

Document reference: IRM/GALOCAD/OUT250-1	Deliverable : OUT250-1	Date: 19-June-2008 Version: 2
Contract ref : GJU/06/2423/CTR/GALOCAD	Written by : H. Brenot, R. Warnant	Verified by : R. Warnant

GALOCAD

Development of a Galileo Local Component for the nowcasting and forecasting of atmospheric disturbances affecting the integrity of high precision Galileo applications.

WP 250 Technical Report:

“Characterization of the tropospheric small-scale activity”

LIST OF ABBREVIATIONS

BDN	Belgian Dense Network
DD	Double Differences of carrier phases
DOY	Day Of Year
EUREF	European Reference Frame
GNSS	Global Navigation Satellite System
GPS	Global Positioning System
IF	Ionosphere-Free combination
IWV	Integrated Water Vapour content
MCS	Mesoscale Convective System
NWP	Numerical Weather Prediction
POH	Probability Of Hail
RINEX	Receiver Independent Exchange format
RMI	Royal Meteorological Institute
ROB	Royal Observatory of Belgium
RTK	Real Time Kinematics
STD	Slant Total Delay
WP	Work Package
ZHD	Zenith Hydrostatic Delay
ZHmD	Zenith Hydrometeors Delay
ZTD	Zenith Total Delay
ZWD	Zenith Wet Delay

TABLE OF CONTENT

List of abbreviations.....	2
Table of Content.....	3
1. Introduction.....	4
2. GNSS measurements of tropospheric delays.....	5
2.1 The tropospheric error.....	5
2.1.1 Contributions to tropospheric error.....	5
2.1.2 Introduction of mapping function.....	6
2.1.3 Notion of ZTD.....	6
2.1.4 Notion of STD.....	7
2.2 Reconstruction of STD.....	7
2.2.1 Isotropic contribution from ZTD to STD.....	7
2.2.2 Anisotropic contribution from gradients of delays to STD.....	11
2.2.3 Final reconstruction of STD and residuals.....	12
3. The different indicators of small-scale tropospheric activity.....	14
3.1 Database and cases studies.....	14
3.2 Tropospheric zenith path delay and their variability.....	15
3.3 Horizontal gradients of delays.....	18
3.3.1 Horizontal gradients from geodetic software.....	18
3.3.2 Baseline index and horizontal gradients from ZTD measurements....	20
3.4 Ionosphere-Free tropospheric index of activity (<i>IF DD Index</i>).....	25
3.4.1 Methodology of IF DD Index.....	25
3.4.2 Process to determine IF DD Index.....	26
3.5 Evaluation of the different candidates.....	31
3.5.1 Event of the 29 th June 2005.....	31
3.5.2 Event of the 8 th June 2003.....	35
3.6 Conclusion on the different candidates.....	37
4. Validation of the IF DD Index.....	38
4.1 Case studies.....	38
4.1.1 Event of the 28 th July 2006.....	38
4.1.2 Tornado of the 1 st October 2006.....	40
4.1.3 Heavy rainfall of the 30 th July 2002.....	47
4.1.4 Rainfall of the 29 th June 2005.....	49
4.1.5 Wet weather of the 19 th October 2005.....	59
4.2 Statistical study of three baselines.....	65
4.2.1 BRUS-BERT and BRUS-OLLN baselines (2005-2007).....	65
4.2.2 BREE-MEEU baseline (1997-2007).....	87
5. Conclusions.....	103
 Annex: BREE-MEEU baseline (1997-2007)	 105
 References.....	 121

1. INTRODUCTION

The neutral atmosphere introduces a delay in the propagation of GNSS signals. This delay essentially due to the troposphere and to the low stratosphere is called “tropospheric delay”. A part of the error source for high accuracy differential GNSS applications comes from the tropospheric delay. GNSS differential applications are based on the assumption that the measurements made by the reference station and by the mobile user are affected in the same way by the different error sources, in particular by the tropospheric effects. The variability of tropospheric delays is mainly due to the tropospheric water vapour. Therefore, differential applications will not be affected by the integrated water vapour content above a GNSS site but mainly by spatial and temporal gradients in water vapour between the reference station and the user.

Small-scale structures in the troposphere are the origin of gradients in water vapour which can degrade the accuracy of differential applications even on distances of a few km. Such events could pose a threat for high accuracy GNSS applications. In this report, we characterize the different small-scale disturbances which can be encountered for stations of the Belgian Dense Network (BDN) during different types of meteorological events.

Different candidates of tropospheric effects indicator which take place in RTK-architecture can be considered. In a first step, we present the tropospheric parameters (*i. e.* ZTD and horizontal gradients) resolved by geodetic software. Interest and limitation of the detection of small-scale tropospheric structures by these tropospheric parameters are discussed. In a second step, considering variability observed in time-series of double differences of the Ionosphere-Free combination, we introduce a new candidate, called “*IF DD Index*”. Considering the rainfall event of the 29th June 2005 and the event of the 8th June 2003, we illustrate the added value of the IF DD Index to detect tropospheric small-scale disturbances (few km) affecting double difference taking place in RTK-architecture. The intensity of this index (which expresses the level of tropospheric activity detected) and the characterization of associated meteorological event are presented for six case studies. A validation of the representativity of IF DD Index is performed mainly based on radar imaging. Finally, considering two baselines of 19 km and 23 km (2 years of data) and one baseline of 7 km (10 years of data) we show the capability of IF DD Index to represent the existence of tropospheric small-scale structures: other techniques of observations (radar imaging and rain gauges measurements) are used to diagnose the tropospheric activity.

2. GNSS MEASUREMENTS OF TROPOSPHERIC DELAYS

2.1 The tropospheric error

The atmosphere affects the propagation of electromagnetic waves. In particular, the neutral atmosphere introduces a delay in the propagation of GNSS signals. The satellites transmit two signals at frequencies L_1 (1575.42 MHz) and L_2 (1227.6 MHz). If multipath effects are neglected, the simplified mathematical model of phase measurements (ϕ_A^i) made by receiver A on satellite i (expressed in cycles) can be written as follows [Seeber, 2003; Leick, 2004]:

$$\phi_A^i = \frac{f}{c} \left(D_A^i + T_A^i - I_A^i + c(\Delta t^i - \Delta t_A) \right) + N_A^i \quad (2.1)$$

with:

D_A^i , the geometric distance between receiver A and satellite i (in meters);

I_A^i , the ionospheric error (in meters);

T_A^i , the tropospheric error (in meters);

Δt_A , the receiver clock error (the synchronisation error of the receiver time scale with respect to GPS time scale);

Δt^i , the satellite clock synchronisation error (the synchronisation error of the satellite time scale with respect to GPS time scale);

N_A^i , the phase ambiguity (integer number);

f , the considered carrier frequency (L_1 or L_2);

c , the speed of electromagnetic waves.

The tropospheric error (T_A^i) is the perturbation induced by the troposphere and the low stratosphere on phase measurements recorded by ground-based receiver.

2.1.1 Contributions to tropospheric error

The tropospheric error (T_A^i), usually called the “*tropospheric path delay*” is defined by three contributions:

$$T_A^i = T_{hydrostatic_A}^i + T_{wet_A}^i + T_{hydrometeors_A}^i \quad (2.2)$$

The tropospheric path delay (T_A^i) is essentially induced by the thickness and the density of the neutral atmosphere. This major contribution (about 90% of T_A^i at the sea level in Belgium), which depends on the altitude and on the absolute pressure at the station, is called the “*hydrostatic delay*” ($T_{hydrostatic_A}^i$) [Saastamoinen, 1972]. Another contribution to

T_A^i takes place at GNSS frequencies. In fact, the molecule of water vapour owns a dipolar moment which has a delay effect on microwave propagation. This second contribution is called the “wet delay” ($T_{wet_A}^i$) [Saastamoinen, 1972]. The variability of the tropospheric error (T_A^i) is mainly controlled by the water vapour density through the atmospheric path travel (from 2% to 20% of T_A^i at the sea level). A third contribution to the tropospheric error exists: this is the contribution of hydrometeors ($T_{hydrometeors_A}^i$) to the total delay of the neutral atmosphere [Solheim et al., 1999; Hajj et al., 2001]. This small contribution to tropospheric path delay owns a relative high variability (from 0% to 3% of T_A^i) [Brenot, 2006]

2.1.2 Introduction of mapping function

The “slant” tropospheric delay (T_A^i) can be converted to a zenith tropospheric delay above a GNSS station A. Taking into account the variable composition and thickness of the neutral atmosphere in the direction of a satellite i (at azimuth α_i and elevation ε_i) visible from station A at time t , an approximation of the vertical tropospheric error ($T_A^{vertical}$) can be expressed using mapping function (MF):

$$T_A^i(t) \cong T_A^{vertical}(t) \cdot MF(t, \alpha_i, \varepsilon_i) \quad (2.3)$$

If the atmosphere were rigorously plan without local tropospheric anisotropy around station A, the simple mapping function (without azimuth dependency) is $\sin^{-1}(\varepsilon_i)$. Nevertheless in practice, for low elevations this simple function is usually not realistic [Resch, 1984; Bevis et al., 1992]. More complicated mapping functions have thus been introduced to convert more precisely slant delays into zenith delays taking into account the more important thickness of the troposphere at low elevation and the error caused by the straight line approximation [Hopfield, 1969; Marini and Murray, 1973; Ifadis, 1986; Herring, 1992; Niell, 1996].

2.1.3 Notion of ZTD

In the literature, the term $T_A^{vertical}$ of Eq. (2.3) is often referred to as the “Zenith Total Delay” of the neutral atmosphere (ZTD). Zenith Total Delay represents the mean propagation delay (expressed in unit of distance) experienced by GNSS signals due to their propagation in the neutral atmosphere (ZTD values are about 2.5 m at the sea level):

$$ZTD = ZHD + ZWD + ZHmD \quad (2.4)$$

The major part of the ZTD depends on the altitude and the absolute atmospheric pressure at the station. This major contribution, called the “Zenith Hydrostatic Delay” (ZHD), is about 2.3 m at the sea level. On the other hand, ZTD variability is essentially driven by the water vapour content over the site: the “Zenith Wet Delay” contribution (ZWD) which

ranges from 0.05 m to 0.50 m. *Brenot et al.* [2006] have shown that an additional contribution to ZTD can be considered during rainfall events: the “*Zenith Hydrometeors Delay*” (ZHmD) with value estimate up to 0.07 m during the flash-flood event which occurred the 8-9th September 2002 over southeastern France.

2.1.4 Notion of STD

In the literature, the term T_A^i of Eq. (2.1), (2.2) and (2.3) is often referred to as the “*Slant Total Delay*” of the neutral atmosphere (STD). Phase measurements are ambiguous (see Eq. 2.1). For this reason, STD can not be directly obtained using phase measurements. Using geodetic software, a reconstruction of STD can be established with two tropospheric parameters: 1) the ZTD, and 2) the horizontal gradients of delays.

2.2 Reconstruction of STD

2.2.1 Isotropic contribution from ZTD to STD

The first tropospheric parameter which can be reconstructed by geodetic software is the “*Zenith Total Delay*” (ZTD) of the neutral atmosphere. To extract the tropospheric error (T_A^i) from the phase measurements (φ_A^i) different steps have to be considered:

Step 1: the Ionosphere-Free combination

Contrary to the ionosphere, the troposphere is non-dispersive for GNSS microwaves. Thus, the Ionosphere-Free combination (IF) allows to remove the first order of ionospheric errors. Considering the simplified mathematical model of phase measurements φ_A^i emitted by satellite i and received by station A , presented Eq. (2.1), and considering $\varphi_{A,1}^i$ and $\varphi_{A,2}^i$, respectively the phase measurements at L_1 and L_2 frequencies, the ionosphere-free combination is given by:

$$\varphi_{A,IF}^i = \alpha_{IF} \varphi_{A,1}^i + \gamma_{IF} \varphi_{A,2}^i \quad (2.5)$$

with

$$\alpha_{IF} = \frac{f_1^2}{(f_1^2 - f_2^2)} \cong 2.546 \quad (2.6)$$

and

$$\gamma_{IF} = -\frac{f_1 f_2}{(f_1^2 - f_2^2)} \cong -1.984 \quad (2.7)$$

If we neglect multipath, the IF phase measurements $\varphi_{A,IF}^i$ made by receiver A on satellite i can be expressed by [Leick, 2004]:

$$\varphi_{A,IF}^i = \frac{f_1}{c} (D_A^i + T_A^i) + f_1 (\Delta t^i - \Delta t_A) + N_{A,IF}^i \quad (2.8)$$

where f_1 is the L₁ frequency, and $N_{A,IF}^i$ the IF combination phase ambiguity (real number) which can be formulated by:

$$N_{A,IF}^i = \alpha_{IF} N_{A,1}^i + \gamma_{IF} N_{A,2}^i \quad (2.9)$$

$N_{A,1}^i$ and $N_{A,2}^i$ are respectively L₁ and L₂ ambiguities.

Step 2: double difference technique

The double difference technique allows removing clock errors from Eq. (2.8). In fact, considering two GNSS stations (*A* and *B*) and two satellites (*i* and *j*), we can form double differences ($\varphi_{AB,IF}^{ij}$) of the ionosphere-free combination observations of the Eq. (2.8):

$$\varphi_{AB,IF}^{ij} = \frac{f_1}{c} (D_{AB}^{ij} + T_{AB}^{ij}) + N_{AB,IF}^{ij} \quad (2.10)$$

with the notation

$$*_{AB,IF}^{ij} = (*_{A,IF}^i - *_{B,IF}^i) - (*_{A,IF}^j - *_{B,IF}^j) \quad (2.11)$$

$$*_{AB}^{ij} = (*_A^i - *_B^i) - (*_A^j - *_B^j) \quad (2.12)$$

Step 3: positions and resolutions of ambiguities to extract tropospheric error

In practice, to reconstruct information about the troposphere (T_{AB}^{ij}), it is necessary:

- 1) to resolve phase ambiguities ($N_{AB,IF}^{ij}$),
- 2) to compute the geometric term (D_{AB}^{ij}); this term can be computed if station *A* and *B* positions are well known.

Step 4: ZTD's adjustments by geodetic softwares and mapping functions

Phases measurements (Eq. 2.1) between each couple of stations and each couple of visible satellites are projected in the zenith direction using mapping function (figure 1). Considering the differential tropospheric error (T_{AB}^{ij}) contained in double differences of ionosphere-free combinations ($\varphi_{AB,IF}^{ij}$), geodetic softwares allow to reconstruct ZTD's for the network of stations selected.

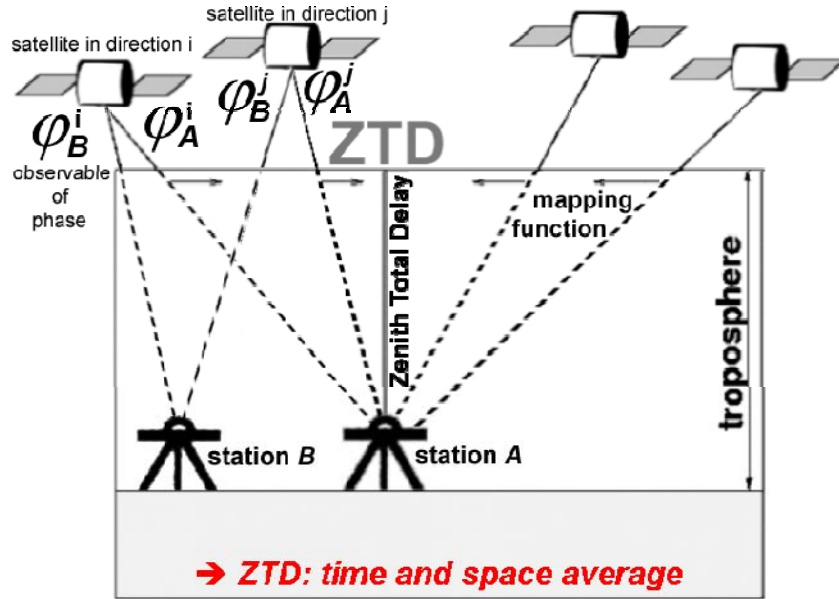


Figure 1: definition of Zenith Total Delay (ZTD) of the neutral atmosphere estimated by geodetic software (a time and space average considering every observable of phase).

For each baseline, an adjustment of the tropospheric error T_{AB}^{ij} is performed, which represents an adjustment of the difference of ZTD between stations A and B:

$$T_{AB}^{ij} = (T_A^i - T_B^i) - (T_A^j - T_B^j) \quad (2.13)$$

where

$$\begin{aligned} T_A^i &\cong ZTD_A \cdot mf_{sym}(\varepsilon_A^i) = L_{sym,A}^i \\ T_B^i &\cong ZTD_B \cdot mf_{sym}(\varepsilon_B^i) = L_{sym,B}^i \\ T_A^j &\cong ZTD_A \cdot mf_{sym}(\varepsilon_A^j) = L_{sym,A}^j \\ T_B^j &\cong ZTD_B \cdot mf_{sym}(\varepsilon_B^j) = L_{sym,B}^j \end{aligned} \quad (2.14)$$

Mean Zenith Total Delays, for example ZTD_A and ZTD_B at stations A and B, are estimated using isotropic mapping functions (mf_{sym}) of Niell [1996] (with spherical symmetry) which depend on elevation (for example elevations $\varepsilon_A^i, \varepsilon_B^i$ and $\varepsilon_A^j, \varepsilon_B^j$ of satellites i and j), and based on the least square adjustments of tropospheric isotropic error delays in direction of each visible satellites (for example $L_{sym,A}^i, L_{sym,B}^i, L_{sym,A}^j$ and $L_{sym,B}^j$) as shown in Eq. 2.14.

ZTD's cannot be reconstructed at each epoch of measurements: this would add two unknowns for each epoch. Therefore, it is assumed that ZTD's remains constant during a given time which ranges from 5 minutes to 2 hours depending on the geodetic software used and on the application. Carrier phase measurements made on all visible satellites ($\varphi_A^i, \varphi_B^i, \varphi_A^j, \varphi_B^j, \dots$) are used to form double differences of the ionosphere-free combination ($\varphi_{AB,IF}^{ij}, \dots$) and used in calculations (space average) during a selected time-window (time average). Resolutions of ambiguities and well known positions of stations

allow estimations of ZTD_A and ZTD_B . Considering k epochs of 30 seconds in the defined time-window used by geodetic software for reconstructions of ZTD (15 minutes for example), and considering the number n_j of visible satellites at each epoch j , ZTD_A can be established by:

$$\left| ZTD_A - \frac{1}{k} \sum_{j=1}^k \left(\frac{1}{n_j} \sum_{i=1}^{n_j} \frac{L_{sym,A}^i(\varepsilon_A^i)}{mf_{sym}(\varepsilon_A^i)} \right) \right| < \mu \quad (2.15)$$

In practice, ZTD_A resolved by geodetic software is the result of the minimization of μ ($\mu \rightarrow 0^+$) obtained during the inversion which adjusts $(k.n_j)$ tropospheric isotropic delays ($L_{sym,A}^i$). ZTD are supposed constant during the time-windows chosen to obtain the adjustment.

Contribution with spherical symmetry (L_{sym}) to STD

Slant Total Delay (STD) of the neutral atmosphere in direction of each visible satellite, which is the tropospheric error T_A^i presented Eq. (2.1) for station A and satellite i , is not directly available. Only the use of the tropospheric model defined by mapping functions allows restitutions of STD. According to ZTD_A , the isotropic delay ($L_{sym,A}^i$) can be reconstructed in direction of satellite i with elevation ε_A^i by:

$$L_{sym,A}^i(\varepsilon_A^i) = ZTD \cdot mf_{sym}(\varepsilon_A^i) \quad (2.16)$$

This isotropic contribution to STD is independent of the azimuth α_A^i of the selected satellite, and can define a cone of path delay around a GNSS site (spherical symmetry).

2.2.2 Anisotropic contribution from horizontal gradients of delays to STD

The number of visible satellites and the accuracy of STD reconstructions are critical to identify exactly the location of small-scale tropospheric structures. For this reason, a second tropospheric parameter has been introduced in the least square adjustment of geodetic software: the horizontal gradients of delays [Chen and Herring, 1997]. These gradients take into account the presence of anisotropies in the troposphere.

Notion of horizontal gradients of delays

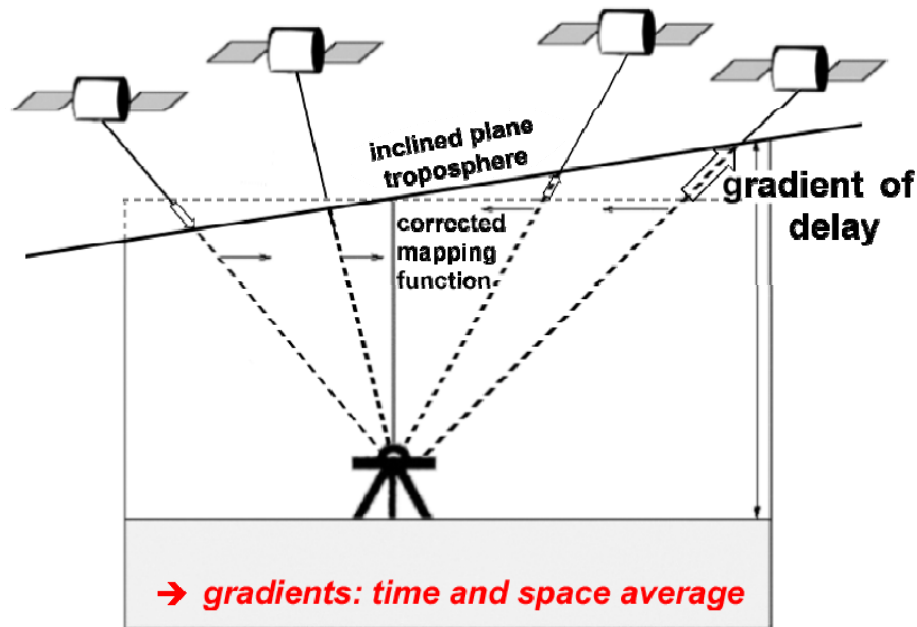


Figure 2: definition of horizontal gradients of delays by geodetic software (anisotropic correction of phase observables residuals projected in the zenith direction).

Horizontal gradients of delays are characterized by two components G_{EW} and G_{NS} (respectively East-West and North-South). GNSS gradients represent a correction of phase residuals projections depending on elevations (ε) and on azimuths (α) of visible satellites (anisotropic contribution). An inclined plane model of troposphere (Fig. 2) schematized by linear thickness and density variations is considered to define horizontal gradients during adjustments of tropospheric parameters [Davis *et al.*, 1993; Gradinarsky, 2002; Brenot, 2006]. The correction provided by GNSS gradients has its own mapping function (mf_{az}) [Chen and Herring, 1997]. The formulation of azimuth anisotropic contribution (L^i_{az}) to STD reconstruction depends on the satellite direction (elevation and azimuth).

GNSS horizontal gradients of delays are expressed by an equivalent additional distance. The convention of GAMIT geodetic software [King and Bock, 2002] is to resolve GNSS gradient components at 10° of elevation (centimeter values), but using mapping functions

measurements of gradients can be converted into the zenith direction (millimeter values). Usually, values of GAMIT gradients components do not exceed 15 cm. In practice, a positive value (of 5 cm for example) of G_{EW} means that the STD at 10° of elevation in the east direction is 5 cm larger than the STD at 10° of elevation in the west direction. Usually considering a cutoff angle of 10° in calculations, GNSS gradients concern an area of 50 km around the GNSS site (assuming that water vapour density over 10 km is negligible). Considering G_{EW} of 5 cm, ZTD of a site located 25 km eastward at the same altitude is about 9 mm larger, which approximately represents, an Integrated Water Vapour content (IWV) about 1.5 kg/m^2 larger. G_{EW} component (of 5 cm) corresponds to a zenith differential value of about 1.6 mm which can allow ZTD imaging from a network of stations. For ZTD resolved every 15 minutes, horizontal gradients are adjusted every 30 minutes. As ZTD, horizontal gradients represent a time and space average adjustment depending on the different visible satellites.

Contribution with azimuthal asymmetry (L_{az}) to STD

The use of a simple model of inclined plane troposphere allows to resolve horizontal gradients of delays (two components G_{EW} and G_{NS}). The first order of the anisotropic contribution to delays ($L_{az,A}^i$) induced by water vapour and hydrometeors (up to 50 km around GNSS station A) in direction of satellite i can be formulated depending on elevation ε_A^i and azimuth α_A^i of this satellite:

$$L_{az,A}^i(\alpha_A^i, \varepsilon_A^i) = mf_{az}(\varepsilon_A^i) \cdot (G_{NS} \cdot \cos(\alpha_A^i) + G_{EW} \cdot \sin(\alpha_A^i)) \quad (2.17)$$

This expression of anisotropic contribution to STD combines a mapping function (mf_{az}), which depends on the elevation ε_A^i , with gradients components connected to the azimuth α_A^i (azimuthal asymmetry).

2.2.3 Final reconstruction of STD and residuals

Geodetic software (BERNESE or GAMIT) consider double differences of linear combinations of carrier phases measurements (contained in RINEX files) to resolve precise positioning solutions and atmospheric parameters [King, 1985; Dong and Bock, 1989; Blewitt, 1989; Leick, 1989; Teunissen et al., 1998]. The two tropospheric parameters adjusted by geodetic software are ZTD and horizontal gradients. These parameters allow a reconstruction of the Slant Total Delay of the neutral atmosphere at station A (STD_A^i) in direction of a satellite i with an elevation ε_A^i and an azimuth α_A^i , which is equivalent to the tropospheric error (T_A^i) of a station A (see Eq. 2.1). To detect small scale structures the addition of $L_{sym,A}^i$ (obtained from ZTD_A) with $L_{az,A}^i$ (obtained from horizontal gradient components) establishes a good reconstruction of STD_A^i :

$$STD_A^i(\alpha_A^i, \varepsilon_A^i) = T_A^i = L_{sym,A}^i(\varepsilon_A^i) + L_{az,A}^i(\alpha_A^i, \varepsilon_A^i) + L_{res,A}^i(\alpha_A^i, \varepsilon_A^i) \quad (2.18)$$

The residual observation $L_{res,A}^i$ is the post-fit phase residual of the inversion calculation performed by geodetic software, called “*One-Way post-fit residual*”. It is the third tropospheric parameters available from geodetic software every epoch of 30 seconds in direction of every satellite. Values of post-fit phase residuals rarely exceed few centimeters. In the practice, these post-fit residuals are not only due to tropospheric effects: they contain all remaining unmodeled effects (specifically multipath). For this reason we will not focus on One-Way post fit residuals and final reconstructions of STD.

From the meteorological point of view, for a ground-based station the best localization of tropospheric structures is defined by the contribution with azimuthal asymmetry (L_{az}) and horizontal gradients. If distances between stations are short enough, detection of small-scale structures can be envisaged.

The aim of our study is to find a good indicator of small-scale tropospheric activity which takes place and has an effect in RTK-architecture. In the following section, we present the database used to study the potential and the limitation of tropospheric delays (ZTD and gradients) to assess tropospheric effects in RTK-architecture. The interest of Belgian Dense Network of GNSS stations for such a study will be discussed. Then, with a new approach based on double difference index of tropospheric activity (called *IF DD Index*) we present another candidate to detect small scale tropospheric structures. Then, the studies of the rainfall of the 29th June 2005 and the 8th June 2003 event show the different advantages of possible indicators of tropospheric activity (ZTD, gradients and IF DD Index). Finally, several case studies and a statistical study present the relevance of IF DD Index.

3.2 Tropospheric zenith path delay and their variability

Zenith Total Delays (ZTD's) represent the path delays induced by the neutral atmosphere compared to an empty space travel for a same time of GNSS signals propagation (ZTD values are about 2.5 m at the sea level). The major part of the ZTD depends on the altitude and on the atmospheric pressure at the station (defined by ZHD contribution to ZTD, about 2.3 m at the sea level) but the ZTD major variability is essentially driven by the water vapour content over the site: the “*Zenith Wet Delay*” contribution ranges from 0.05 m to 0.50 m. To study the evolution of ZTD and to detect small-scale structures, we have estimated for the whole ZTD-database equivalent ZTD at the sea level. In fact to compute this altitude correction we have considered an atmosphere in hydrostatic equilibrium with a humidity of 50% (standard conditions for the ground pressure and temperature).

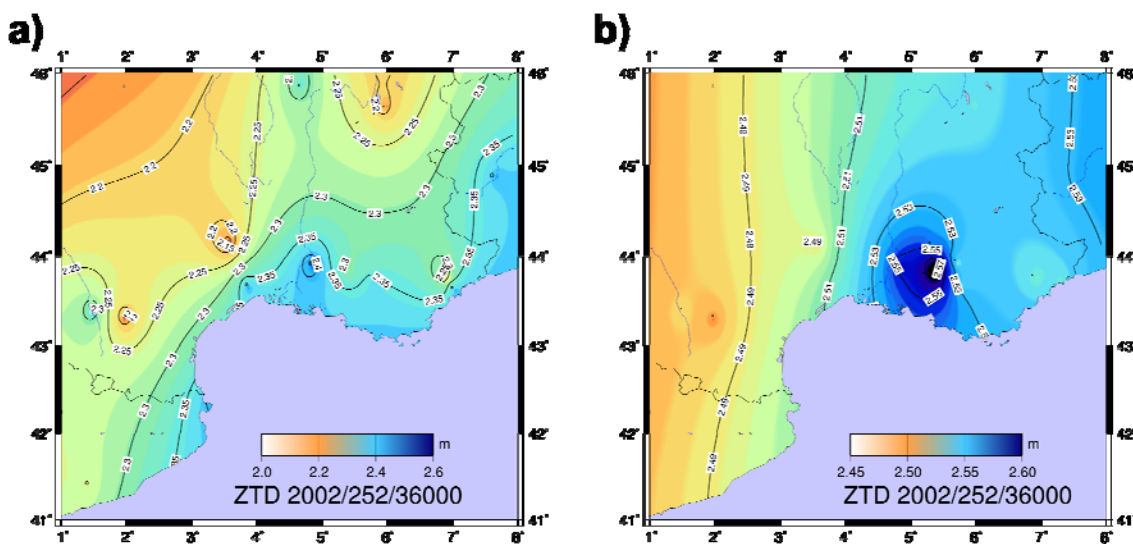


Figure 4: a) ZTD imaging at 10H UTC the 9th September 2002 without altitude correction;
b) same ZTD with altitude correction.

Figure 4 illustrates the importance of this ZTD altitude correction to allow a 2D-field visualization of small-scale structures (flash-flood of the *Gard* in southeastern France the 8-9th September 2002). Afterwards, ZTD altitude correction will systematically be applied on time-series and imaging of ZTD.

To analyze the effect of tropospheric activity on RTK, we are trying to find an indicator which allows to detect small-scale tropospheric structures.

We have studied the ZTD variability (using one station data) to see in how far this one-station ZTD variability could be an indication of small-scale activity in the vicinity of the station considered. For all the ZTD data we have produced index, called *ZTD variation Level*. This index considers the ZTD variability from t_0-3h to t_0 . Figure 5 illustrates the use of ZTD variability to characterize the 29th June 2005 rainfall event. At 15H UTC, we can observe that NAMR station shows a loading period while ONHA presents a discharge period.

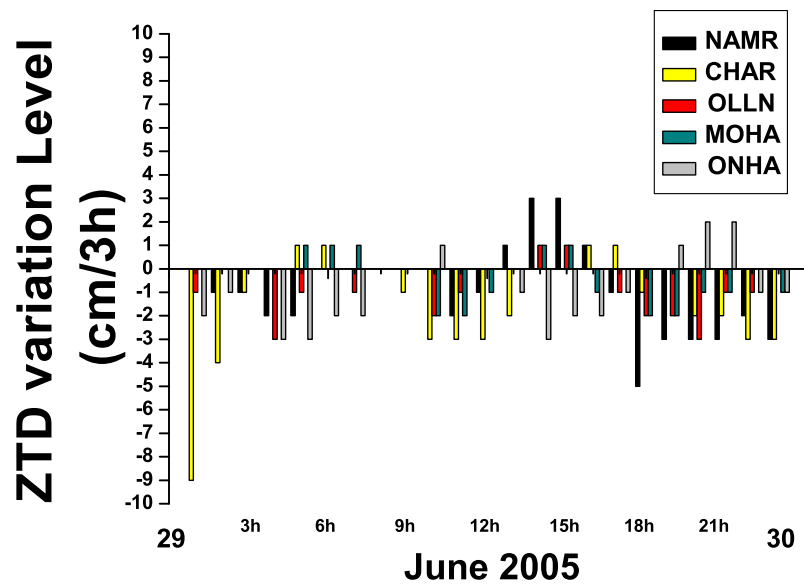


Figure 5: Level of activity considering ZTD variation from t_0-3h to t_0 .

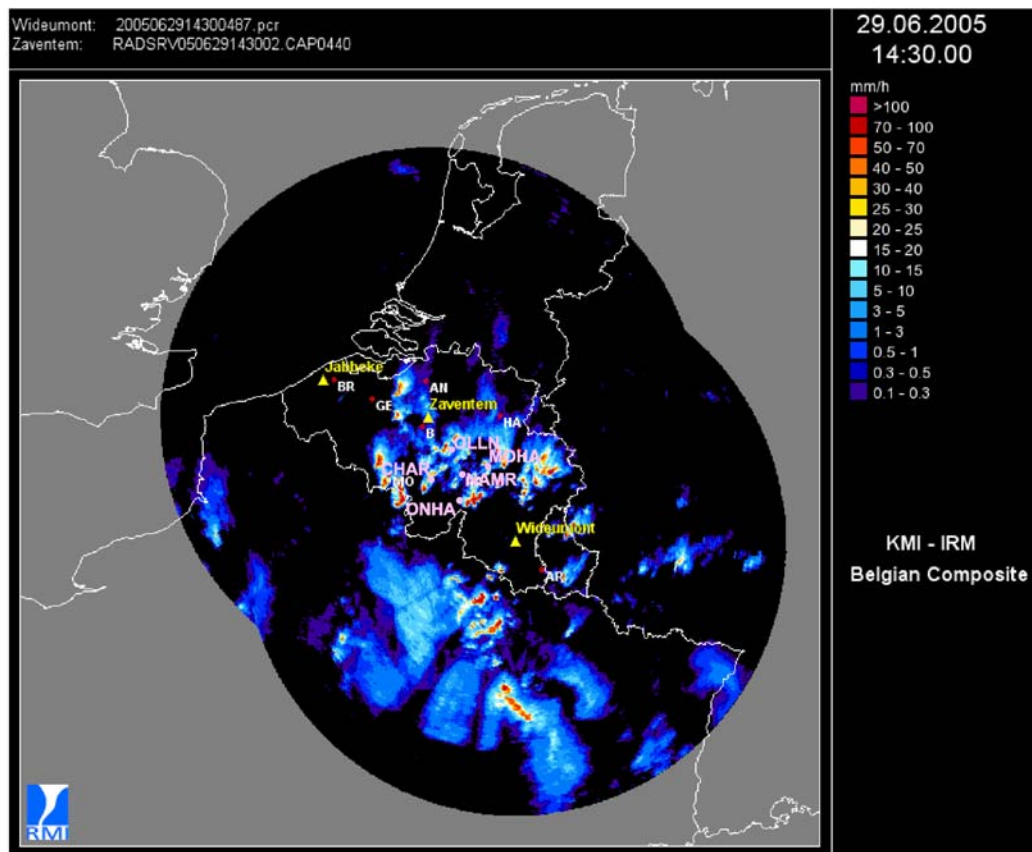


Figure 6: radar imaging of precipitations at 14H30 UTC the 29th June 2005.

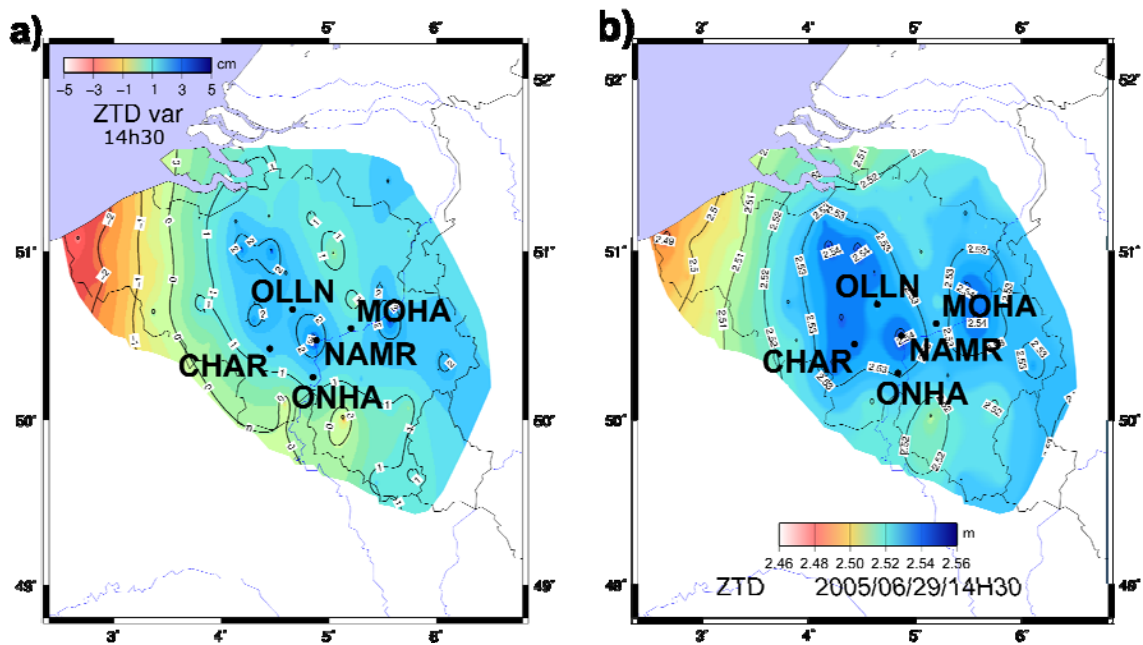


Figure 7: ZTD imaging at 14H30 UTC the 29th June 2005 a) bias to the mean value noted ZTD var; b) ZTD with altitude correction. The white area shows the absence of data.

Radar and ZTD imaging (Fig. 6 and 7) confirm that small-scale tropospheric structures were present above NAMR station. In an equivalent way of doing than the altitude correction, figure 7a shows the bias of ZTD to the mean value of the ZTD time-series studied from the 25th June to the 1st July 2005. Figure 7b shows ZTD corrected to the altitude of the sea level.

3.3 Horizontal gradients of delays

3.3.1 Horizontal gradients from geodetic software

Horizontal gradients of delays are the second tropospheric parameter adjusted by geodetic software (see section 2.2.2). Two components are resolved to establish the horizontal gradient vector $\vec{G} = (G_{NS}, G_{EW})$, respectively North-South and East-West component. With GAMIT software, this vector represents the azimuth direction of the maximal anisotropy (normalized at 10° of elevation) induced by water vapour and hydrometeors around a GNSS site. Except for rainfall events, horizontal gradients components do not exceed few centimetres.

In figure 8, we illustrate the interest of horizontal gradients during the flash-flood event of 8-9 September 2002. Considering radar imaging of reflectivity in dBZ (equivalent to precipitations), we superposed horizontal GNSS gradients with the plot of the tropospheric activity zone (dot line circle with a radius 50 km). During the three phases of the 8-9th September 2002 flash-flood event [Delrieu *et al.*, 2005], the GNSS gradients of the four stations concerned (baselines from 60 km to 150 km) detect exactly the location of Mesoscale Convective Systems (MCS).

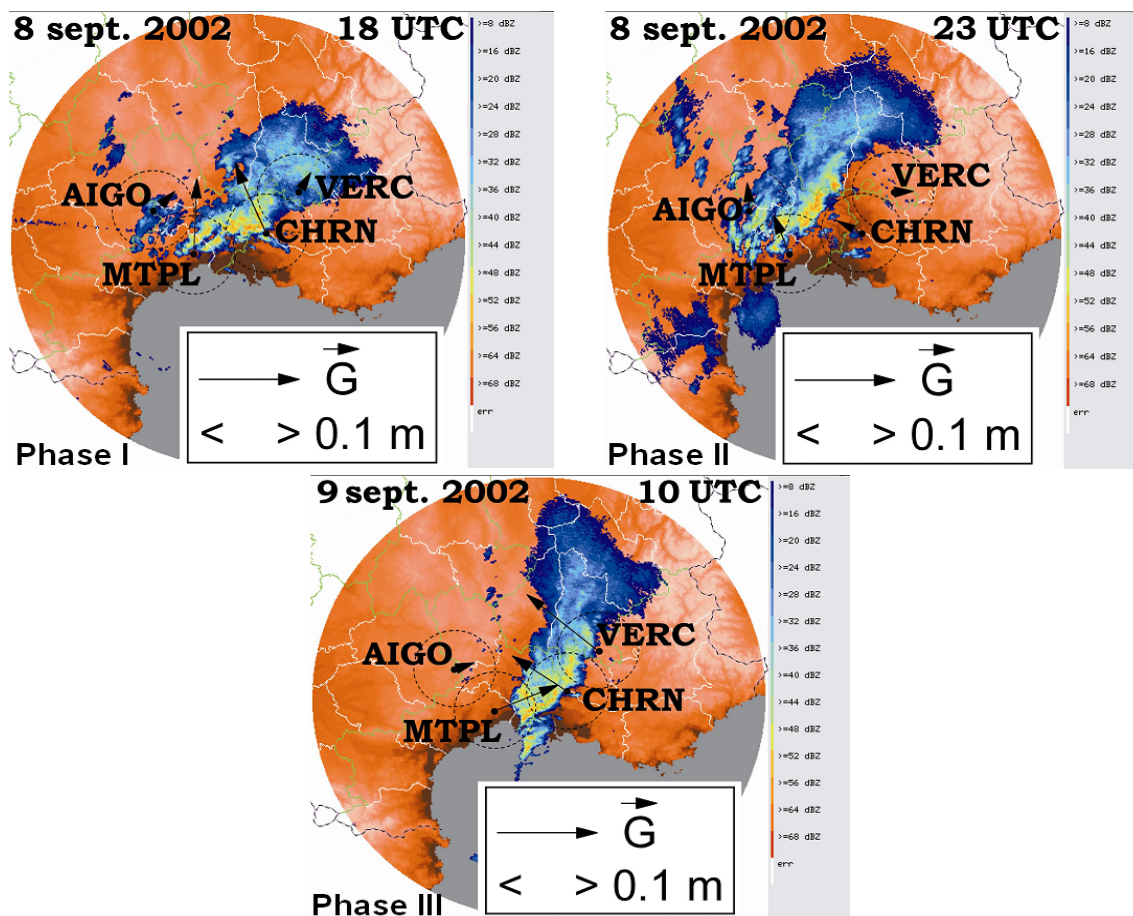


Figure 8: GNSS gradients superposed to radar imaging for the 8-9th September flash-flood event.

Brenot [2006] demonstrated that liquid and solid tropospheric water processes (with maximal humidity) give the main contribution to the local tropospheric anisotropy. In phase I (formations of MCS) and phase III (sweeping of them by a front perturbation) of this event, we estimated that conversions of the hydrometeors delay anomaly (with mapping functions) observed by GNSS gradients represent an increase larger than 2 cm of ZTD observations at CHRN station.

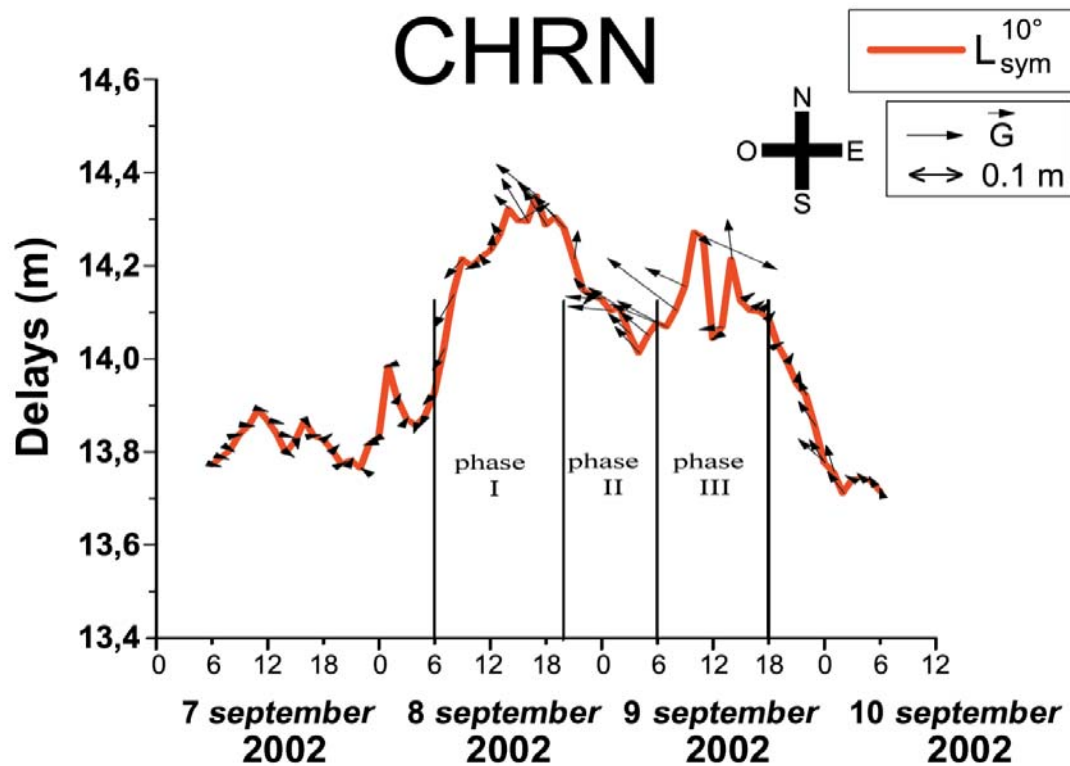


Figure 9: Horizontal gradients plot on each isotropic delays observations (ZTD) projected at 10° of elevation ($L_{sym}^{10^\circ}$).

In figure 9, we present the plot of horizontal gradients (at 10°) on the time-series of ZTD projected at 10° ($L_{sym}^{10^\circ}$ around 14 m, see Eq. 3.1).

$$L_{sym}^{10^\circ} = ZTD \cdot mf_{sym}(10^\circ) \quad (3.1)$$

The combination of ZTD and horizontal gradients of delays can be useful to detect and qualify the water vapour and the hydrometeors contributions to delay caused by MCS existence.

3.3.2 Baseline index and horizontal gradients from ZTD measurements

The difference of ZTD between two stations (Δ ZTD) defining a baseline is a key parameter to characterize tropospheric small-scale structures. For this reason we have established for all the ZTD-data index of tropospheric activity relative to each baseline smaller than 30 km, index called “ Δ ZTD Baseline Index”. Figure 10 shows time-series of this index which represent biases between the ZTD of two stations (altitude corrections have been applied) the 29th June 2005. We can see considering baselines NAMR-CHAR, NAMR-OLLN, NAMR-MOHA, NAMR-ONHA, that NAMR station presents a ZTD from 1 cm to 4 cm larger than the other stations (at 14H UTC). The high tropospheric activity around NAMR points a structure above this station according to ZTD observations (see radar and ZTD imaging figures 6 and 7 for validation).

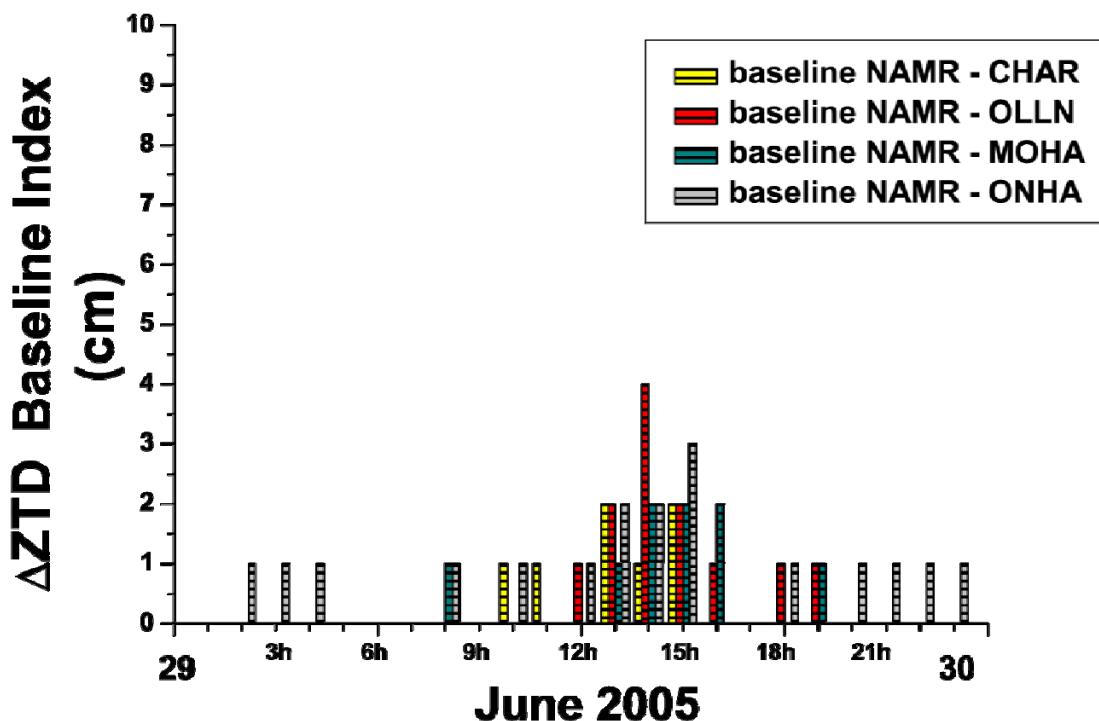


Figure 10: Time-series of Baseline index estimated from ZTD bias (altitude correction) according to NAMR station the 29th June 2005.

Let's remark that, in this case study, we can see the importance to have a dense network of GNSS stations: figure 11 compares the resolution obtained with a sub-set of the Belgian Dense Network (BDN) and with the full BDN.

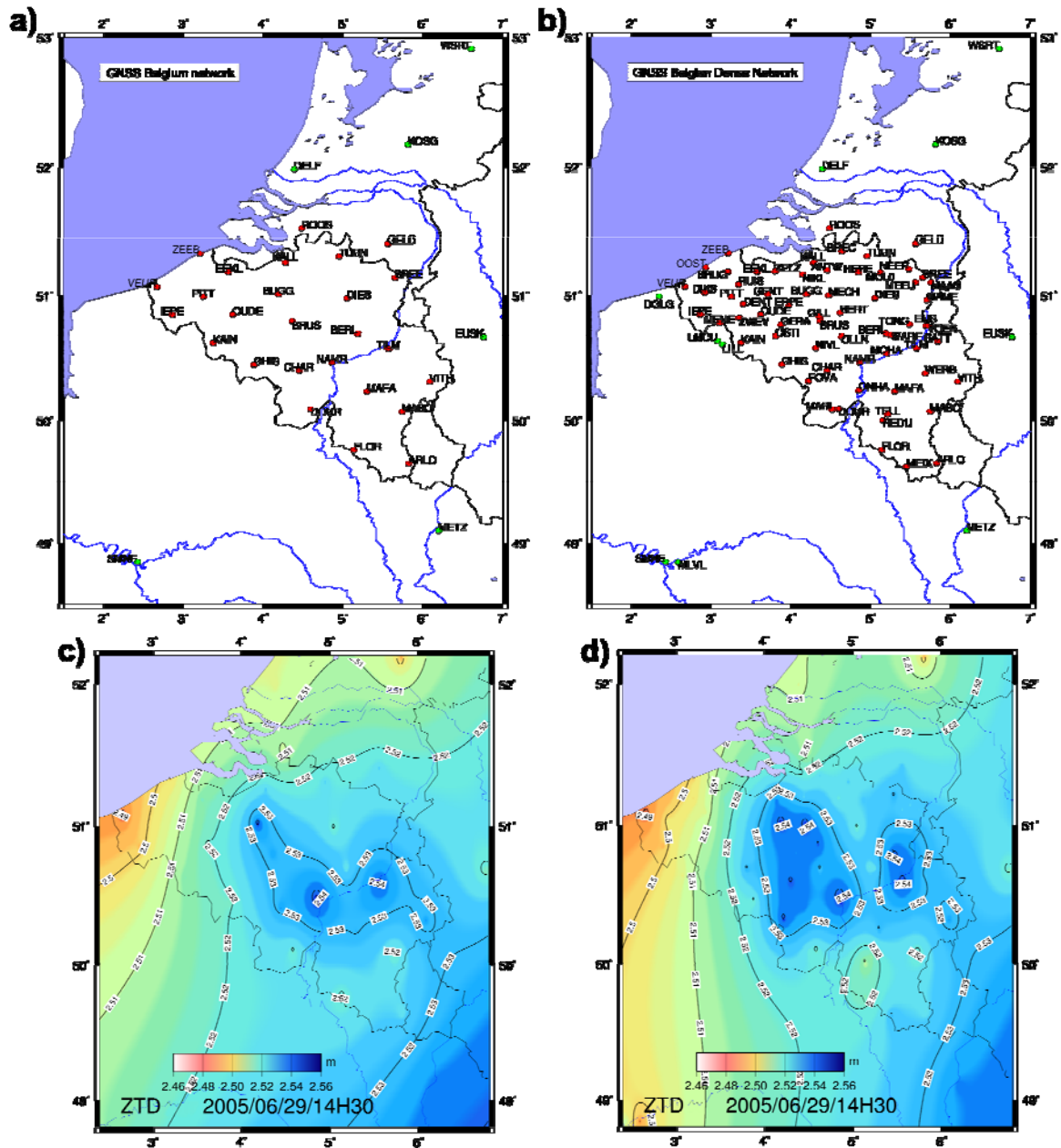


Figure 11: GNSS network of stations a) low density, b) high density. ZTD imaging (with altitude corrections) at 14H30 UTC the 29th June 2005 c) with the low density network, d) with the high density network.

The resolution of ZTD imaging (Figure 11c) with a low density network (Figure 11a) is clearly affected compared to the ZTD imaging (Figure 11d) with the full BDN (Figure 11b).

Horizontal gradients from geodetic software are not available for EUREF stations (2001-2005). For this reason, using a least square adjustment, we have produced horizontal gradients from ZTD data (*i. e.* differences of ZTD between stations with altitude correction and adjustment of North-South and East-West components), called afterwards $\overrightarrow{Grad}^{ZTD} = (G_{NS}^{ZTD}, G_{EW}^{ZTD})$ [Brenot, 2006]:

$$\begin{aligned} G_{NS}^{ZTD} &= \frac{\overline{\cos(\alpha)\sin(\alpha)} \cdot \overline{\sin(\alpha)\Delta ZTD} - \overline{\sin^2(\alpha)} \cdot \overline{\cos(\alpha)\Delta ZTD}}{\overline{\cos(\alpha)\sin(\alpha)^2} - \overline{\sin^2(\alpha)} \cdot \overline{\cos^2(\alpha)}} \\ G_{EW}^{ZTD} &= \frac{\overline{\cos(\alpha)\sin(\alpha)} \cdot \overline{\cos(\alpha)\Delta ZTD} - \overline{\cos^2(\alpha)} \cdot \overline{\sin(\alpha)\Delta ZTD}}{\overline{\cos(\alpha)\sin(\alpha)^2} - \overline{\sin^2(\alpha)} \cdot \overline{\cos^2(\alpha)}} \end{aligned} \quad (3.2)$$

where $\overline{\cos(\alpha)\sin(\alpha)} = \sum_{i=1}^k (\cos(\alpha_i)\sin(\alpha_i))$, $\overline{f(\alpha)\Delta ZTD} = \sum_{i=1}^k (f(\alpha_i)\Delta ZTD_i)$, and $\overline{f^2(\alpha)} = \sum_{i=1}^k f^2(\alpha_i)$, with f function \cos or \sin and $\Delta ZTD_i = ZTD^{ref} - ZTD_i^{other}$. ZTD^{ref} is ZTD of the reference station chosen to estimate horizontal gradients $\overrightarrow{Grad}^{ZTD}$, ZTD_i^{other} are ZTD of BDN stations located at a distance smaller than 50 km from the reference station. Horizontal gradients from ZTD have been calculated if North-South and East-West geometric repartition factor (respectively $\xi_{NS} \in [0,100]$ and $\xi_{EW} \in [0,100]$) of these stations, expressed in %, are satisfactory (*i. e.* between 45% and 55%). The formulation of geometric repartition factors of the other stations around the reference station is the following:

$$\begin{aligned} \xi_{NS} &= 100 \cdot \frac{\sum_{i=1}^n \left(d_i \cdot \left| \frac{\alpha_i - \pi}{\pi} \right| \right)}{\sum_{i=1}^n d_i} \\ \xi_{EW} &= 100 \cdot \frac{\sum_{i=1}^n \left(d_i \cdot \left| 1 - \frac{\pi - \left| \alpha_i - \frac{\pi}{2} \right|}{\pi} \right| \right)}{\sum_{i=1}^n d_i} \end{aligned} \quad (3.3)$$

with n the number of stations located at a distance smaller than 50 km from the reference station, α_i the azimuthal direction of stations according to the reference station, and d_i the distance between the reference station and one other station (baseline smaller than 50 km). Some indications allow to better understand the meaning of geometric factors: if all the other stations are located in the north direction $\xi_{NS} = 100\%$, all in the south direction $\xi_{NS} = 0\%$; if all the other stations are located in the east direction $\xi_{EW} = 100\%$, all in the west direction $\xi_{EW} = 0\%$. Note that a perfect

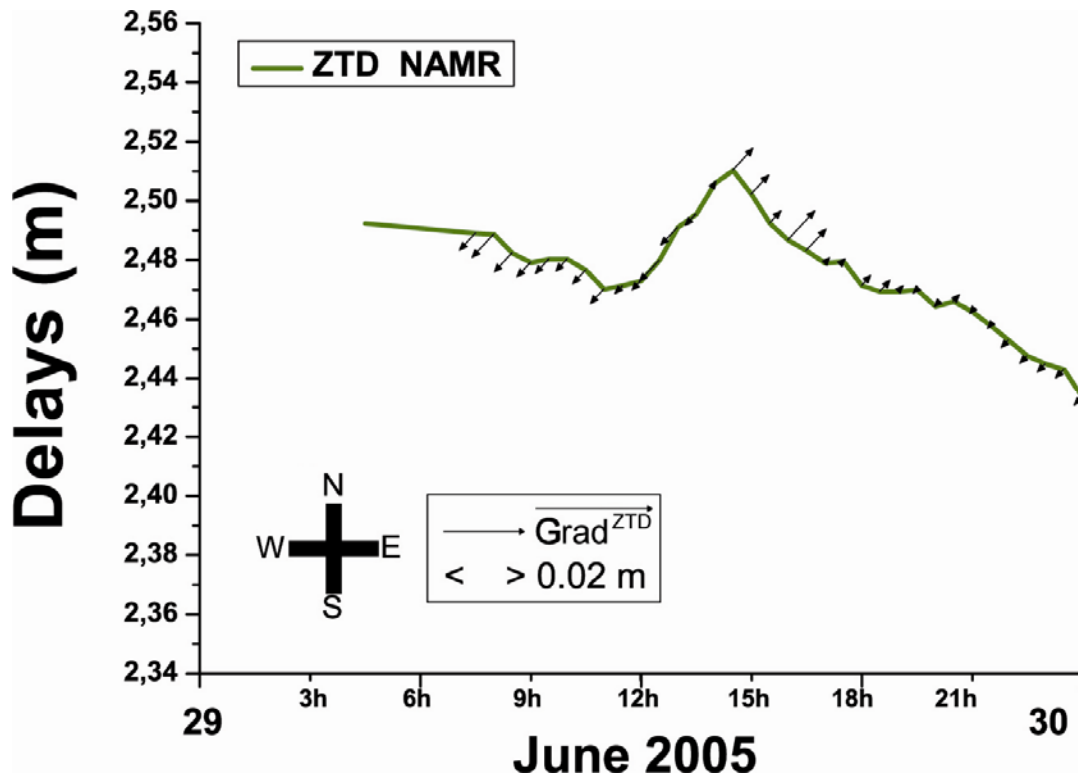


Figure 13: Horizontal gradients plot on each ZTD observations at NAMR stations the 29th June 2005.

Equivalent horizontal gradients from ZTD observations ($\overline{Grad^{ZTD}}$) point the local anisotropy around NAMR what can be useful to validate the occurrence of local tropospheric activity. Nevertheless, it cannot be used to detect periods where small-scale tropospheric activity could affect RTK accuracy. In fact, considering the rainfall event of the 29th June 2005 we will see in section 3.5 that ZTD and horizontal gradients present a limitation for the detection of very small-scale tropospheric structures (in our RTK-architecture). ZTD and horizontal gradients from geodetic software (\tilde{G}) or horizontal gradients from ZTD ($\overline{Grad^{ZTD}}$) represent an average in time and space which smoothes tropospheric structures (see section 2, figure 1 and Eq. 2.15 for a description of ZTD assessments by geodetic software, and section 2, figure 2 and Eq. 3.2 for horizontal gradients).

In the following section, we will present a new candidate to identify tropospheric activity. This candidate is based on time-series of double differences observations considering the ionosphere-free combination. To establish a new indicator, we focus on double differences observation due to the fact that they are the basic observable used in RTK to compute positions.

3.4 Ionosphere-Free tropospheric index of activity (*IF DD Index*)

3.4.1 Methodology of *IF DD Index*

Double differences (L_1, L_2) of the ionosphere-free combination of GNSS phase observations can be used to detect the presence of small-scale structures in the troposphere. The basic observables used for this purpose are explained in section 2.1 and 2.2.1 of this report. The presence of small-scale structures in the troposphere induces variability in phase measurements. As we are using stations of which positions are precisely known (BDN stations), geometric distances D_{AB}^{ij} in double differences are known. The tropospheric effect T_{AB}^{ij} and the ambiguity $N_{AB,IF}^{ij}$ remain the only unknowns in the double difference of phase of the ionosphere-free (IF) combination $\varphi_{AB,IF}^{ij}$, presented Eq. (2.10). Let's call $\Phi_{AB,IF}^{ij}$, the double difference phase observation corrected for the geometric term D_{AB}^{ij} :

$$\Phi_{AB,IF}^{ij} = \varphi_{AB,IF}^{ij} - \frac{f_1}{c} D_{AB}^{ij} = \frac{f_1}{c} T_{AB}^{ij} + N_{AB,IF}^{ij} \quad (3.4)$$

The ambiguity term ($N_{AB,IF}^{ij}$) has the following expression according to Eq. (2.11):

$$N_{AB,IF}^{ij} = (N_{A,IF}^i - N_{B,IF}^i) - (N_{A,IF}^j - N_{B,IF}^j) \quad (3.5)$$

Ambiguities ($N_{A,IF}^i, N_{B,IF}^i, N_{A,IF}^j$ and $N_{B,IF}^j$) are defined in Eq. (2.9). The phase ambiguity term ($N_{AB,IF}^{ij}$) is a real number with a constant value. In figure 14, we show an example of $\Phi_{AB,IF}^{ij}$ (called IF Double Difference) for the 29th of June 2005, satellite pair 27-08 and baseline BRUS-GILL (4 km): as can be seen from Eq. (3.4), $\Phi_{AB,IF}^{ij}$ should remain close to a constant value in the absence of residual tropospheric error (T_{AB}^{ij}).

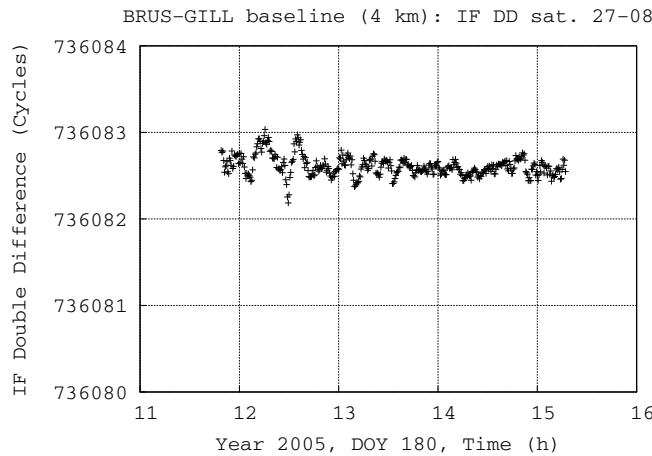


Figure 14: IF Double Difference of BRUS-GILL baseline the 29th June 2005 (DOY 180).

We see clearly the variability induced by the troposphere on the Ionosphere-Free Double Difference observable $\Phi_{AB,IF}^{ij}$ (IF Double Difference) time-series presented figure 14 mainly between 12H UTC and 13H UTC.

3.4.2 Process to determine atmospheric index of activity

Our RTK-architecture requires the resolution of ambiguities, but all the possible couples of satellites are not considered. During a studied Day Of Year (DOY) reference satellites are chosen to form Double Difference (DD) to maximize the time period when the couple is visible by the two stations considered. Nevertheless, the atmospheric scan by these couples of satellites is sufficient to estimate a representative activity index. Considering NAMR-OLLN baseline for DOY 180 of 2005 (couple of satellites 10-21) and BRUS-BERT baseline DOY 365 of 2006 (couple of satellites 16-19), we present in figure 15 the **Ionosphere-Free (IF) Double Difference time-series** (observable of phase $\Phi_{AB,IF}^{ij}$ of Eq. 3.4) for these two baselines (called IF DD plot with crosses):

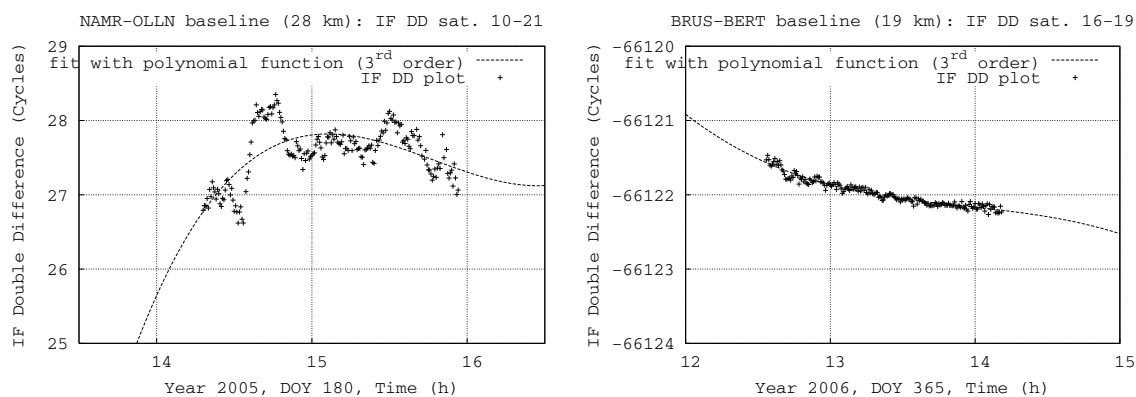


Figure 15: IF Double Difference of NAMR-OLLN baseline the 29th June 2005 event (DOY 180) on the left, BRUS-BERT baseline on the right (no meteorological event 31 December 2006, DOY 365). Fits of DD time-series with polynomial functions of the 3rd order are presented.

Specifically for the tropospheric activity, the impact on DD depends on the elevation of considered satellites. In order to display only the influence of small-scale structures on DD time-series, we assess fits of IF Double Difference time-series with polynomial functions of the 3rd order (dashed line figure 15) and consider **biases between IF DD and their respective fits**, called IF DD Residuals figure 16.

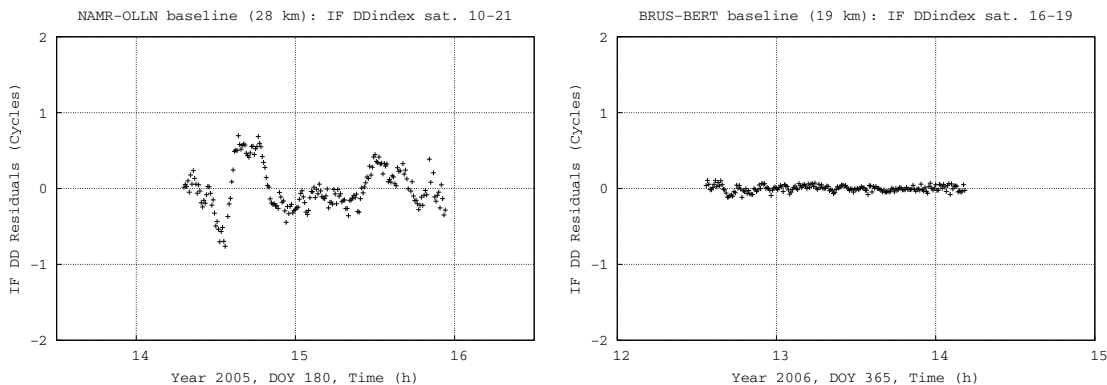


Figure 16: IF DD Residuals time-series of NAMR-OLLN baseline the 29th June 2005 event (left), BRUS-BERT baseline on the right (no meteorological event 31 December 2006).

Bias to the fit removes elevation effects (see figures 15 and 16) and allows to identify the presence of small scale structures.

Small-scale structures are clearly identified for NAMR-OLLN baseline the 29th June 2005 (figure 16 between 14H and 15H UTC). To obtain IF DD Index of the tropospheric activity presented figure 17, **we convert absolute values of IF DD Residuals (in cycles) to centimeters** (multiplying by the L_1 wave length: 19.029 cm).

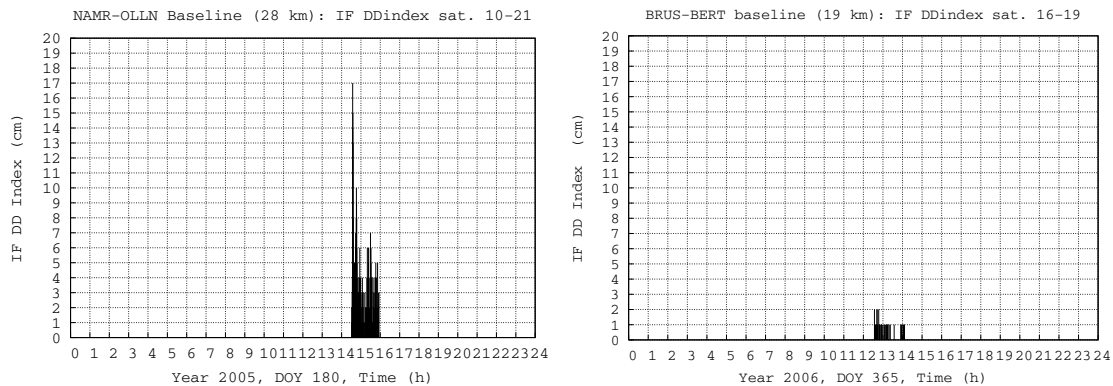


Figure 17: IF DD Index of tropospheric activity of NAMR-OLLN baseline the 29th June 2005 event (left), BRUS-BERT baseline on right (no meteorological event 31 December 2006).

According to radar imaging of rain rate (Fig. 19), the tropospheric small-scale activity around *Namur* (NAMR and OLLN stations) during DOY 180 of 2005 can be easily observed between 14H UTC and 15H UTC. No tropospheric activity is present around *Brussels* (station BRUS) DOY 365 of 2006 at 13H15 UTC on radar imaging figure 20.

Considering all the couples of satellites for a selected baseline and all the available phase measurements, we can show **the daily tropospheric activity** (superposition of all the IF DD Index *i. e.* for all the available couples of satellites) in Fig. 18 and 19.

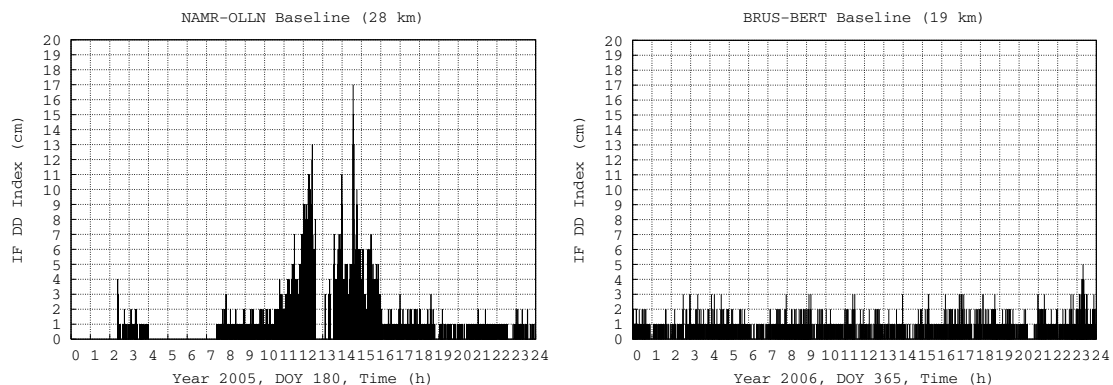


Figure 18: daily IF DD tropospheric index of activity of NAMR-OLLN baseline the 29th June 2005 event, and of BRUS-BERT baseline (no meteorological event 31 December 2005).

No data are available for OLLN station between 0H UTC and 2H30 UTC and for NAMR station between 4H UTC and 7H30 UTC and between 12H40 UTC and 13H30 UTC. This explains the gaps in Fig. 18.

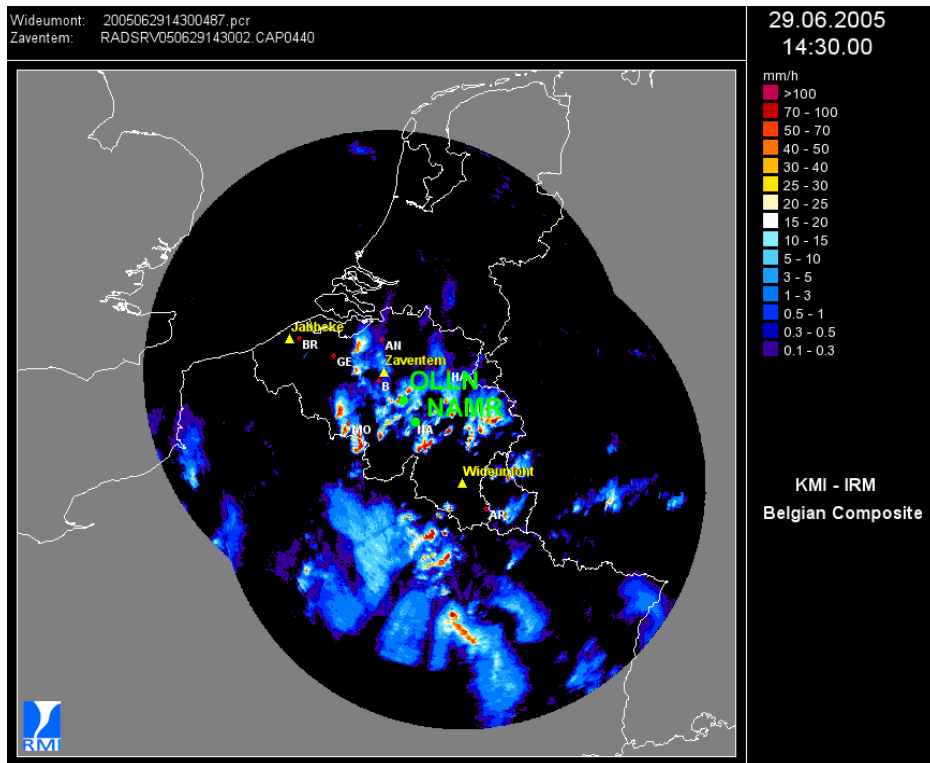


Figure 19: radar imaging the 29th June 2005 at 14H30 UTC.

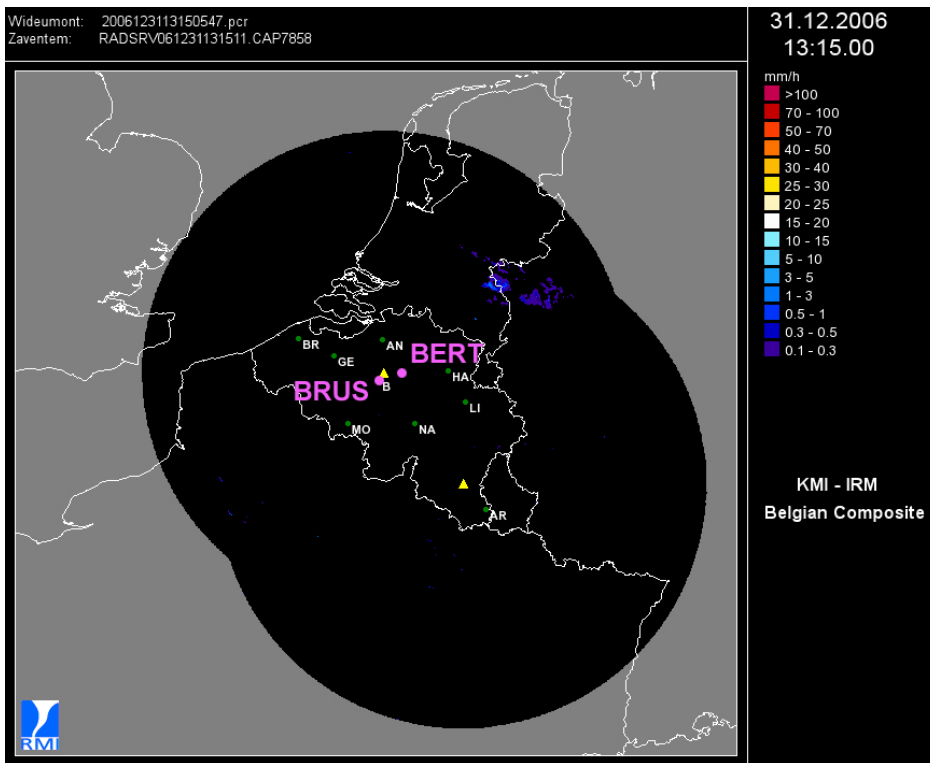


Figure 20: radar imaging 31 December 2006 at 13H15 UTC.

Considering every baseline in the BDN, **IF DD Index imaging** can be shown (Fig. 21). In this imaging, geometric segments (each one corresponding to a baseline) are characterized by a value which represents the largest IF DD Index value among all the IF DD Index values for all couples observed at a given time (14H30 UTC and 13H15 UTC for the two cases presented in figure 21).

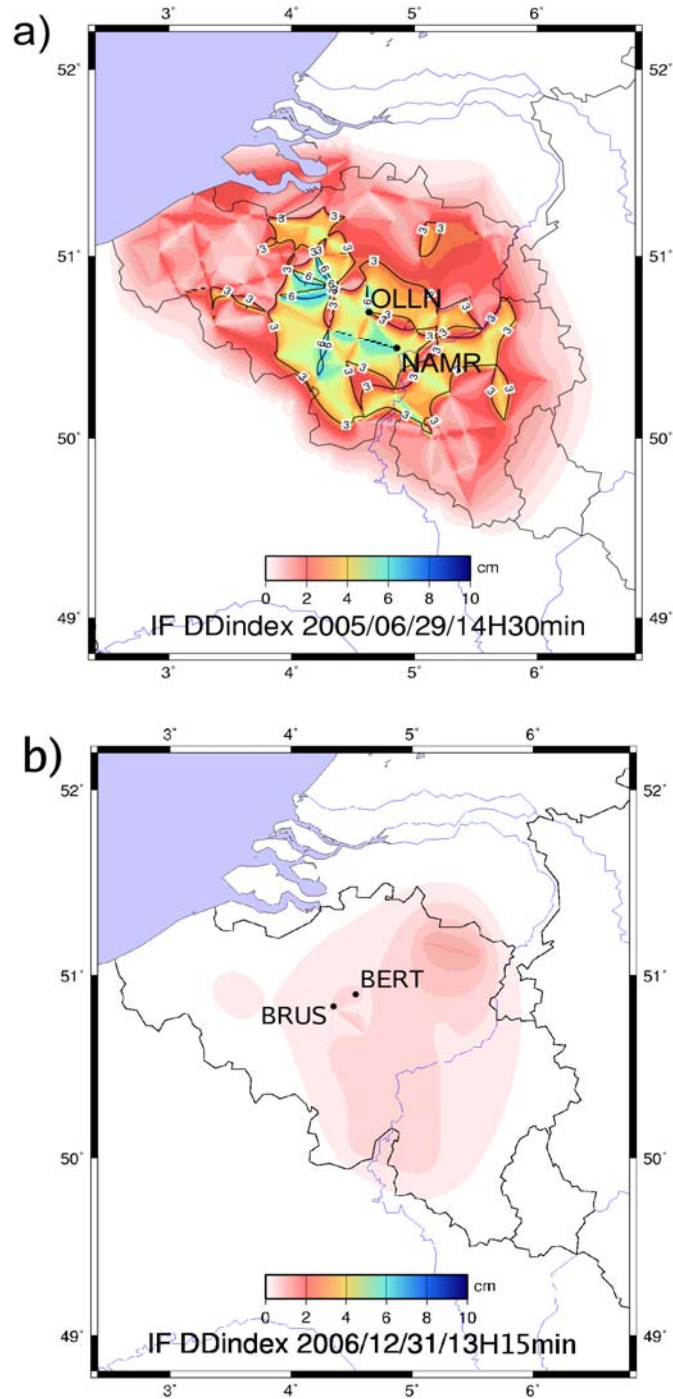


Figure 21: imaging of maximal IF DD Index detected in our RTK-architecture,
a) 29 June 2005 at 14H30 UTC; b) 31 December 2006 at 13H15 UTC.

White areas presented figure 21 show that no data are available.

For DOY 365 of 2006, increased tropospheric activity is observed between 23H UTC and 24H UTC (see daily IF DD Index on the right of figure 18 and on figure 22).

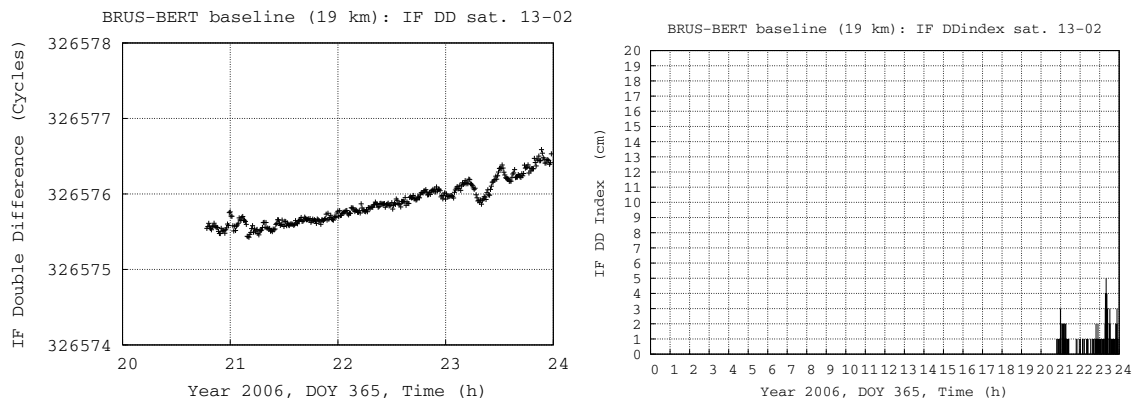


Figure 22: IF Double Difference (expressed in cycles) and IF DD Index (expressed in cm) for BRUS-BERT baseline the 31st December 2006 (satellites 13 and 02).

In practice, radar imaging of precipitations (Fig. 23) shows that tropospheric activity was present around BRUS and BERT stations at 23H20 the 31st December 2006.

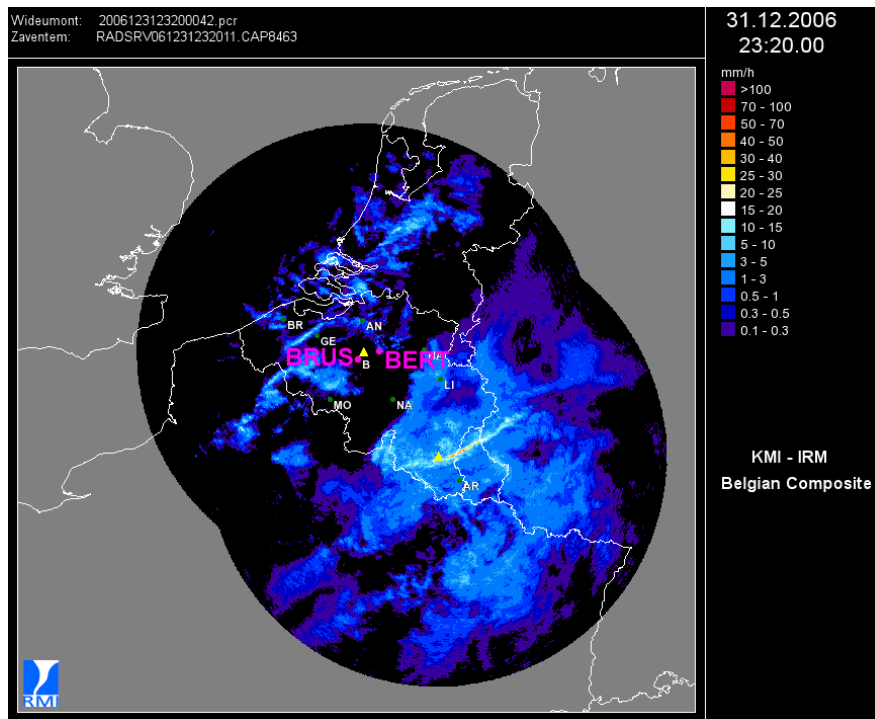


Figure 23: radar imaging of precipitations (31 December 2006 at 23H20 UTC).

For DOY 180 of 2005 (between 11H UTC and 16H UTC), **high index of troposphere activity** (larger than 10 cm) are induced by **important density of water vapour and hydrometeors** close to NAMR and OLLN stations. For DOY 365 of 2006 (at 23H20 UTC), hydrometeors are more discrete and it is essentially the water vapour close to BRUS and BERT stations which contributes to the tropospheric activity (around 5 cm).

3.5 Evaluation of the different candidates

3.5.1 Event of the 29th June 2005

Considering the rainfall event of the 29th June 2005 (see 1h radar precipitation accumulation figure 24 which describes the tropospheric activity of this day), we present the different interest of three GNSS candidates to detect tropospheric structures which influence RTK accuracy: ZTD, horizontal gradients of delays, and the IF DD Index.

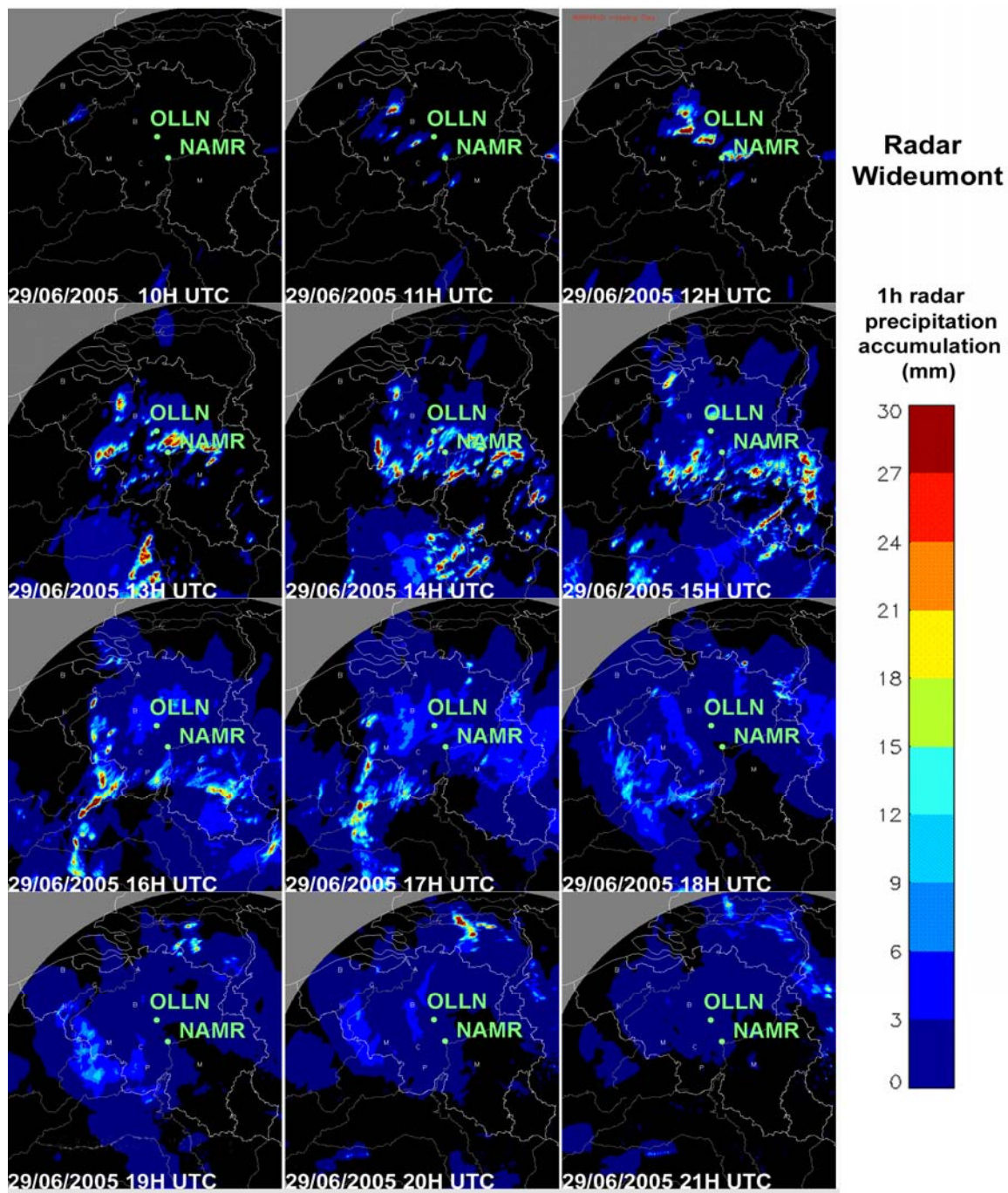


Figure 24: 1h radar precipitation accumulation (29/06/2005).

We can see on radar precipitations (Fig. 24 and 26) that tropospheric structures with a high level of activity fly over OLLN station between 12H30 and 13H UTC. According to ZTD imaging of the BDN (Fig. 25a) and Baseline index estimated from ZTD biases (Fig. 10), a weak horizontal variation of ZTD is observed around OLLN station. Tropospheric small-scale structures are not shown by ZTD imaging.

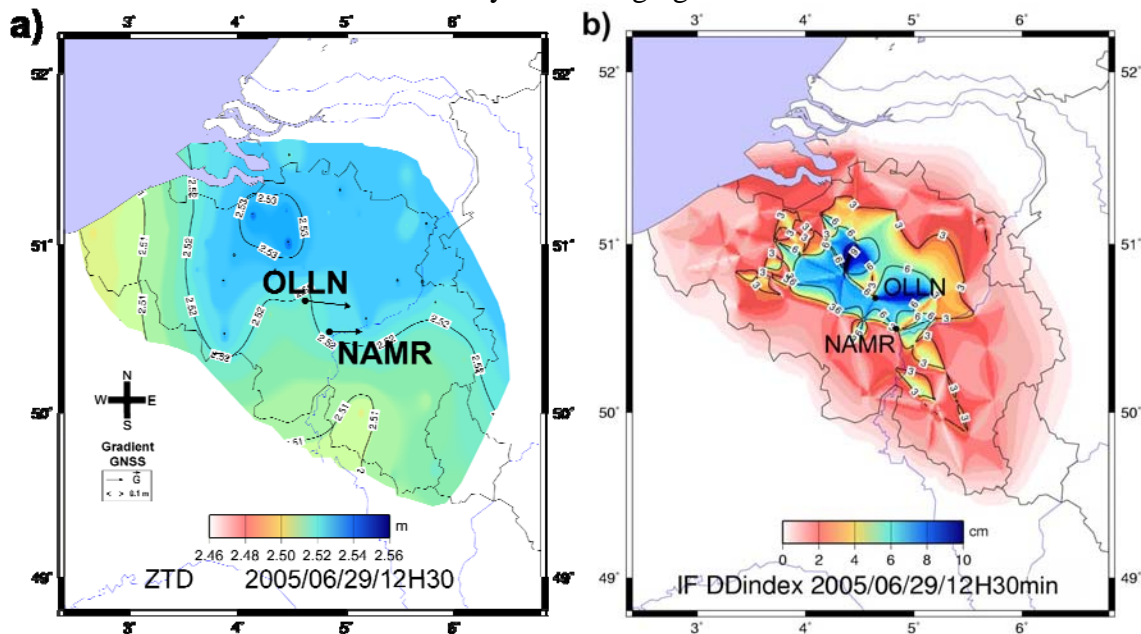


Figure 25: a) GNSS horizontal gradients of delays superposed to ZTD imaging, b) IF DD Index imaging the 29th June 2005 at 12H30 UTC.

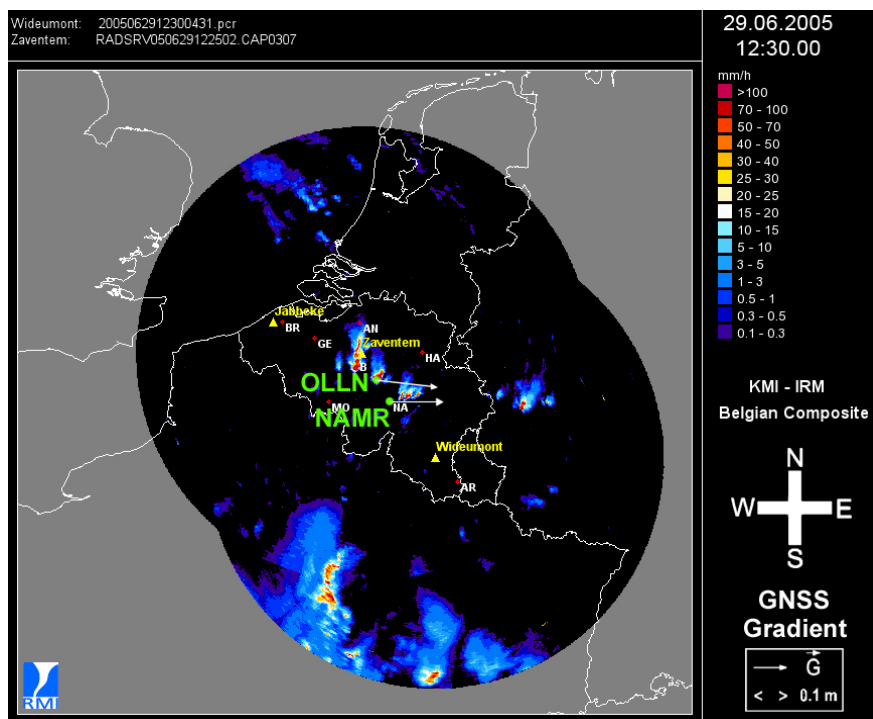


Figure 26: GNSS horizontal gradients of delays (GAMIT software) superposed to radar imaging of precipitations the 29th June 2005 at 12H30 UTC.

Nevertheless strong horizontal gradients \vec{G} from geodetic software (about 0.2 m at 10° of elevation) are observed eastside of OLLN and NAMR stations (see figure 25a and 26) what allows to detect tropospheric structures. However the rainfall cell present over OLLN station does not appear with ZTD imaging due to the time and space average. Horizontal gradients of delays \vec{G} points to a direction where the local anisotropy is maximal, but these gradients represent a time and space average which at a given time (*i. e.* 12H30 UTC) do not show exactly the location of small-scale structures (in the north-east direction of OLLN station).

According to radar imaging (Fig. 26) important precipitations (larger than 100 mm/h) which took place over and north-east of OLLN station at 12H30 UTC the 29th June 2005 show clearly the location of strong tropospheric activity. The maximal humidity and existence of hydrometeors induces a strong perturbation of atmospheric refractivity [Brenot *et al.*, 2006]. Perturbation of refractivity can clearly explain sudden variability of tropospheric error T_A^i measured by station A for a signal emitted by satellite i . The following expression presents the relation between tropospheric error T_A^i (*i. e.* usually called STD) with neutral atmosphere refractivity (R):

$$T_A^i = 10^{-6} \int R ds \quad (3.6)$$

ds is a infinitesimal distance on the receiver A to satellite i path.

The tropospheric error T_{AB}^{ij} , which induces the perturbation of phase observable $\Phi_{AB,IF}^{ij}$ defined Eq. 3.4 (double difference of the ionosphere-free combination corrected for geometric distances), has the following expression:

$$T_{AB}^{ij} = (T_A^i - T_B^i) - (T_A^j - T_B^j) \quad (3.7)$$

Sudden perturbations of tropospheric errors (T_A^i, T_B^i, T_A^j and T_B^j) by small-scale structures induce directly perturbations of T_{AB}^{ij} and $\Phi_{AB,IF}^{ij}$. Considering two epochs of measurements (epoch t_0 and epoch $t_0 + \Delta t$, for example $\Delta t = 5$ min), figure 27 illustrates direct impact of the occurrence of a small-scale tropospheric structure on phase measurements (observables $\Phi_{AB,IF}^{ij}$ and T_{AB}^{ij}).

Contrary to ZTD imaging and horizontal gradients (\vec{G}) measurements by geodetic software, the IF DD Index imaging (Fig. 25b) is clearly sensitive to sudden perturbation of tropospheric activity. In other words, the IF DD Index is sensitive to the occurrence of tropospheric small-scale structures which locally affect couples of satellites considered in our RTK-architecture at a given epoch what is not the case of ZTD's and horizontal gradients which are averaged in space and time. IF DD Index shows strong perturbations of GNSS signal propagation induced by the troposphere around OLLN station between 12H UTC and 13H UTC (see IF Double Difference time-series figures 28 and 29 for the couples of satellites 04-23 and 04-02). The presence of water vapour and hydrometeors above OLLN and on the north-east side affects Double-Difference observations for OLLN-NAMR baseline the 29th June 2005 (DOY 180).

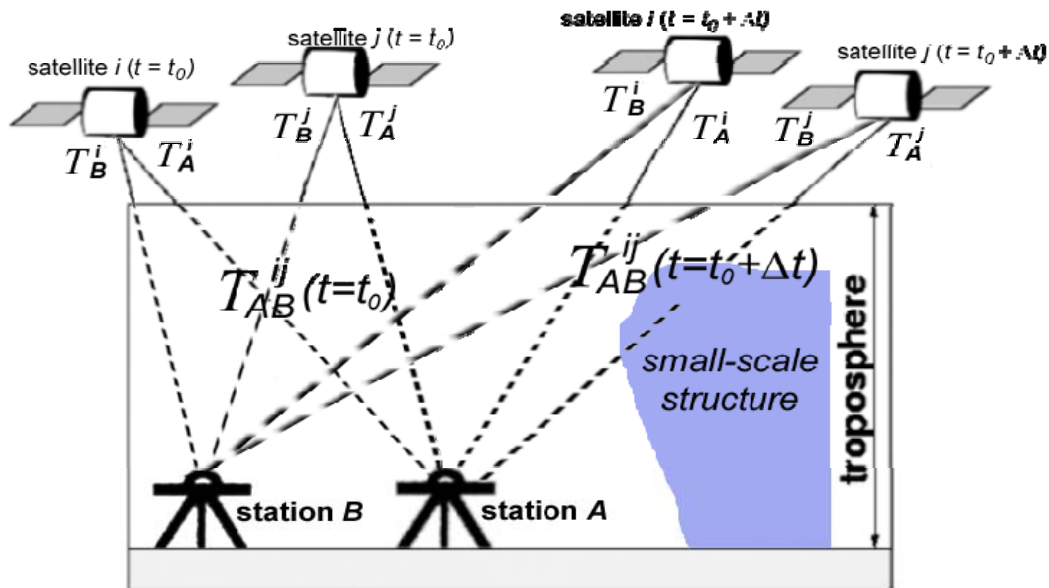


Figure 27: perturbation of T_{AB}^{ij} induced by a small-scale tropospheric structure for two epochs of measurements (epoch $t = t_0$ and epoch $t = t_0 + \Delta t$).

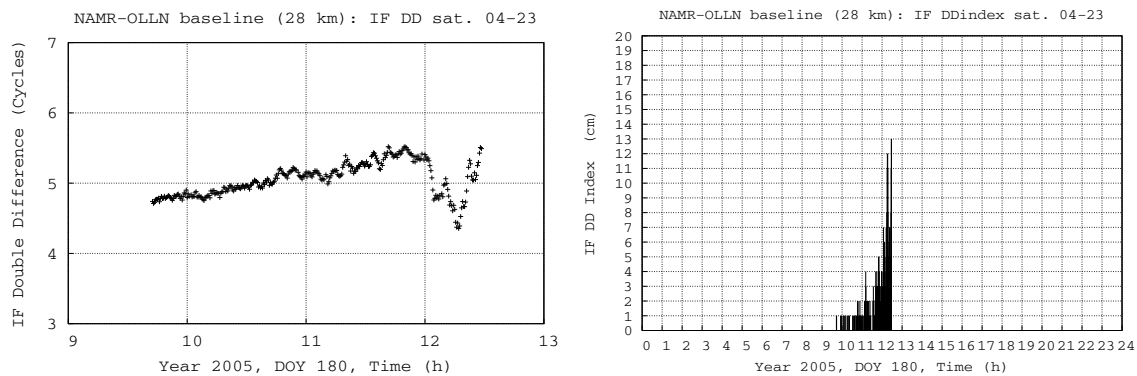


Figure 28: IF Double Difference time-series and IF DD tropospheric index of activity of NAMR-OLLN baseline during the 29th June 2005 event (couple of satellites 04-23).

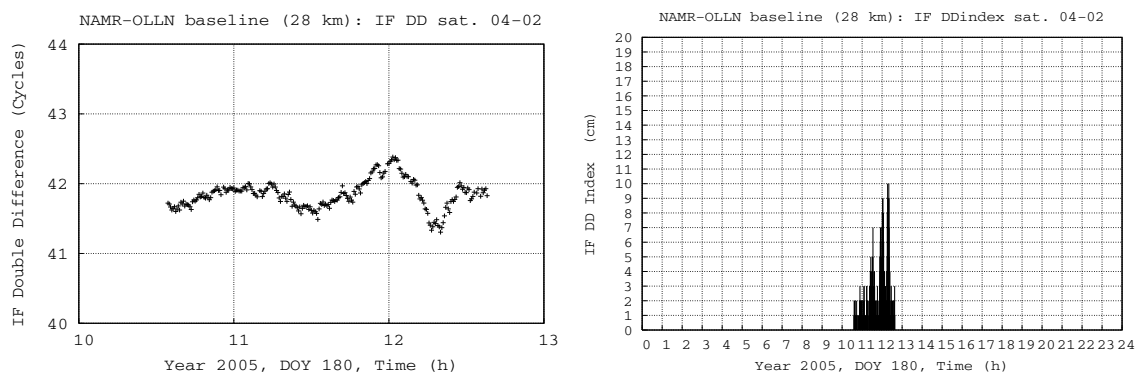


Figure 29: IF Double Difference and tropospheric index of activity of NAMR-OLLN baseline during the 29th June 2005 event (couple of satellites 04-02).

The tropospheric activity detected by IF DD Index (figures 18 and 25b) is validated by radar imaging (Fig. 24 and 26).

3.5.2 Event of the 8th June 2003

Considering the event of the 8th June 2003, we show the added value in terms of time resolution of IF DD Index compared to ZTD observations. The 8th June 2003, a large line of hailstone has travelled from south-west to north-east over Belgium (from 7H to 11H UTC). At 10H UTC storm cells fly close to MEEU and BREE stations, as shown by radar imaging figure 30. At 16H UTC, maximal humidity conditions were present. Creation of several convective systems has taken place around MEEU and BREE stations (see radar Fig. 31).

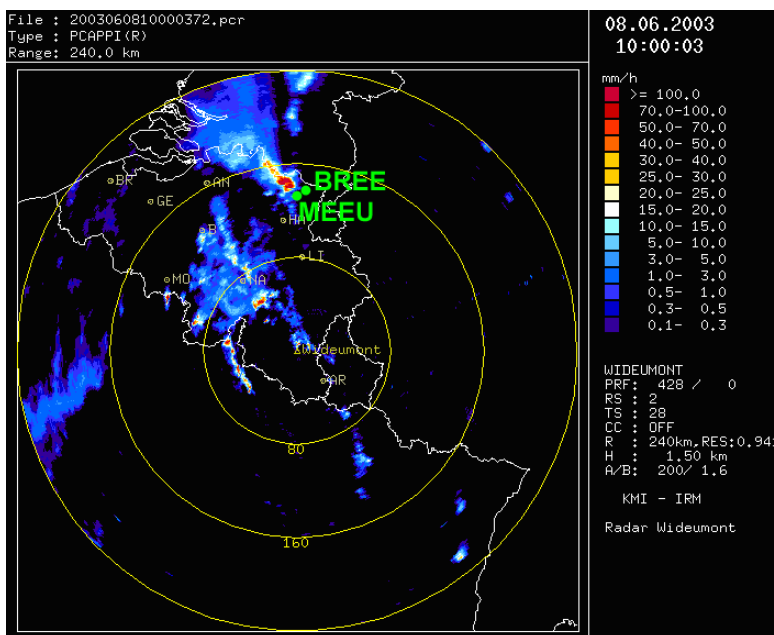


Figure 30: radar imaging of precipitations the 8th June 2003 at 10H UTC.

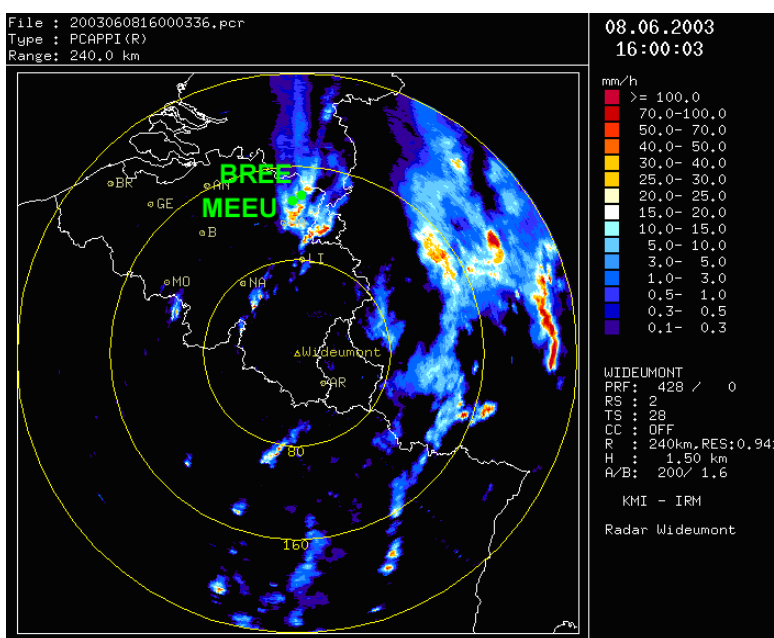


Figure 31: radar imaging of precipitations the 8th June 2003 at 16H UTC.

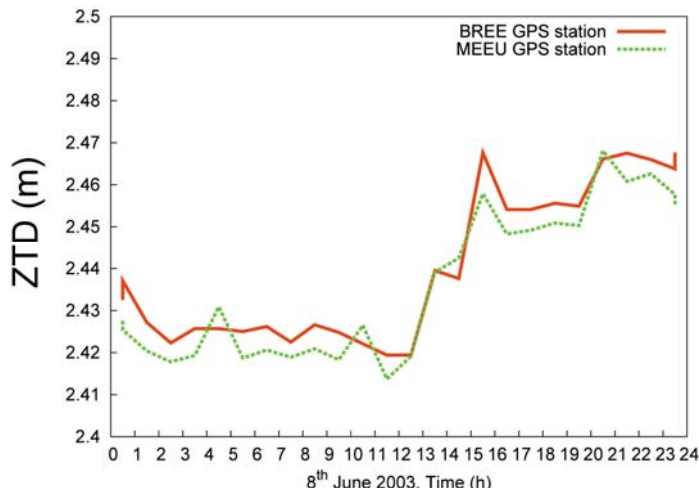


Figure 32: ZTD for BREE and MEEU stations the 8th June 2003.

The distance between BREE and MEEU station is about 7 km, for respective altitudes of 89 m and 119 m. Corrected ZTD's at the sea level are shown figure 32. ZTD's have been calculated every hour. The time and space averages of ZTD's do not show the passage of the hailstone structure close to these GPS stations, but the formation of Mesoscale Convective Systems (MCS) above these stations is observed by ZTD's (loading 3 hours before 16H UTC and dump at 16H UTC).

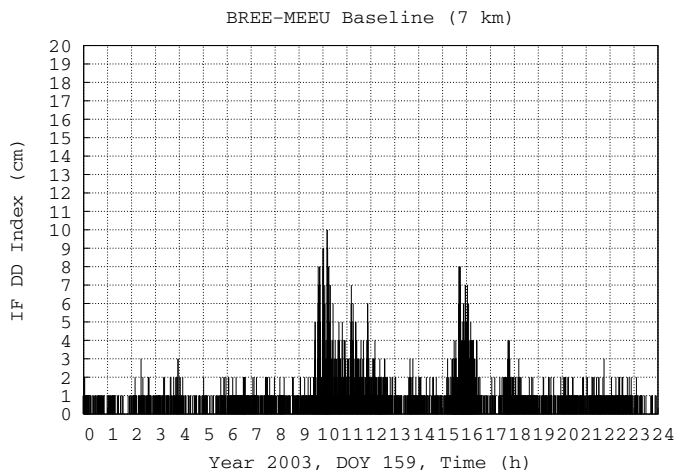


Figure 33: daily IF DD Index of tropospheric activity of BREE-MEEU baseline the 8th June 2003.

On the other hand, a high activity is detected by IF DD Index at 10H UTC and 16H UTC (even on such a short baseline) when radar imaging shows tropospheric activity. The daily IF DD Index (Fig. 33) is validated by radar imaging (Fig. 30 and 31).

Considering the passage of a very small-scale structure (persistent hailstone structure), we can see the advantage of IF DD Index which has a higher spatial and temporal resolution than ZTD measurements. The existence and the creation of MCS are clearly detected by ZTD, but the quick passage of small-scale structures and the associated tropospheric activity are smoothed by time and space average tropospheric parameters computed from geodetic software.

3.6 Conclusion on the different candidates

Our study of different meteorological situations in Belgium and France, in particular the flash-flood event of south-eastern France in September 2002 [Brenot *et al.*, 2006], have shown that ZTD measurements are representative of the mesoscale tropospheric activity above considered stations. Nevertheless, ZTD's are obtained from a time and space average of tropospheric activity above GNSS sites. The 8th June 2003 event, characterized by the passage of persistent small-scale hailstone structures, has shown that ZTD measurements do not detect tropospheric activity (see figure 32), whereas IF DD Index, figure 33, clearly identifies these structures and the tropospheric activity associated (validated by radar imaging of precipitations) during the morning of the 8th June 2003.

Horizontal gradients of delay are the most relevant GNSS measurements from the meteorological point of view (see figure 8 and the detection of MCS). But these measurements are also the result of time and space averages. For this reason, like for ZTD measurements, sudden changes of the tropospheric activity are smoothed. We can see for the 29th June 2005 rainfall event in Belgium that, very small-scale convective systems have moved quickly around OLLN station. For this reason, the tropospheric anisotropy (induced by water vapour and hydrometeors) detected by horizontal gradients from geodetic software does not precisely localize small-scale tropospheric structures (see figure 26). On the other hand, IF DD Index shows a higher spatial and temporal resolution referring to the quickness of the tropospheric activity during the 29th June 2005 rainfall event.

From the study performed in this paragraph, we can draw the following conclusions:

- Low time and space resolution inherent to the computation of GNSS path delays (ZTD and horizontal gradients) is a clear limitation for the detection of small-scale tropospheric activity. These indicators are not able to detect the sudden occurrence of very small-scale structures which can affect RTK.
- As expected, the availability of BDN data clearly improves the resolution we can obtain in small-scale structures detection (notably with ZTD biases according to a baseline, called ZTD baseline index).
- IF DD Index shows a higher spatial and temporal resolution than the other candidates, for this reason we will afterwards focus on this indicator to detect small-scale tropospheric activity taking affecting RTK.

4. VALIDATION OF THE IF DD INDEX

We have seen the limitation of ZTD observations to detect very localized small-scale structures. In practice, the double differences are the basic observables used in RTK-positioning. The IF DD Index which expresses the tropospheric activity is based on Double Difference of the Ionosphere-Free combination (and the knowledge of BDN stations positions). In the following section ZTD and horizontal gradients measurements, radar imaging of precipitations and rain gauges measurements will be used to validate our IF DD Index. Six cases studies will be considered. After that, considering two baselines of 19 km and 23 km (2 years of data) and one baseline of 7 km (10 years of data), we will show the capability of IF DD Index to detect the presence of tropospheric small-scale structures: other techniques of observations (radar imaging and rain gauges measurements) are used to diagnose the tropospheric activity.

4.1 Case studies

Our methodology has been applied to six case studies which show distinct meteorological events (the case study of the 8th June 2003 has been presented section 3.5).

4.1.1 Event of the 28th July 2006

During this event, tropospheric structures (convective cells) have been characterized by a long line of convergence (low layer) which takes place from *North Sea* nearly up to the French *Massif Central* (consequence of the synoptic conditions, see radar Fig. 34a).

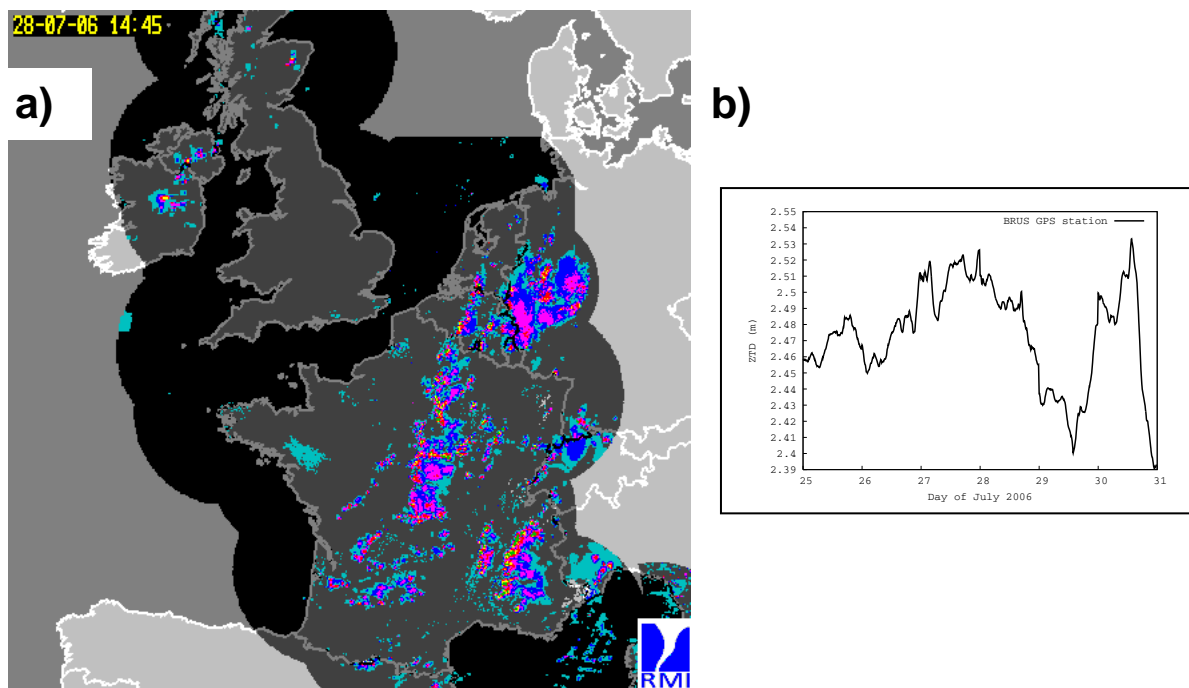


Figure 34: a) European composite radar imaging of precipitations the 28th July 2006 at 14H45 UTC; b) ZTD time-series of BRUS station.

ZTD time-series show that a loading period occurred two days before the heavy rainfall of the 28th July 2006 (Fig. 34b). Precipitations are characterized by the discharge period during the afternoon of the 28th July 2006. For this period, only ZTD's from BRUS are available. Detection of small-scale structures can not be established only with ZTD of BRUS station.

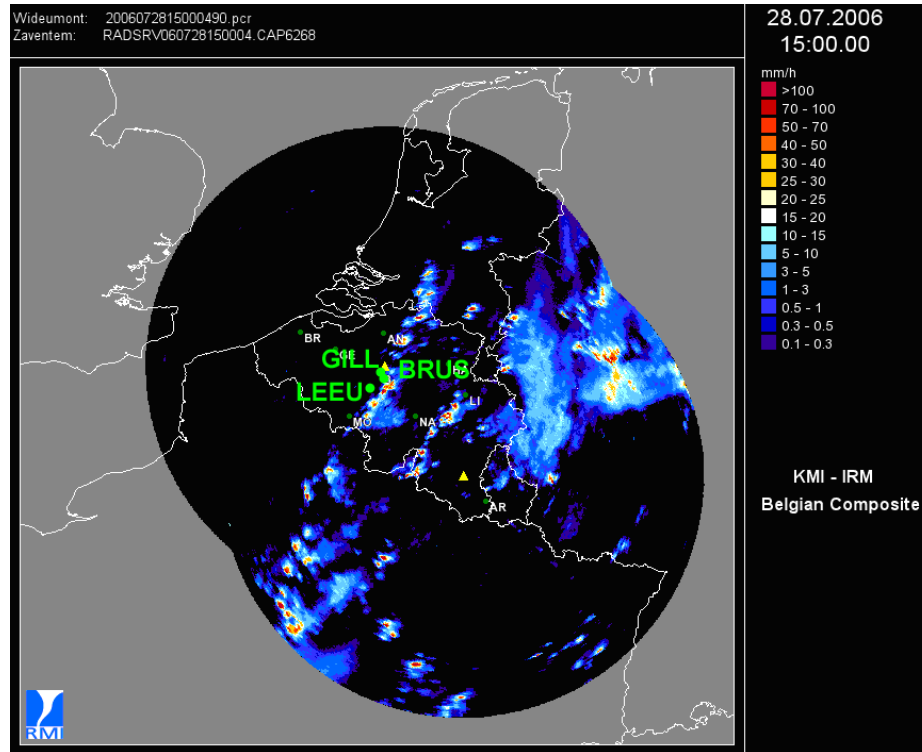


Figure 35: Belgian composite radar imaging of precipitations the 28th July 2006 at 15H UTC.

Small-scale tropospheric structures are detected by IF DD analysis (baselines smaller than 10 km). High levels of activity (larger than 10 cm) are shown on daily IF DD Index of tropospheric activity figure 36.

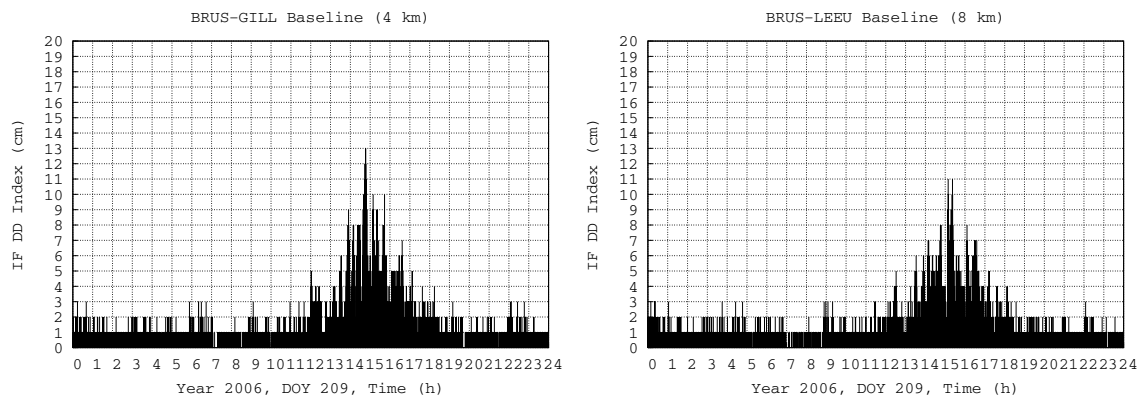


Figure 36: daily IF DD Index of tropospheric activity of BRUS-GILL and BRUS-LEEUE baselines the 28th July 2006.

The daily IF DD Index of BRUS-GILL and BRUS-LEEUE baselines (respectively of 4 km and 8 km), agree with radar imaging at 15H UTC (2006/07/28) presented figure 35.

4.1.2 Tornado of the 1st October 2006



Figure 37: photography of the tornado.

A super-cell can exist during few hours keeping its tropospheric activity. This structure has given specific conditions to permit the formation of such a tornado (see photography figure 37). This super-cell (rainfall from a cumulonimbus) visible on radar imaging close to BRUS and LEEU stations has generated this tornado close to *Brussels* (Fig. 38).

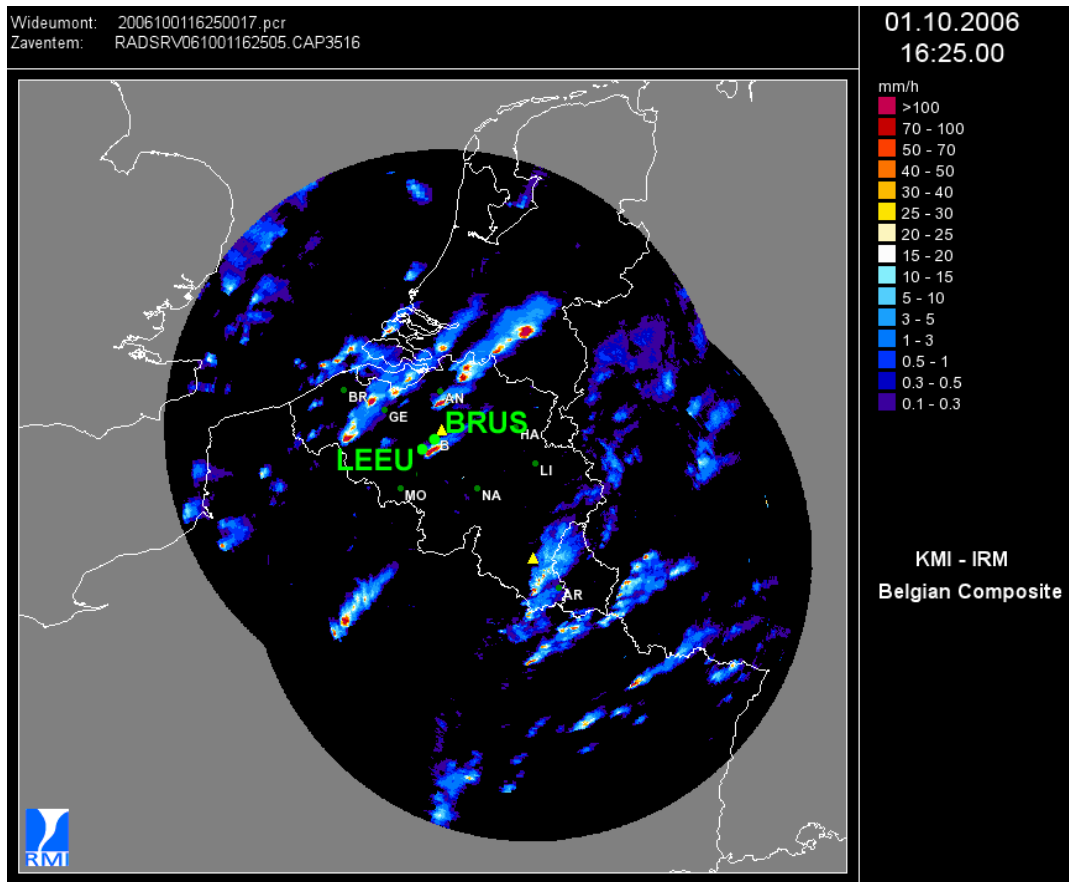


Figure 38: Belgian composite radar imaging the 1st October 2006 at 16H25 UTC.

The passage of the super-cell close to *Brussels* (BRUS station) and *Sint-Pieters-Leeuw* (LEEU station) can clearly be observed by the daily IF DD Index (Fig. 39) of this baseline of 8 km.

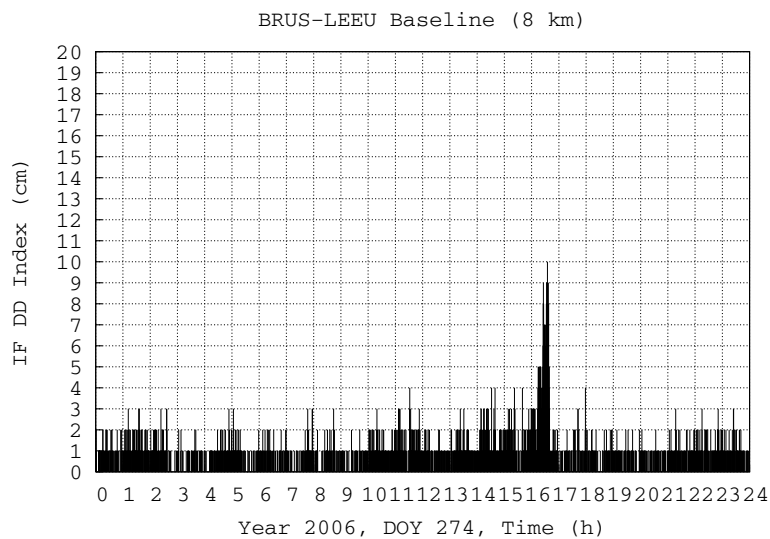


Figure 39: daily IF DD Index of tropospheric activity of BRUS-LEEU baseline 1st October 2006.

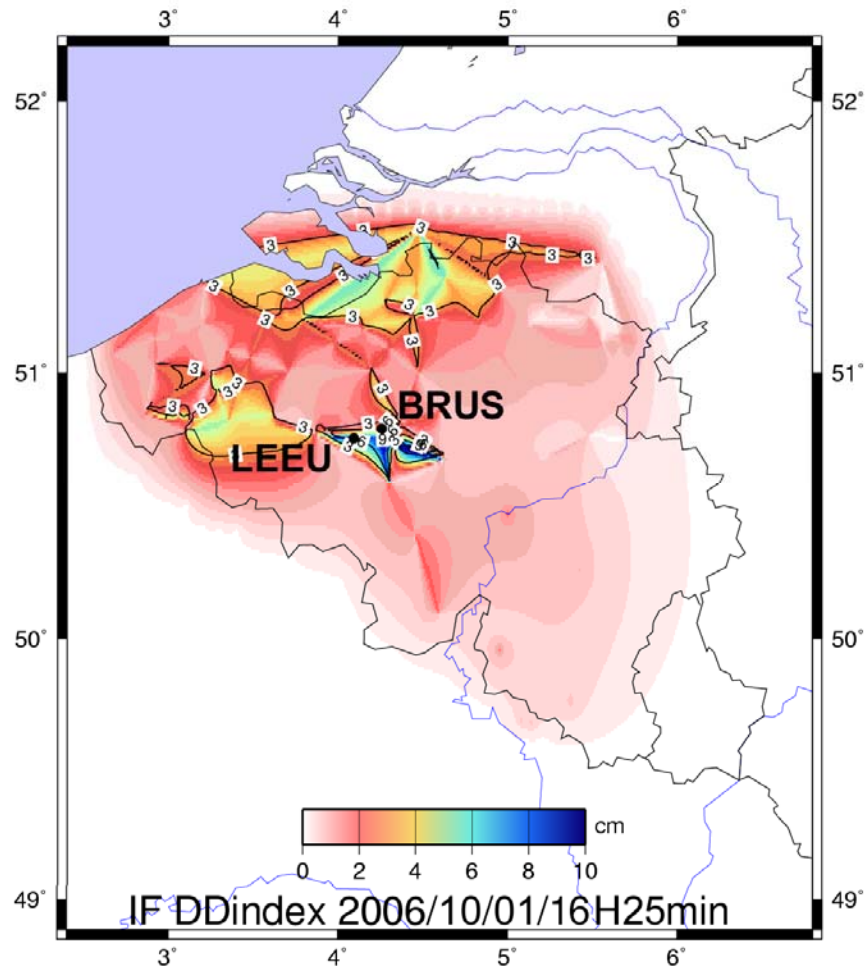


Figure 40: imaging of maximal IF DD Index detected at 16H25 the 1st October 2006.

In Figure 40, the IF DD Index imaging at 16H25 UTC shows high level of activity (larger than 10 cm). Note that isolines of IF DD Index are plotted every 3 level of activity (*i. e.* 3 cm, 6cm, 9cm, 12 cm ...).

On 1st October 2006, tropospheric activity takes place all the day. Operational hail detection products at RMI are derived from the height of the freezing level and from 45 dBZ echotop values provided by single-polarization C-band weather radar [Delobbe and Holleman, 2006]. Figure 41 presents the probability of hail (maximum values during 24h) during the 1st October 2006 event (DOY 274). We can see the passage of the super-cell close to *Brussels*. Other super-cells are also shown. The tropospheric daily IF DD Index detects strong activity DOY 274 for baseline ANTW-KALL. On the other hand a quiet tropospheric activity can be observed for the baseline VOER-TONG (Fig. 42). This analysis is in agreement with Figure 41.

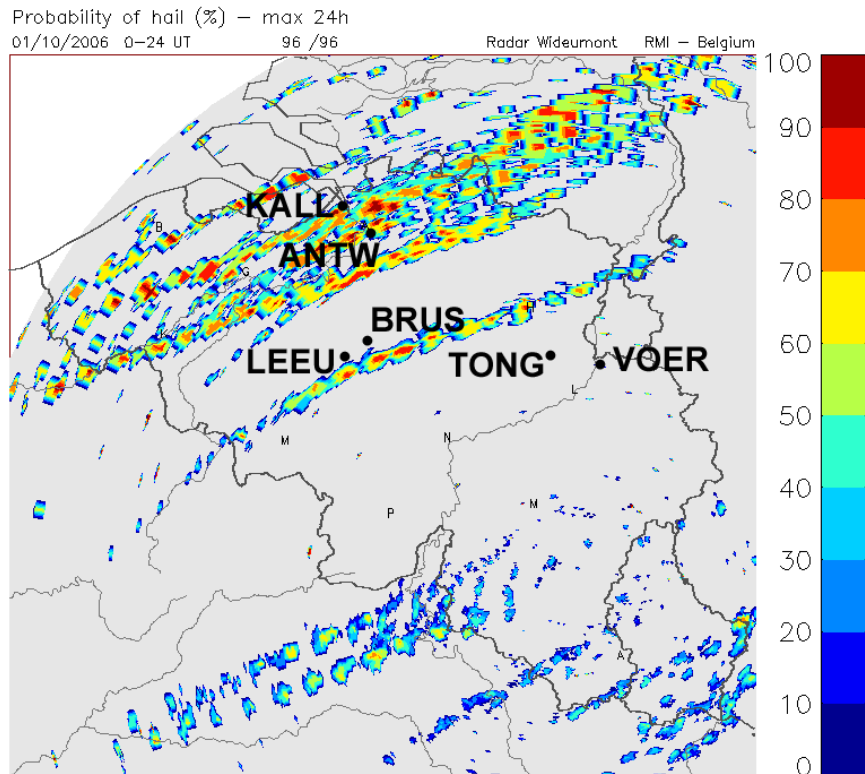


Figure 41: daily probability of hail (POH) the 1st October 2006.

The interest to look at the radar imaging of the Probability Of Hail (POH) is that the possible production of hail requires an important vertical extension characterized by a large layer of water vapour associated with hydrometeors existence.

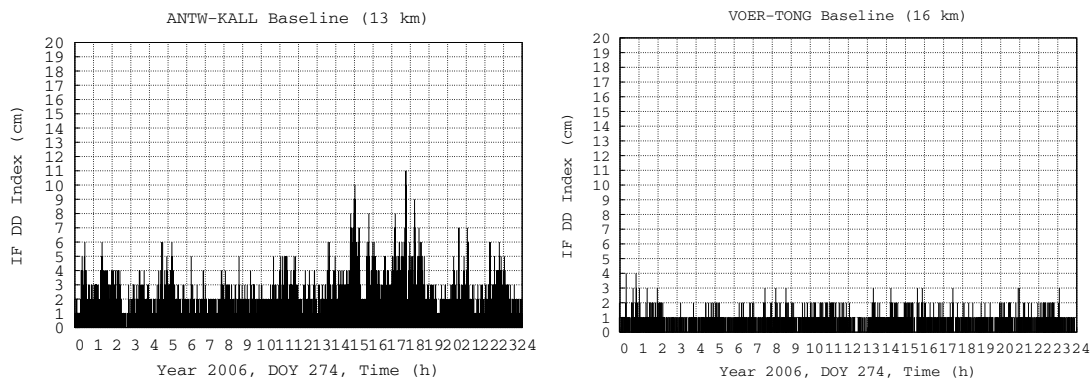


Figure 42: daily IF DD Index of tropospheric activity of ANTW-KALL and VOER-TONG baselines (2006/10/01).

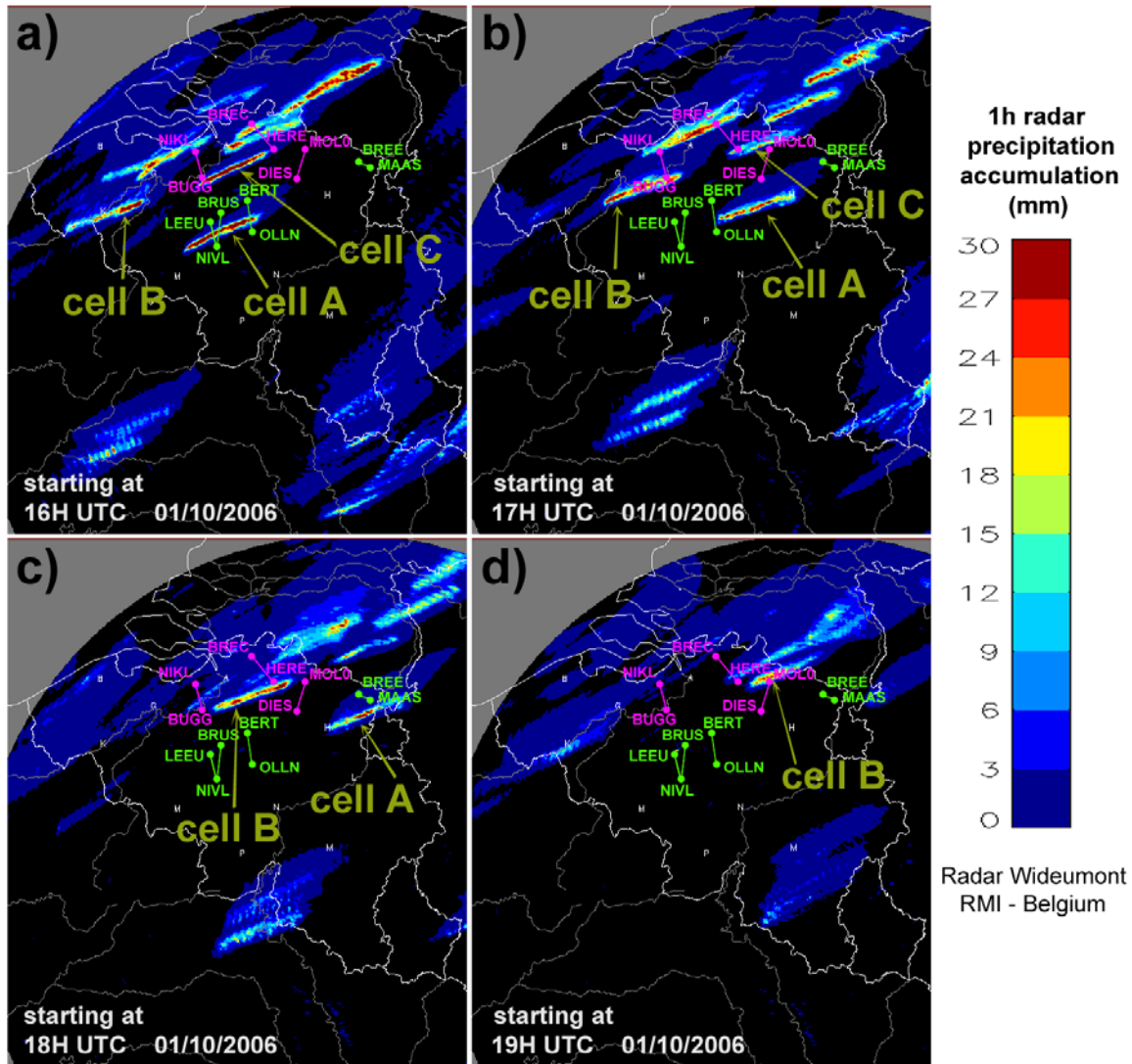


Figure 43: 1h radar precipitation accumulation starting at 16H UTC, 17H UTC, 18H UTC and 19H UTC the 1st October 2006.

We can see on 1h radar precipitation accumulation (Fig. 43) that super-cells have travelled from south-west to north-east. Baselines BUGG-NIKL, BREC-HERE, DIES-MOLO, LEEU-NIVL, BRUS-NIVL, BERT-OLLN and BREE-MAAS are plotted on these radar imaging. For these baselines, IF DD Index tropospheric activities are shown figure 44 and 45.

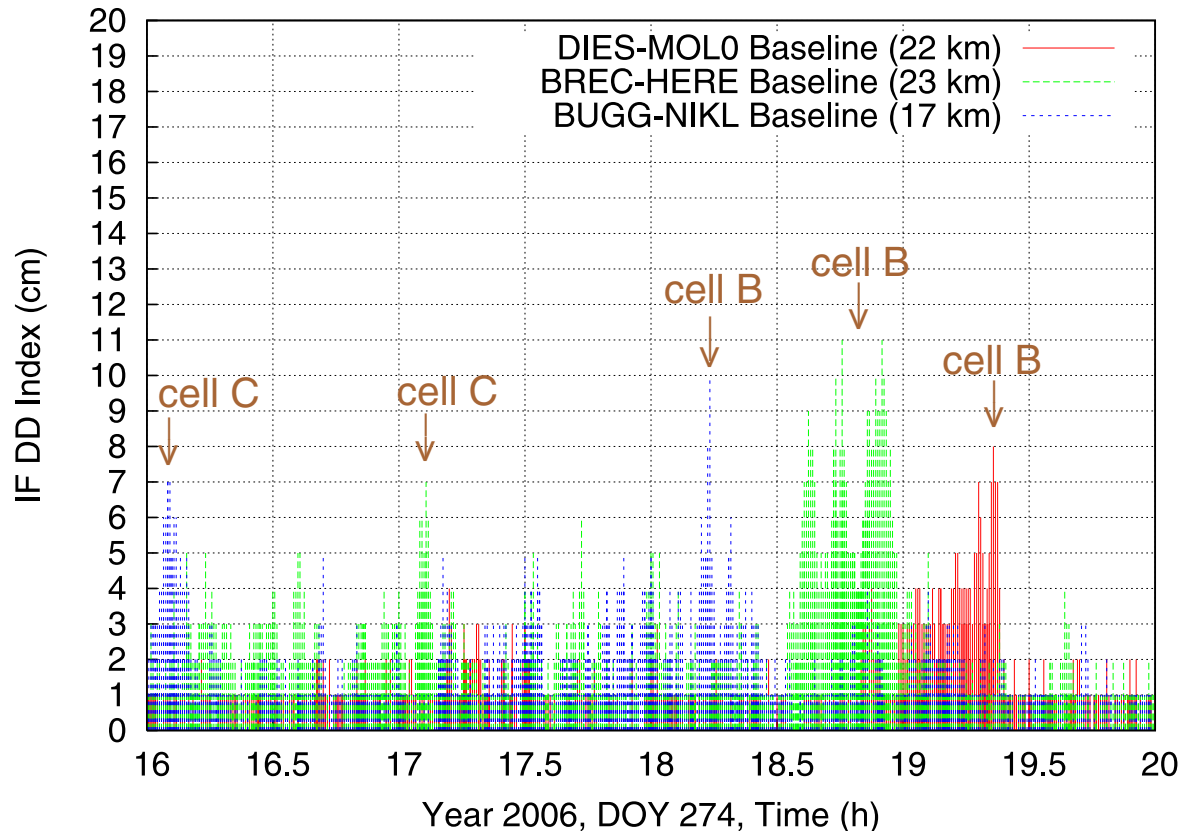


Figure 44: daily IF DD Index of tropospheric activity of BUGG-NIKL, BREC-HERE and DIES-MOLO baselines (2006/10/01).

According to 1h radar precipitation accumulation imaging (Fig. 43), the description of figure 44 is the following: at about 16H UTC, tropospheric activity for baseline BUGG-NIKL (up to 7 cm) is detected when cell C is close to BUGG station (Fig. 43a). This same cell C was close to HERE station at about 17H UTC and induced an IF DD Index up to 7 cm for BREC-HERE baseline. Around 18H UTC the cell B was approaching over BUGG station (*i. e.* figure 43b) and inducing IF DD Index up to 10 cm for BUGG-NIKL baseline. The passage of the cell B can clearly be observed with IF DD Index presented figure 44 between 18H and 19H30 UTC. Around 19H UTC the cell B (Fig. 43c) is located above HERE station (IF DD Index up to 11 cm for BREC-HERE baseline) and at 19H20 UTC (Fig. 43d) above MOL0 station (IF DD Index up to 8 cm for DIES-MOLO baseline).

The contribution of hydrometeors in association with water vapour bubble to strong IF DD Index of tropospheric activity is indisputable. The bubble of water vapour surrounds the rainfall cells with a high vertical extension.

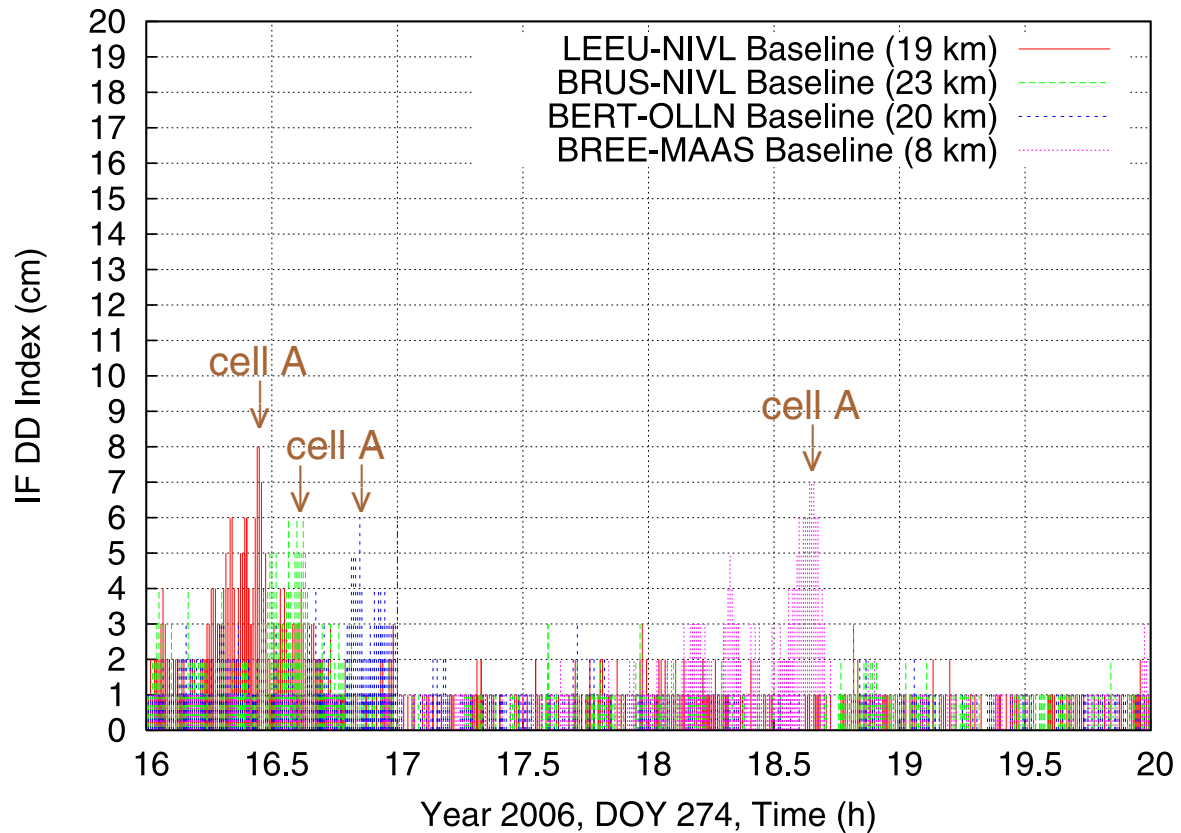


Figure 45: daily IF DD Index of tropospheric activity of LEEU-NIVL, BRUS-NIVL, BERT-OLLN and BREE-MAAS baselines (2006/10/01).

According to 1h radar precipitation accumulation imaging (Fig. 43), the description of figure 45 is the following: at 16H20 UTC, tropospheric activity has taken place around LEEU and NIVL stations (IF DD Index up to 8 cm for baseline LEEU-NIVL). Between 16H30 and 17H UTC the super-cell A has moved from south-west to the east of *Brussels* (successively IF DD Index of 6 cm for BRUS-NIVL and BERT-OLLN baselines). Around 18H40 UTC, the cell A was close to MAAS station and induced IF DD Index up to 7 cm for BREE-MAAS baseline. The passage of the super-cell A is clearly shown from 16H to 19H UTC on IF DD Index figure 45.

4.1.3 Heavy rainfall of the 30th July 2002

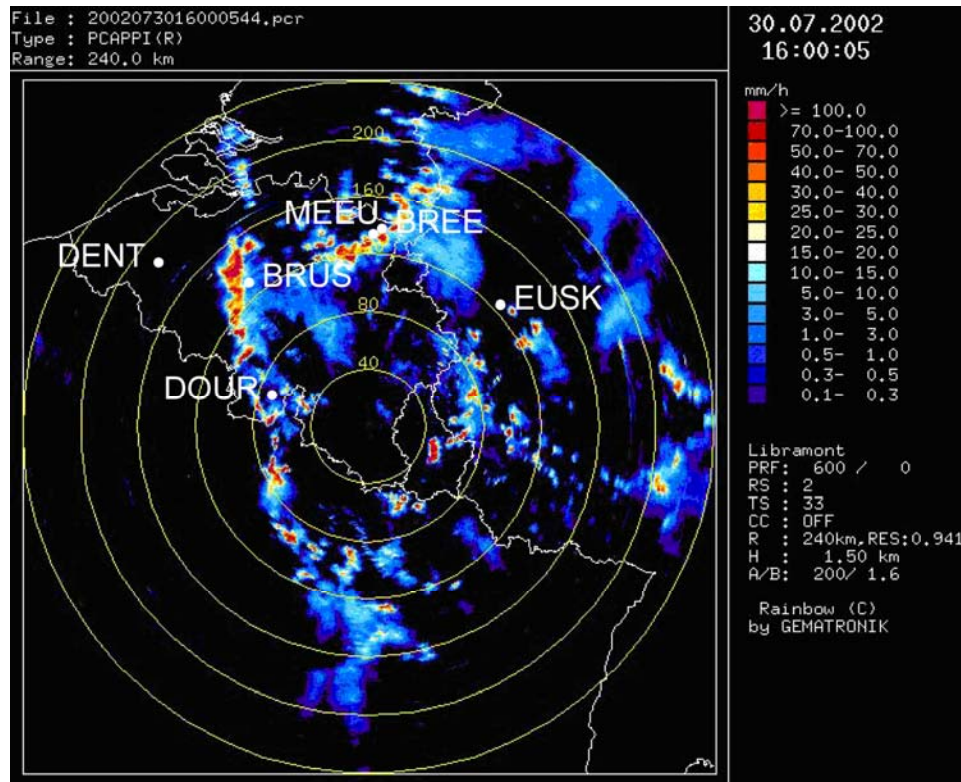


Figure 46: radar imaging of precipitations at 16H UTC the 30th July 2002.

Important accumulations of rainfall (larger than 100 mm/hour) have been observed the 30th July 2002 (DOY 211) by radar imaging (Fig. 46). This event is one of the strongest summer rainfalls which occurred in Belgium this century.

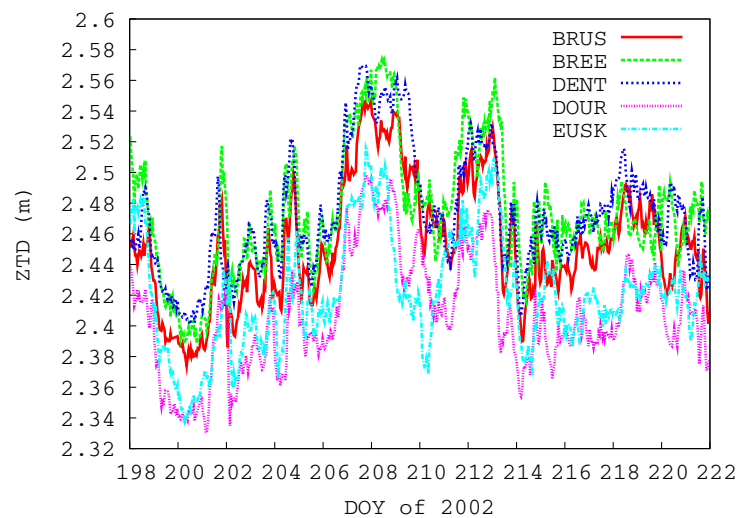


Figure 47: ZTD time-series for BRUS, BREE, DENT, DOUR and EUSK stations from 15th July (DOY 196) to the 10th August 2002 (DOY 222).

In figure 47, the analysis of ZTD time-series of BREE, BRUS, DENT, DOUR and EUSK stations clearly shows an important loading of water vapour all over Belgium the 3 days before this event (from DOY 207 to 210). The extreme nature of this strong event is characterized by a radical drop of ZTD the 30th July 2002 (DOY 211) when rainfalls are observed (ZTD decrease about 10 cm). Two loading periods (207-210 and 212-214 DOY periods) of water vapour surround precipitations of DOY 211.

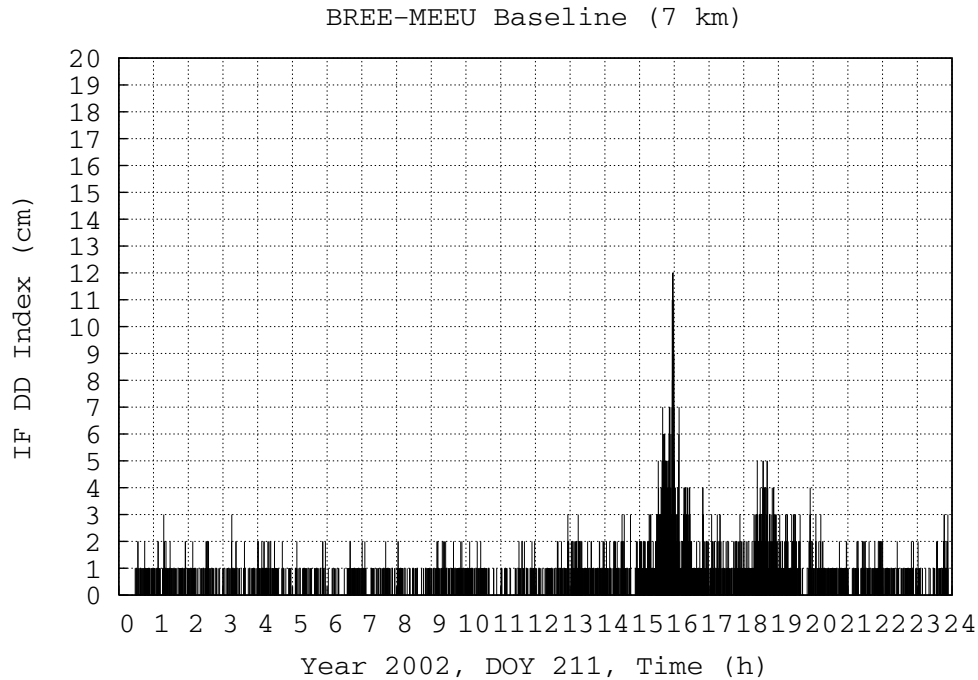


Figure 48: daily IF DD Index of tropospheric activity of BREE-MEEU baseline the 30th July 2006 (DOY 211).

The presence of convective systems close to BREE and MEEU stations (baseline of 7 km) at 16H UTC the 30th July 2002 has caused high level of tropospheric activity detected by daily IF DD Index figure 48 (up to 12 cm). Unfortunately, no BDN were available in 2002.

4.1.4 Rainfall of the 29th June 2005

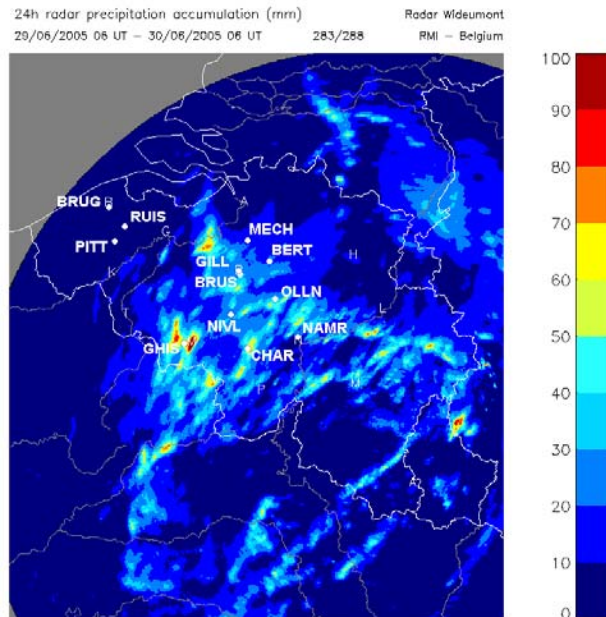


Figure 49: 24h radar precipitation accumulation the 29th June 2005.

This event is characterized by the formation of small-scale stormy cells which have travelled above different GNSS stations over Belgium. Figure 49 presents the tropospheric activity (24h radar precipitation accumulation). A strong tropospheric activity is observed around GHIS station on the 29th June 2005. A high tropospheric activity has also been identified around BRUS and OLLN stations on radar imaging (figure 52) and on IF DD Index imaging (up to 15 cm between for BRUS-OLLN baseline figure 51).

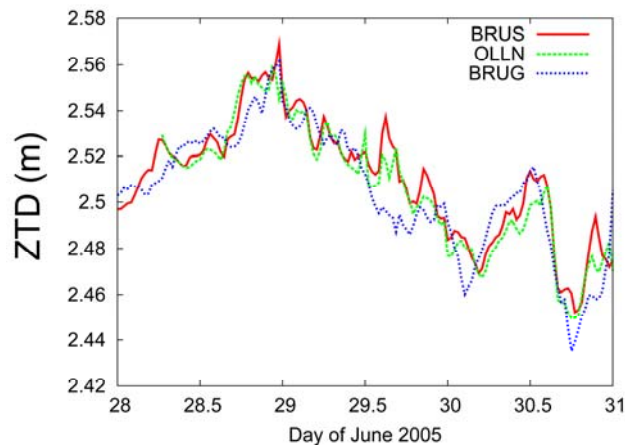


Figure 50: ZTD times series for BRUS, OLLN and BRUG stations (from the 28th June to the 31st June 2005).

Considering ZTD time-series, we can see that tropospheric activity has taken place at BRUS and OLLN stations during the afternoon of the 29th June 2005 (Fig. 50). On the other hand a low tropospheric activity has been observed around BRUG station (see ZTD figure 50 and daily IF DD Index for baselines BRUG-RUIS and BRUG-PITT figure 51).

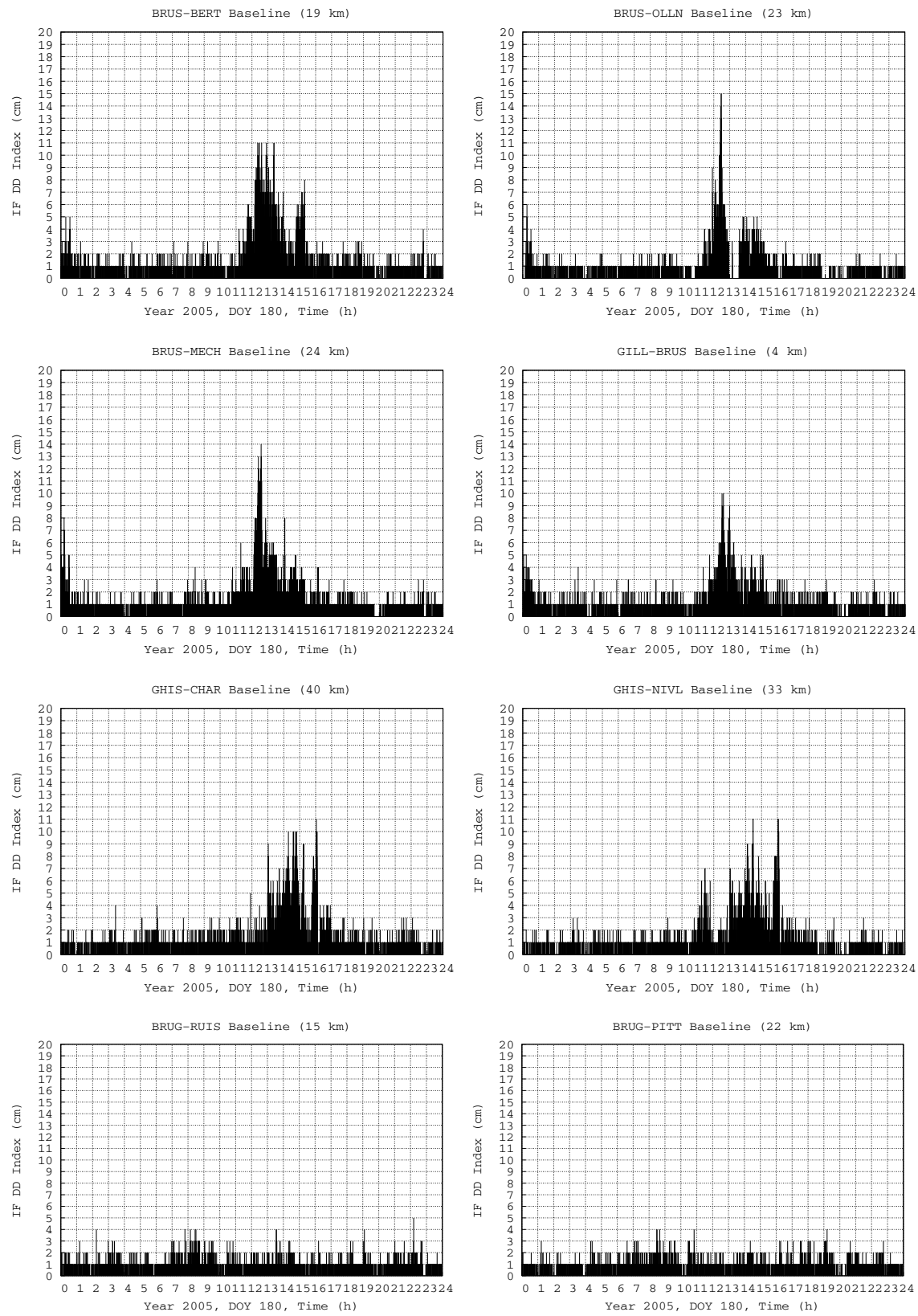


Figure 51: daily IF DD Index of tropospheric activity of BRUS-BERT, BRUS-OLLN, BRUS-MECH, GILL-BRUS, GHIS-CHAR, GHIS-NIVL, BRUG-RUIS and BRUG-PITT baselines (2005/06/29).

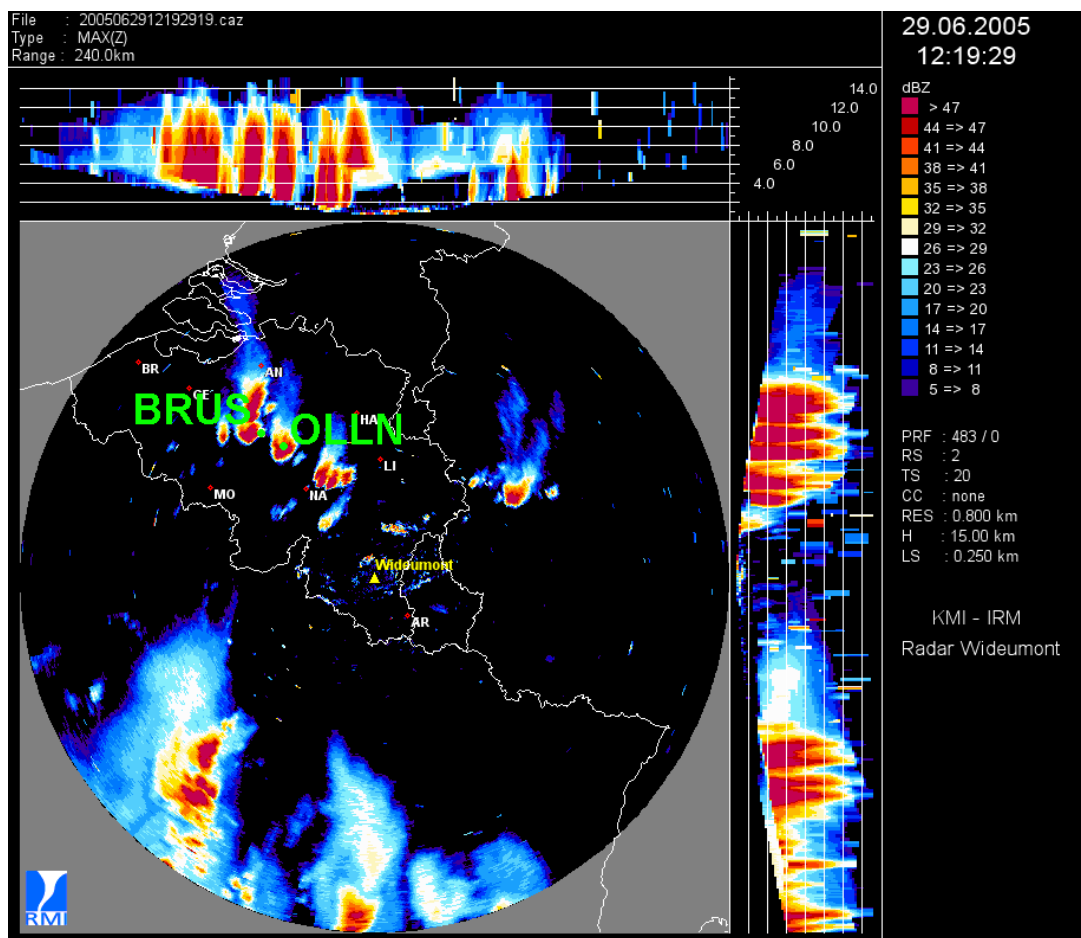


Figure 52: radar reflectivity imaging (max values) and projections in North and East directions.

High vertical extensions of tropospheric structures (vertical extension larger than 10 km shown figure 52) induce important perturbations on GNSS phases measurements around 12H30 UTC the 29th June 2005 (see daily IF DD Index Fig. 51 and some examples of IF DD time-series and tropospheric index of activity for NAMR-OLLN baseline Fig. 15 and 56, and for BRUS-MECH, BRUS-OLLN and GILL-BRUS baselines Fig. 53, 54 and 55).

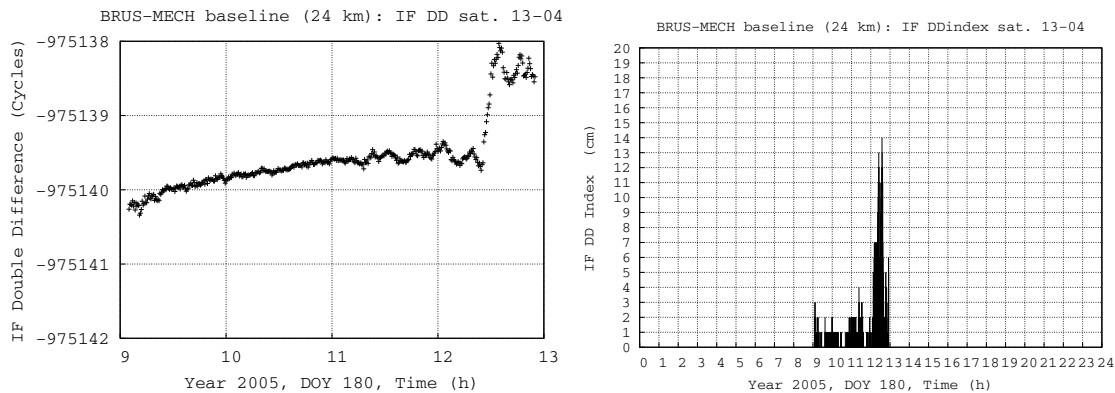


Figure 53: IF Double Difference and tropospheric index of activity of BRUS-MECH baseline DOY 180 of 2005 (couple of satellites 13-04).

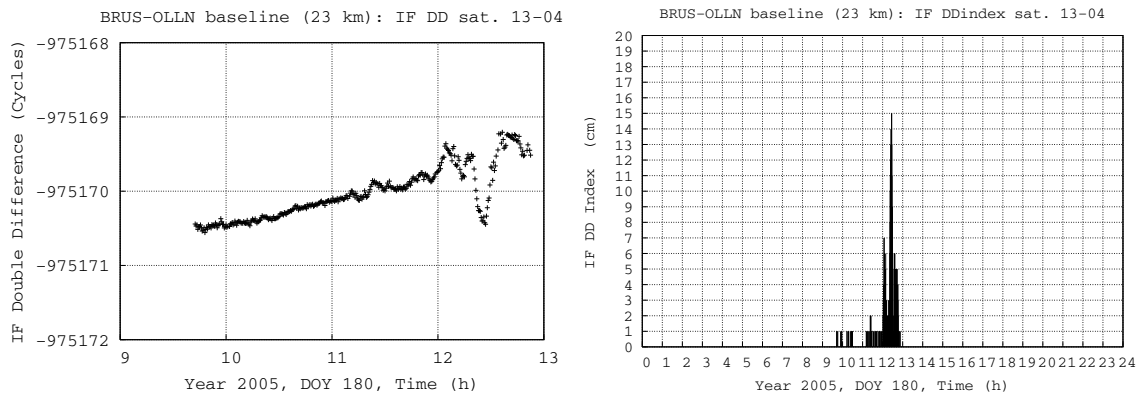


Figure 54: IF Double Difference and tropospheric index of activity of BRUS-OLLN baseline DOY 180 of 2005 (couple of satellites 13-04).

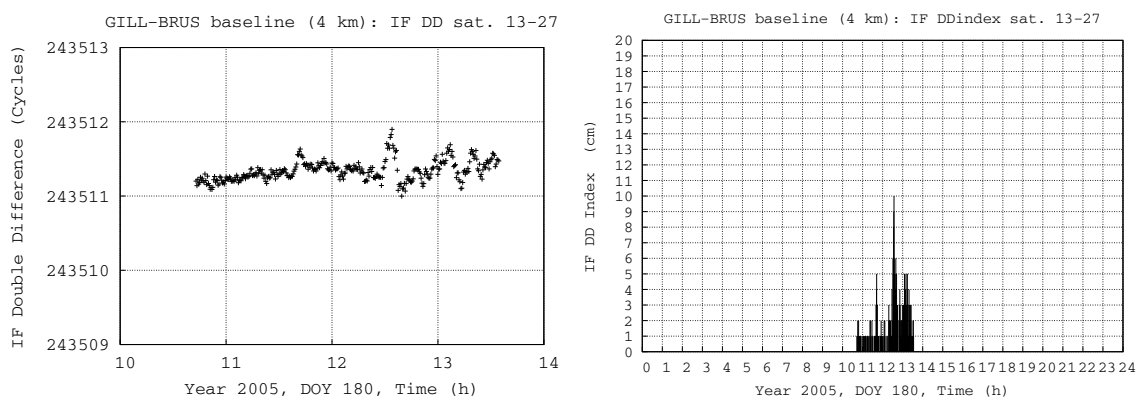


Figure 55: IF Double Difference and tropospheric index of activity of GILL-BRUS baseline DOY 180 of 2005 (couple of satellites 13-27).

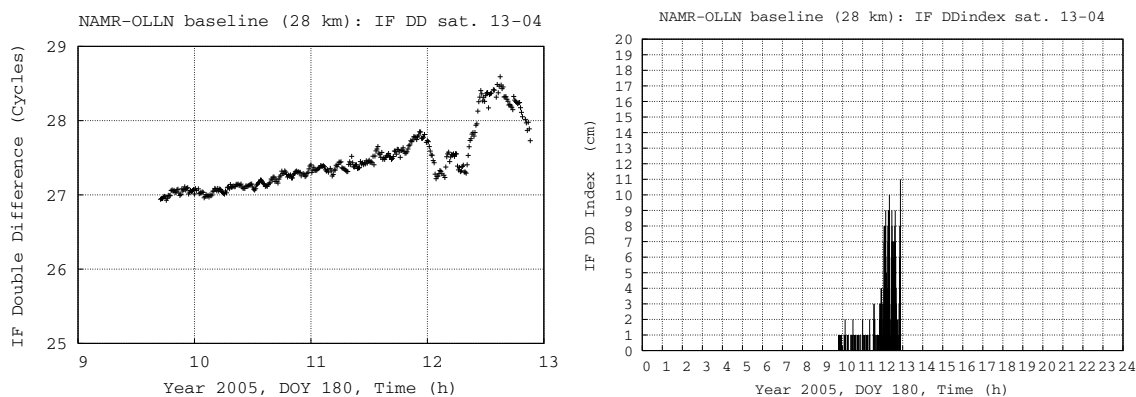


Figure 56: IF Double Difference and tropospheric index of activity of NAMR-OLLN baseline DOY 180 of 2005 (couple of satellites 13-04).

The trajectories of visible satellites from BRUS station are presented figure 57. In RTK positioning, a satellite is chosen among the other to form double differences with each visible satellite (method of the “reference satellite”). From 10H UTC to 14H UTC, the reference satellite is the number 13. The high vertical extension (figure 52) is associated with a high probability of hail (see figure 58). According to radar imaging, a large thickness of tropospheric structures and solid hydrometeors are located above BRUS and

OLLN stations at 12H19 UTC. The low elevation of satellite 4 at 12H30 UTC and a high change in refractivity during the path travel of GNSS signals have induced a high perturbation of the double-difference time-series (Fig. 53, 54 and 56). However, a low elevation of one of the two satellites selected in double-difference does not explain the high perturbation observed in DD time-series. In fact for a short baseline of 4 km (GILL-BRUS), high IF DD Indexes are observed (up to 10 cm) at 12H30 UTC the 29th June 2005 (see figure 55). The couple of satellites considered is 13-27 with elevation of about 60° at 12H30 UTC (see skyplot figure 57). Therefore, we can consider that the change in refractivity (which can be induced by water vapour and hydrometeors) is the key parameter to explain the sudden change observed in IF DD Index.

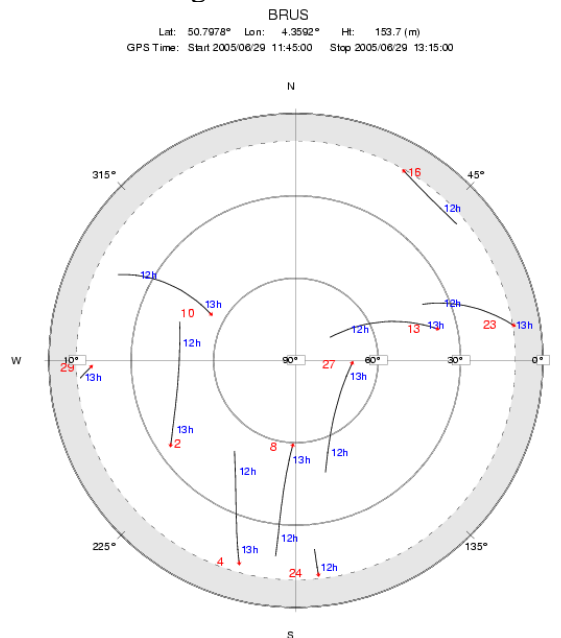


Figure 57: skyplot of visible satellites from BRUS station between 11H45 UTC and 13H15 UTC.

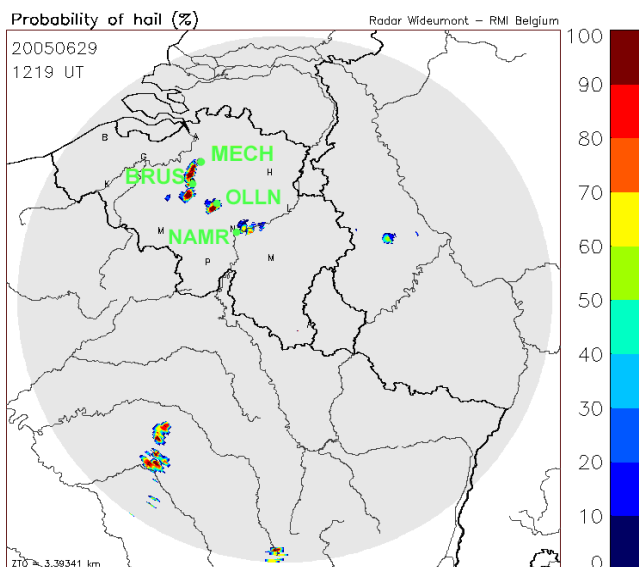


Figure 58: probability of hail at 12H19 UTC the 29th June 2005.

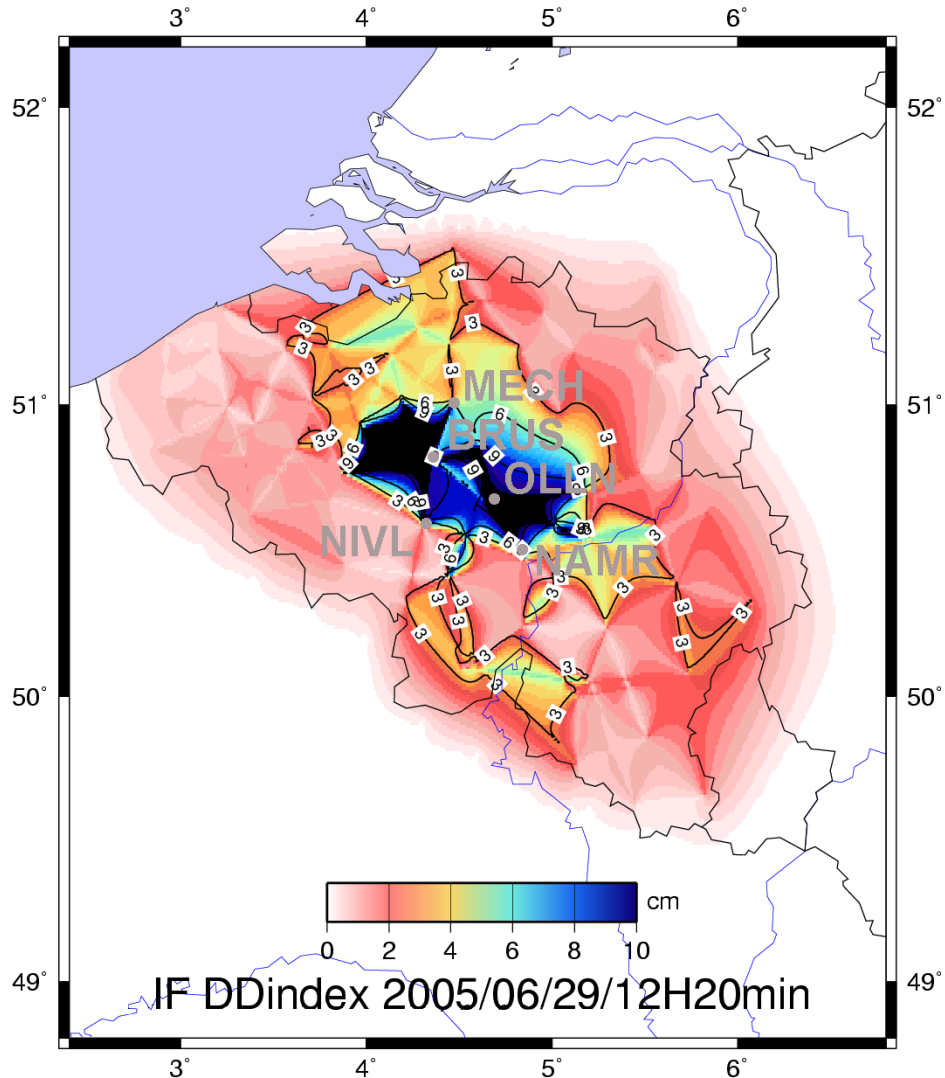


Figure 59: imaging of maximal IF DD Index detected the 29th June 2005 at 12H20 UTC.

We can notice that all baselines considered around BRUS and OLLN stations are affected by the presence of small-scale tropospheric structures with high vertical extension (see IF DD Index imaging figure 59).

At 16H UTC the 29th June 2005, tropospheric activity has been observed over the major part of the Belgium. We can see the location of small-scale structures on radar imaging of precipitations (Belgian composite figure 60) at 16H05 UTC the 29th June 2005. GHIS and MABO stations are close to these tropospheric structures. We can observe high IF DD Index at 16H UTC (see figure 51) for GHIS-CHAR and GHIS-NIVL baseline (up to 11 cm). For baselines REDU-MABO and MABO-LEGL, the daily IF DD Index show activity at 16H UTC, but the perturbation of DD time-series does not exceed 6 cm (see figure 61). The key parameter to explain this difference of the tropospheric activity level detected by IF DD Index is the change in refractivity induced by tropospheric structures and the thickness of the vertical extension.

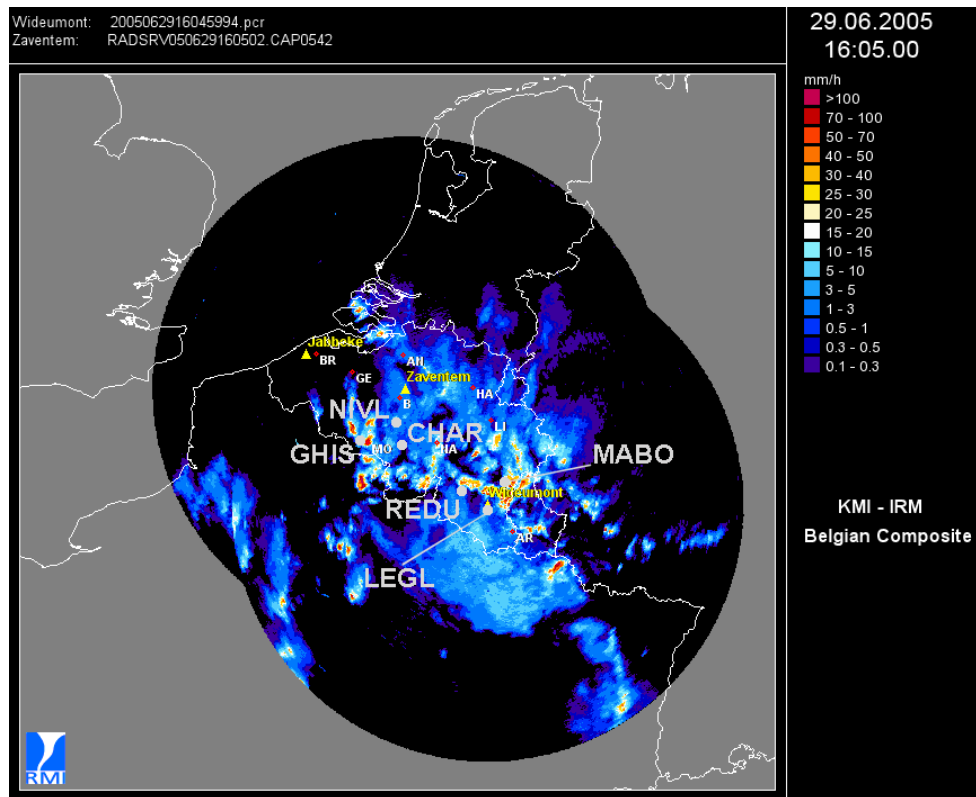


Figure 60: radar imaging of precipitations (29 June 2005 at 16H05 UTC).

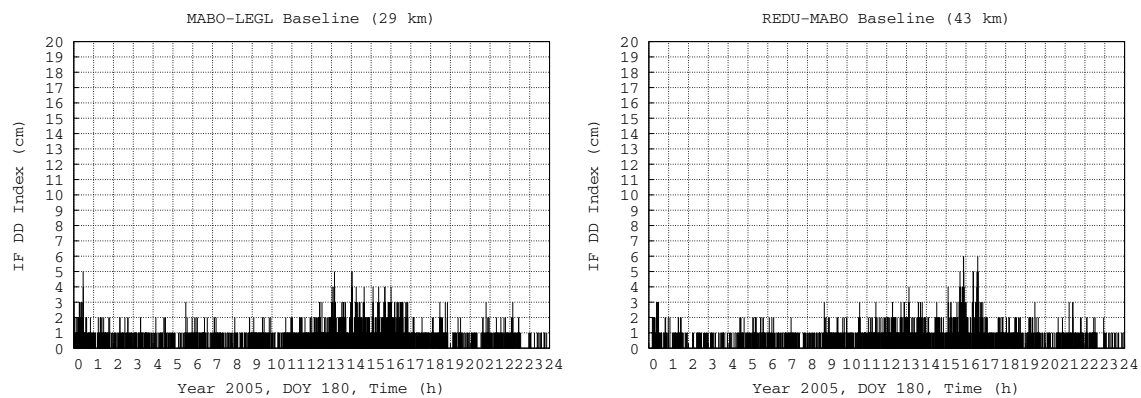


Figure 61: daily IF DD Index of tropospheric activity of MABO-LEGL and REDU-MABO baselines (2005/06/29).

Radar imaging of maximum values of reflectivity and specifically projections in the north and east directions (see figure 62) allow us to estimate the vertical extension of tropospheric structures close to GHIS station (larger than 10 km) and MABO station (about 8 km). In practice, an additional vertical extension of 2 km (water vapour only) for GHIS station would induce that ZTD at GHIS station is about 1 cm larger than for MOHA station (correction of altitude applied). In the present case, the difference of 5 cm in the IF DD Index between GHIS-CHAR and REDU-MABO at 16H UTC can not be explained only by the presence of water vapour (see figure 51 for GHIS-CHAR baseline and figure 61 for REDU-MABO baseline).

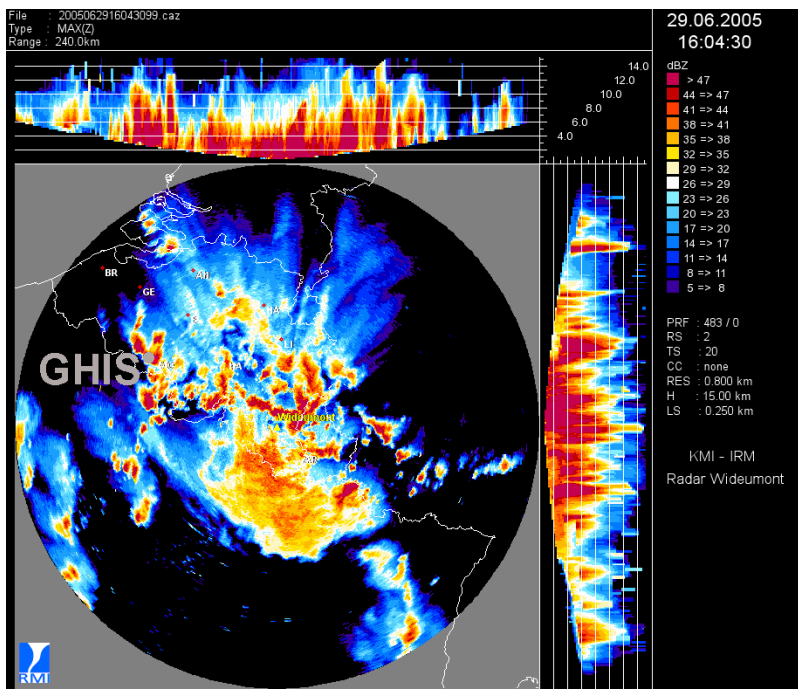


Figure 62: radar reflectivity imaging (max values) and projections in North and East directions.

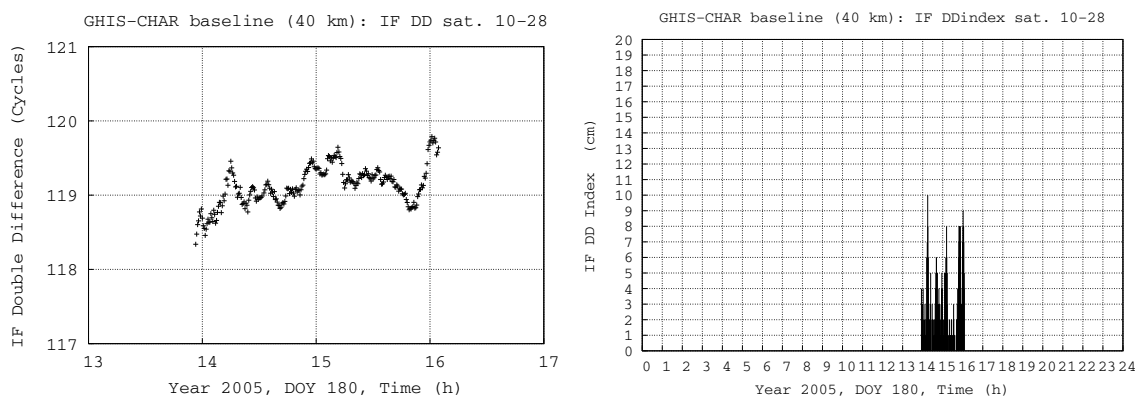


Figure 63: IF Double Difference and tropospheric index of activity of GHIS-CHAR baseline DOY 180 of 2005 (couple of satellites 10-28).

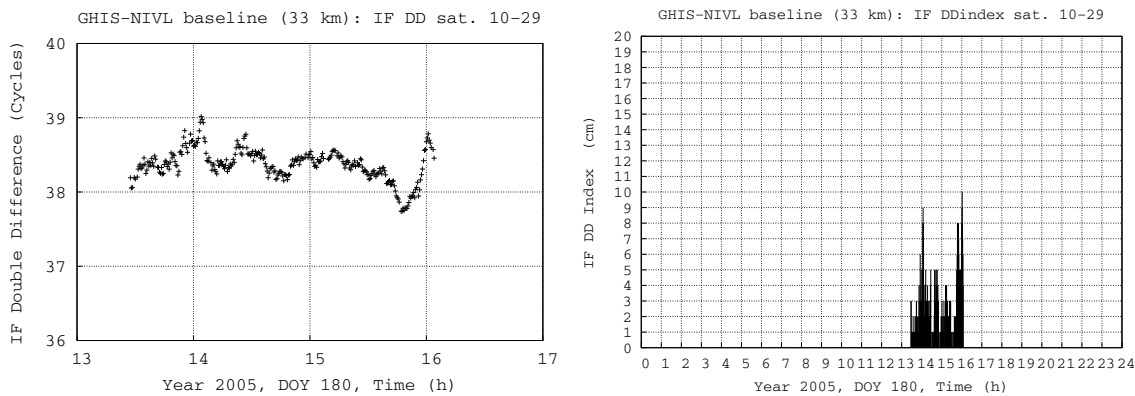


Figure 64: IF Double Difference and tropospheric index of activity of GHIS-NIVL baseline DOY 180 of 2005 (couple of satellites 10-29).

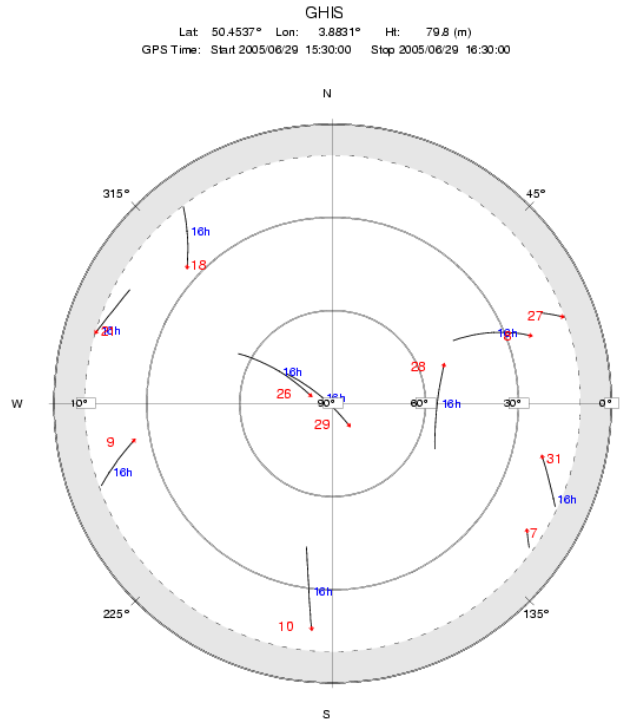


Figure 65: skyplot of visible satellites from GHIS station between 15H30 UTC and 16H30 UTC (29/06/2005).

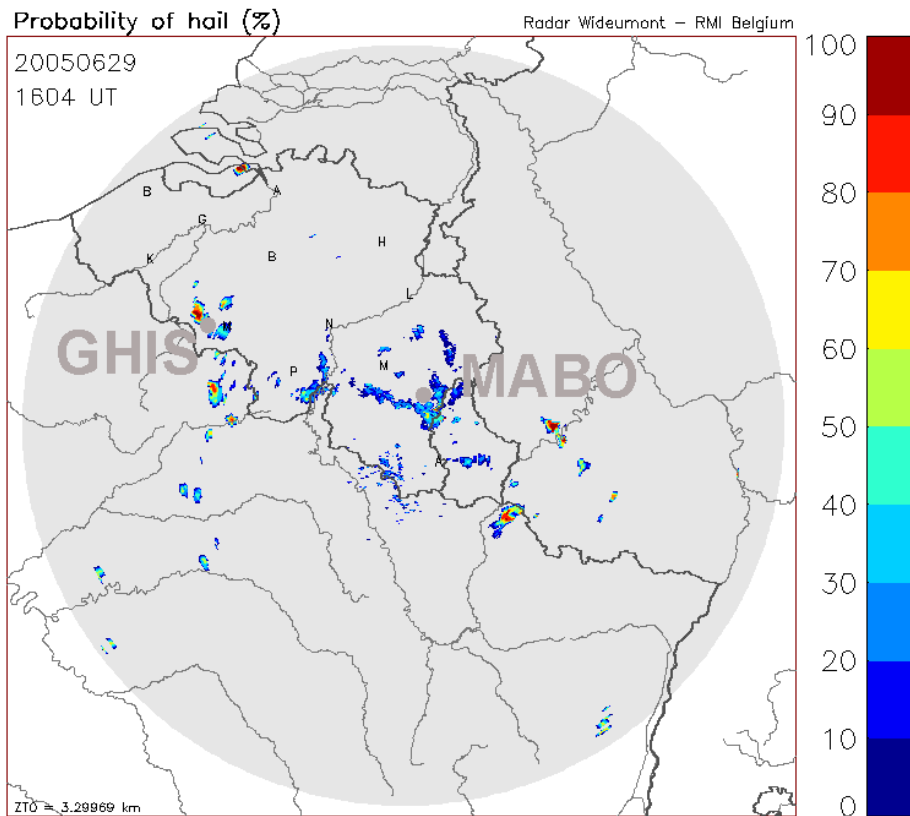


Figure 66: probability of hail at 16H04 UTC the 29th June 2005.

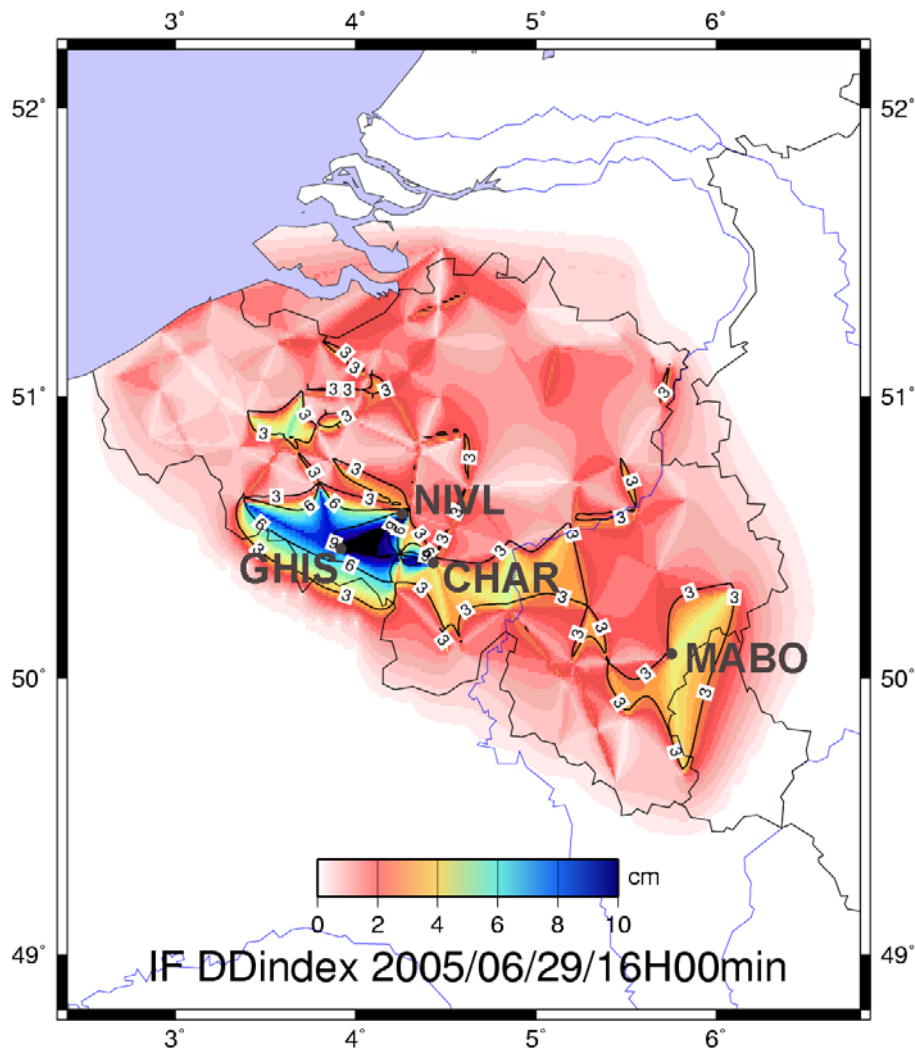


Figure 67: imaging of maximal IF DD Index detected the 29th June 2005 at 16H00 UTC.

The occurrence of hydrometeors (hail induced by important vertical extension, see figure 62 and 66) can explain a contrast of delays of few centimeters in the zenith direction [Brenot *et al.*, 2006]. The change in refractivity induced by hydrometeors can clearly be observed in IF DD time-series and in tropospheric index of activity of GHIS-CHAR and GHIS-NIVL baselines figure 63 and 64. According to the skyplot of visible satellites from GHIS station between 15H30 and 16H30 UTC the 29th June 2005 (Fig. 65) and according to the location of the high probability of hail (Fig. 66), the path travel of GNSS signals recorded at GHIS station have been affected by hydrometeors. We can see on IF DD Index imaging at 16H00 UTC the 29th June 2005 (Fig. 67) that all the double-differences established from GHIS station are highly disturbed (up to 11 cm). On the other hand, double-differences established from MABO station are affected by an IF DD Index of about 5 cm at 16H UTC. Therefore, we can conclude that strong IF DD Indexes (larger than 10 cm) are very probably induced by hydrometeors.

4.1.5 Wet weather of the 19th October 2005

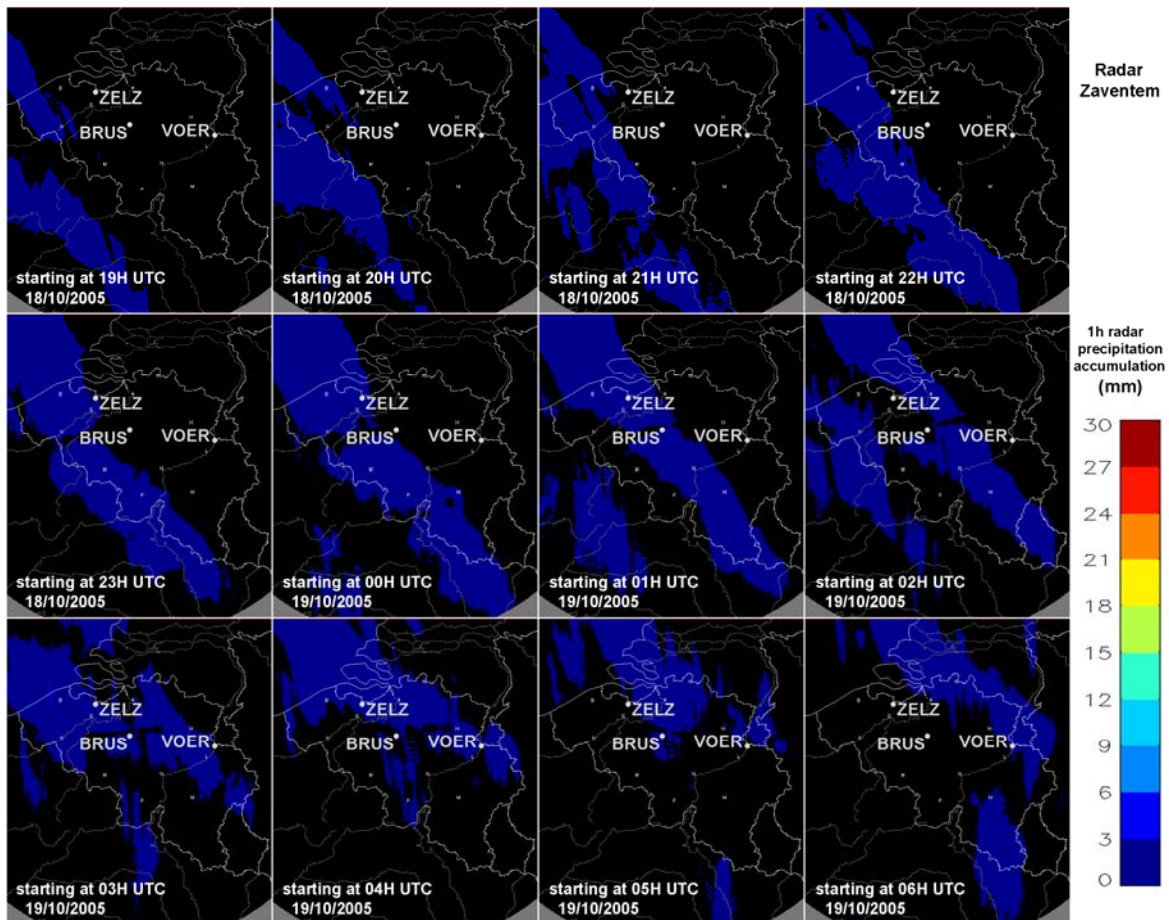


Figure 68: 1h radar precipitation accumulation from 19H UTC (18/10/2005) to 7H UTC (19/10/2005).

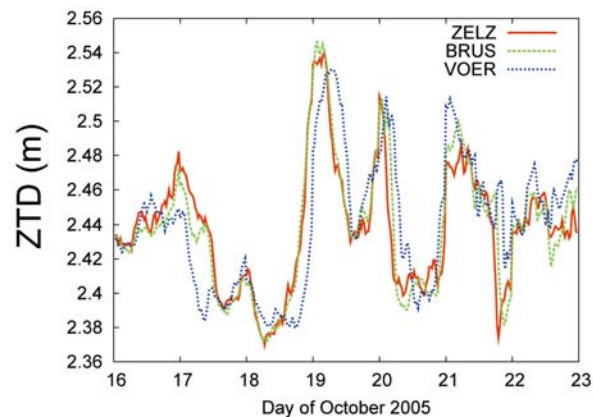


Figure 69: ZTD time-series of ZELZ, BRUS and VOER in October 2005.

During this event, an important ZTD-loading has been observed by all Belgian GNSS stations, but the daily precipitations have been smaller than 30 mm/day. Small-scale structures are rather weak during this event (see radar imaging figure 68) which corresponds to the passage of a weather front from south-west to north-east, but a ZTD-drop between two loading periods is observed the 19th October 2005 (Fig. 69).

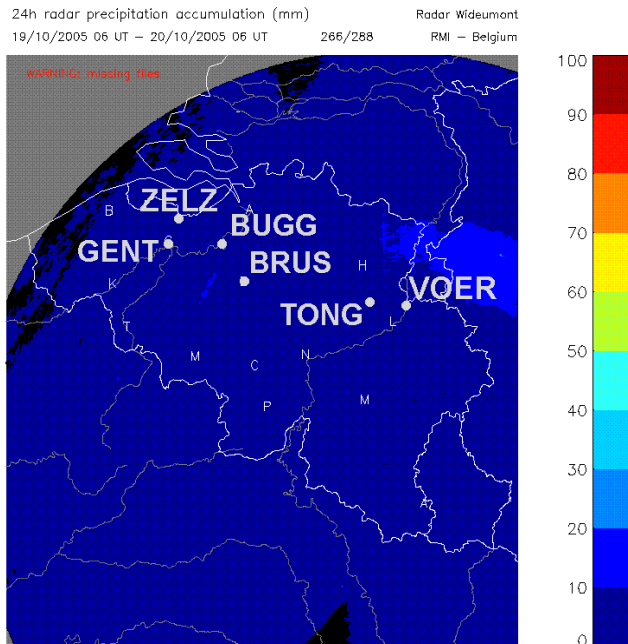


Figure 70: 24h radar precipitation accumulation the 19th October 2005.

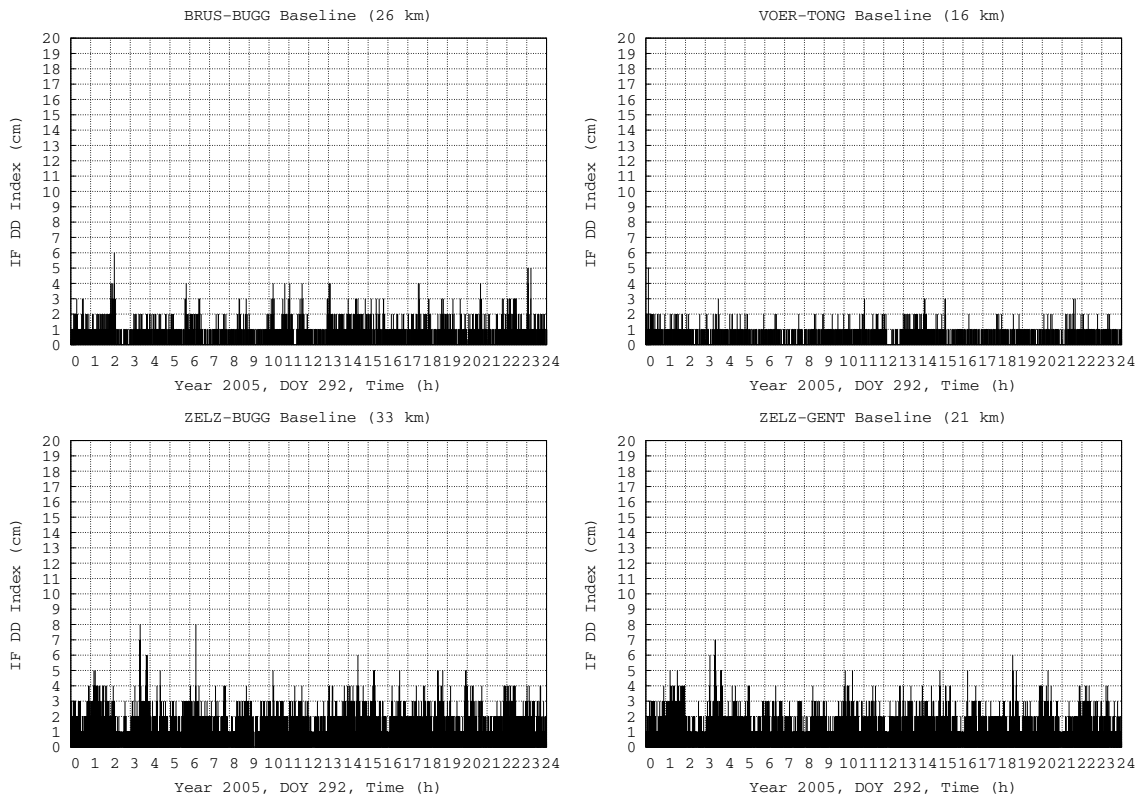


Figure 71: daily IF DD Index of tropospheric activity of BRUS-BUGG, VOER-TONG, ZELZ-BUGG and ZELZ-GENT baselines (2005/10/19).

A low 24h precipitation accumulation has been observed by radar imaging (Fig. 70). The daily IF DD Index activity observed the 19th October 2005 is moderate (see figure 71). IF DD Index up to 8 cm are obtained for ZELZ-BUGG baseline.

We present IF DD time-series and tropospheric index of activity of ZELZ-GENT baseline (Fig. 72 to Fig. 77). The reference satellite used to form double-difference is number 13. The other satellites visible at 03H30 UTC are numbers 02, 04, 20, 23, 24, 27. The skyplot of these satellites is presented figure 78.

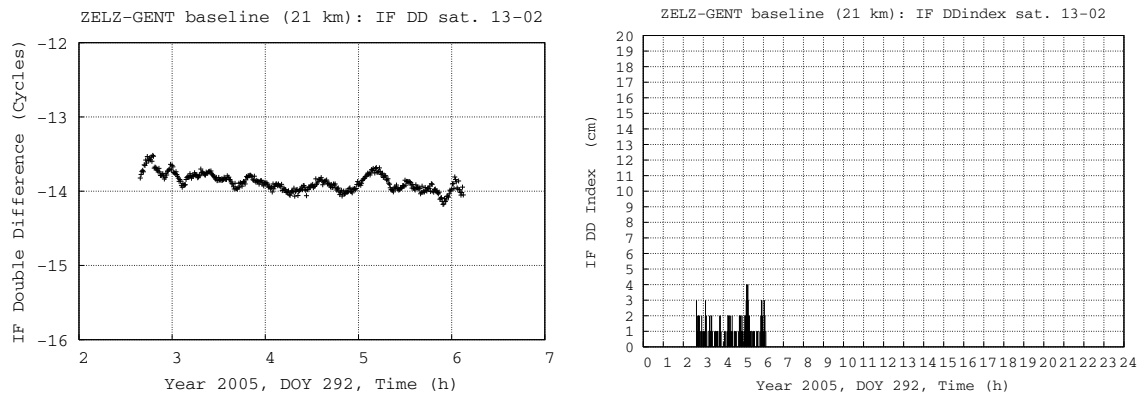


Figure 72: IF Double Difference and tropospheric index of activity of ZELZ-GENT baseline DOY 292 of 2005 (couple of satellites 13-02).

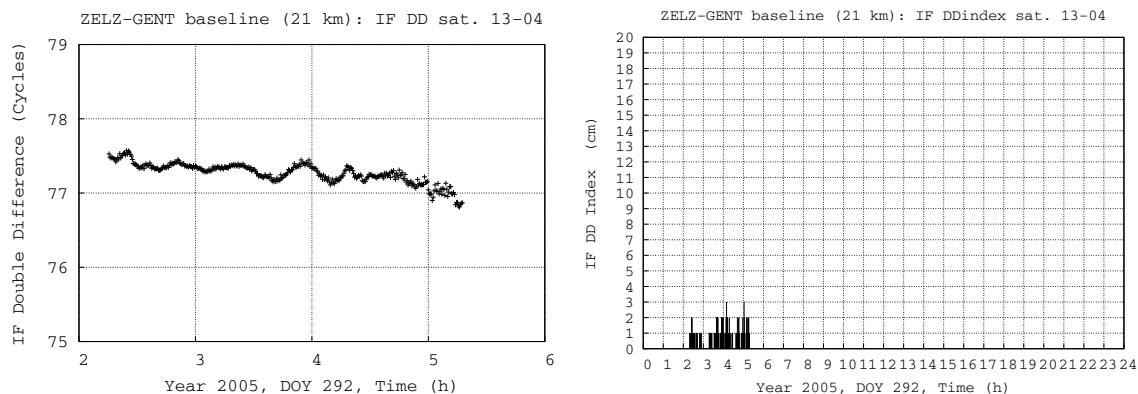


Figure 73: IF Double Difference and tropospheric index of activity of ZELZ-GENT baseline DOY 292 of 2005 (couple of satellites 13-04).

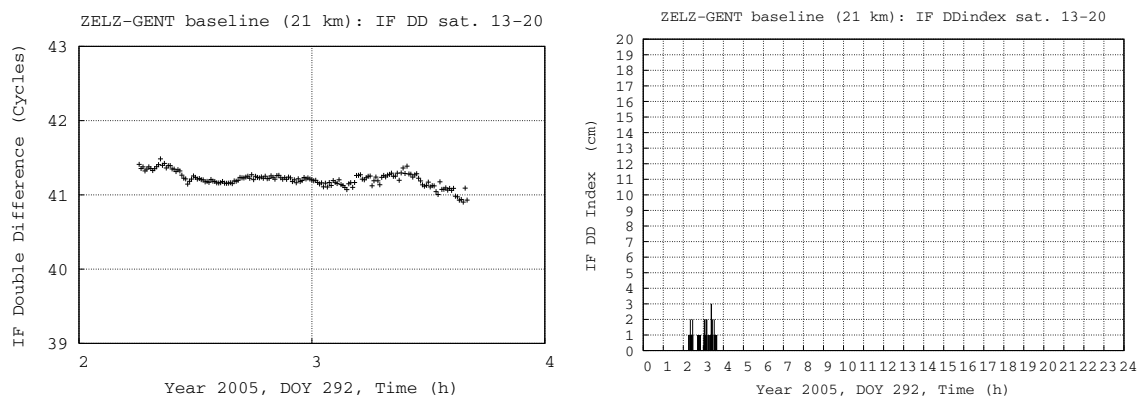


Figure 74: IF Double Difference and tropospheric index of activity of ZELZ-GENT baseline DOY 292 of 2005 (couple of satellites 13-20).

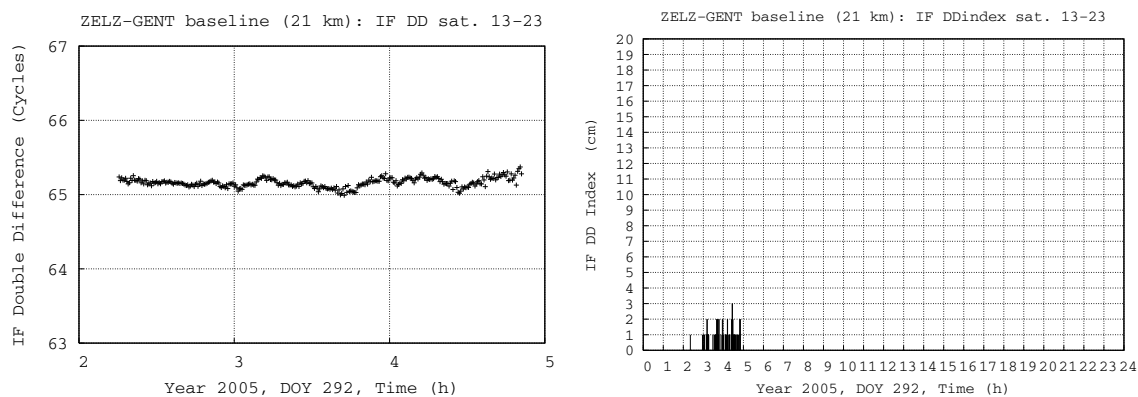


Figure 75: IF Double Difference and tropospheric index of activity of ZELZ-GENT baseline DOY 292 of 2005 (couple of satellites 13-23).

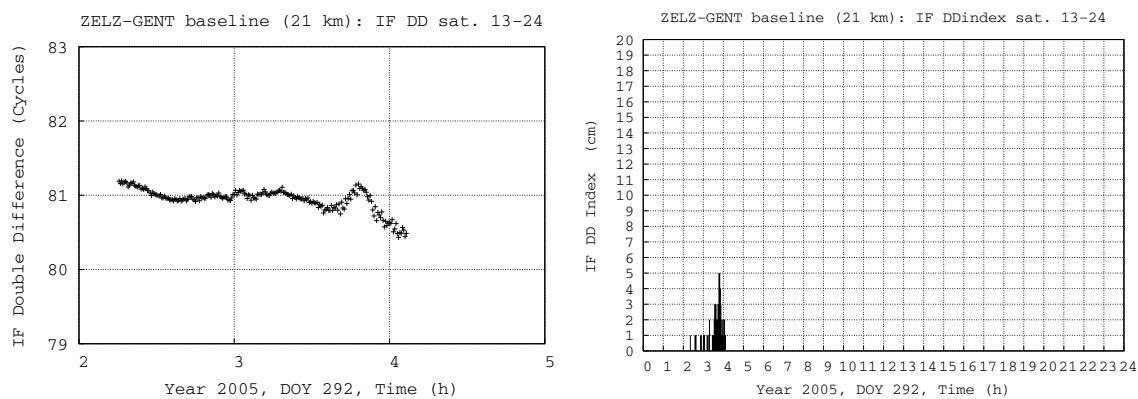


Figure 76: IF Double Difference and tropospheric index of activity of ZELZ-GENT baseline DOY 292 of 2005 (couple of satellites 13-24).

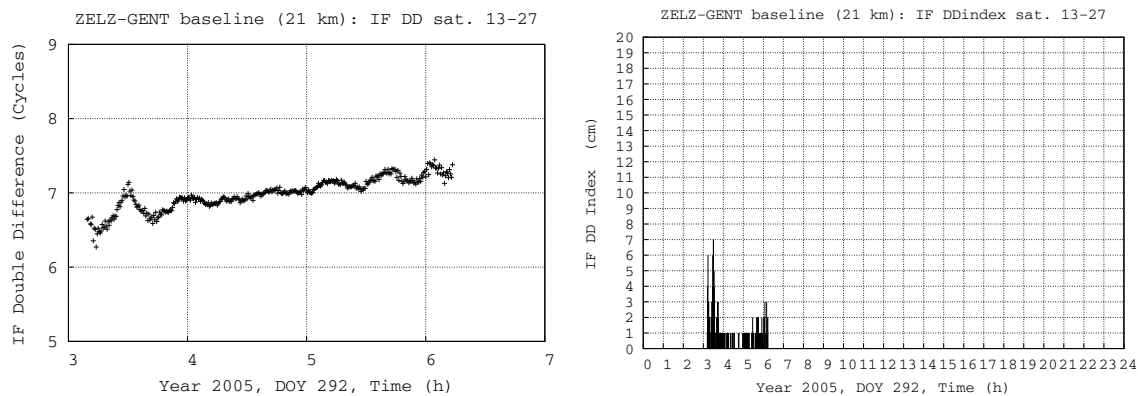


Figure 77: IF Double Difference and tropospheric index of activity of ZELZ-GENT baseline DOY 292 of 2005 (couple of satellites 13-27).

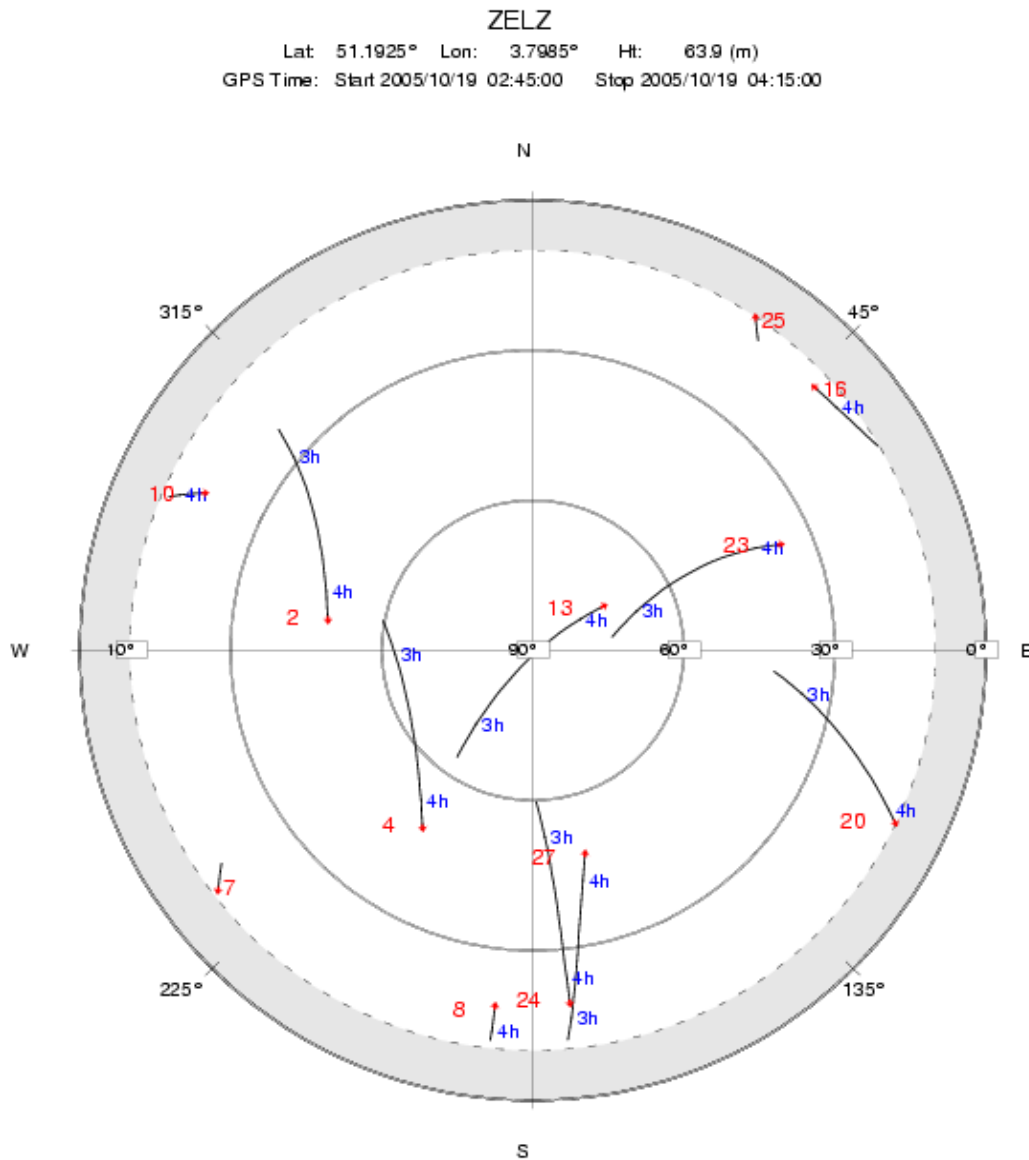


Figure 78: skyplot of visible satellites from ZELZ station between 02H45 UTC and 04H15 UTC (19/10/2005).

From figure 78, we can see that satellite 13 flies at the zenith of ZELZ station between 03H UTC and 04H UTC on 19th October 2005. Considering different couples of satellites (13-02, 13-04, 13-20, 13-23, 13-24 and 13-27) we observe maximal IF DD Index from 3 cm to 7 cm. The localization of the tropospheric structure can be estimated according to the different trajectory of visible satellites (02, 04, 20, 23, 24 and 27). High IF DD Indexes are observed for couple of satellites 13-24 and 13-27 (respectively up to 5 cm at 03H50 UTC and 7 cm at 03H30 UTC); that means that tropospheric structures are located to the south of ZELZ station or to the south of GENT station (from few kilometers to 20 km) at about 45° of elevation.

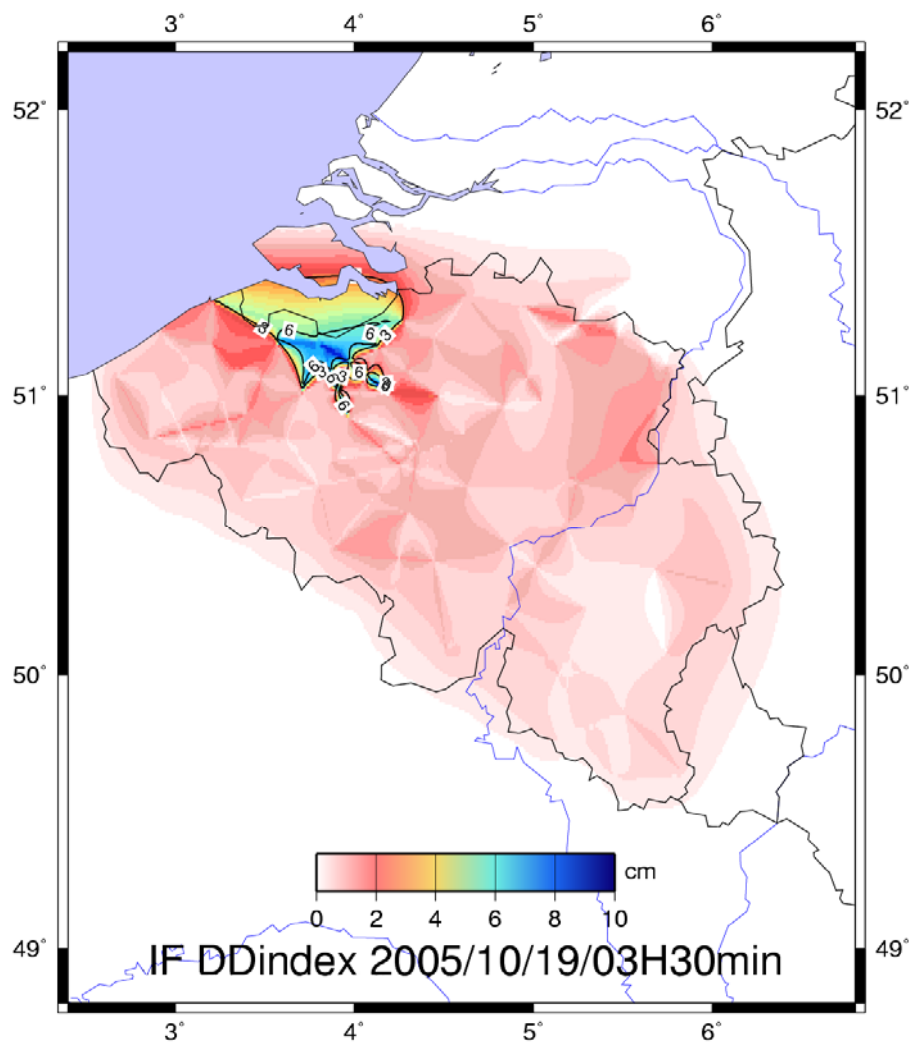


Figure 79: imaging of maximal IF DD Index detected the 19th October 2005 at 03H30 UTC.

According to radar imaging and the fact that a weak content of hydrometeors (probability of hail about 0% over Belgium) occurs, we can conclude that the IF DD Index activity detected figure 79 at 03H30 UTC the 19th October 2005 is probably the result of a bubble of water vapour.

4.2 Statistical study of three baselines

In this section, we analyse the frequency of occurrence of high tropospheric IF DD Indexes of activity. To achieve this goal, we have processed baselines BRUS-BERT and BRUS-OLLN from May 2005 to April 2007 and baseline BREE-MEEU from July 1997 to May 2007 (see figure 80 for localization of these stations). These baselines have respectively a length of about 19 km, 23 km and 7 km.

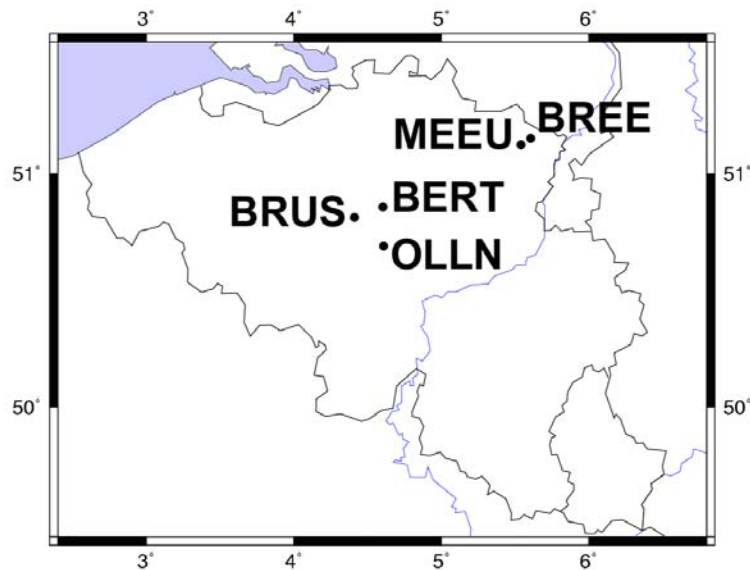


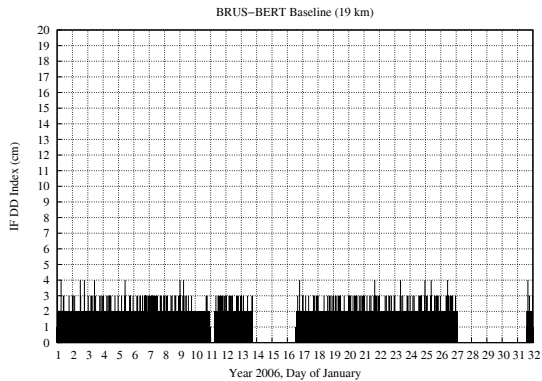
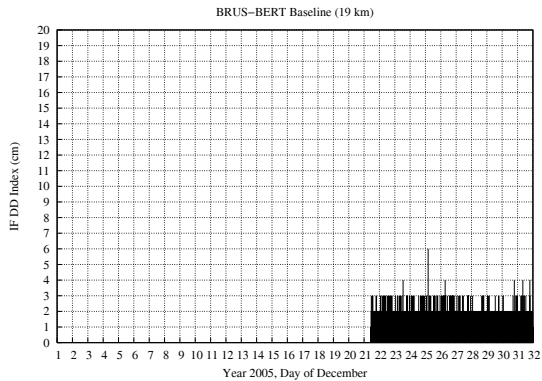
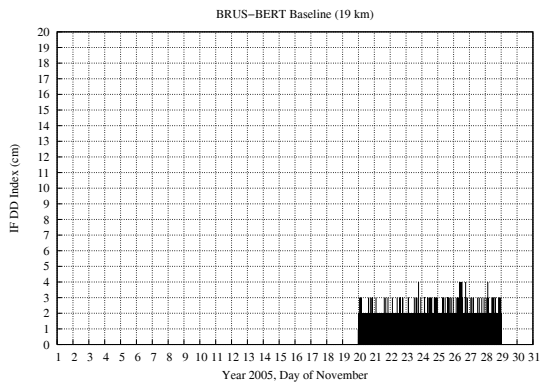
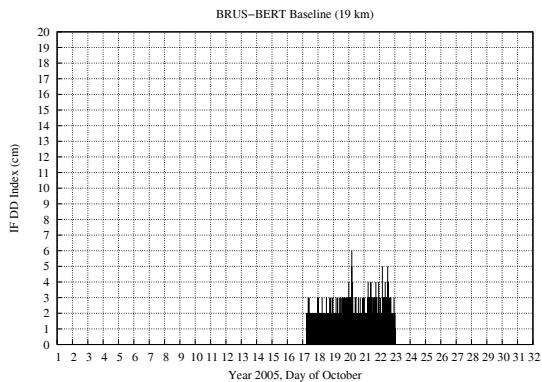
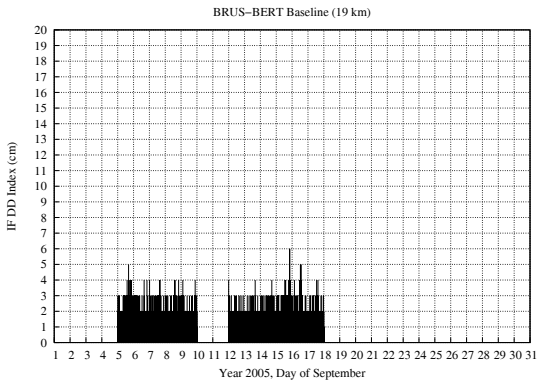
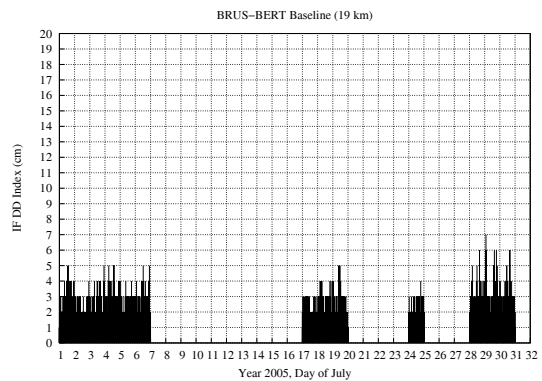
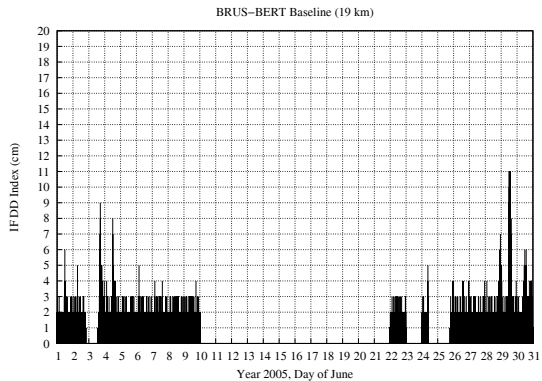
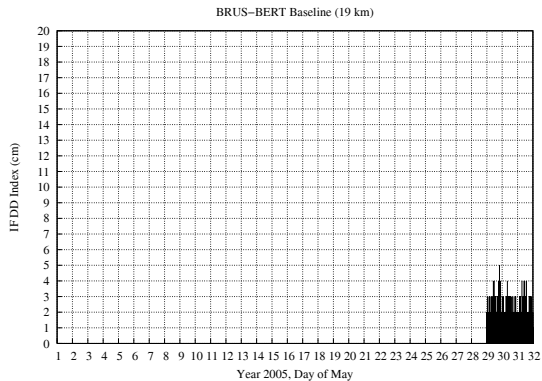
Figure 80: location of BRUS, BERT, OLLN, BREE and MEEU stations.

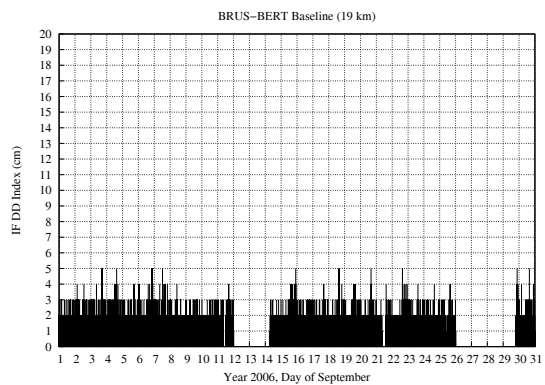
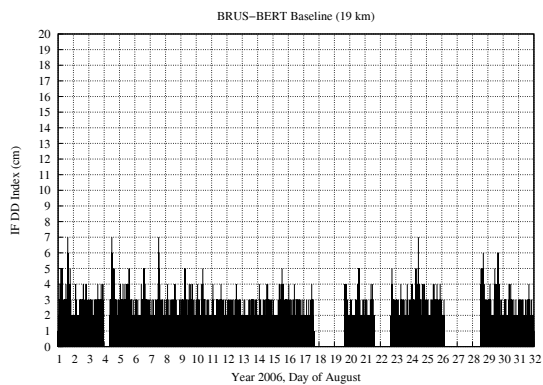
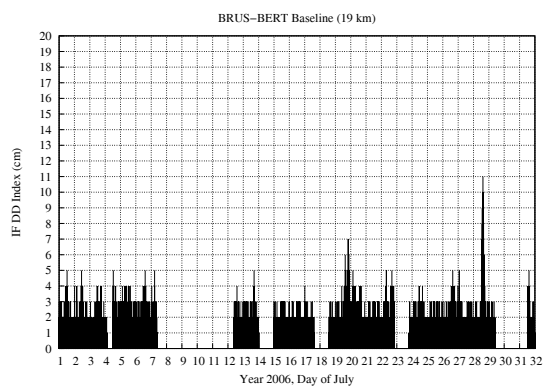
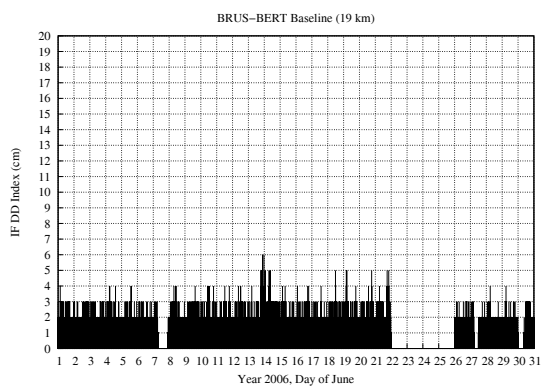
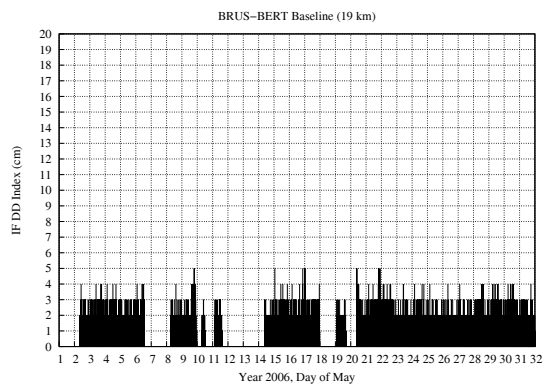
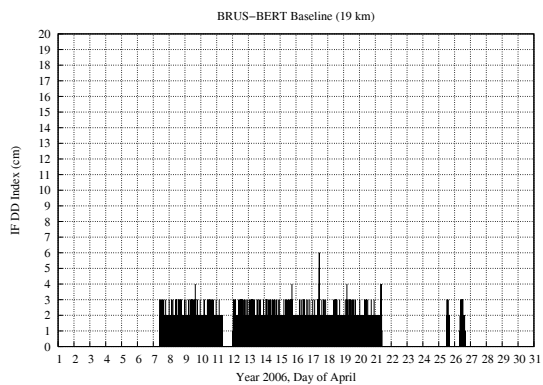
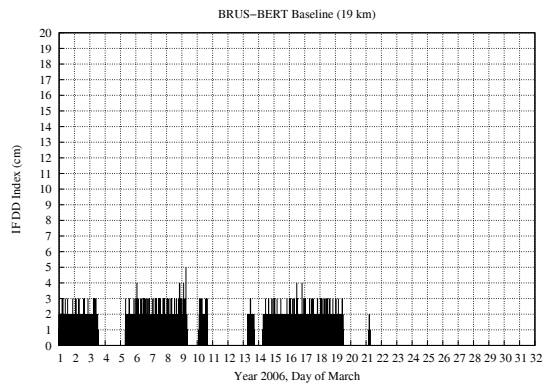
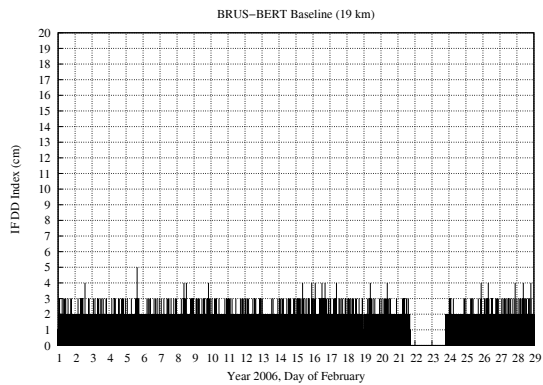
4.2.1 BRUS-BERT and BRUS-OLLN baselines from May 2005 to April 2007

The following graphics (Fig. 81 and 82) present monthly IF DD Index of tropospheric activity of BRUS-BERT and BRUS-OLLN baselines from May 2005 to April 2007. Note that periods where no index is shown correspond to periods where no data is available.

Statistical studies are presented in Tables 1 and 2 to estimate the occurrence of the different index of tropospheric activity established by DD analysis. A level 0 indicates that the IF DD Index relative to a baseline and a couple of satellites is larger or equal to 0 cm and smaller than 1 cm. A level 4 indicates that the IF DD Index relative to a baseline and a couple of satellites is larger or equal to 4 cm and smaller than 5 cm. A level 5+ indicates that the IF DD Index according to a baseline and a couple of satellites is larger than 5 cm. Considering every couples of satellites during a month we present the proportion of events which belongs to a defined level (expressed in %).

Figure 83 presents the global occurrence and selected tropospheric events detected for these two baselines from May 2005 to April 2007. As expected, we can see that major rainfall events with high tropospheric activities occur in summer.





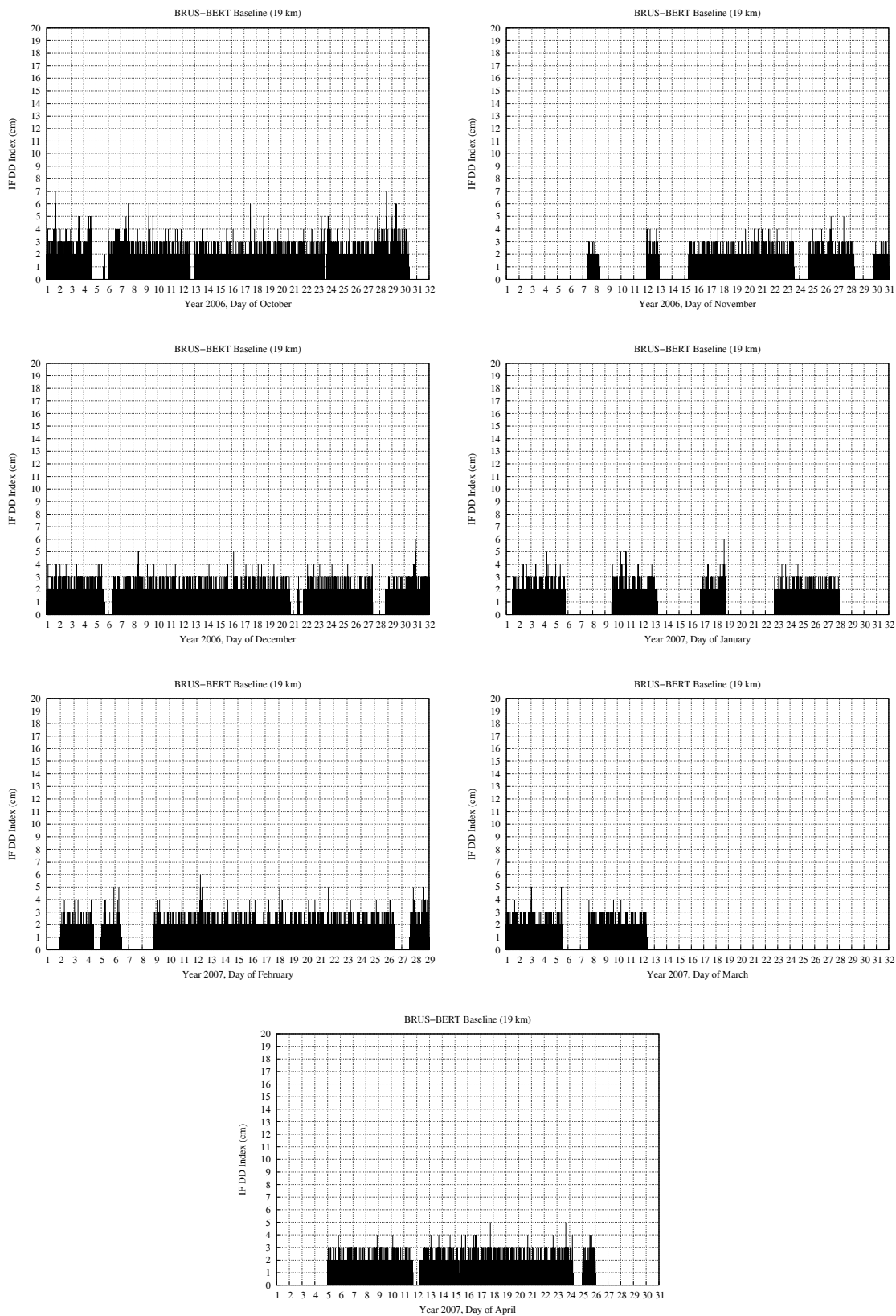
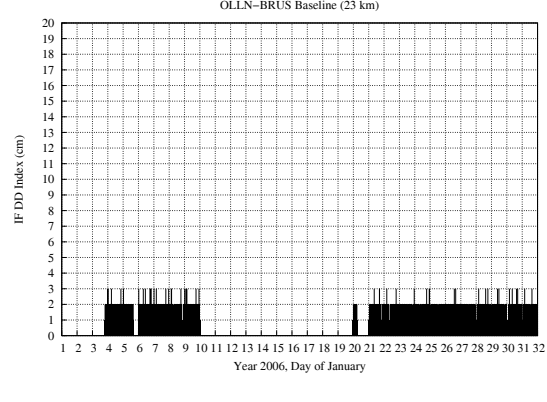
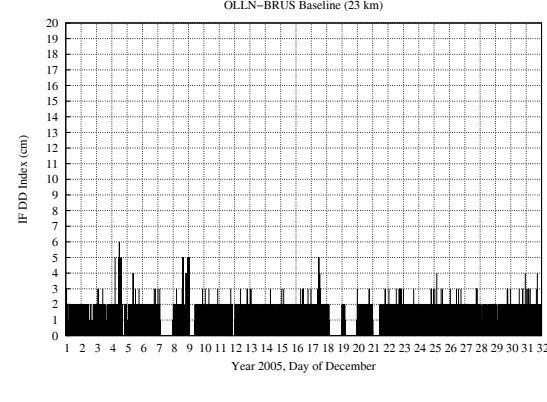
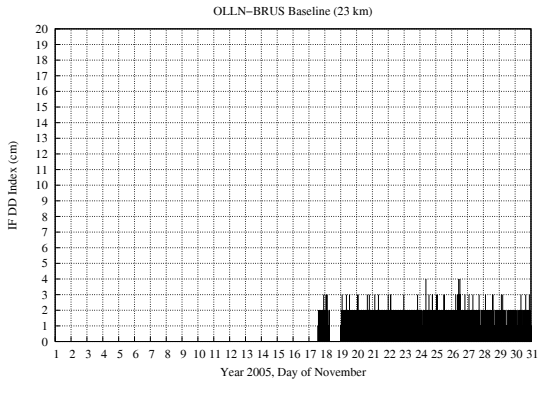
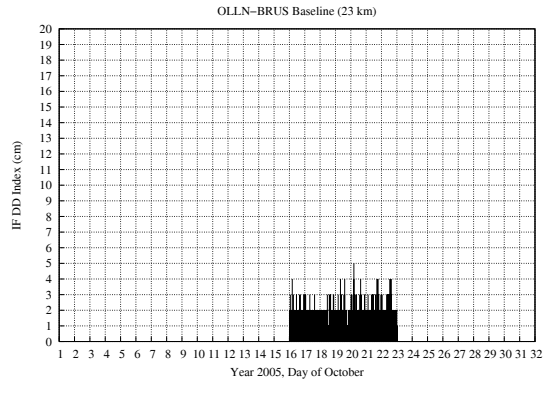
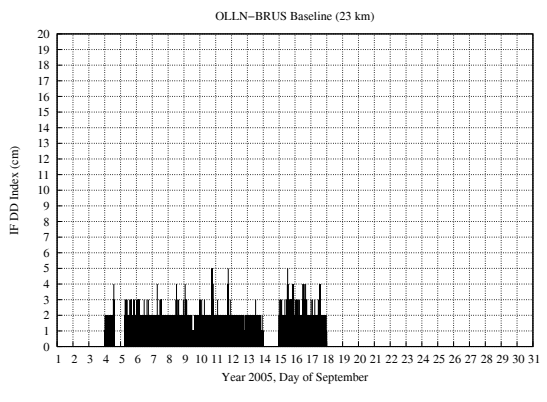
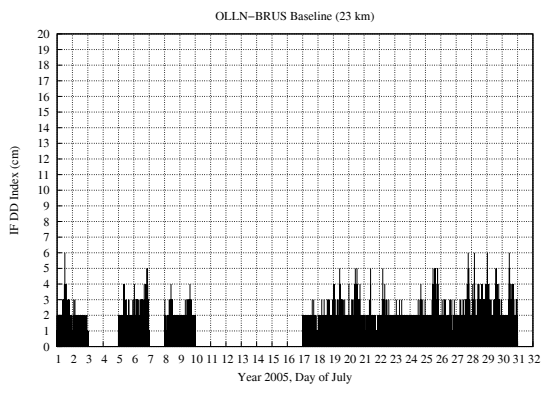
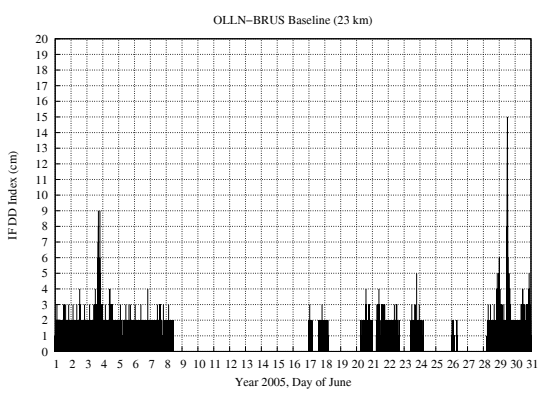
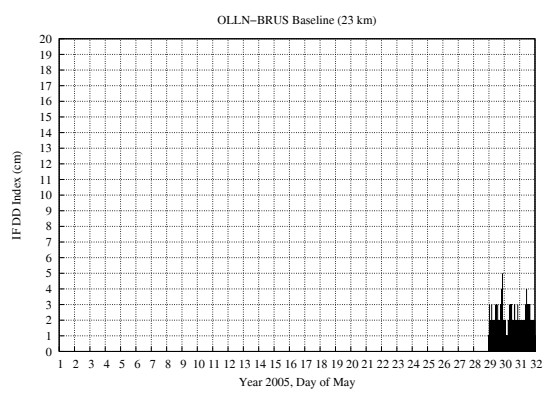
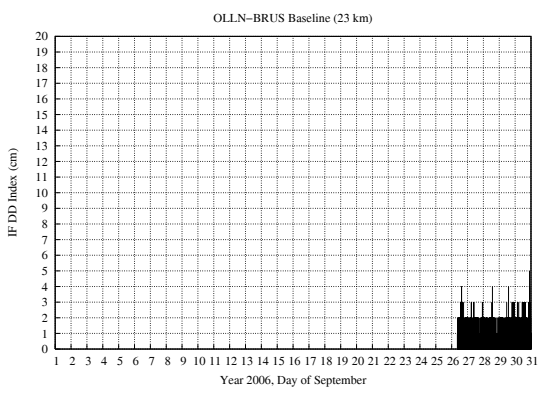
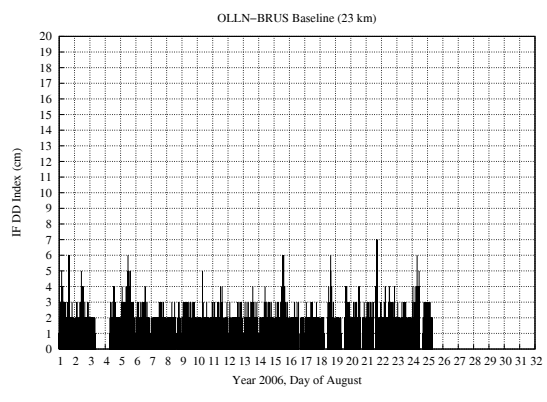
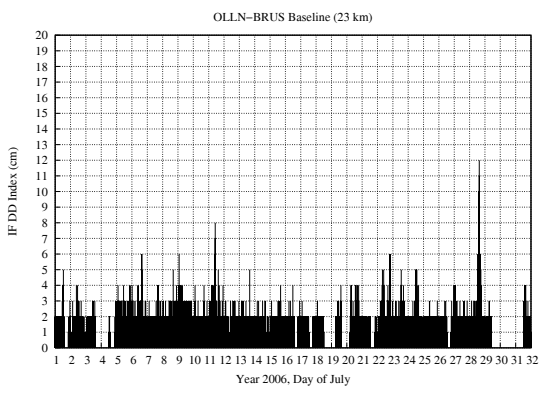
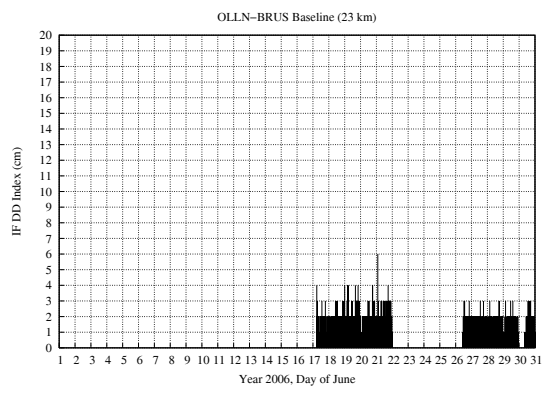
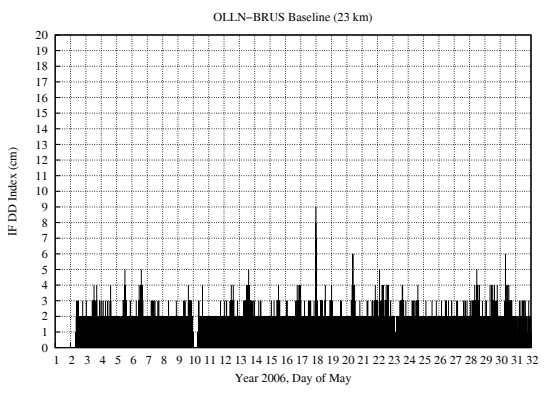
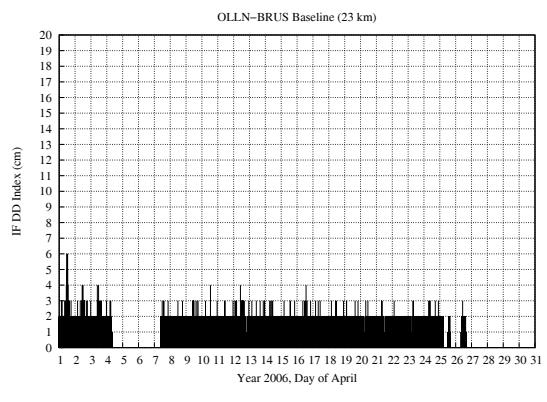
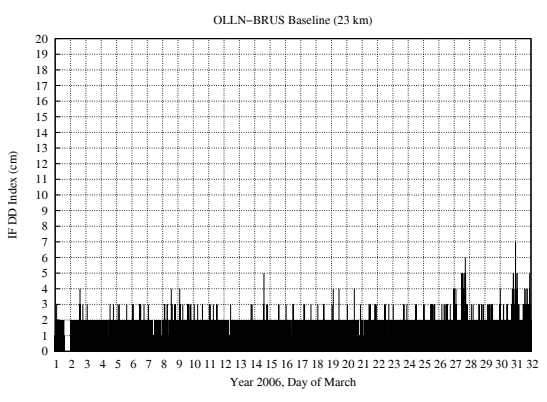
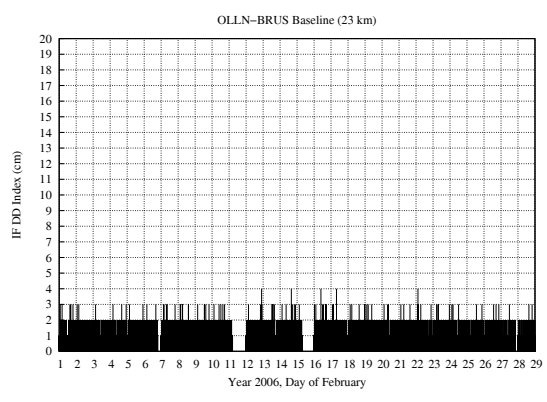


Figure 81: monthly IF DD Index of tropospheric activity of BRUS-BERT baseline from May 2005 to April 2007.

Baseline BRUS-BERT (19 km)							
Periods	Number Of DD-analysis (time-series)	% of tropospheric events					
		level 0	level 1	level 2	level 3	level 4	level 5+
May 2005	40188	80.69	16.40	2.48	0.38	0.05	0.00
June 2005	205920	82.10	15.03	2.17	0.39	0.13	0.18
July 2005	180307	77.38	18.66	3.19	0.60	0.14	0.03
September 2005	149591	81.04	16.47	2.17	0.29	0.03	0.00
October 2005	79623	82.56	15.39	1.81	0.20	0.03	0.01
November 2005	124692	85.68	13.06	1.15	0.10	0.01	0.00
December 2005	147222	85.89	12.82	1.20	0.09	0.00	0.00
January 2006	324283	86.46	12.35	1.12	0.07	0.00	0
February 2006	376849	85.39	13.36	1.16	0.09	0.00	0.00
March 2006	178598	85.16	13.54	1.21	0.09	0.00	0.00
April 2006	202279	83.84	14.53	1.52	0.11	0.00	0.00
May 2006	319846	81.23	16.38	2.08	0.26	0.04	0.01
June 2006	337977	82.21	15.60	1.91	0.24	0.03	0.01
July 2006	290287	77.94	18.55	2.84	0.47	0.11	0.09
August 2006	350990	78.67	17.93	2.82	0.46	0.10	0.02
September 2006	312120	81.62	15.97	2.10	0.26	0.04	0.01
October 2006	396067	82.08	15.59	2.03	0.25	0.04	0.01
November 2006	213976	83.98	14.39	1.51	0.11	0.01	0.00
December 2006	422726	83.62	14.60	1.61	0.15	0.02	0.00
January 2007	217772	83.42	14.84	1.58	0.14	0.02	0.00
February 2007	349544	83.27	14.92	1.63	0.16	0.02	0.00
March 2007	135104	83.11	15.02	1.70	0.16	0.01	0.00
April 2007	296042	83.90	14.41	1.53	0.15	0.01	0.00
All periods (2005-2007)	5652003	82.65	15.23	1.84	0.22	0.04	0.02

Table 1: statistical study of the occurrence of tropospheric index of activity by DD analysis (IF DD Index) for the BRUS-BERT baseline from May 2005 to April 2007.





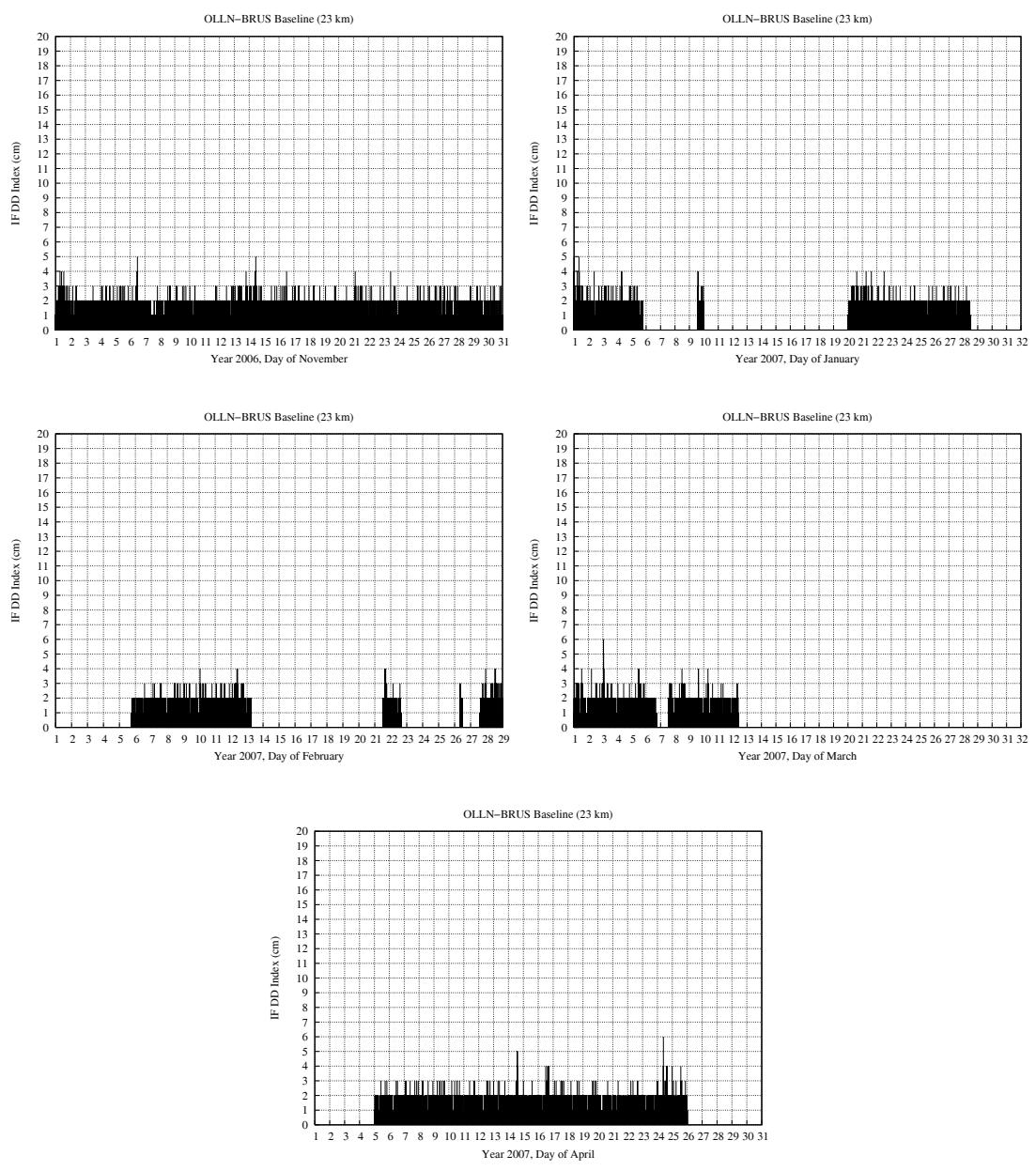


Figure 82: monthly IF DD Index of tropospheric activity of OLLN-BRUS baseline from May 2005 to April 2007.

Baseline BRUS- OLLN (23 km)							
Periods	Number Of DD-analysis (time-series)	% of tropospheric events					
		level 0	level 1	level 2	level 3	level 4	level 5+
May 2005	30402	83.88	14.32	1.60	0.19	0.01	0.00
June 2005	189268	83.57	14.33	1.63	0.30	0.09	0.08
July 2005	270973	83.40	14.43	1.82	0.28	0.06	0.01
September 2005	161628	85.46	13.02	1.33	0.15	0.04	0.00
October 2005	88845	85.80	12.89	1.18	0.12	0.01	0.00
November 2005	169580	88.97	10.35	0.64	0.04	0.00	0
December 2005	360026	87.99	11.21	0.72	0.05	0.02	0.01
January 2006	233518	89.43	10.03	0.52	0.02	0	0
February 2006	367042	88.24	11.08	0.65	0.03	0.00	0
March 2006	413021	86.87	12.07	0.95	0.09	0.01	0.01
April 2006	306750	86.25	12.73	0.95	0.06	0.01	0.00
May 2006	399052	83.34	14.87	1.58	0.17	0.03	0.01
June 2006	114037	84.91	13.85	1.14	0.09	0.01	0.00
July 2006	341576	82.19	15.57	1.83	0.28	0.07	0.06
August 2006	306759	83.65	14.33	1.72	0.25	0.04	0.01
September 2006	62207	86.14	12.53	1.16	0.15	0.02	0.00
November 2006	419273	87.97	11.16	0.81	0.05	0.01	0.00
January 2007	202416	88.20	10.86	0.85	0.08	0.01	0.00
February 2007	148926	86.85	11.99	1.06	0.09	0.01	0
March 2007	151037	87.23	11.71	0.97	0.07	0.02	0.00
April 2007	313609	88.02	11.14	0.79	0.05	0.00	0.00
All periods (2005-2007)	5049945	86.19	12.54	1.12	0.12	0.02	0.01

Table 2: statistical study of the occurrence of tropospheric index of activity by DD analysis (IF DD Index) for the OLLN-BRUS baseline from May 2005 to April 2007.

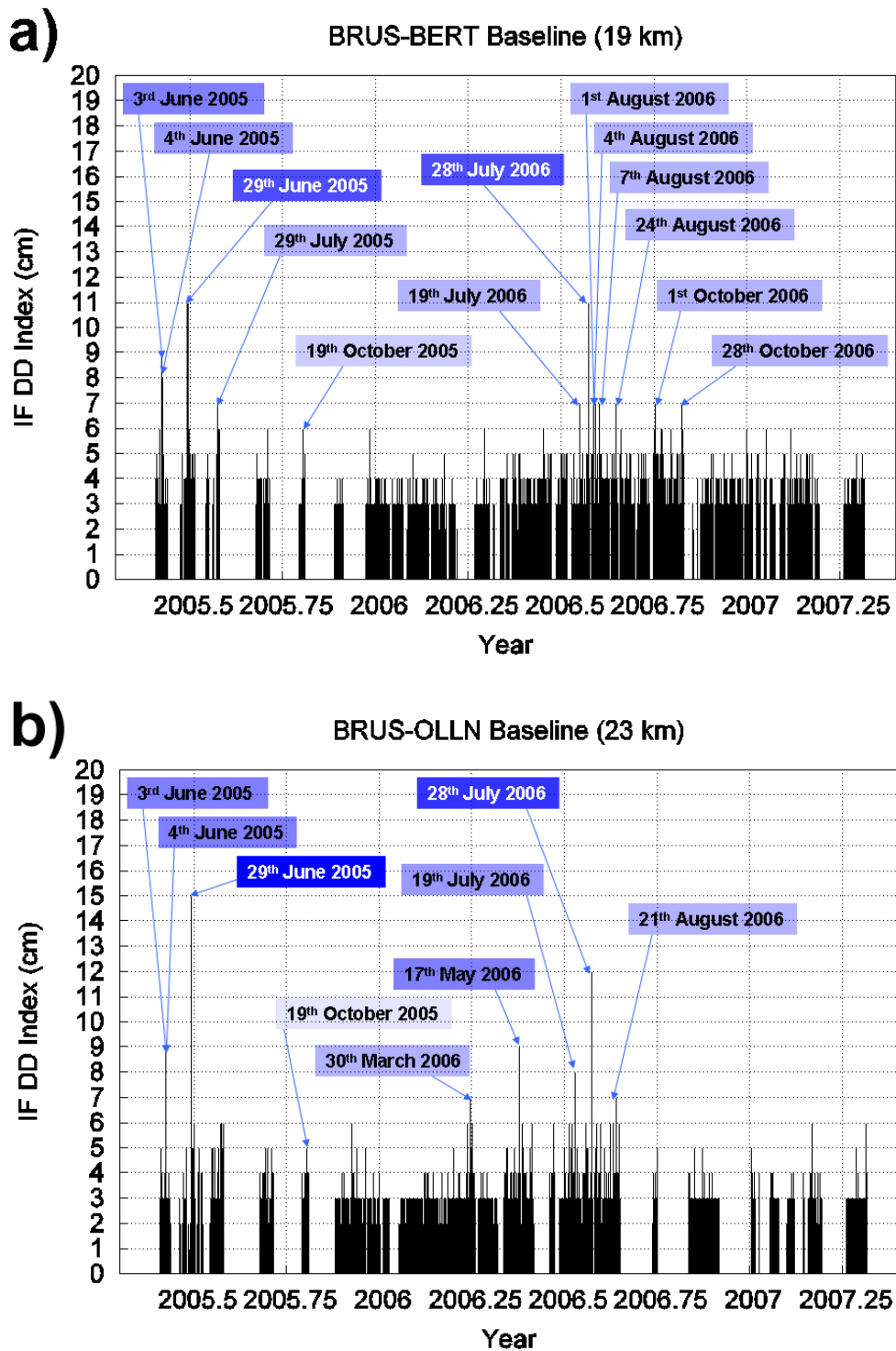


Figure 83: events detected by IF DD Index for a) BRUS-BERT baseline; b) BRUS-OLLN baseline

For both baselines we can see that the most important events are the rainfall of the 29th June 2005 and the super-cell formation of the 28th July 2006. These events have been studied section 4.1. In figure 83, we show the dates where events with IF DD Indexes larger or equal to 7 cm are detected, except for the 19th October 2005 event presented section 4.1 (where the data from the whole BDN were available).

We present a validation of the major events shown in figure 83.

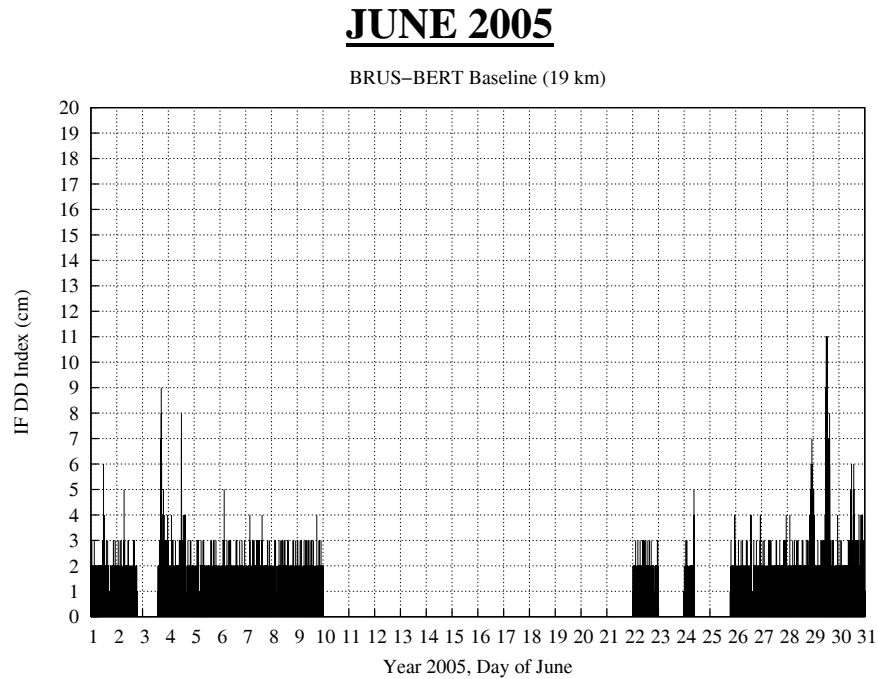


Figure 84: monthly IF DD Index of tropospheric activity of BRUS-BERT baseline (June 2005).

June 2005 is the most active period of study for the troposphere from 2005 to 2007. In figure 84, 5 days present IF DD Index larger than 6 cm (DOY 154, 155, 179, 180 and 181):

The 3rd JUNE (17H30)

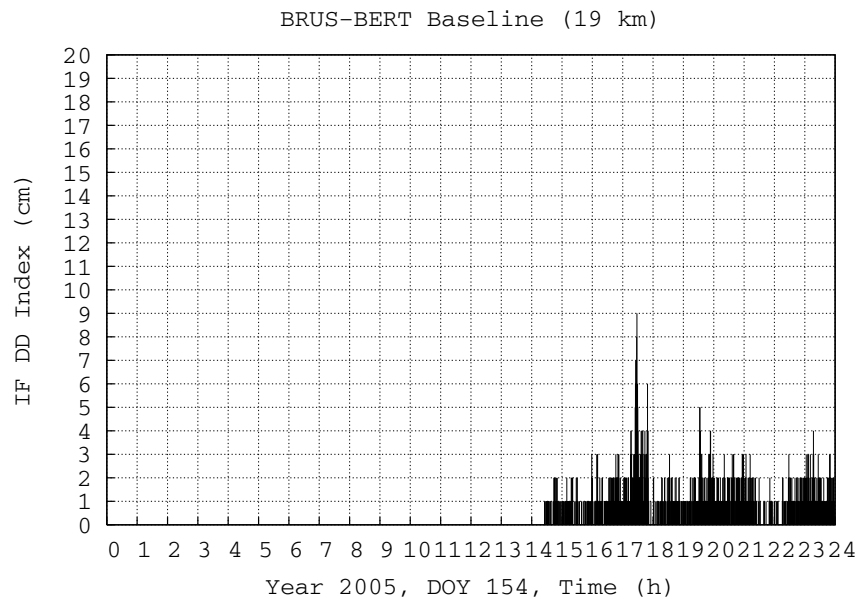


Figure 85: daily IF DD Index of tropospheric activity of BRUS-BERT baseline (29th June 2005).

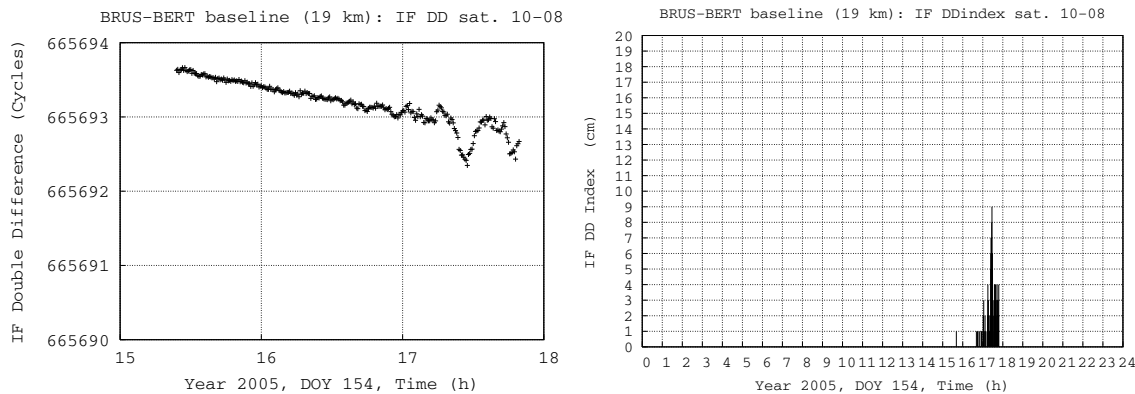


Figure 86: IF Double Difference and tropospheric index of activity of BRUS-BERT baseline the 3rd June 2005 for couple of satellites 10-08.

On June 3rd 2005, tropospheric activity is characterized by an IF DD Index of 9 cm for the couple 10-08 of satellites (Fig. 85 and 86). Indexes of 6 cm are found for satellites pairs 10-28 and 10-29. Index of 4 cm is found for the couple 10-26. The skyplot of satellites trajectories (Fig. 87) shows that from 17H to 18H UTC the elevation of satellite 10 ranges from 50° to 20° (which corresponds to a tropospheric layer ranging from 7.5 km to 3.5 km) with an azimuth ranging from 190° to 180° (south direction). Satellite 29 passes close to the zenith direction; satellite 26 flies with about 60° of elevation in the west direction at 17H30 UTC. Satellites 28 and 08 are in the east direction with respectively 55° and 40° of elevation at 17H30 UTC. We can not conclude about the localization of tropospheric activity detected from satellites signals. In fact the detailed analysis of this case would require to use another strategy to form DD: in our RTK-architecture, we are using the method of the reference satellite. That means that we would need to consider all possible couples of satellites available to characterize tropospheric structures detected by IF DD Index. Nevertheless, radar imaging shows there is indeed tropospheric activity when IF DD Index detects activity (Fig. 88).

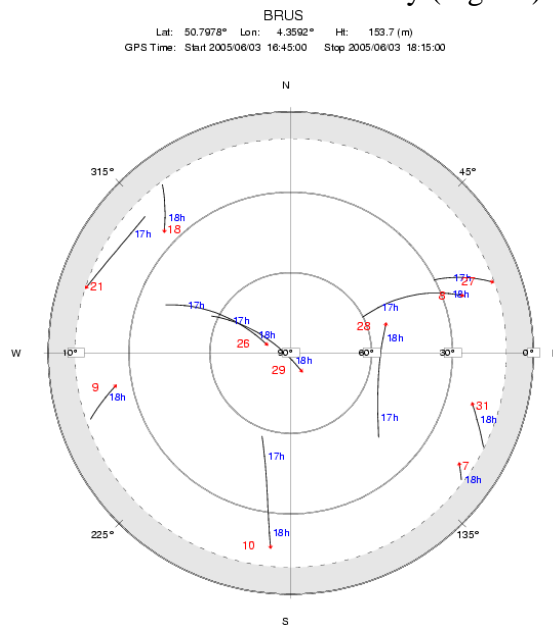


Figure 87: skyplot of visible satellites from BRUS station between 16H45 UTC and 18H15 UTC.

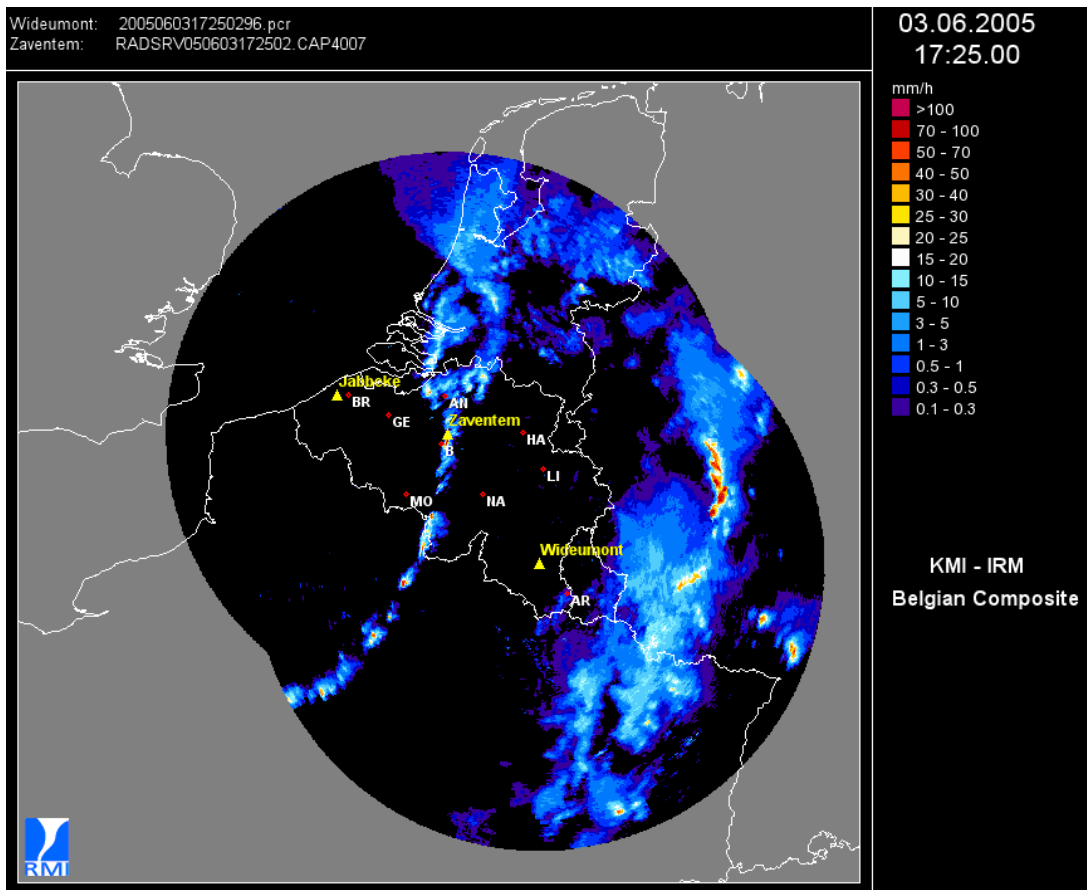


Figure 88: Belgian composite radar imaging of precipitations DOY 154 of 2005 at 17H25 UTC.

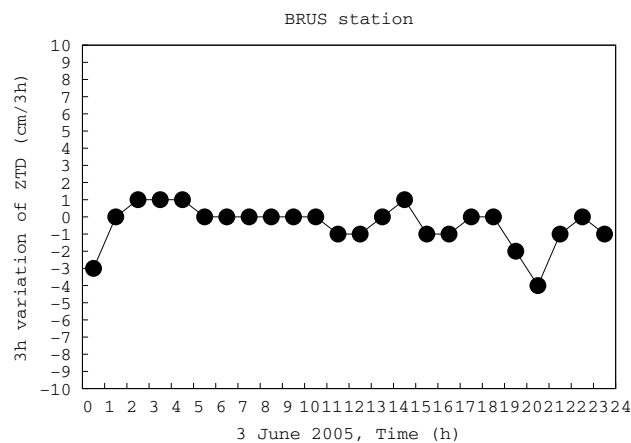


Figure 89: temporal ZTD gradient index (expressed in cm/3h) at BRUS station DOY 154 of 2005 (the 3rd June).

3 hourly variation of ZTD (Fig. 89) at BRUS station does not allow to detect the occurrence of small-scale tropospheric structure at 17H30 UTC, but clearly radar imagery (Fig. 88) validates the activity detected by IF DD Index. The mean time and space averages inherent to ZTD's do not allow to detect this tropospheric activity.

The 3rd JUNE (19h30)

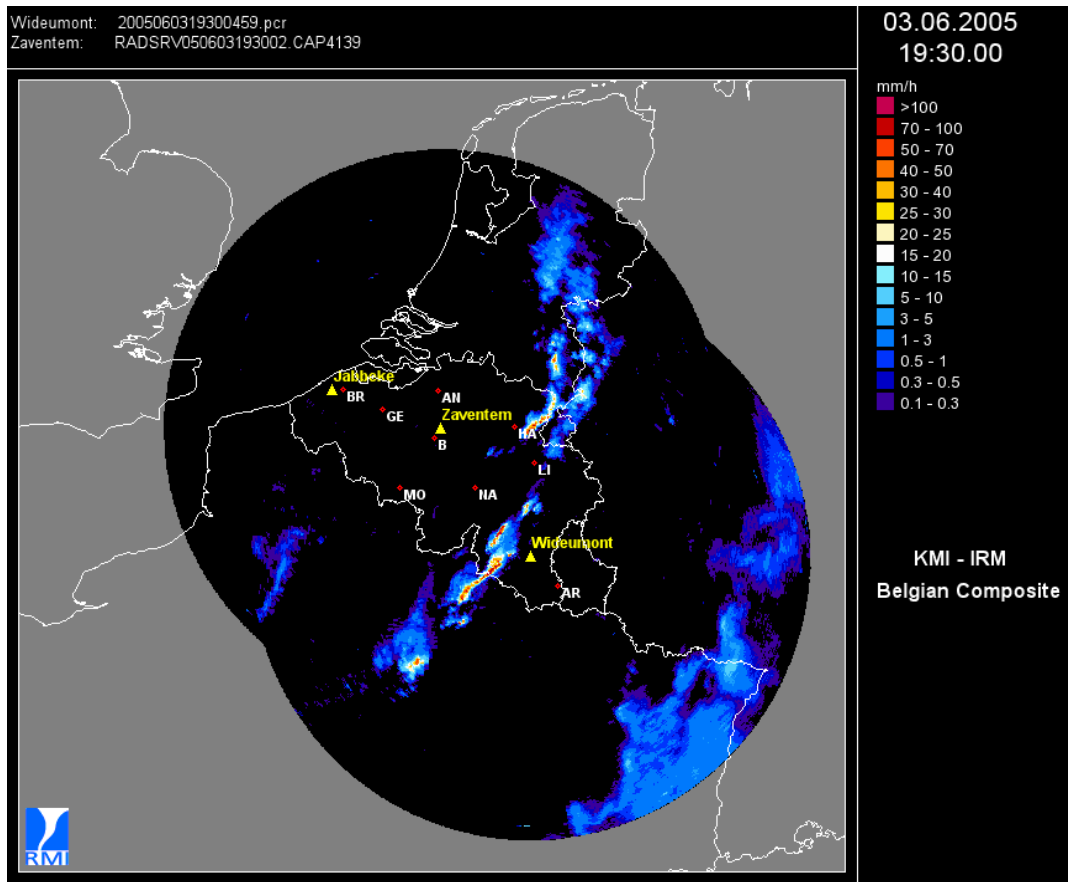


Figure 90: Belgian composite radar imaging of precipitations DOY 154 of 2005 at 19H30 UTC.

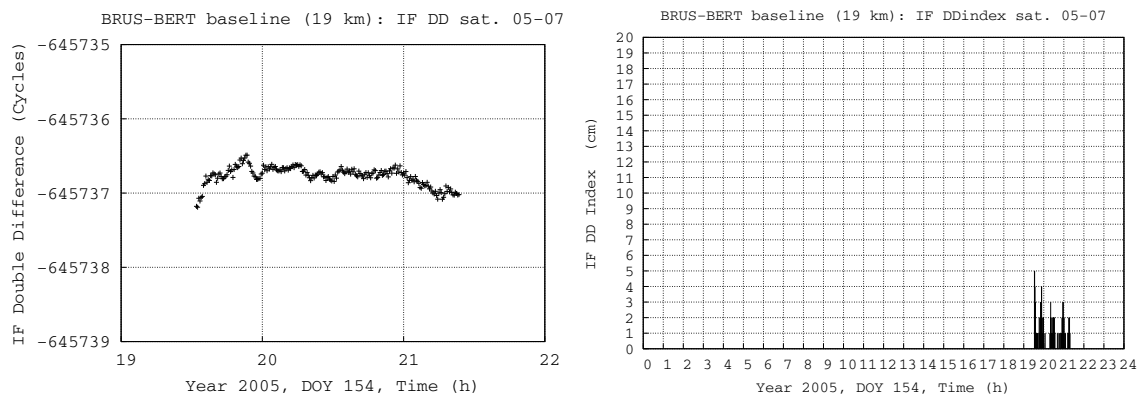


Figure 91: IF Double Difference and tropospheric index of activity of BRUS-BERT baseline the 3rd June 2005 for couple of satellites 05-07.

Tropospheric activity detected by IF DD Index at 19H30 UTC (Fig. 91) is not the result of hydrometeors (see radar imaging figure 90), but time-series of ZTD at BRUS, DENT, DOUR and WARE stations show that tropospheric activity appears from west to east over BRUS station (Fig. 92 on the left) justifying the fact that a water vapour layer flies over *Brussels*.

At 19H UTC, the skyplot of satellites trajectories (Fig. 93) shows that horizontal gradients from ZTD ($\overrightarrow{Grad}^{ZTD}$) points the azimuth direction of satellite 05 (figure 92 on the right). Tropospheric activity detected by IF DD Index (Fig. 91) is induced by a bubble of water vapour which has travelled from west to east over Belgium in direction of satellite 05 at 19H UTC .

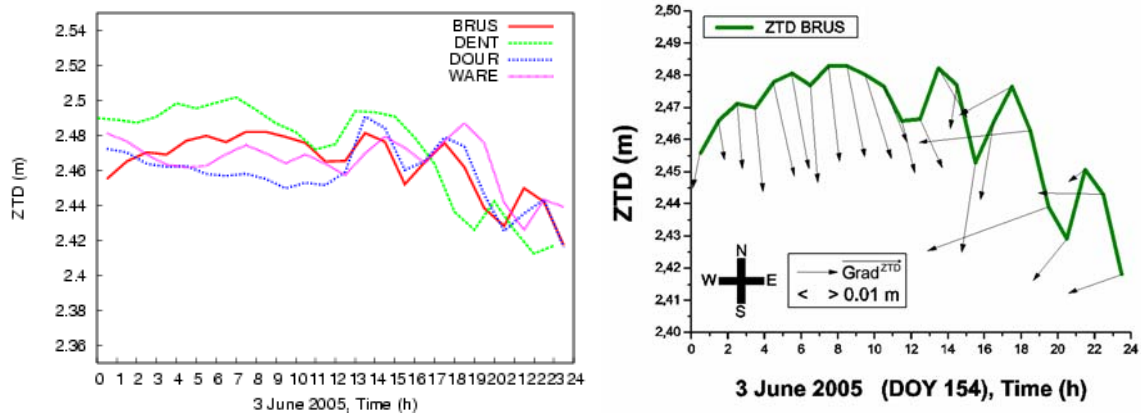


Figure 92: ZTD time-series DOY 154 of 2005 for BRUS, DENT, DOUR and WARE stations (on the left); horizontal gradients (deduced from ZTD of EUREF network) superposed to the ZTD time-series of BRUS station.

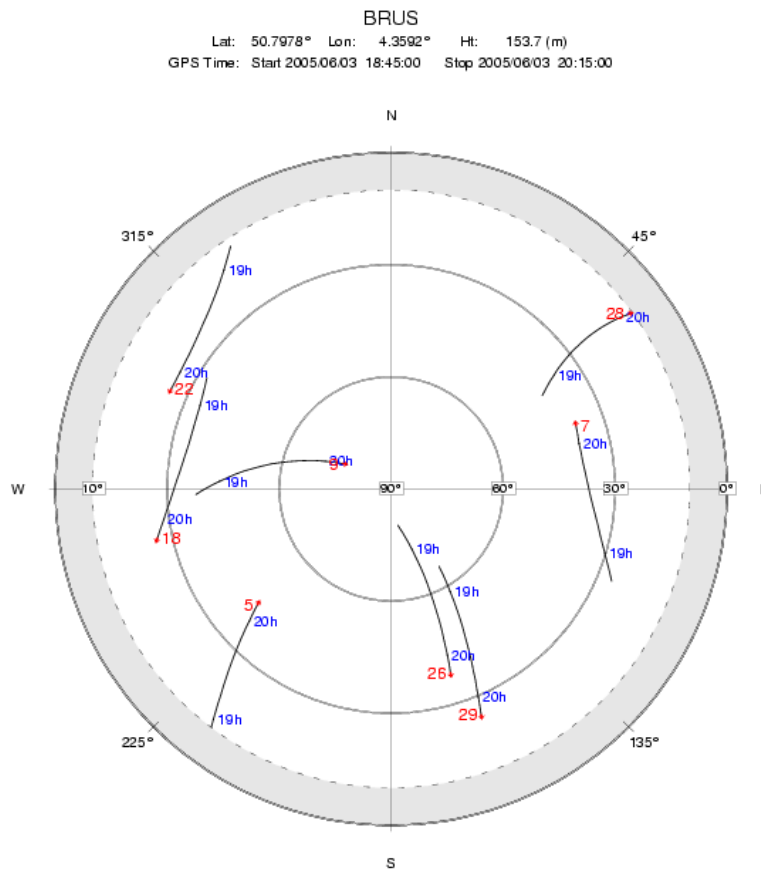


Figure 93: skyplot of visible satellites from BRUS station between 18H45 UTC and 19H15 UTC.

The 29th JUNE

A strong tropospheric activity can be observed around BRUS station between 11H and 16H UTC (see radar imaging figure 97 and 98). Daily IF DD Index shows tropospheric activity during the same period (Fig. 94). ZTD imaging the 29th June 2005 at 14H30 UTC (bias to the mean value during the period of study, *i.e.* from the 25th June to the 1st July 2005) shows that a tropospheric structure has taken place around BRUS and BERT stations (Fig. 95).

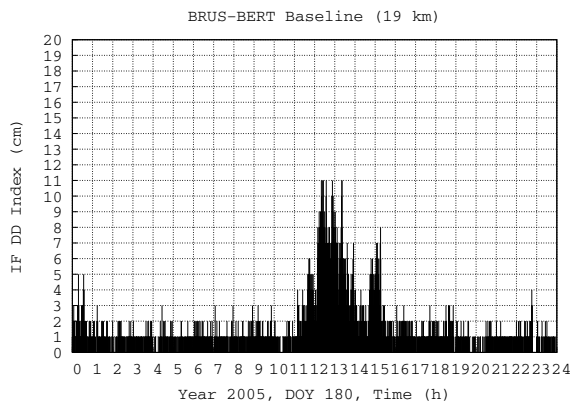


Figure 94: daily IF DD Index of tropospheric activity of BRUS-BERT baseline (29th June 2005).

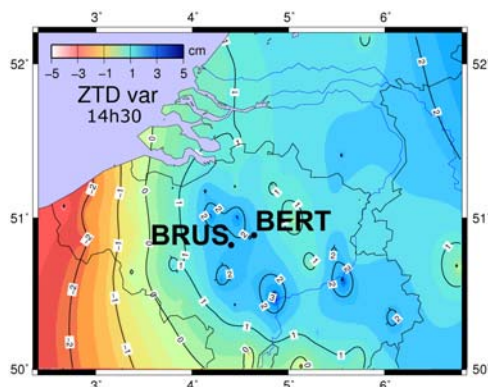


Figure 95: ZTD imaging (bias to the mean value) at 14H30 UTC the 29th June 2005.

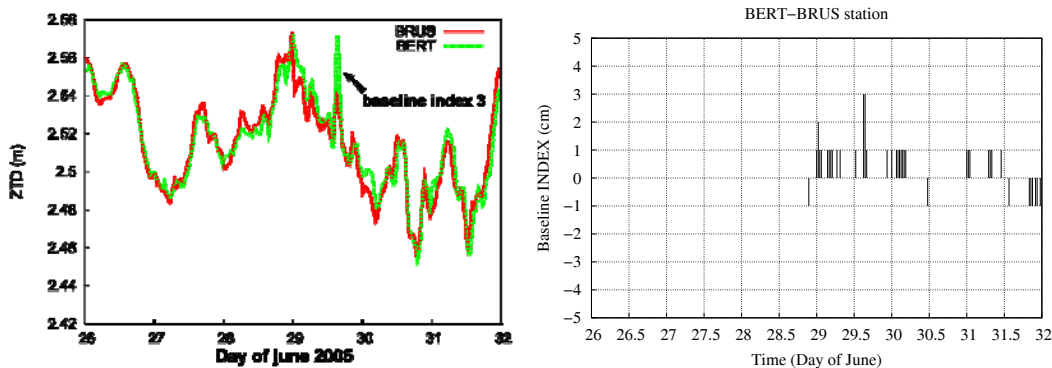


Figure 96: ZTD times-series for BRUS and BERT stations from the 26th June 2005 to the 31st June 2005 (on the left); Bias between ZTD at BRUS station and ZTD at BERT station, *i. e.* Baseline INDEX expressed in cm (on the right).

In that case, Baseline index (bias of ZTD between two stations figure 96) represents an indication of the tropospheric activity detected by daily IF DD Index (Fig. 94).

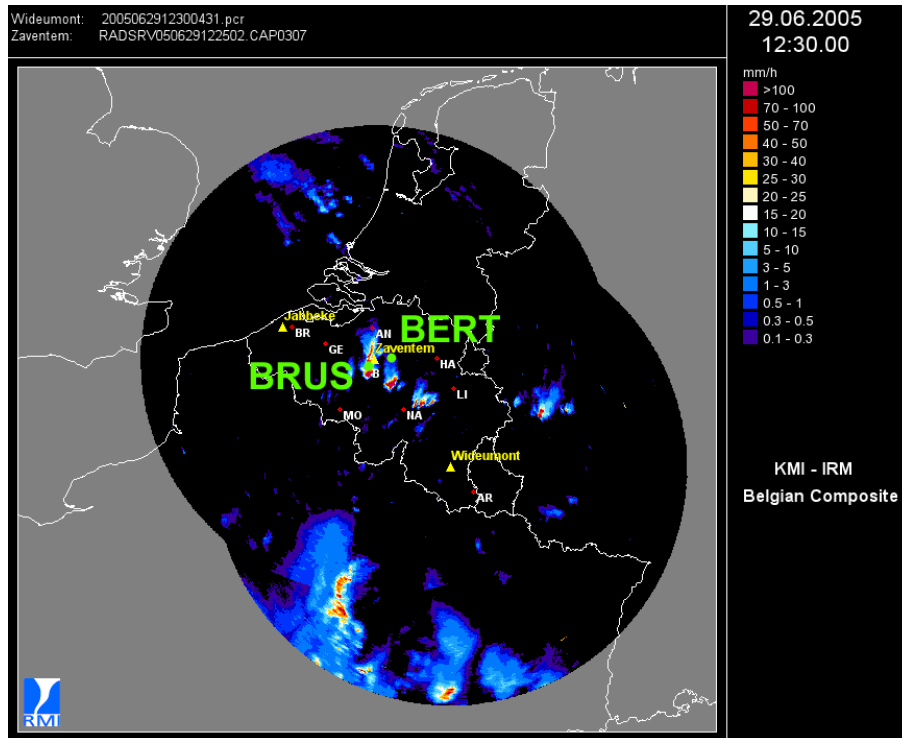


Figure 97: radar imaging of precipitations at 12H30 UTC the 29th June 2005.

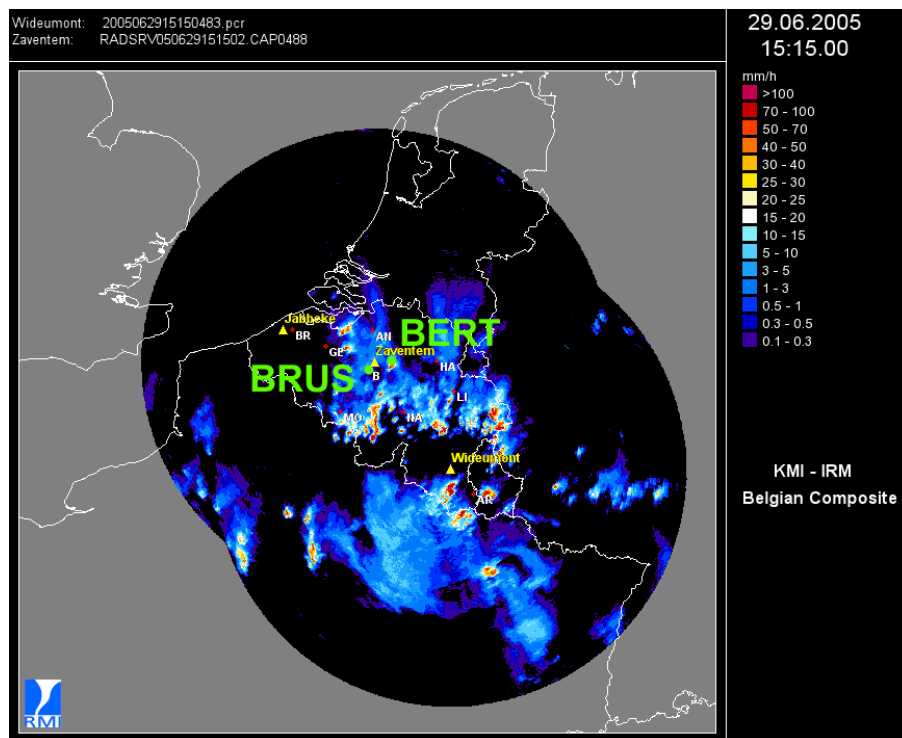


Figure 98: radar imaging of precipitations at 15H15 UTC the 29th June 2005.

In Figure 97 and 98, tropospheric activity is clearly detected by radar at 12H30 UTC and at 15H15 UTC (a strong thunderstorm flies over BRUS station at 12H30 UTC and over BERT station at 15H15 UTC). DD-analysis shows the following index of tropospheric activity: up to 11 cm between 12H15 and 13H30 UTC and up to 9 cm at 15H15 UTC (Fig. 94).

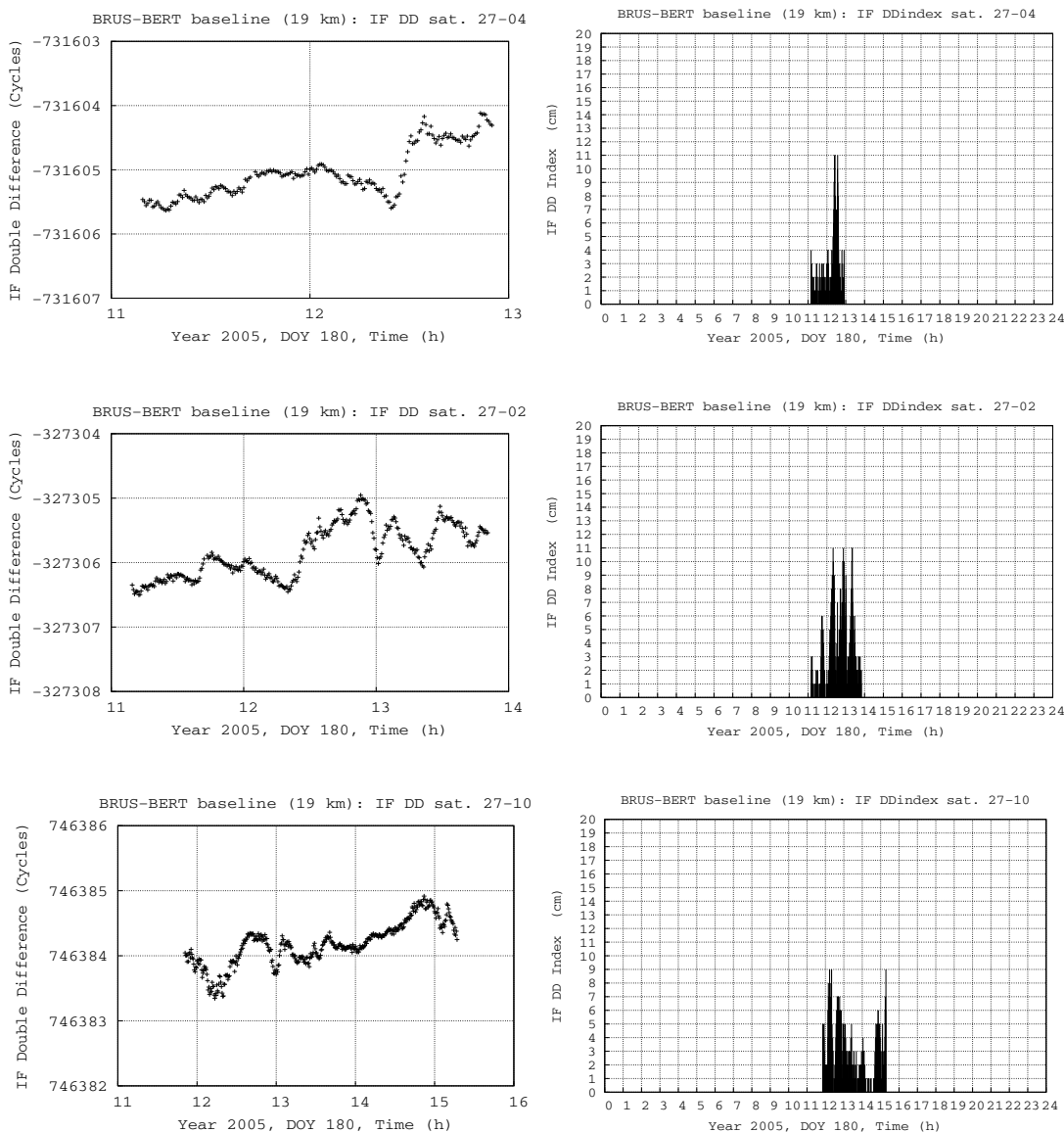


Figure 99: IF Double Difference and tropospheric index of activity of BRUS-BERT baseline DOY 180 of 2005 (couples of satellites 27-4, 27-2 and 27-10).

The storm is detected by baseline index (larger values of ZTD for BERT station at 14H UTC due to the thunderstorm which occurred at 15H UTC), but baseline index does not show important activity at 12H30 while tropospheric activity is clearly detected by radar. Time and space averages of ZTD measurements do not detect very small-scale structures, but IF DD Indexes detect these structures.

The 17th MAY 2006 (23h30)

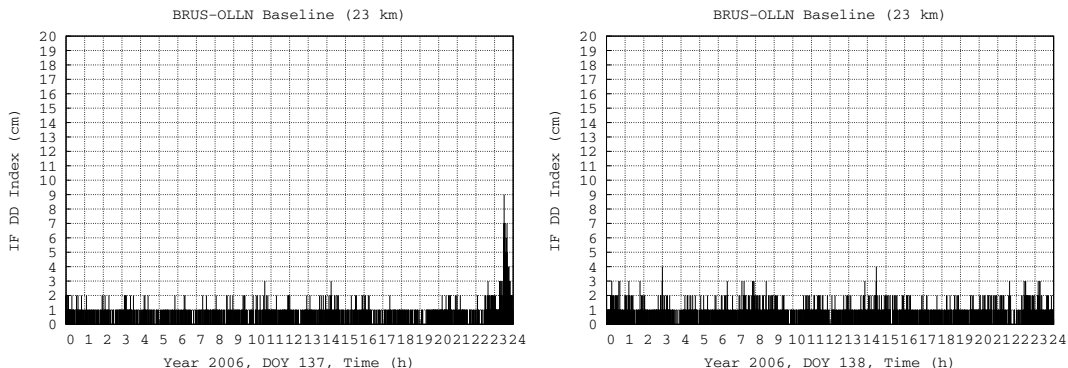


Figure 100: daily IF DD Index of tropospheric activity of OLLN-BRUS baseline (17 and 18 May 2006).

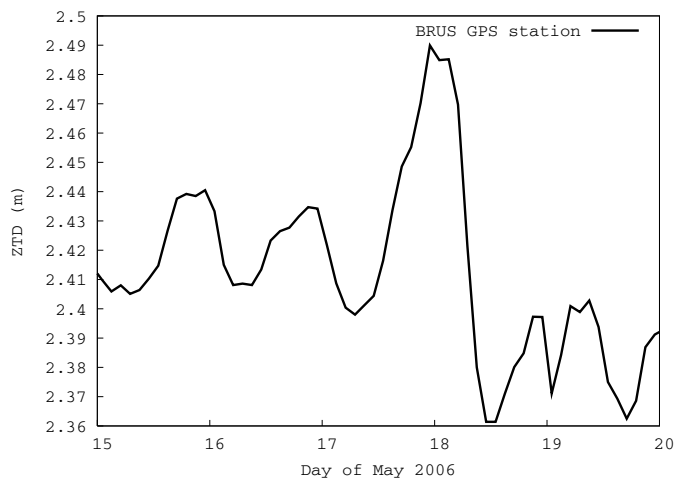


Figure 101: ZTD time-series from BRUS stations from the 15th May to the 20th May 2006.

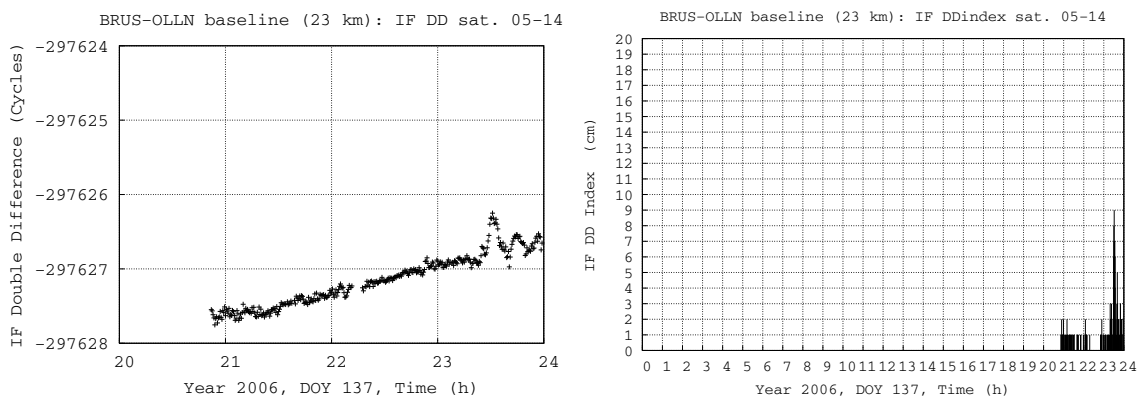


Figure 102: IF Double Difference and tropospheric index of activity of BRUS-OLLN baseline DOY 137 of 2006 (the 17th May) for the couple of satellites 05-14.

Tropospheric activity is clearly identified by ZTD measurements at BRUS station during the night of 17th to the 18th May 2006 (see figure 101). A strong loading period has been observed during the afternoon and the evening of the 17th May. At 04H00 UTC on 18th May 2006, ZTD (and of water vapour content above *Brussels*) starts to decrease. This tropospheric activity is validated by radar precipitations imaging on 17th May 2006 at 23H30 UTC (Fig. 103). At 00H00 UTC the 18th May 2006, IF DD Index are smaller than 4 cm (Fig. 100). We can see on radar imaging (Fig. 104) that rainfall cells are not any more above BRUS and OLLN stations. In figures 100 and 102, the change of tropospheric refractivity and IF DD Index of 9 cm at 23H30 UTC the 17th May 2006 has been induced by hydrometeors and water vapour and not only by water vapour.

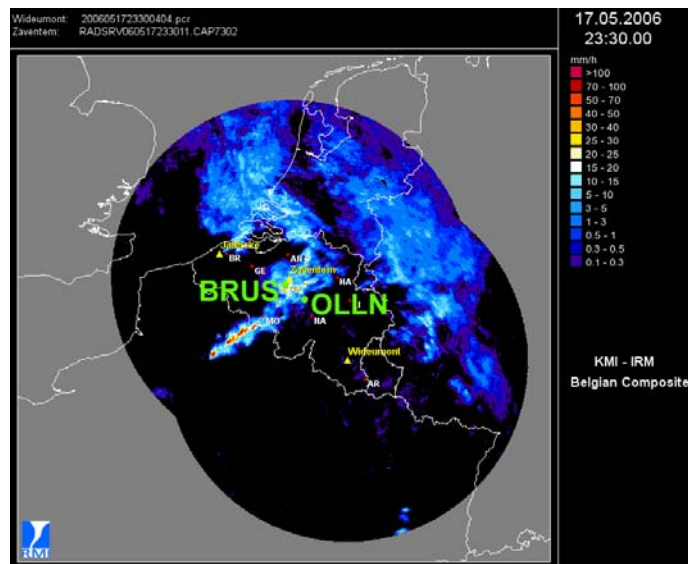


Figure 103: radar imaging of precipitations at 23H30 UTC the 17th May 2006.

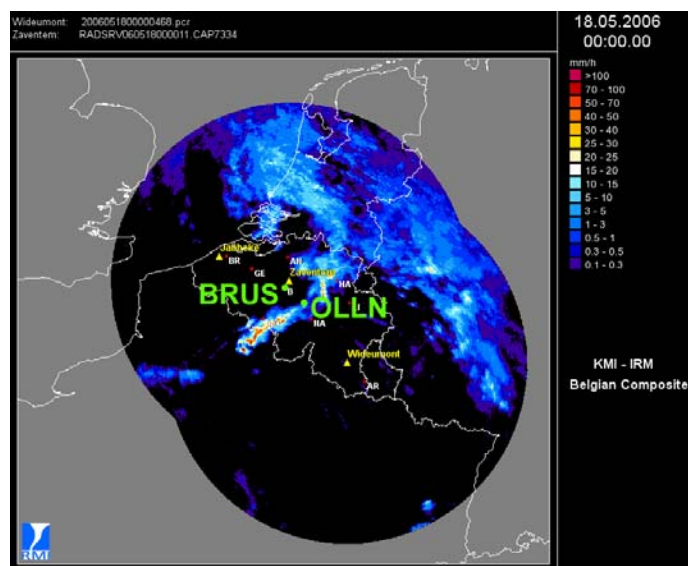


Figure 104: radar imaging of precipitations at 00H00 UTC the 18th May 2006.

The maximum IF DD Index (up to 9 cm) observed in our RTK-architecture the 17th May 2006 corresponds to the couple of satellites 05-14 at 23H30 UTC (see figure 102).

The 28th JULY 2006 (afternoon)

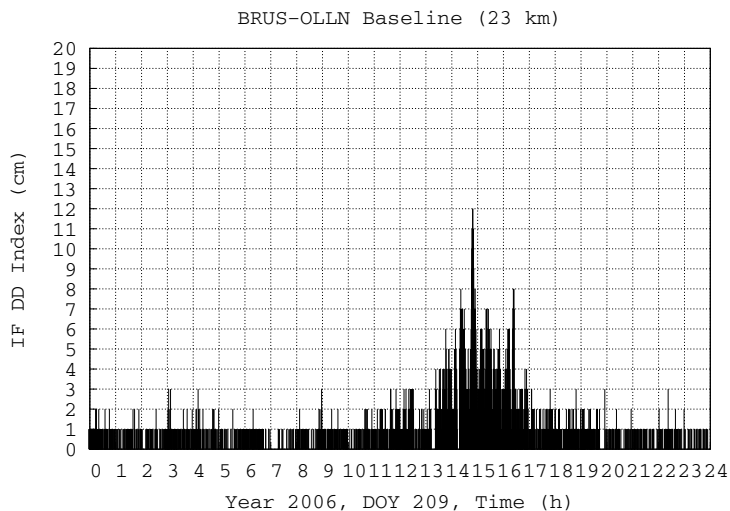


Figure 105: daily IF DD Index of tropospheric activity of OLLN-BRUS baseline (28th July 2006).

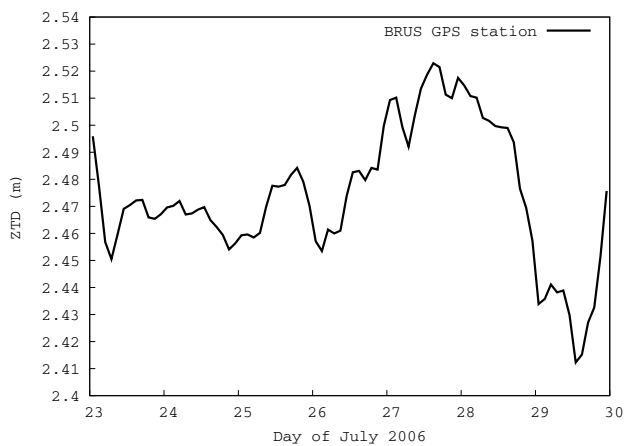


Figure 106: ZTD time-series from BRUS stations from the 23rd July to the 30th July 2006.

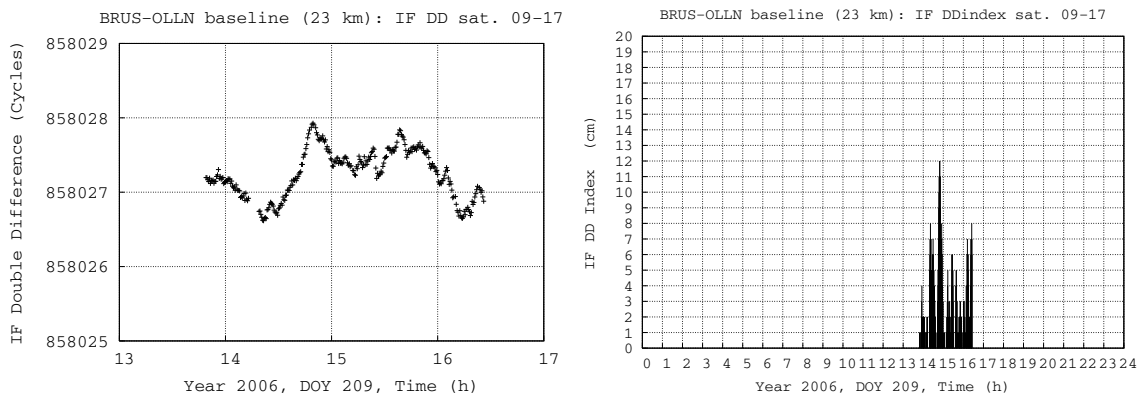


Figure 107: IF Double Difference and tropospheric index of activity of BRUS-OLLN baseline DOY 209 of 2006 (the 28th July) for the couple of satellites 09-17.

Formation of super-cells during the 28th July 2006 has been presented section 4.1. A strong tropospheric activity has also been observed around *Brussels* stations (see radar imaging figure 108), but this meteorological situation is very different of the previous. From the 26th July 2006 a large increase in ZTD is observed at BRUS station (loading period during two days, see figure 106). Note that the mean ZTD is 5 cm larger during the 28th July event than during the 17th May event (more humidity). The discharge of ZTD associated with precipitations has taken place during the afternoon of the 28th July 2006.

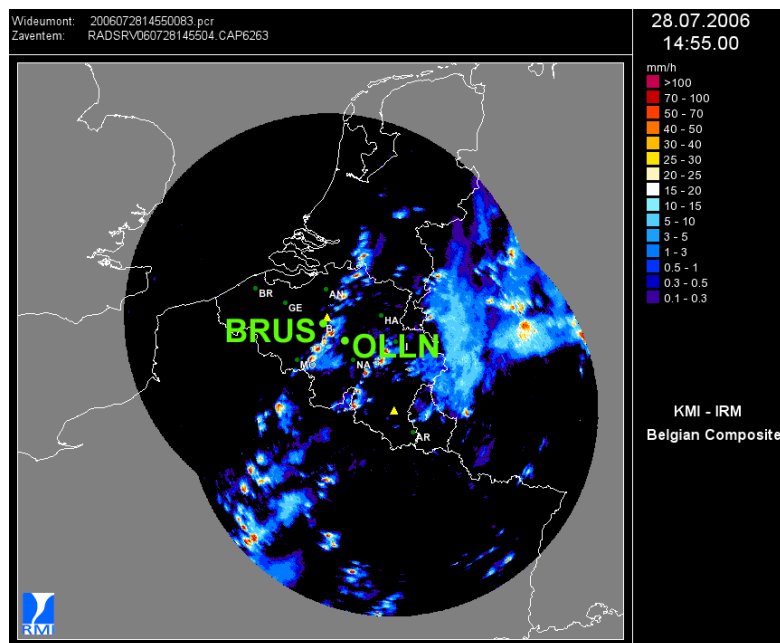


Figure 108: radar imaging of precipitations at 14H55 UTC the 28th July 2006.

In figure 105, the maximum IF DD Index (up to 12 cm) observed in our RTK-architecture the 28th July 2006 corresponds to the couple of satellites 09-17 around 15H UTC (Fig. 107).

Conclusion of this study

- The tropospheric activity detected by IF DD Index is validated for BRUS-BERT and BRUS-OLLN baselines from May 2005 to April 2007 based on ZTD and radar observations.
- The two strong rainfall events observed around *Brussels* from May 2005 to April 2007 (the 29th June 2005 event and the 28th July 2006 event) show the largest IF DD Index observed during these two years.
- The study of the 3rd June 2005 rainfall event shows that a bubble of water vapour was present in direction of satellite 05 at 19H UTC: our IF DD Index allows to detect such phenomena.
- For events described by IF DD Index larger than 7 cm, hydrometeors are present systematically above one of the two station of the considered baseline.

4.2.2 BREE-MEEU baseline from 1997 to 2007

Our IF DD Index has been validated for a period of two years and for two baselines. But are the occurrences of the different levels of IF DD Index during these two years representative? To answer to this question, knowing that no data from the BDN is available before 2003, we will study a baseline (smaller than 20 km to be sensitive to small-scale structures) for which data is available since 1997: BREE-MEEU baseline (7 km).

Following graphics (figures 109 to 119) presents monthly IF DD Index of tropospheric activity of BREE-MEEU baseline from July 1997 to May 2007. Let us note that periods where no index is shown correspond to periods where no data are available.

Figure 120 presents the IF DD Index for BREE-MEEU baseline from July 1997 to May 2007 and displays the main events detected on this period. As expected, we can see that major rainfall events with high tropospheric activities occur in summer. Days with IF DD Indexes larger than 9 cm are showed on figure 120.

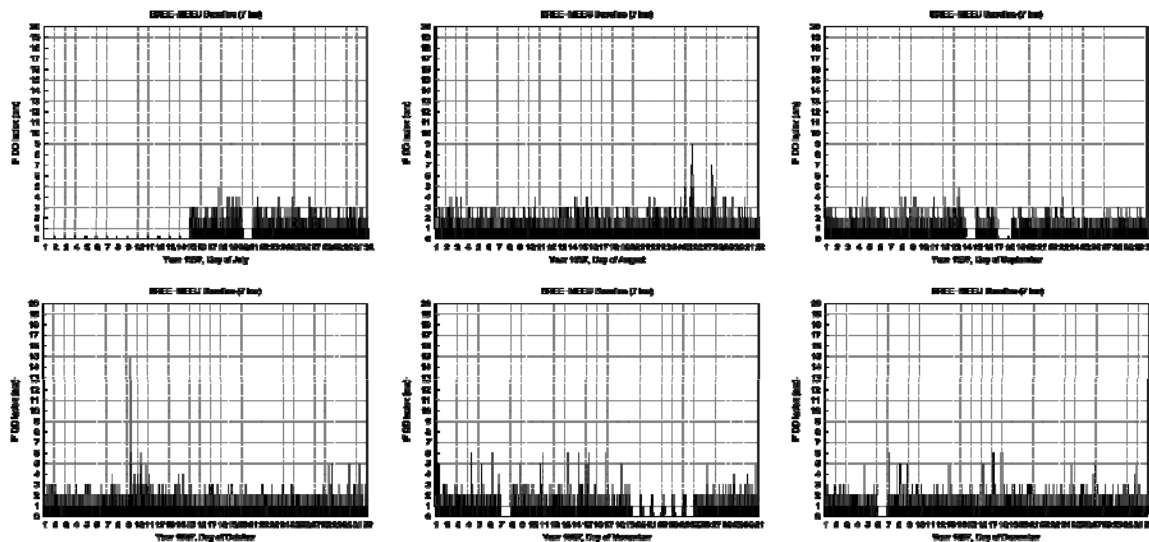


Figure 109: monthly IF DD Index of tropospheric activity of BREE-MEEU baseline (Year 1997).

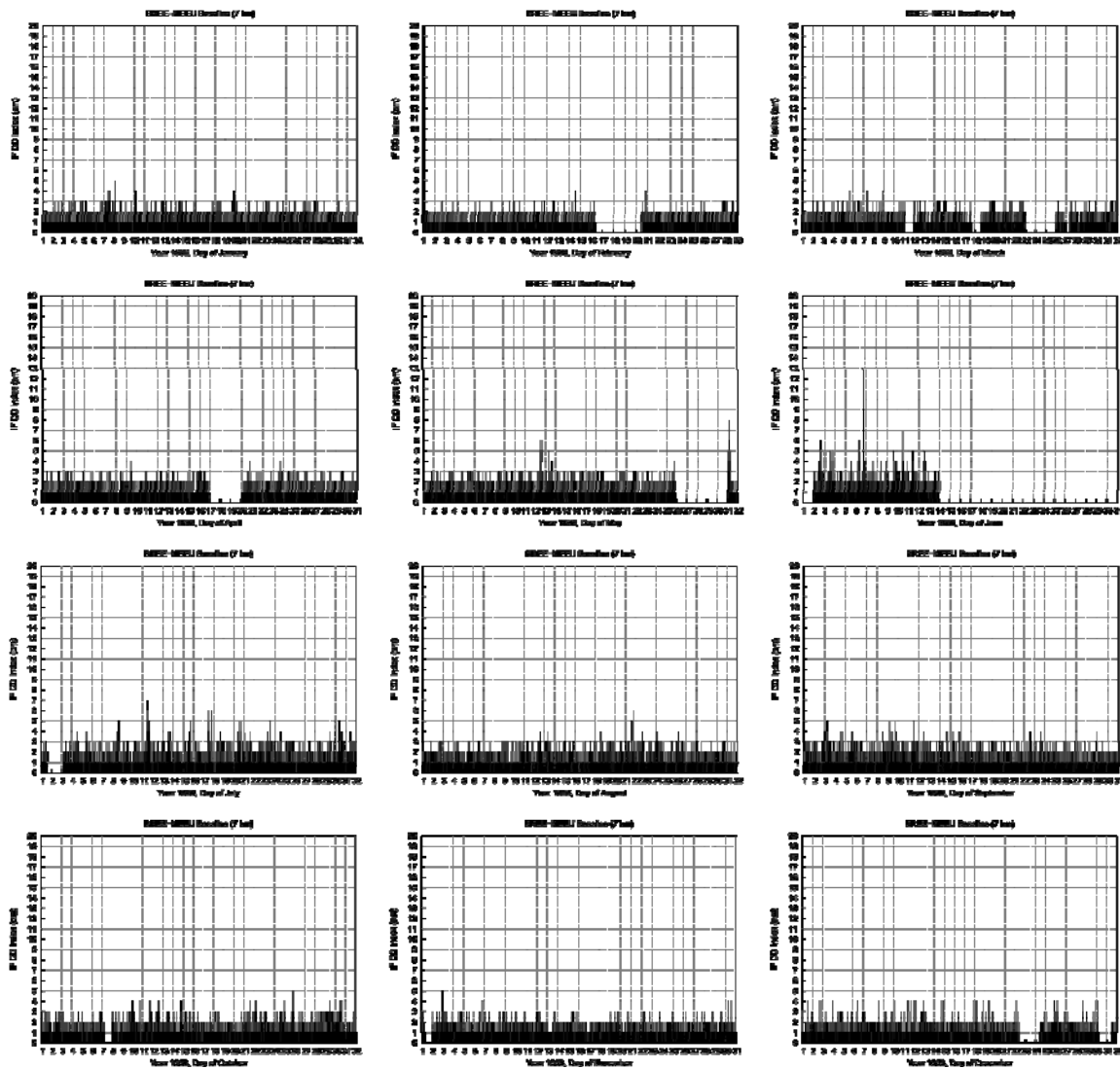


Figure 110: monthly IF DD Index of tropospheric activity of BREE-MEEU baseline (Year 1998).

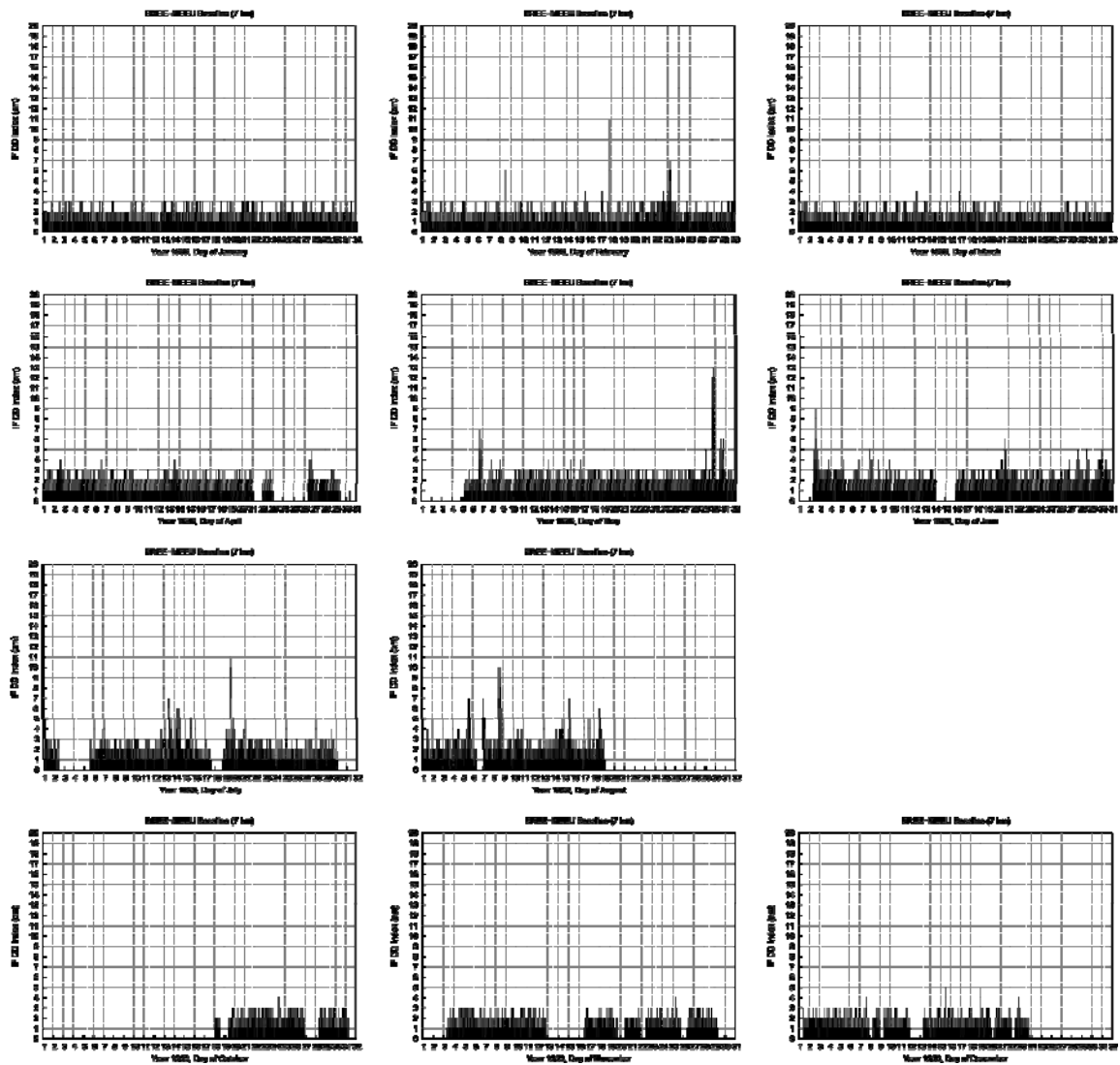


Figure 111: monthly IF DD Index of tropospheric activity of BREE-MEEU baseline (Year 1999).

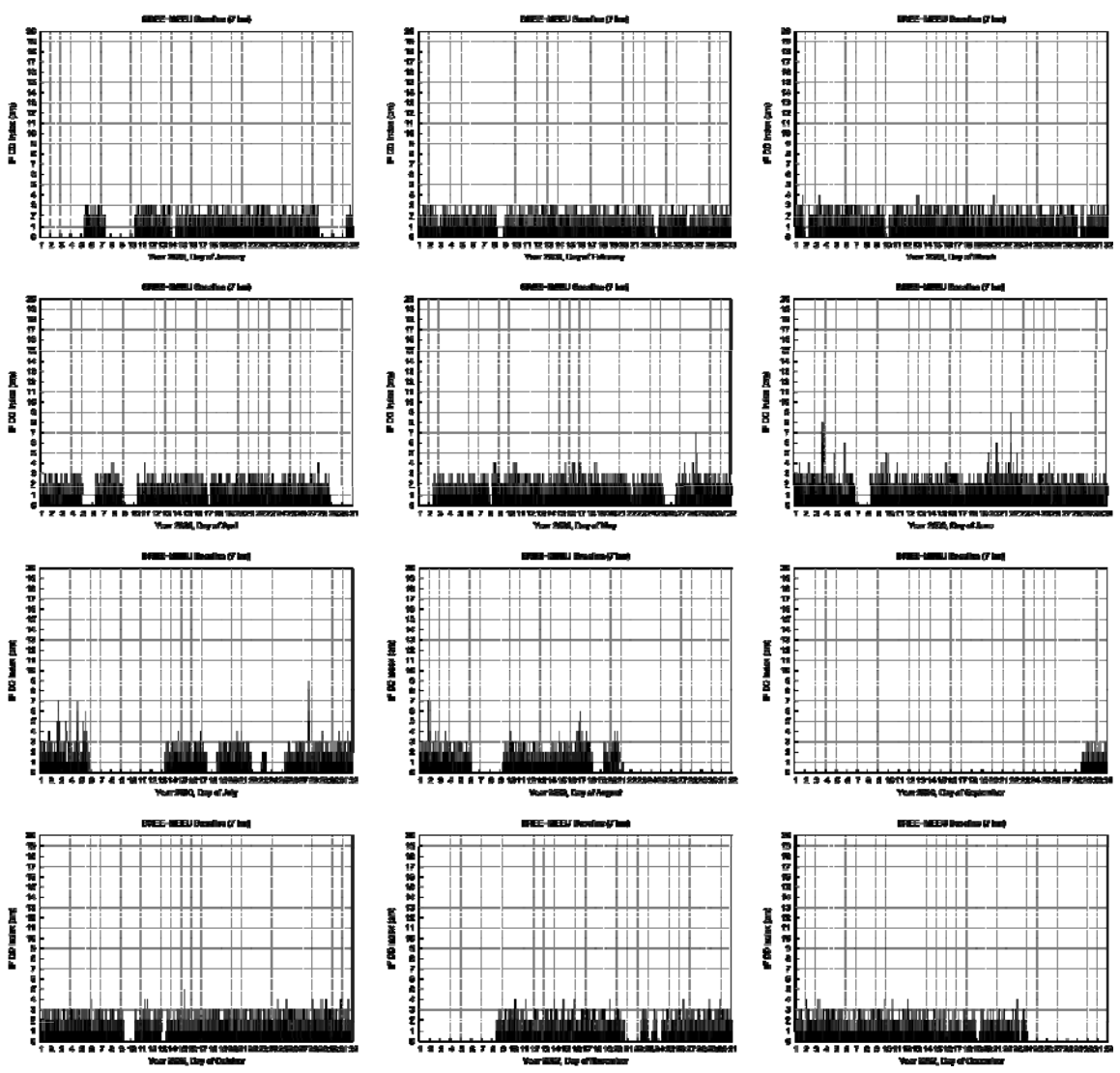


Figure 112: monthly IF DD Index of tropospheric activity of BREE-MEEU baseline (Year 2000).

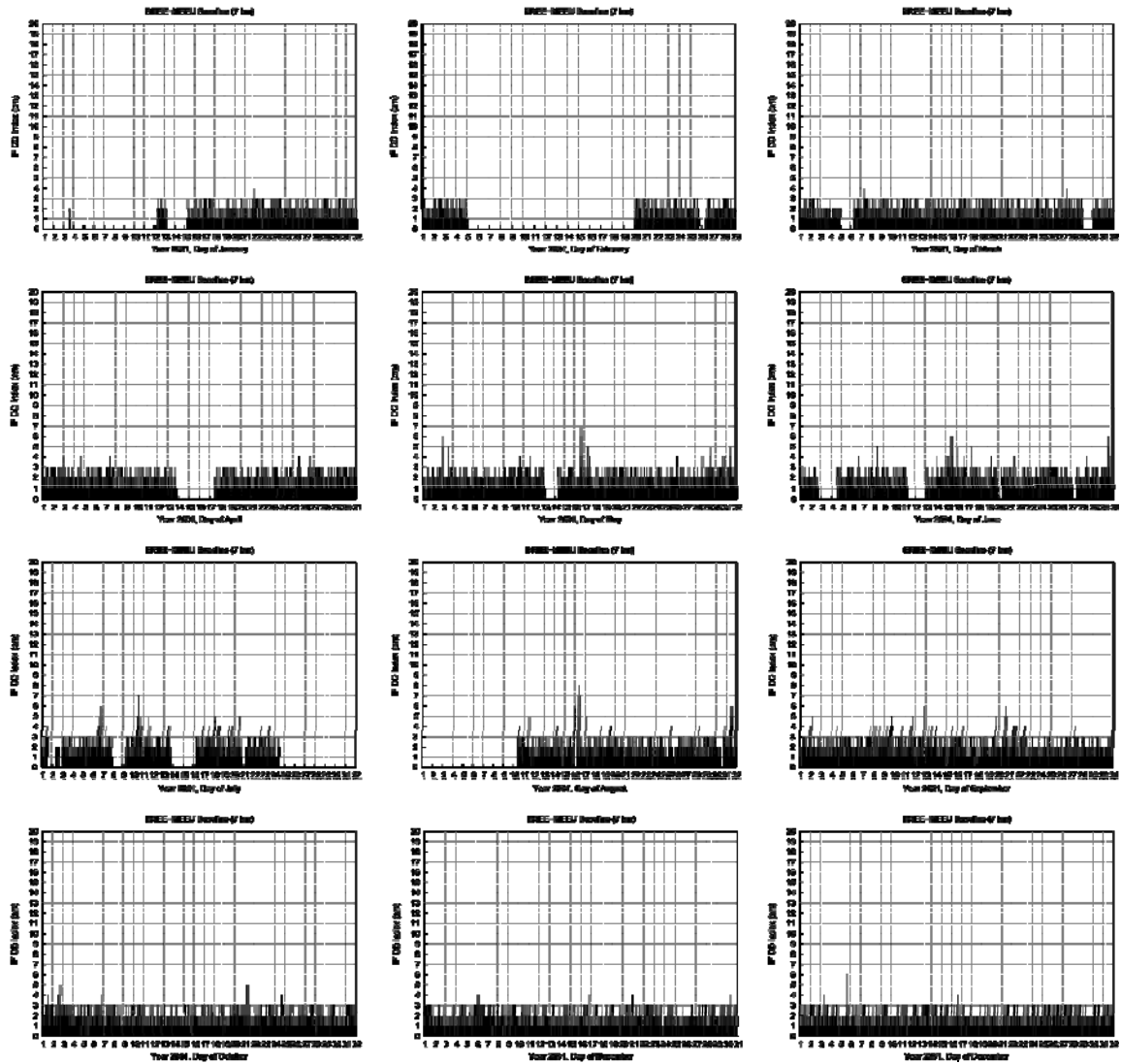


Figure 113: monthly IF DD Index of tropospheric activity of BREE-MEEU baseline (Year 2001).

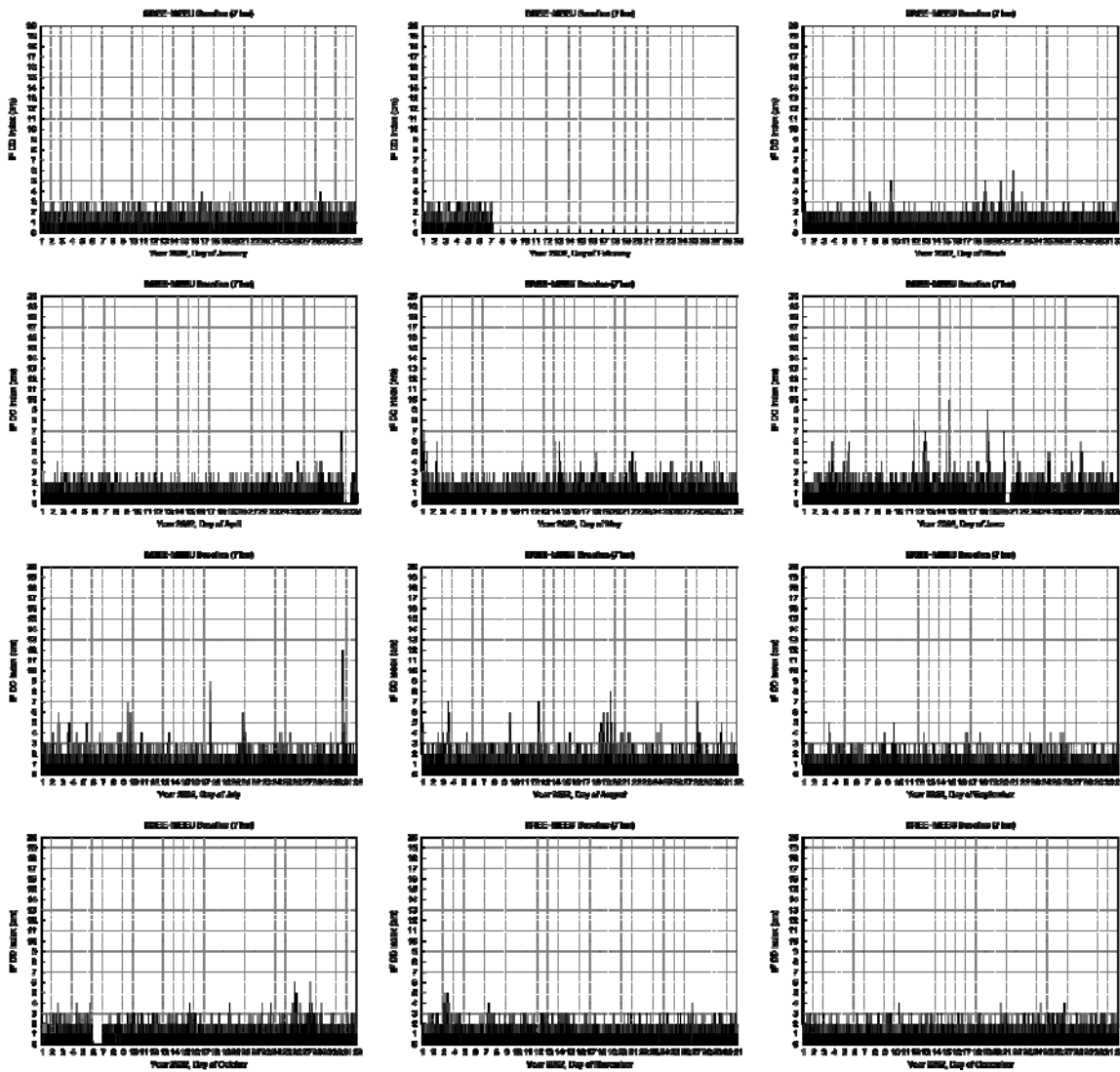


Figure 114: monthly IF DD Index of tropospheric activity of BREE-MEEU baseline (Year 2002).

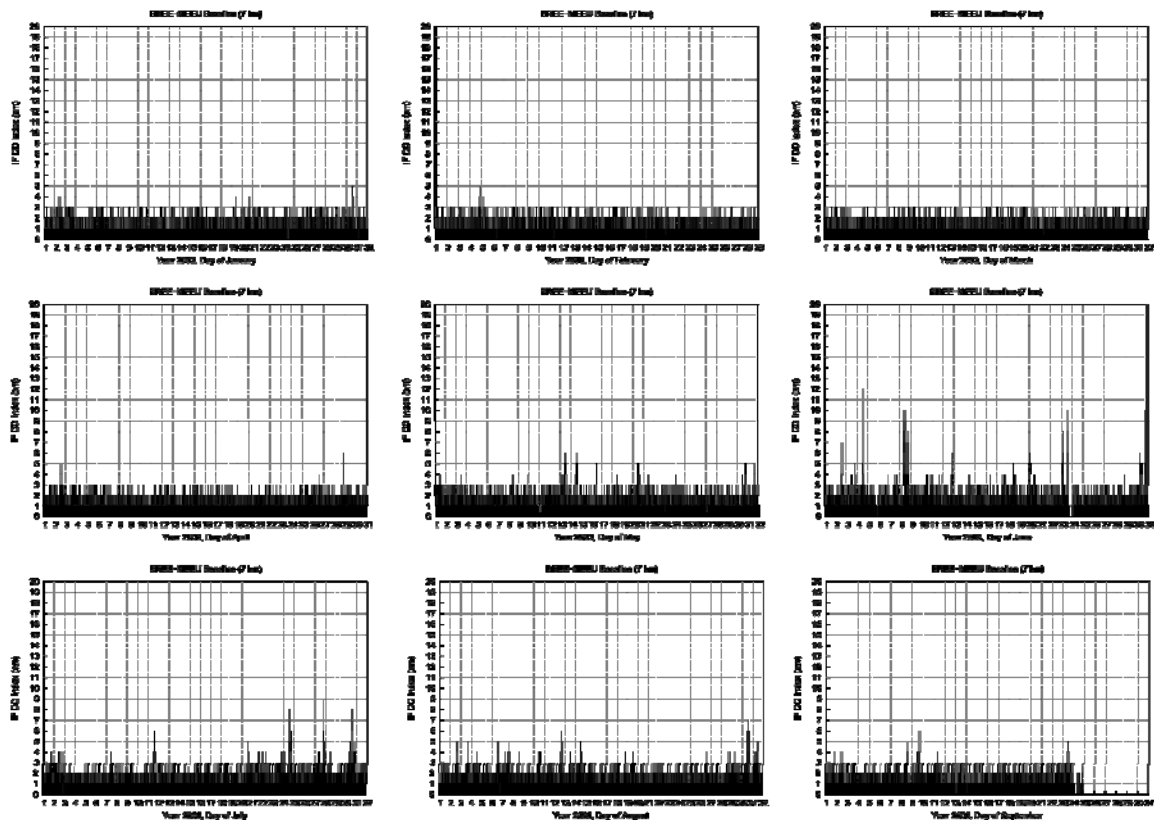


Figure 115: monthly IF DD Index of tropospheric activity of BREE-MEEU baseline (Year 2003).

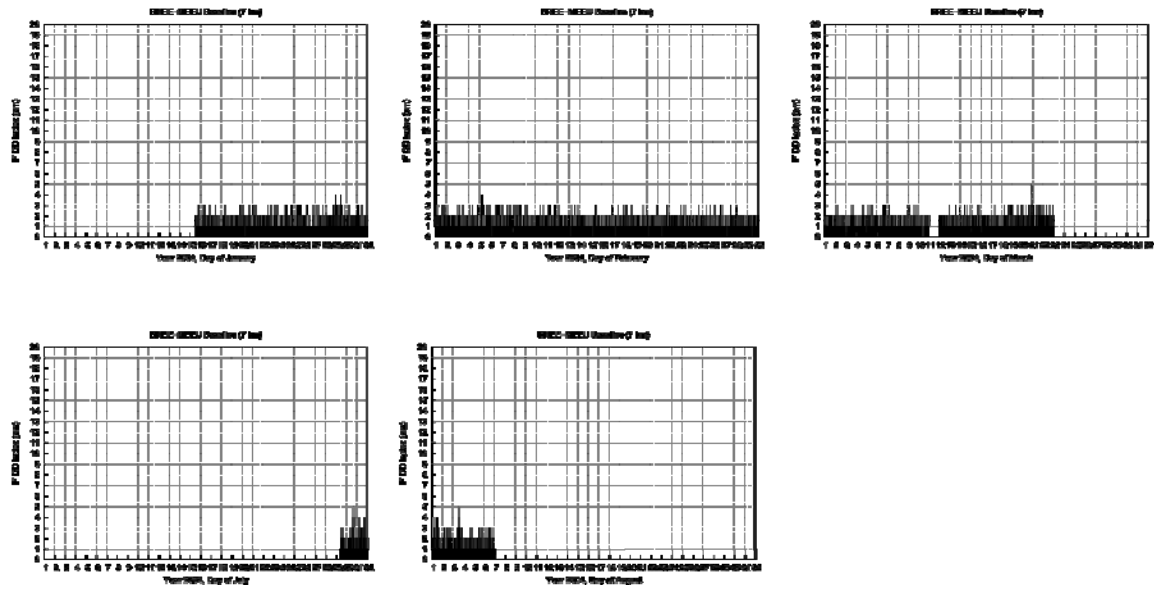


Figure 116: monthly IF DD Index of tropospheric activity of BREE-MEEU baseline (Year 2004).

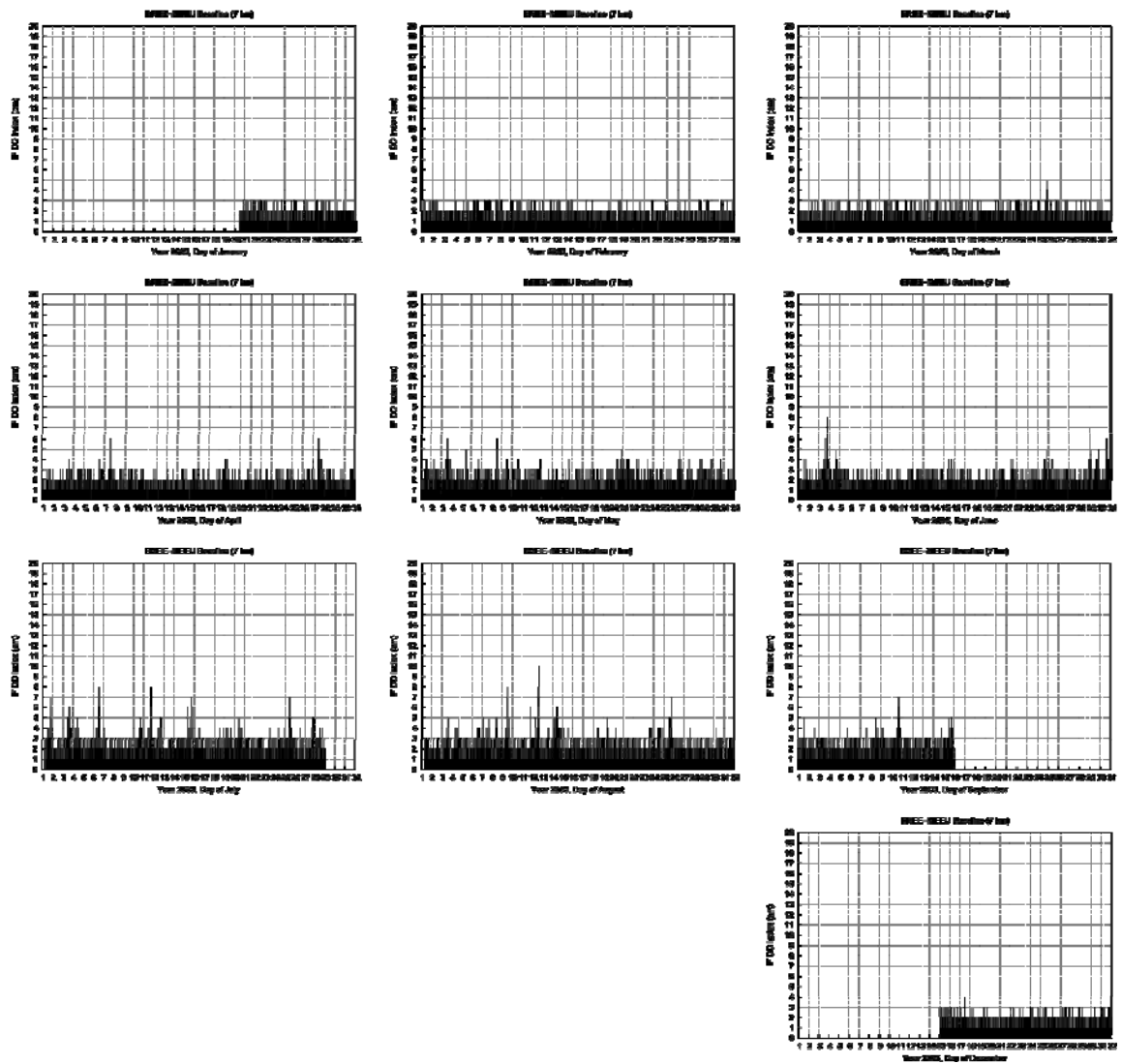


Figure 117: monthly IF DD Index of tropospheric activity of BREE-MEEU baseline (Year 2005).

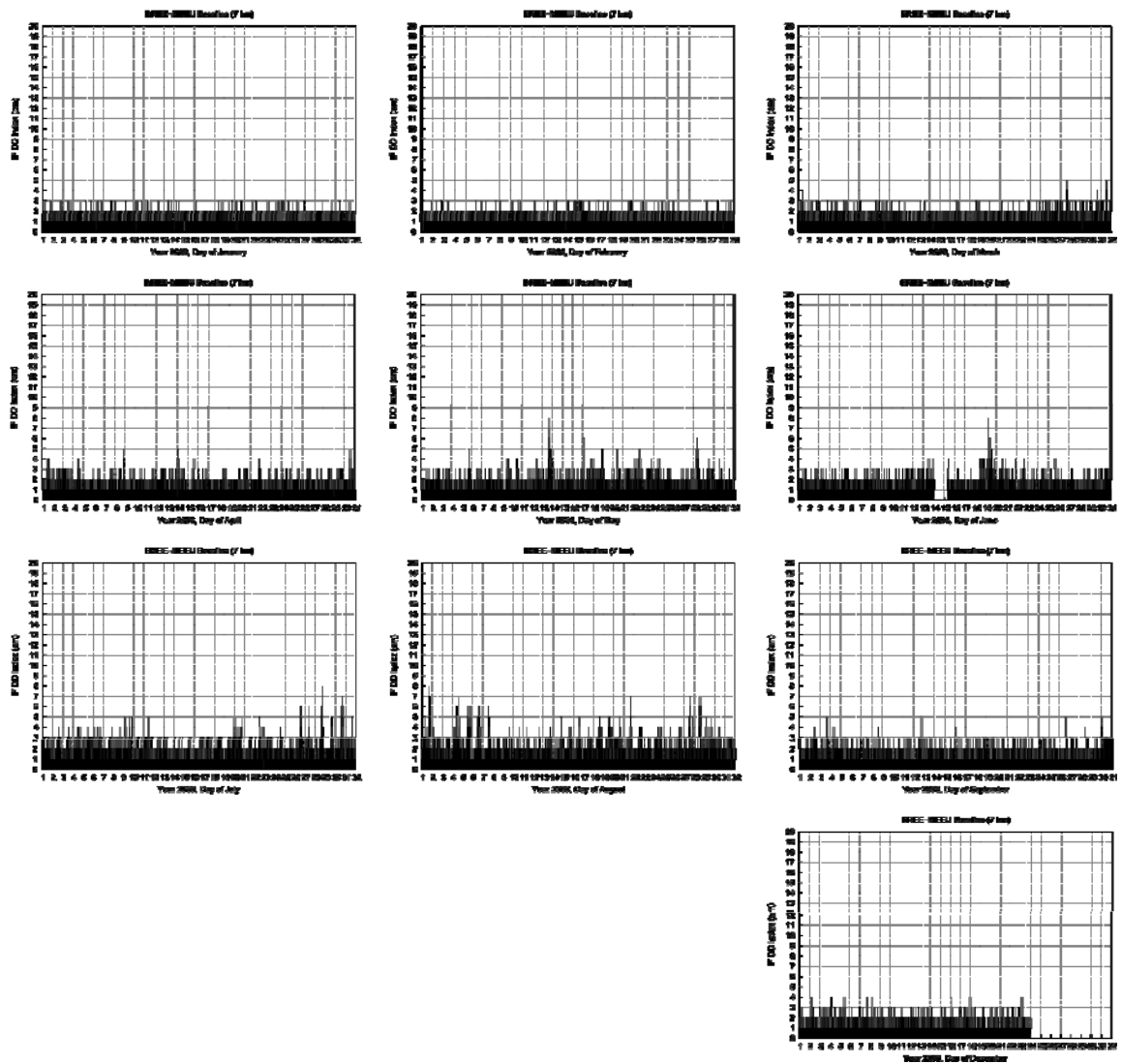


Figure 118: monthly IF DD Index of tropospheric activity of BREE-MEEU baseline (Year 2006).

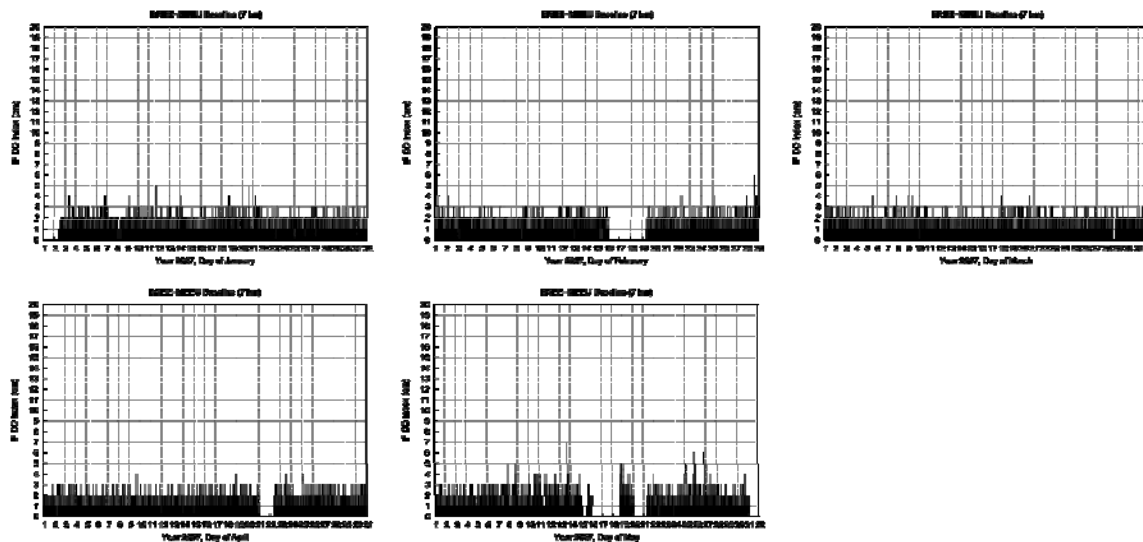


Figure 119: monthly IF DD Index of tropospheric activity of BREE-MEEU baseline (Year 2007).

For each month a statistical study is presented Table 3 to estimate the occurrence of the different index of tropospheric activity detected by DD analysis. Considering every couple of satellites during a month we present the proportion of events which belong to a defined level (in %). Table 4 presents the proportion of events which belong to each level of activity for each month of the year for the whole period 1997-2007 (for example January 1997 to January 2007). This allows to have an idea about seasonal behaviour of small scale structures. The table 4 shows that large IF DD Indexes are mainly detected during summer what is the behaviour we could expect. The same table also shows the proportion of the different levels of activity per year. It can be seen that the proportion of the different activity levels remains very similar from year to year what is an indication of the representativity of our IF DD Index. Occurrences of the different level of IF DD Index are similar for BREE-MEEU baseline (Table 3 and 4, from July 1997 to May 2007) to occurrences of BRUS-BERT and BRUS-OLLN baselines (Table 1 and 2, from May 2005 to April 2007).

Baseline BREE-MEEU (7 km)							
Periods	Number Of DD-analysis (time-series)	% of tropospheric events					
		level 0	level 1	level 2	level 3	level 4	level 5+
July 1997	180324	87.17	11.43	1.23	0.16	0.01	0.00
August 1997	358012	86.92	11.46	1.32	0.21	0.06	0.03
September 1997	319223	90.78	8.46	0.67	0.08	0.01	0.00
October 1997	358662	91.74	7.52	0.61	0.09	0.02	0.02
November 1997	277294	93.29	6.35	0.32	0.03	0.00	0.01
December 1997	333842	93.05	6.45	0.45	0.04	0.00	0.01
January 1998	348497	92.92	6.60	0.44	0.04	0.00	0.00
February 1998	260495	93.53	6.11	0.33	0.03	0.00	0
March 1998	279462	93.11	6.47	0.38	0.04	0.00	0
April 1998	288111	91.68	7.72	0.54	0.06	0.00	0
May 1998	272469	91.24	7.97	0.65	0.11	0.02	0.01
June 1998	128868	84.68	12.88	1.82	0.42	0.12	0.08
July 1998	318588	86.82	11.38	1.47	0.25	0.06	0.02
August 1998	341869	89.77	9.30	0.81	0.11	0.01	0.00
September 1998	329579	89.75	9.19	0.88	0.14	0.03	0.01
October 1998	327874	91.11	8.15	0.65	0.08	0.01	0.00
November 1998	318918	92.95	6.64	0.38	0.03	0.00	0.00
December 1998	304404	93.02	6.54	0.40	0.03	0.01	0
January 1999	335556	93.73	5.96	0.28	0.03	0	0
February 1999	299943	92.53	6.84	0.50	0.09	0.03	0.01
March 1999	337307	93.62	6.06	0.29	0.03	0.00	0
April 1999	263930	92.12	7.27	0.52	0.08	0.01	0.00
May 1999	277169	89.34	9.28	1.04	0.23	0.07	0.04
June 1999	270860	88.17	10.32	1.22	0.24	0.05	0.00
July 1999	279316	87.95	10.51	1.24	0.22	0.04	0.04

August 1999	194110	85.21	12.24	1.85	0.48	0.15	0.07
October 1999	117014	90.82	8.31	0.78	0.09	0.00	0
November 1999	216253	92.75	6.75	0.45	0.05	0.00	0
December 1999	207367	91.51	7.90	0.53	0.05	0.01	0
January 2000	218773	92.78	6.67	0.49	0.06	0	0
February 2000	278122	91.83	7.53	0.57	0.07	0	0
March 2000	296758	91.37	7.82	0.69	0.12	0.00	0
April 2000	242868	89.42	9.60	0.87	0.11	0.00	0
May 2000	284790	87.24	11.22	1.32	0.20	0.02	0.00
June 2000	312304	86.50	11.62	1.53	0.28	0.05	0.02
July 2000	208207	87.37	10.87	1.33	0.33	0.08	0.02
August 2000	163061	86.90	11.42	1.41	0.22	0.04	0.01
September 2000	27874	90.43	8.79	0.71	0.07	0	0
October 2000	320035	89.86	9.08	0.92	0.14	0.00	0
November 2000	195118	91.58	7.63	0.69	0.10	0.00	0
December 2000	246706	91.74	7.57	0.61	0.08	0.00	0
January 2001	180071	92.34	7.01	0.57	0.08	0.00	0
February 2001	129493	92.05	7.32	0.56	0.07	0	0
March 2001	306984	91.65	7.60	0.61	0.09	0.03	0.02
April 2001	285908	89.58	9.46	0.86	0.10	0.00	0
May 2001	309352	88.25	10.44	1.12	0.17	0.02	0.00
June 2001	275907	87.41	11.11	1.24	0.21	0.03	0.00
July 2001	192113	85.59	12.33	1.69	0.32	0.06	0.01
August 2001	228547	86.40	11.94	1.37	0.23	0.04	0.02
September 2001	328302	87.05	11.34	1.36	0.22	0.03	0.00
October 2001	319771	89.35	9.59	0.92	0.13	0.01	0
November 2001	306719	91.17	8.10	0.63	0.10	0.00	0
December 2001	322844	91.36	7.86	0.68	0.10	0.00	0.00
January 2002	329568	91.22	8.10	0.60	0.08	0.00	0
February 2002	68791	90.86	8.35	0.66	0.13	0	0

March 2002	420426	87.88	11.19	0.83	0.08	0.02	0.00
April 2002	385146	87.00	11.91	0.95	0.10	0.03	0.01
May 2002	409789	85.46	13.08	1.30	0.14	0.02	0.00
June 2002	388070	82.43	15.15	1.98	0.35	0.07	0.02
July 2002	410332	83.40	14.58	1.71	0.24	0.05	0.02
August 2002	412049	84.07	13.85	1.69	0.31	0.07	0.01
September 2002	393864	86.52	12.32	1.06	0.09	0.01	0
October 2002	378143	86.15	12.50	1.19	0.14	0.02	0.00
November 2002	394976	87.32	11.61	0.99	0.07	0.01	0
December 2002	410456	88.13	10.86	0.94	0.06	0.01	0
January 2003	407608	88.00	11.03	0.91	0.06	0.00	0
February 2003	376499	88.76	10.29	0.89	0.06	0.00	0
March 2003	428817	88.89	10.30	0.77	0.04	0	0
April 2003	419757	87.13	11.78	1.03	0.06	0.00	0.00
May 2003	437261	84.73	13.49	1.55	0.20	0.03	0.00
June 2003	409571	82.74	14.96	1.92	0.29	0.06	0.03
July 2003	431839	83.46	14.40	1.80	0.27	0.05	0.01
August 2003	433092	83.84	14.23	1.70	0.20	0.03	0.00
September 2003	315867	86.65	11.97	1.22	0.15	0.01	0.00
January 2004	227464	89.28	9.98	0.69	0.05	0.00	0
February 2004	385978	90.13	9.21	0.62	0.04	0.00	0
March 2004	267179	89.52	9.78	0.65	0.05	0.00	0.00
July 2004	38184	81.08	16.38	2.22	0.27	0.05	0.00
August 2004	86570	83.79	14.58	1.50	0.13	0.00	0.00
January 2005	172772	89.20	10.07	0.69	0.04	0	0
February 2005	422870	89.66	9.69	0.62	0.03	0	0
March 2005	449900	88.40	10.73	0.81	0.06	0.00	0
April 2005	434068	87.41	11.44	1.04	0.10	0.01	0.00
May 2005	449356	84.01	14.06	1.68	0.22	0.03	0.00
June 2005	436269	85.29	13.07	1.43	0.18	0.03	0.00

July 2005	396266	82.55	14.83	2.14	0.40	0.07	0.01
August 2005	442483	84.21	13.61	1.78	0.32	0.07	0.01
September 2005	217377	84.76	13.33	1.57	0.27	0.06	0.01
December 2005	247890	88.95	10.39	0.63	0.03	0.00	0
January 2006	450478	90.27	9.23	0.47	0.03	0	0
February 2006	407028	89.87	9.56	0.55	0.02	0	0
March 2006	445844	88.71	10.43	0.79	0.07	0.00	0
April 2006	439196	87.49	11.44	0.99	0.07	0.01	0
May 2006	454524	84.89	13.41	1.47	0.19	0.04	0.00
June 2006	417171	85.10	13.33	1.36	0.17	0.03	0.01
July 2006	454813	82.18	15.49	2.01	0.27	0.04	0.01
August 2006	453721	81.78	15.26	2.38	0.46	0.11	0.01
September 2006	435163	85.62	13.03	1.23	0.11	0.01	0
October 2006	464809	86.61	12.21	1.08	0.09	0.01	0.00
November 2006	457050	88.05	10.96	0.92	0.06	0.01	0.00
December 2006	366609	88.74	10.46	0.74	0.05	0.00	0
January 2007	458187	87.79	11.29	0.85	0.07	0.00	0
February 2007	378944	87.88	11.24	0.81	0.06	0.01	0.00
March 2007	472974	88.02	11.13	0.80	0.05	0.00	0
April 2007	449231	87.63	11.44	0.87	0.06	0.00	0
May 2007	394013	84.44	13.66	1.65	0.21	0.03	0.01

Table 3: statistical study of the occurrence of tropospheric index of activity by DD analysis (IF DD Index) for the BREE-MEEU baseline from July 1997 to May 2007.

Baseline BREE-MEEU (7 km)							
Periods	Number Of DD-analysis (time-series)	% of tropospheric events					
		level 0	level 1	level 2	level 3	level 4	level 5+
January (1997-2007)	3128974	90.54	8.80	0.61	0.05	0.00	0.00
February (1997-2007)	3008163	90.36	8.96	0.63	0.05	0.00	0.00
March (1997-2007)	3705651	89.80	9.44	0.69	0.06	0.01	0.00
April (1997-2007)	3208215	88.48	10.55	0.88	0.08	0.01	0.00
May (1997-2007)	3288723	86.17	12.23	1.36	0.19	0.03	0.02
June (1997-2007)	2639020	85.06	13.04	1.56	0.26	0.05	0.03
July (1997-2007)	2909982	84.54	13.40	1.70	0.28	0.05	0.03
August (1997-2007)	3113514	85.05	12.95	1.63	0.28	0.06	0.03
September (1997-2007)	2367249	87.35	11.36	1.12	0.14	0.02	0.01
October (1997-2007)	2286308	89.04	9.94	0.90	0.11	0.01	0.00
November (1997-2007)	2166328	90.54	8.73	0.67	0.06	0.00	0.00
December (1997-2007)	2440118	90.67	8.63	0.64	0.06	0.00	0.00

YEAR 1997	1827357	90.65	8.47	0.75	0.10	0.02	0.01
YEAR 1998	3519134	91.13	8.06	0.68	0.10	0.02	0.01
YEAR 1999	2798825	90.93	8.14	0.75	0.14	0.03	0.01
YEAR 2000	2794616	89.70	9.18	0.95	0.15	0.02	0.00
YEAR 2001	3186011	89.30	9.56	0.97	0.15	0.02	0.00
YEAR 2002	4401610	86.32	12.29	1.20	0.15	0.03	0.01
YEAR 2003	3660311	85.96	12.54	1.32	0.15	0.02	0.01
YEAR 2004	1005375	88.89	10.27	0.78	0.06	0.00	0.00
YEAR 2005	3669251	86.25	12.27	1.28	0.17	0.03	0.00
YEAR 2006	5246406	86.55	12.11	1.18	0.14	0.02	0.00
YEAR 2007	2153349	87.21	11.71	0.98	0.09	0.01	0.00
All periods (1997-2007)	34262245	88.09	10.71	1.04	0.13	0.02	0.01

Table 4: monthly and yearly statistical study of the occurrence of tropospheric index of activity by DD analysis (IF DD Index) for the BREE-MEEU baseline from July 1997 to May 2007.

According to statistical study we can notice that high level of activity (larger or equal to 5) do not exceed 0.01 % during the 10 years considered in our study. Tropospheric events mainly occur during the summer (see Table 4 and figure 121).

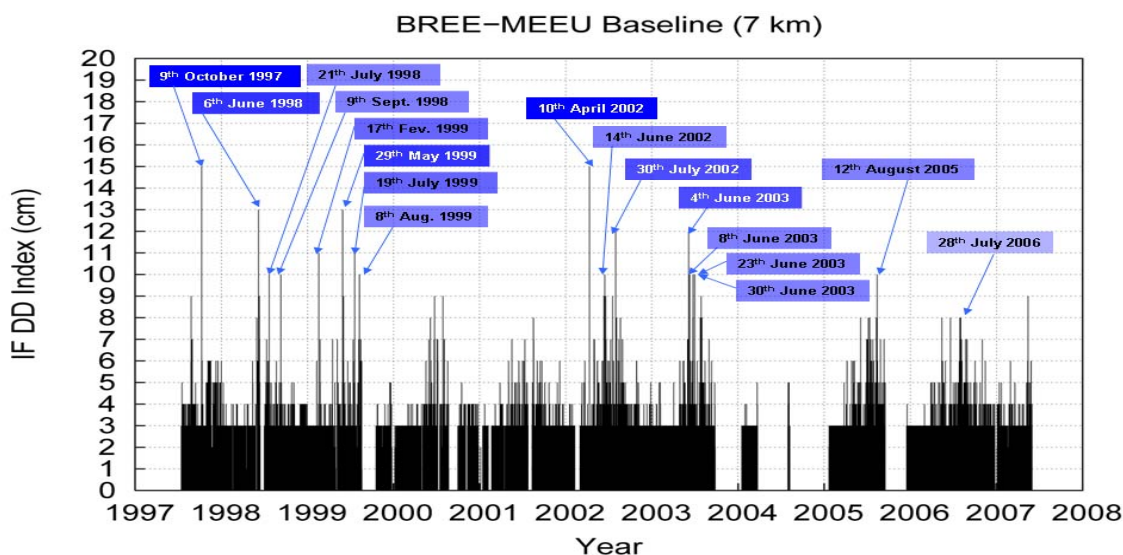


Figure 120: IF DD Index from July 1997 to May 2007. Days with IF DD Index > 9 cm are showed.

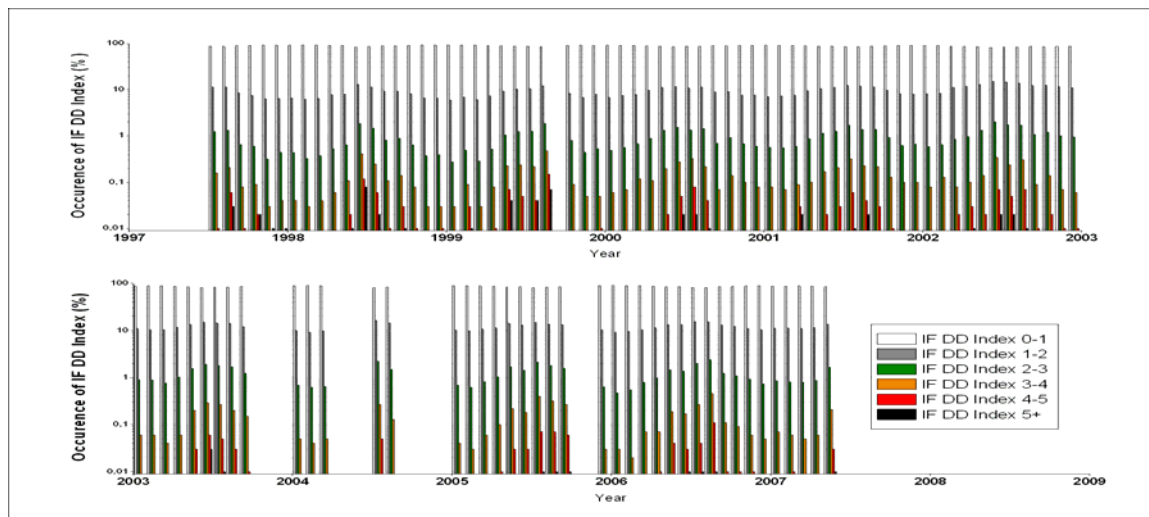


Figure 121: occurrence of IF DD Index for BREE-MEEU baseline from July 1997 to May 2007 (logarithmic scale).

As a last validation, we would like to show that all high IF DD Indexes detected using our method correspond to a real “tropospheric event”. It is not possible to analyze every rainfall event in details. As radar imaging is not available before 2002, we have studied the pluviometry of *Meeuwen* station where one of the two GNSS stations considered for BREE-MEEU baseline is located. Using rain gauges of *Meeuwen* station we prove in the Annex of this report the existence of tropospheric activity corresponding to high IF DD Index. This is not a full validation of IF DD Index but this is a good indicator. From July 1997 to May 2007, rain gauges measurements of *Meeuwen* station “validate” every event with IF DD Index larger than 9 cm. Rain

gauges measurements of events detected by IF DD Index range from 0.5 mm/day to 35 mm/day.

5. CONCLUSIONS

The goal of this WP was to characterize small-scale structures in the troposphere (water vapour) which could pose a threat for high accuracy real time GNSS applications.

To reach that objective, we had first to develop an automated procedure allowing the detection of small-scale structures in water vapour which can be observed during different types of meteorological events. So-called tropospheric parameters (Zenith Total Delays and horizontal gradients of delays) reconstructed by geodetic software offer valuable information about tropospheric activity but, due to the way they are computed, they are only representative of “mean” tropospheric conditions in time and in space around the considered GPS stations. Therefore, we have introduced a new tropospheric activity index called the Ionosphere-Free Double Difference Index (IF DD Index) which is computed from double differences of the ionospheric-free combination. This combination is “sensitive” to local tropospheric effects which are smoothed out during the reconstruction of tropospheric parameters by geodetic software. This statement has been illustrated in several case studies. Then, we have validated our new index based on 6 case studies where we demonstrated that large values of this index are due to disturbed tropospheric conditions of which the existence is confirmed mainly by analyzing radar imaging: in the practice, this index has proved to be capable to detect different types of small-scale structures in the troposphere (stormy cells, bubbles of water vapour, passage of weather front, existences of super-cells, occurrences of hydrometeors). In particular, we showed that a stormy cell with wide vertical extension (i.e. with high water vapour content) associated with hydrometeors (hail in particular) can be the origin of strong variability in GNSS double difference phase measurement (15 cm in the IF DD Index in a few minutes on a 23 km baseline on 29th of June 2005). Such variability can also be observed on short baselines like BREE-MEEU (7 km). We also demonstrated that our index combined with satellite skyplots can also help to identify the location of tropospheric structures with respect to the analyzed baseline.

As an additional validation, we have computed our IF DD Index for 2 baselines on a period of 2 years and demonstrated that the largest indexes correspond to “real” tropospheric disturbances. Again, this validation is based on radar imaging but also on tropospheric parameters reconstructed with geodetic software. Finally, we have computed our index for a 7 km baseline on a period of 10 years in order to further demonstrate that large values of the index are representative of disturbed tropospheric conditions. In this case, in the absence of radar imaging data, the largest values of the index have been validated by rain gauges measurements.

In practice, we demonstrated that our index can be used to select (worst-) case studies to assess the influence of atmospheric threats on high accuracy real time GNSS applications in WP 230.

ANNEX: BREE-MEEU baseline (1997-2007)

As a last validation, we would like to show that all high IF DD Indexes detected using our method correspond to a real “tropospheric event”. It is not possible to analyze every rainfall event in details. As radar imaging is not available before 2002, we have studied the pluviometry of *Meeuwen* station where one of the two GNSS stations considered for BREE-MEEU baseline is located. Daily measurements of rain gauges are estimated from 08H00 UTC during a period of 24H. Daily precipitations are estimated in (l/m²)/day or mm/day. Using rain gauges of *Meeuwen* station we want to prove existence of tropospheric activity corresponding to high IF DD Index. This is not a full validation of IF DD Index but this is a good indicator.

We present the major events of figure 120.

The 9th OCTOBER 1997 (08H00)

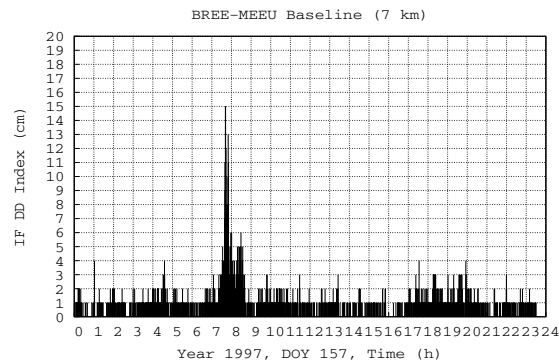


Figure 122: daily IF DD Index of tropospheric activity of BREE-MEEU baseline (the 9th October 1997).

Important IF DD Indexes are observed between 07H00 and 09H00 UTC (Fig. 122). Time-series of IF Double Difference and IF DD Index are presented for the couple of satellites 31-01 (Fig. 123).

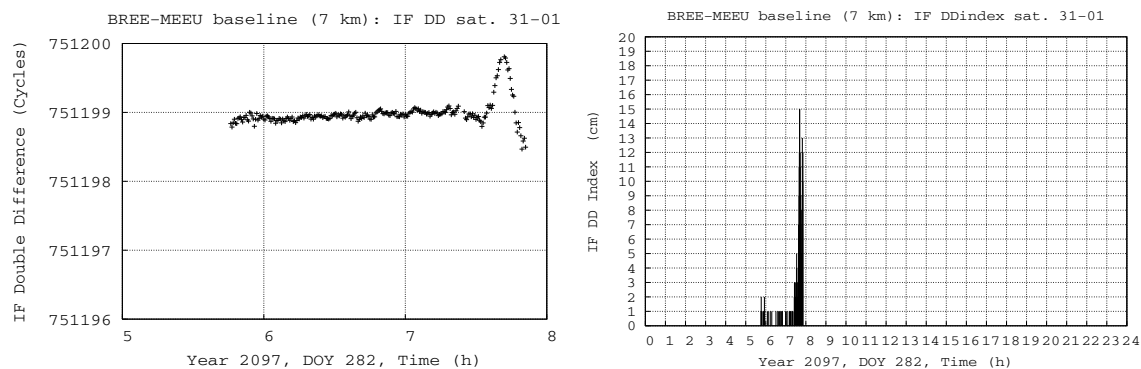


Figure 123: IF Double Difference and tropospheric index of activity of BREE-MEEU baseline the 9th October 1997 for couple of satellites 31-01.

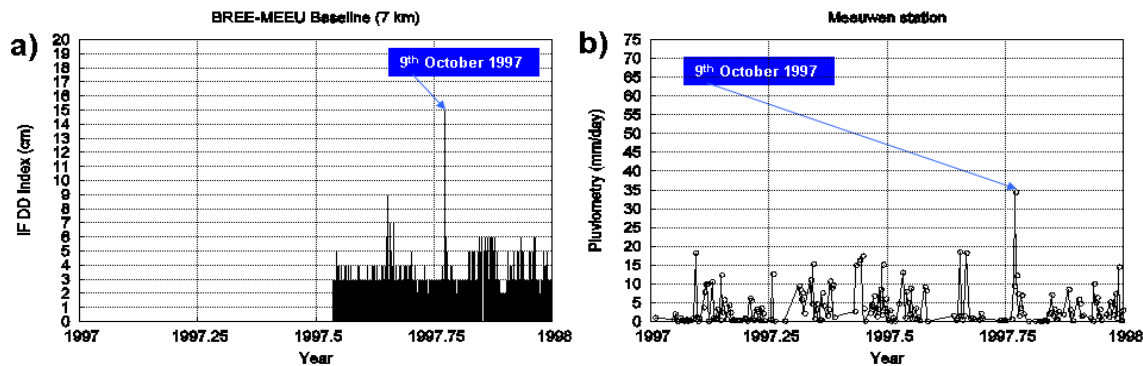


Figure 124: a) Time-series of IF DD Index for BREE-MEEU baseline during year 1997, b) Daily precipitations for Meeuwen station during year 1997.

The tropospheric activity is indicated by rain gauges with precipitations of 9.3 mm/day the 8th October and 34.4 mm/day the 9th October 1997 (see figure 124).

The 6th JUNE 1998 (17H00)

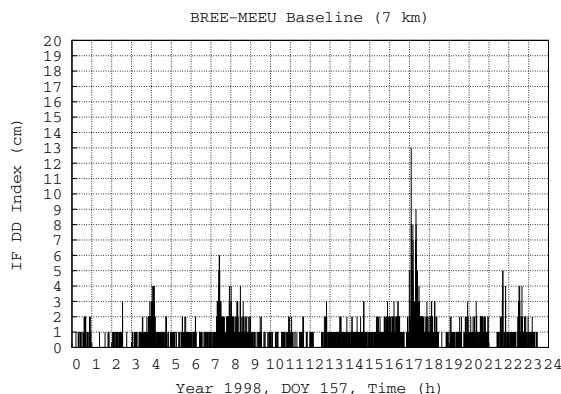


Figure 125: daily IF DD Index of tropospheric activity of BREE-MEEU baseline (the 6th June 1998).

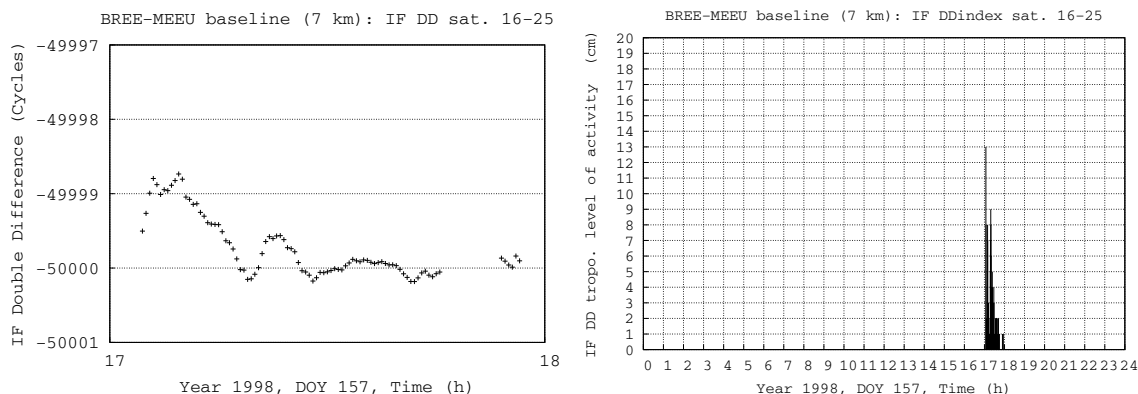


Figure 126: IF Double Difference and tropospheric index of activity of BREE-MEEU baseline the 6th June 1998 for couple of satellites 16-25.

The tropospheric activity of the 6th June 1998 (Fig. 125 and 126) is validated by rain gauges with precipitations of 11.5 mm/day (see figure 131).

The 21th JULY 1998 (14H30)

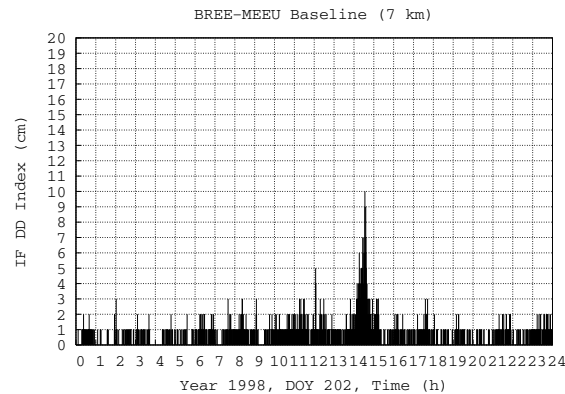


Figure 127: daily IF DD Index of tropospheric activity of BREE-MEEU baseline (the 21th July 1998).

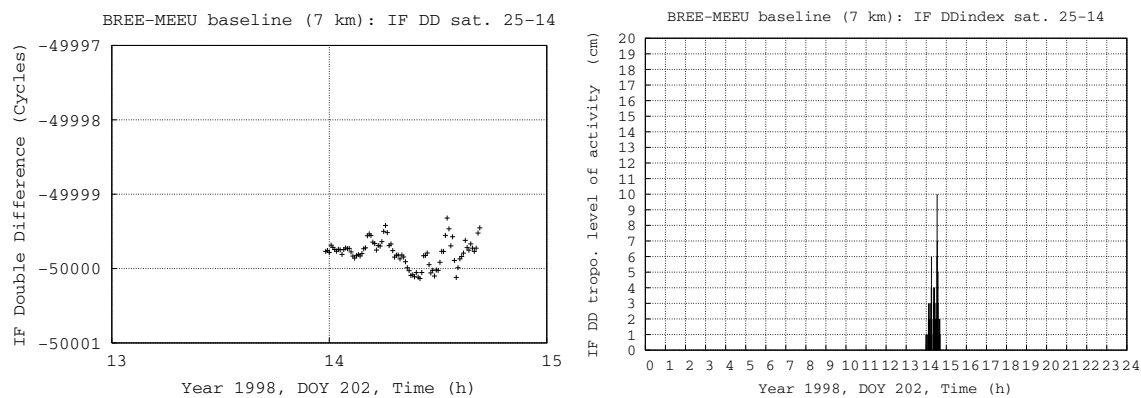


Figure 128: IF Double Difference and tropospheric index of activity of BREE-MEEU baseline the 21th July 1998 for couple of satellites 25-14.

The tropospheric activity of the 21st July 1998 (Fig. 127 and 128) is validated by rain gauges with precipitations of 8.4 mm/day (see figure 131).

The 9th SEPTEMBER 1998 (17H30)

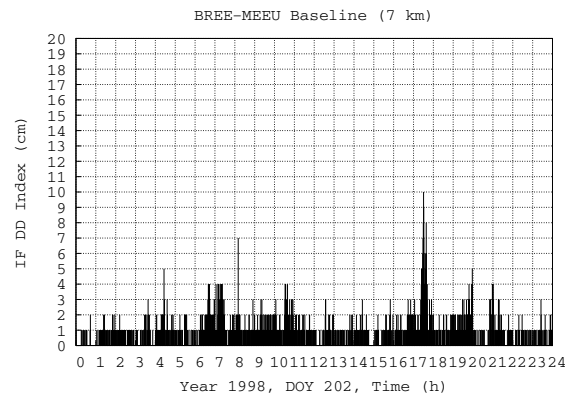


Figure 129: daily IF DD Index of tropospheric activity of BREE-MEEU baseline (the 9th September 1998).

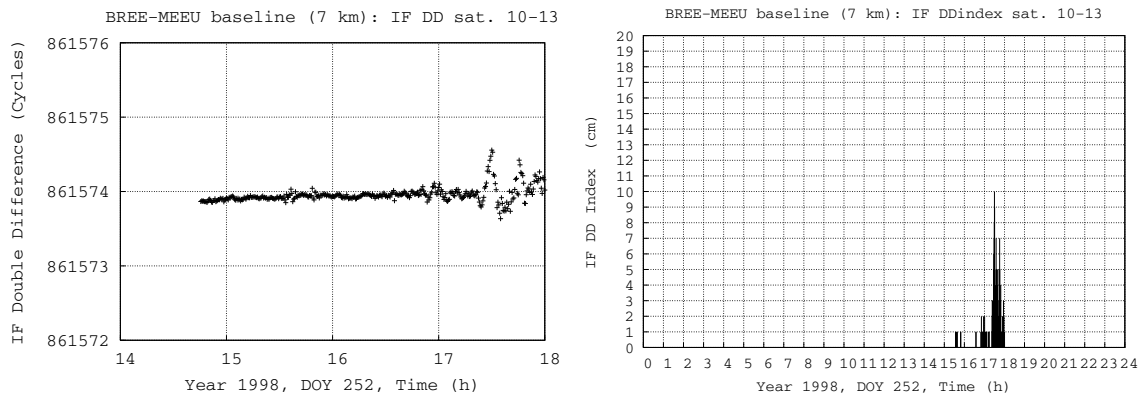


Figure 130: IF Double Difference and tropospheric index of activity of BREE-MEEU baseline the 9th September 1998 for couple of satellites 10-13.

The tropospheric activity of the 9th September 1998 (Fig. 129 and 130) is validated by rain gauges with precipitations of 21.7 mm/day (see figure 131).

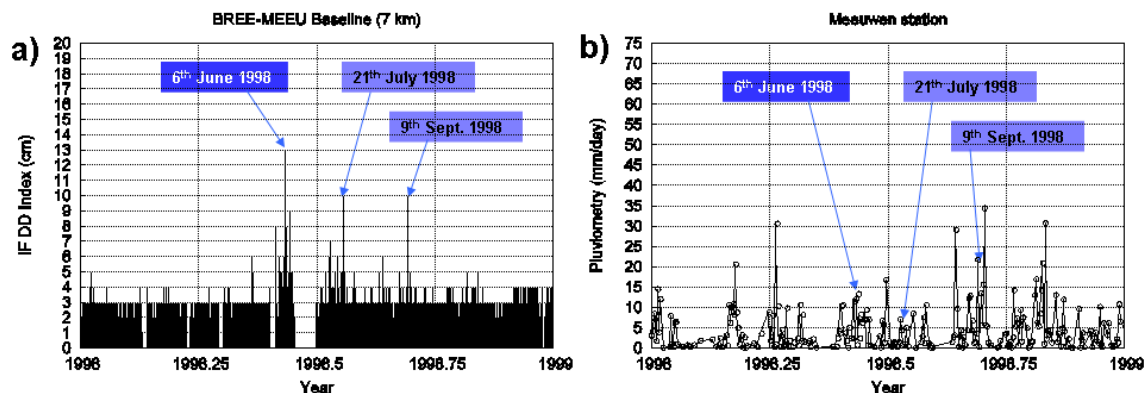


Figure 131: a) Time-series of IF DD Index for BREE-MEEU baseline during year 1998, b) Daily precipitations for Meeuwen station during year 1998.

The 17th FEBRUARY 1999 (19H45)

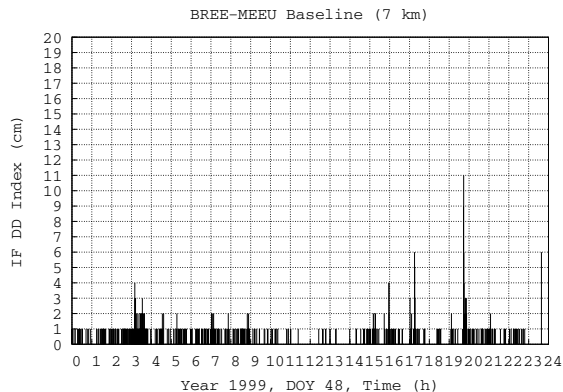


Figure 132: daily IF DD Index of tropospheric activity of BREE-MEEU baseline (the 17th February 1999).

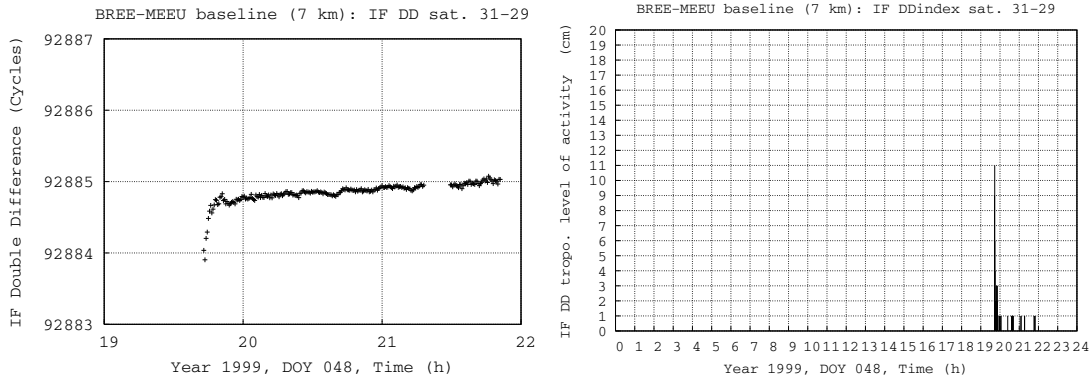


Figure 133: IF Double Difference and tropospheric index of activity of BREE-MEEU baseline the 17th February 1999 for couple of satellites 31-29.

The tropospheric activity of the 17th February 1999 (Fig. 132 and 133) is validated by rain gauges with precipitations of 4.2 mm/day (see figure 140).

The 29th MAY 1999 (afternoon)

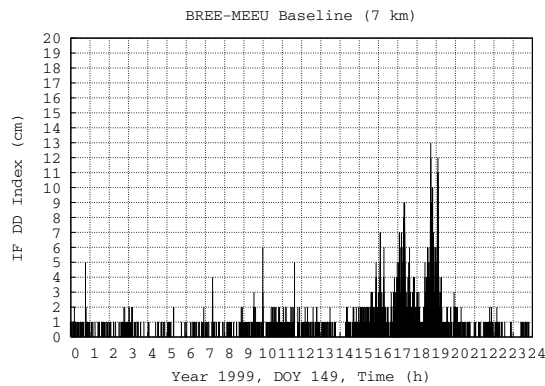


Figure 134: daily IF DD Index of tropospheric activity of BREE-MEEU baseline (the 29th May 1999).

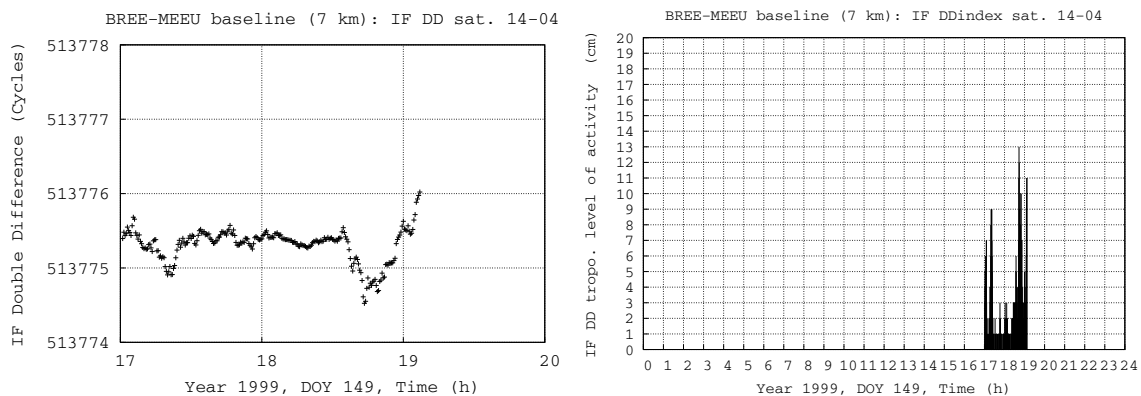


Figure 135: IF Double Difference and tropospheric index of activity of BREE-MEEU baseline the 29th May 1999 for couple of satellites 14-04.

The tropospheric activity of the 29th May 1999 (Fig. 134 and 135) is validated by rain gauges with precipitations of 10.5 mm/day (see figure 140).

The 19th JULY 1999 (14H00)

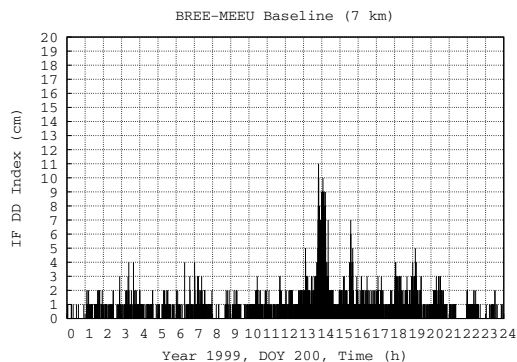


Figure 136: daily IF DD Index of tropospheric activity of BREE-MEEU baseline (the 19th July 1999).

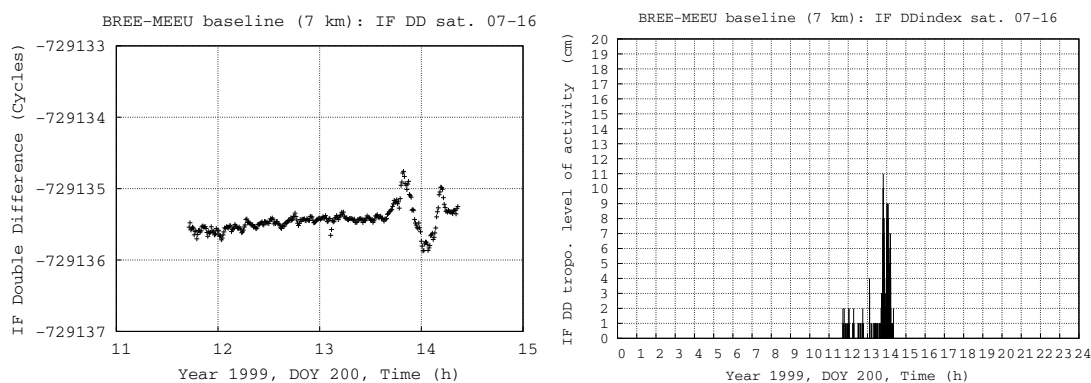


Figure 137: IF Double Difference and tropospheric index of activity of BREE-MEEU baseline the 19th July 1999 for couple of satellites 07-16.

No rain gauge measurement is available.

The 8th AUGUST 1999 (afternoon)

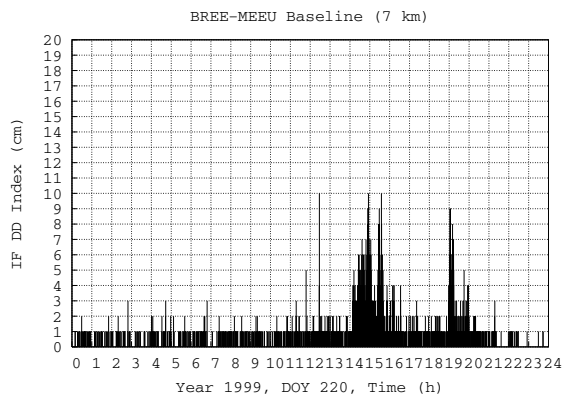


Figure 138: daily IF DD Index of tropospheric activity of BREE-MEEU baseline (the 8th August 1999).

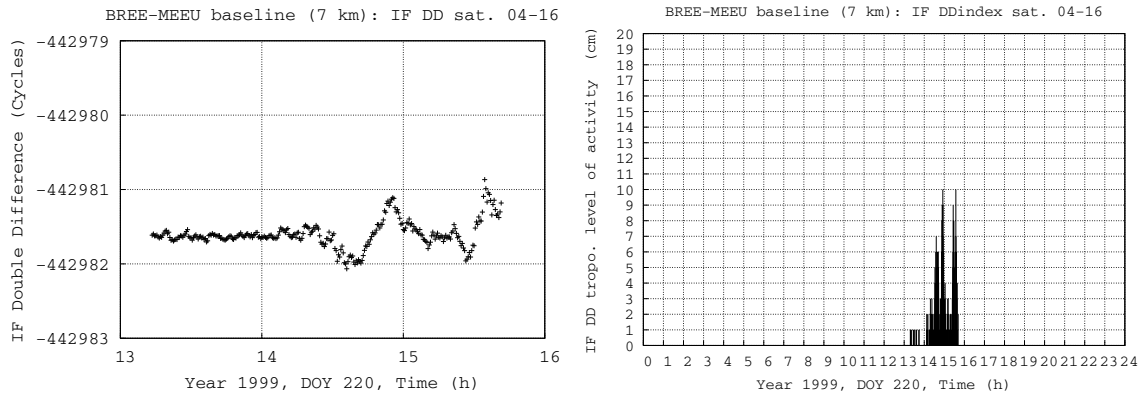


Figure 139: IF Double Difference and tropospheric index of activity of BREE-MEEU baseline the 8th August 1999 for couple of satellites 04-16.

The tropospheric activity of the 8th August 1999 (Fig. 138 and 139) is validated by rain gauges with precipitations of 1.8 mm/day the 8th August 1999 and of 11.9 mm/day the 9th August 1999 (see figure 140).

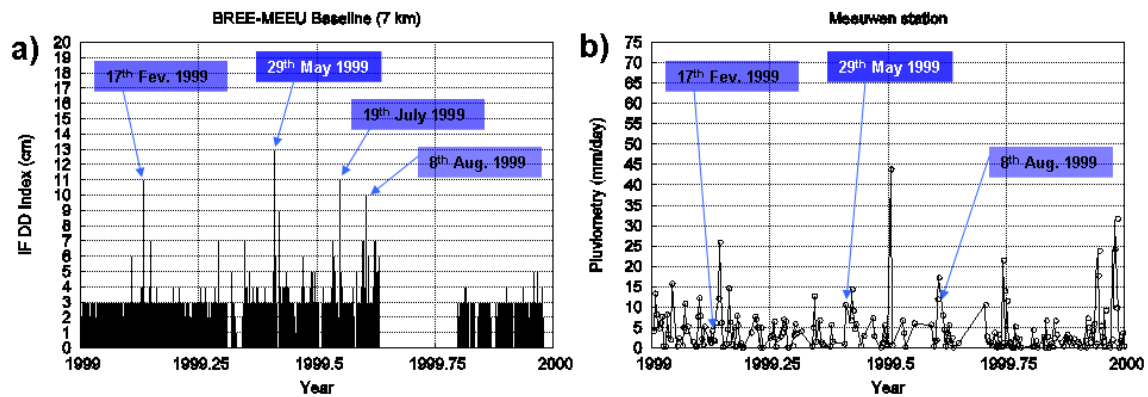


Figure 140: a) Time-series of IF DD Index for BREE-MEEU baseline during year 1999, b) Daily precipitations for Meeuwen station during year 1999.

No major event with IF DD Index larger than 9 cm occurred during year 2000, nevertheless we see that strong rainfalls were observed on the 4th July 2000 with rain gauges precipitations up to 70 mm/day (see figure 141).

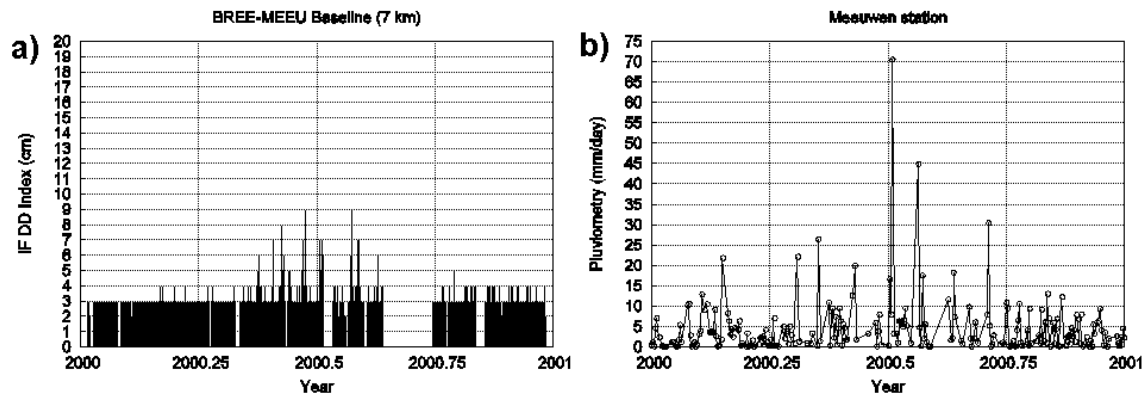


Figure 141: a) Time-series of IF DD Index for BREE-MEEU baseline during year 2000, b) Daily precipitations for Meeuwen station during year 2000.

Despite IF DD Indexes are not larger than 7 cm the 4th July 2000, an increased tropospheric activity is observed by IF DD Index between 16H and 17H UTC (Fig. 142).

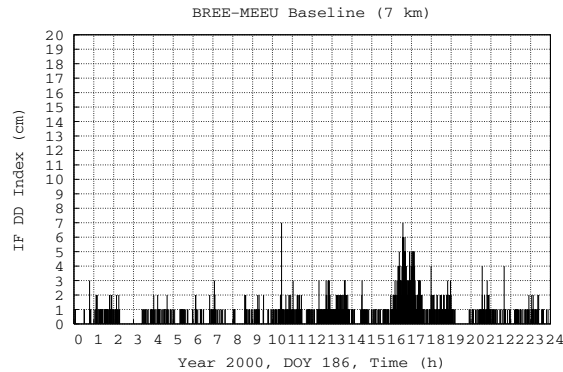


Figure 142: daily IF DD Index of tropospheric activity of BREE-MEEU baseline (the 4th July 2000).

No major event with IF DD Index larger than 9 cm occurred during year 2001, but we see that a consequent tropospheric activity was present the 19th September 2001 with rain gauges precipitations up to 60 mm/day (see figure 143).

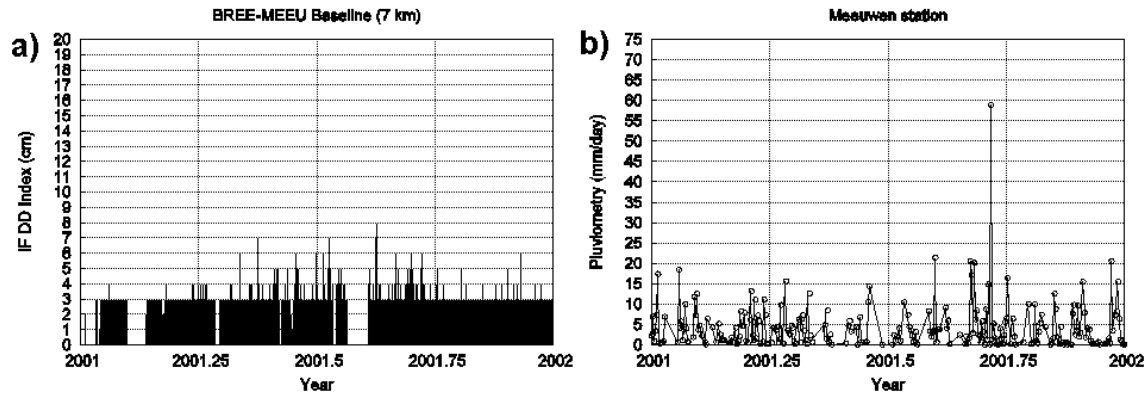


Figure 143: a) Time-series of IF DD Index for BREE-MEEU baseline during year 2001, b) Daily precipitations for Meeuwen station during year 2001.

Despite IF DD Indexes are not larger than 8 cm the 19th September 2001, an important tropospheric activity is observed by IF DD Indexes at 07H20 UTC and between 16H30 UTC and 17H30 UTC (see figure 144).

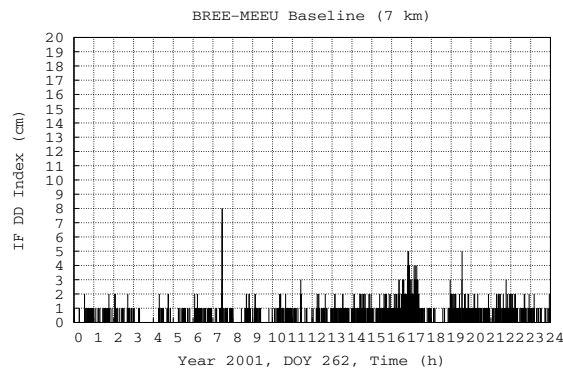


Figure 144: daily IF DD Index of tropospheric activity of BREE-MEEU baseline (the 19th September 2001).

The 14th JUNE 2002 (22H00)

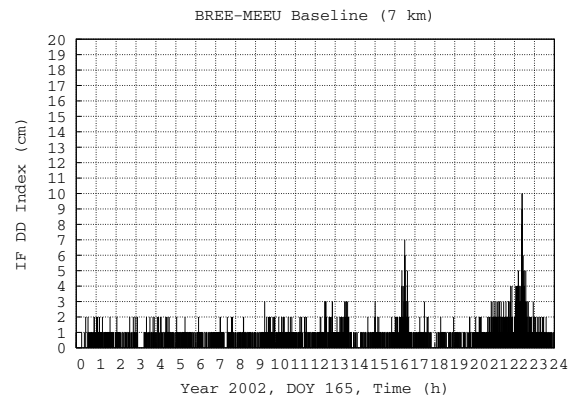


Figure 145: daily IF DD Index of tropospheric activity of BREE-MEEU baseline (the 14th June 2002).

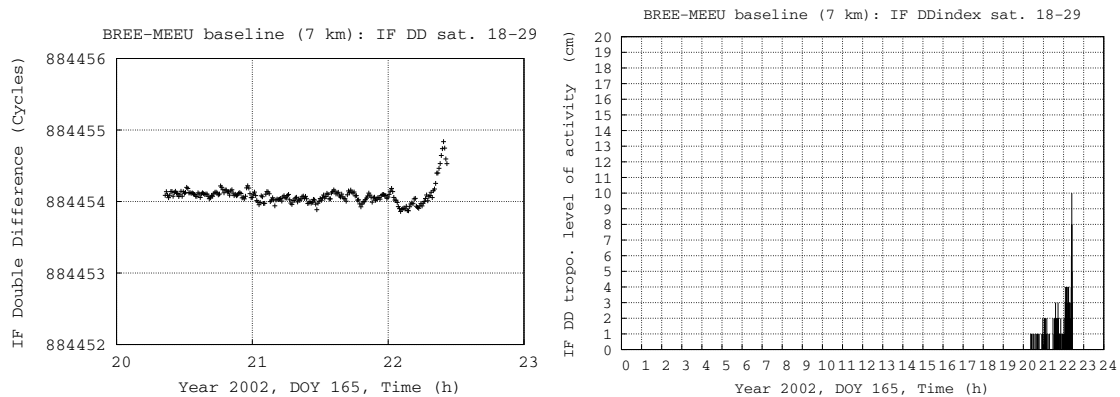


Figure 146: IF Double Difference and tropospheric index of activity of BREE-MEEU baseline the 14th June 2002 for couple of satellites 18-29.

The tropospheric activity of the 14th June 2002 (Fig. 145 and 146) is validated by rain gauges with precipitations of 13.0 mm/day (see figure 149).

The 30th JULY 2002 (16H00)

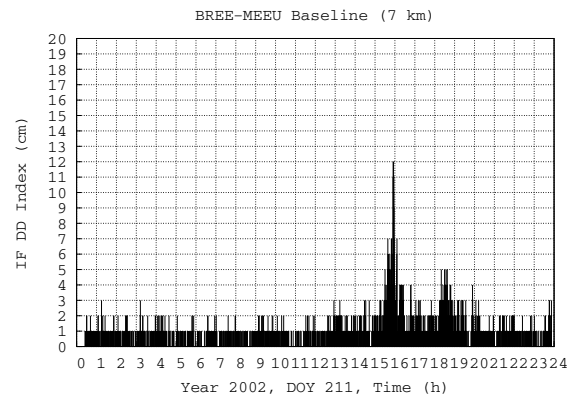


Figure 147: daily IF DD Index of tropospheric activity of BREE-MEEU baseline (the 30th July 2002).

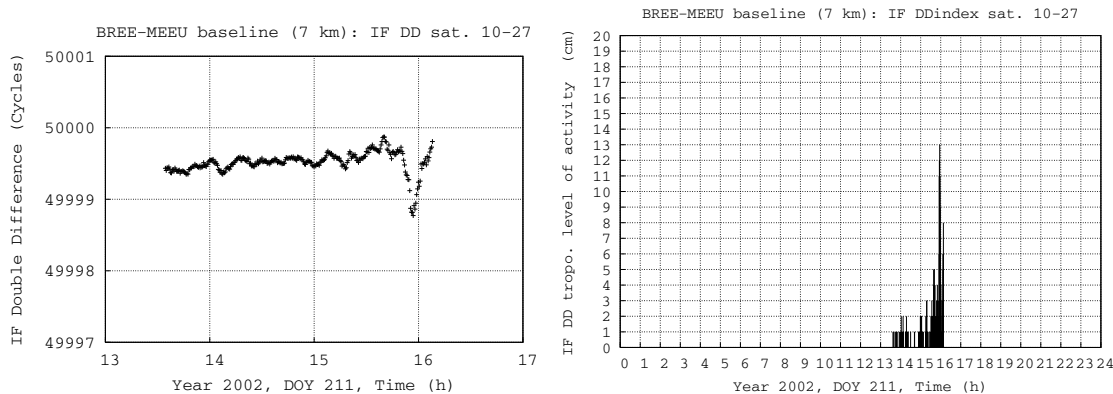


Figure 148: IF Double Difference and tropospheric index of activity of BREE-MEEU baseline the 30th July 2002 for couple of satellites 10-27.

This event has been studied in section 4.1. The tropospheric activity of the 30th July 2002 (Fig. 147 and 148) is indicated by rain gauges with precipitations of 17.4 mm/day the 30th July 2002 and 33.6 mm/day the 31st July 2002 (see figure 149).

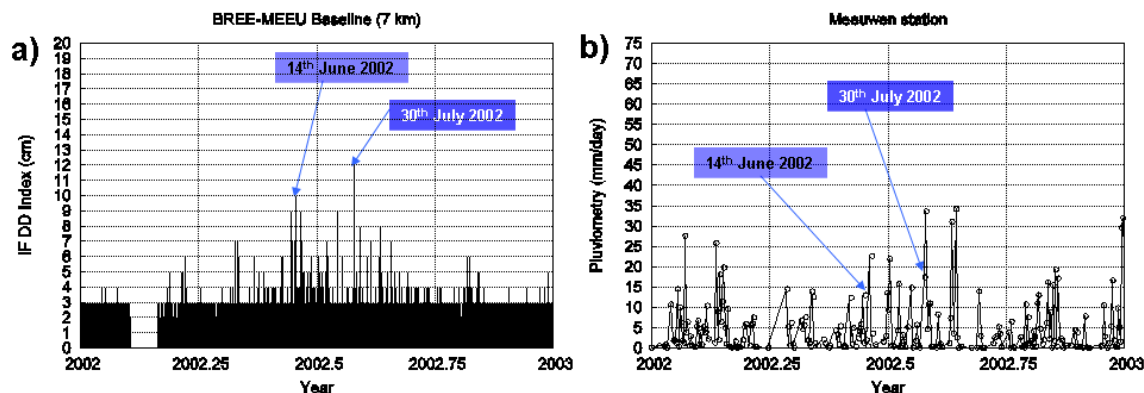


Figure 149: a) Time-series of IF DD Index for BREE-MEEU baseline during year 2002, b) Daily precipitations for Meeuwen station during year 2002.

The 4th JUNE 2003 (14H00)

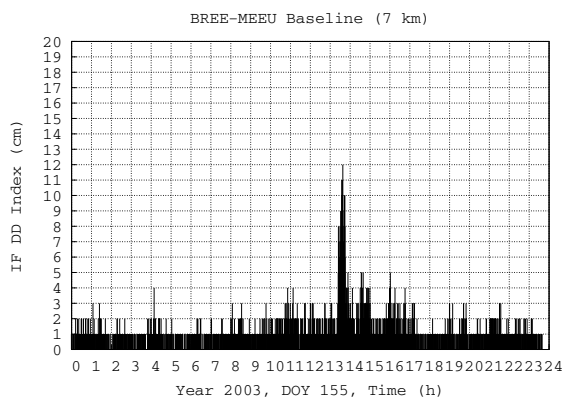


Figure 150: daily IF DD Index of tropospheric activity of BREE-MEEU baseline (the 4th June 2003).

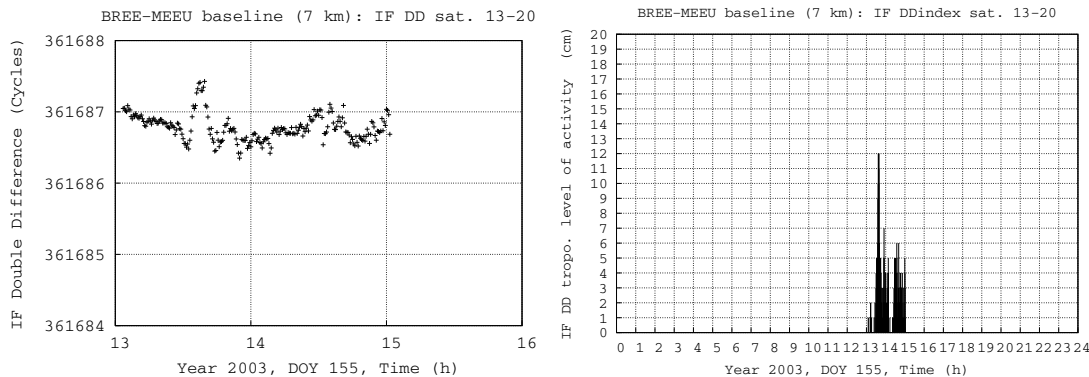


Figure 151: IF Double Difference and tropospheric index of activity of BREE-MEEU baseline the 4th June 2003 for couple of satellites 13-20.

The tropospheric activity of the 4th June 2003 (Fig. 150 and 151) is validated by rain gauges with precipitations of 8.1 mm/day (see figure 158).

The 8th JUNE 2003 (10H00)

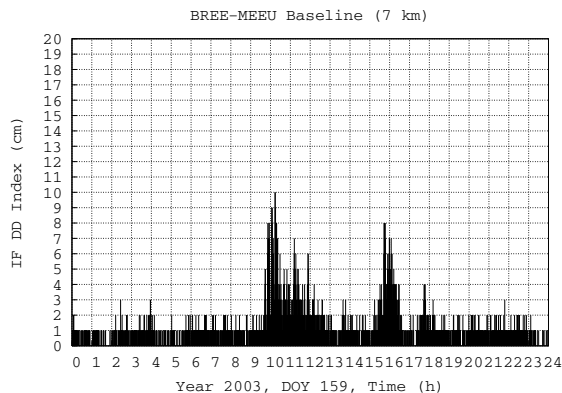


Figure 152: daily IF DD Index of tropospheric activity of BREE-MEEU baseline (the 8th June 2003).

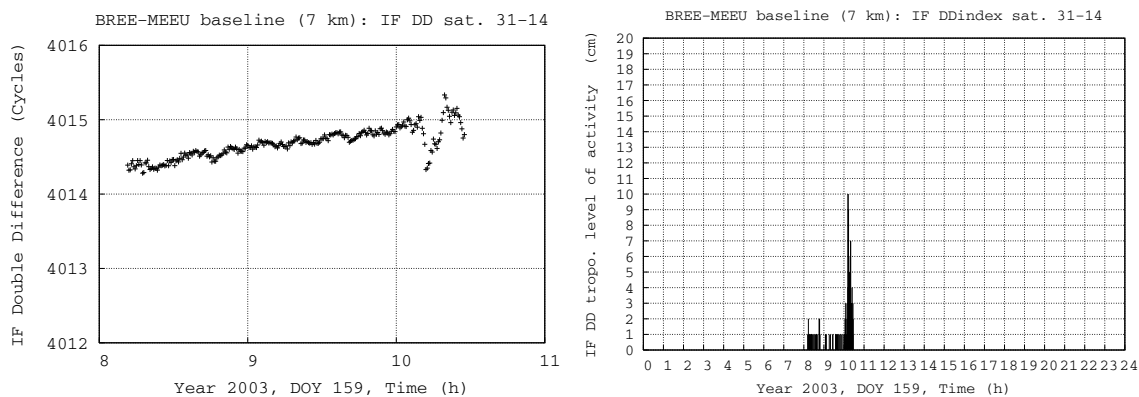


Figure 153: IF Double Difference and tropospheric index of activity of BREE-MEEU baseline the 8th June 2003 for couple of satellites 31-14.

This event has been studied in section 4.1. The tropospheric activity of the 8th June 2003 (Fig. 152 and 153) is validated by rain gauges with precipitations of 20.9 mm/day (see figure 158).

The 23th JUNE 2003 (13H30)

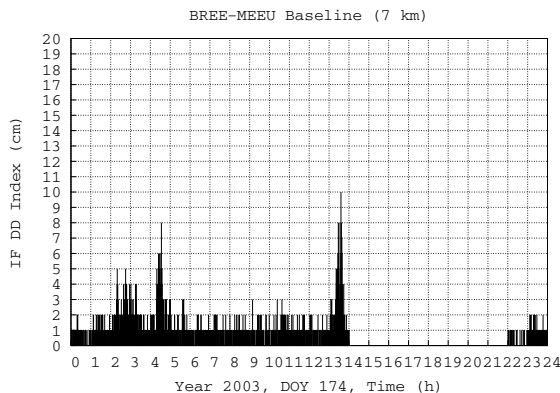


Figure 154: daily IF DD Index of tropospheric activity of BREE-MEEU baseline (the 23th June 2003).

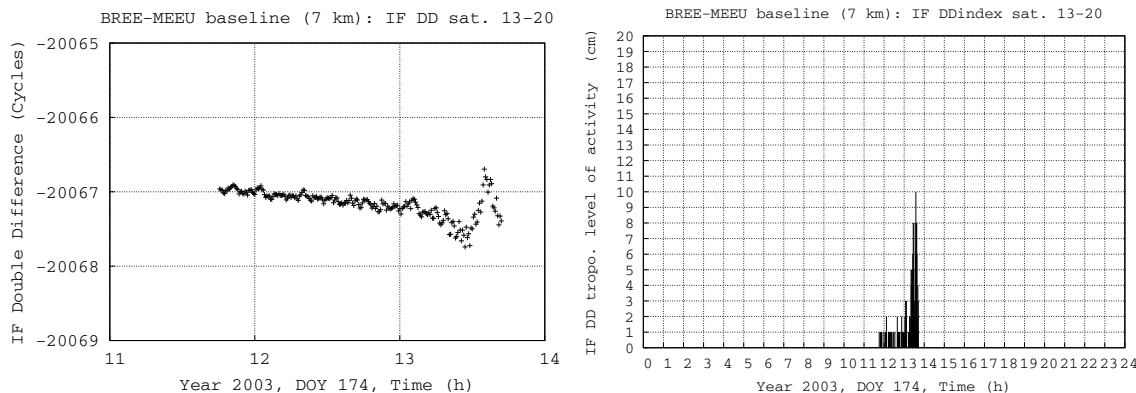


Figure 155: IF Double Difference and tropospheric index of activity of BREE-MEEU baseline the 23th June 2003 for couple of satellites 13-20.

No rain gauge measurement is available.

The 30th JUNE 2003 (20H00)

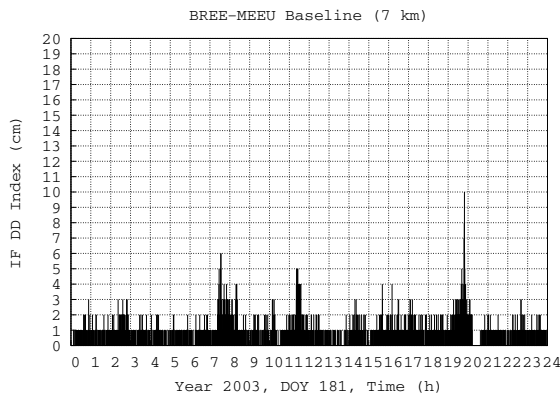


Figure 156: daily IF DD Index of tropospheric activity of BREE-MEEU baseline (the 30th June 2003).

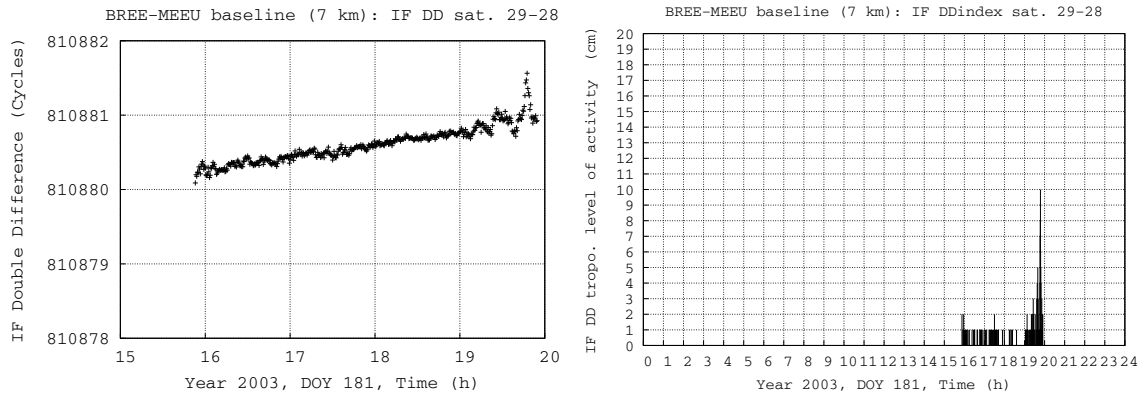


Figure 157: IF Double Difference and tropospheric index of activity of BREE-MEEU baseline the 30th June 2003 for couple of satellites 29-28.

The tropospheric activity of the 30th June 2003 (Fig. 156 and 157) is validated by rain gauges with precipitations of 17.0 mm/day (see figure 158).

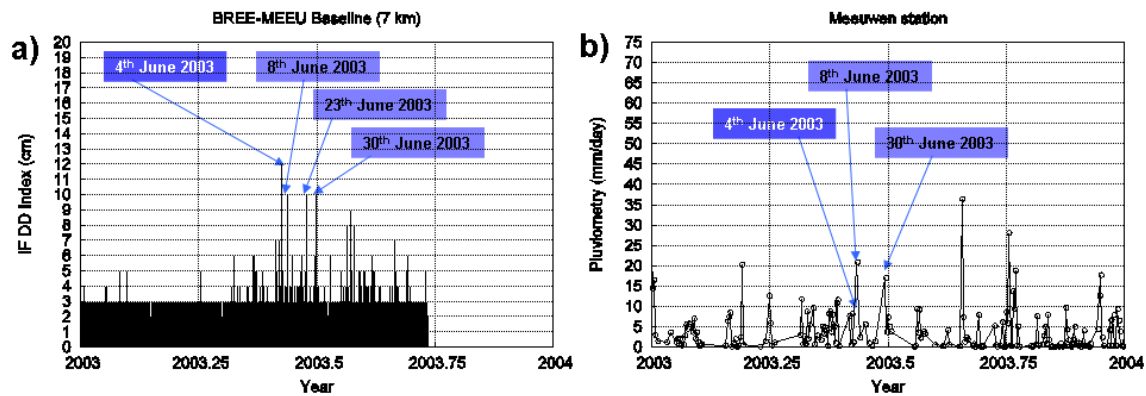


Figure 158: a) Time-series of IF DD Index for BREE-MEEU baseline during year 2003, b) Daily precipitations for Meeuwen station during year 2003.

No major event with IF DD Index larger than 9 cm occurred during year 2004. We see that a consequent tropospheric activity was present the 19th November 2004 with rain gauges precipitations up to 45 mm/day (see figure 159), but no GPS data is available.

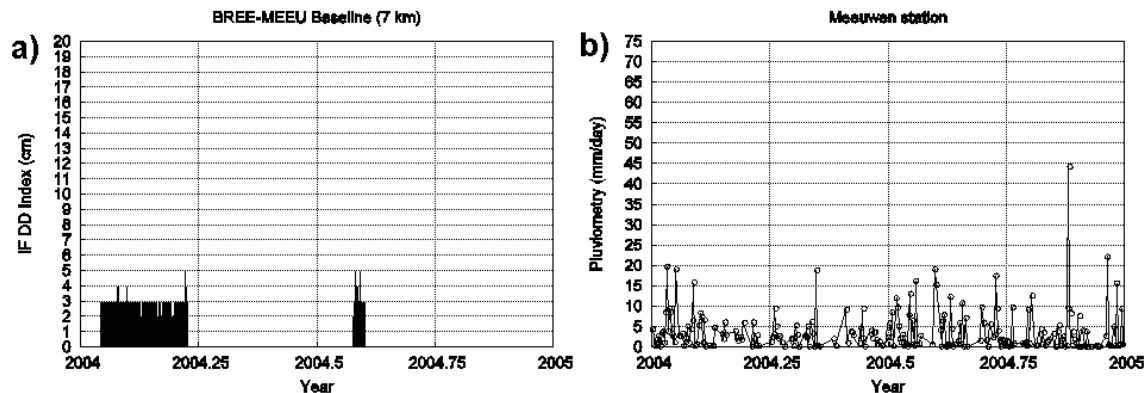


Figure 159: a) Time-series of IF DD Index for BREE-MEEU baseline during year 2004, b) Daily precipitations for Meeuwen station during year 2004.

The 12th AUGUST 2005 (15H00)

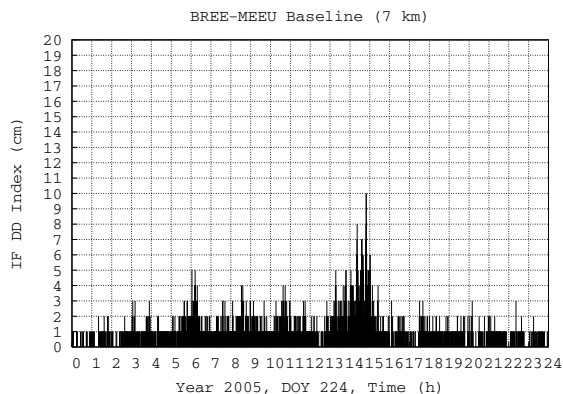


Figure 160: daily IF DD Index of tropospheric activity of BREE-MEEU baseline (the 12th August 2005).

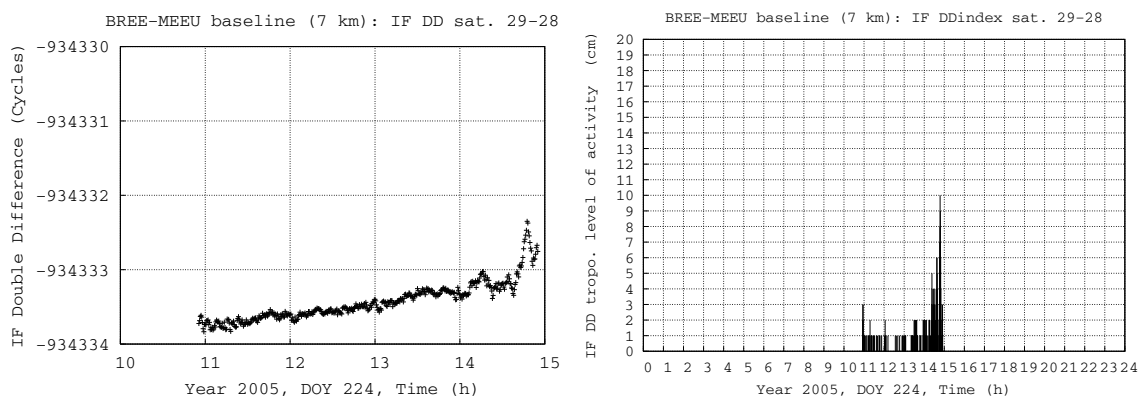


Figure 161: IF Double Difference and tropospheric index of activity of BREE-MEEU baseline the 12th August 2005 for couple of satellites 29-28.

The tropospheric activity of the 12th August 2003 (Fig. 160 and 161) is validated by rain gauges with precipitations of 0.5 mm/day the 12th August 2003 and 9.3 mm/day the 13th August 2005 (see figure 162).

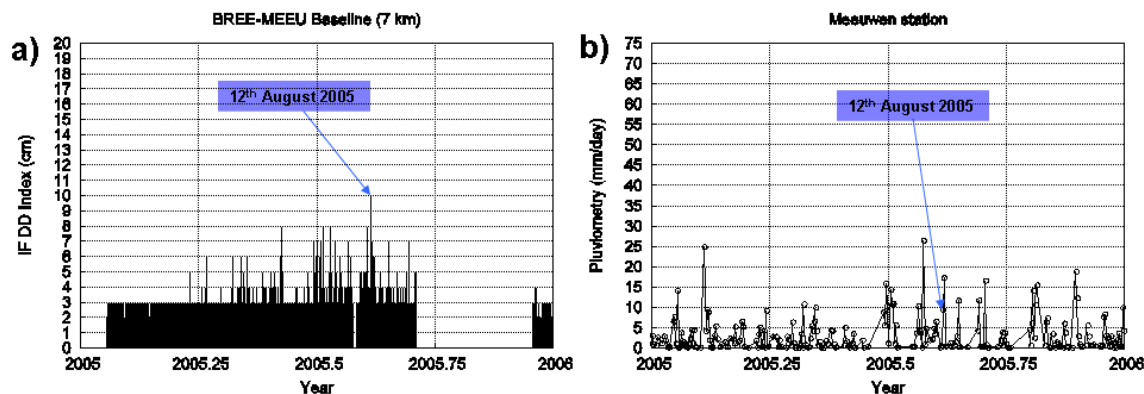


Figure 162: a) Time-series of IF DD Index for BREE-MEEU baseline during year 2005, b) Daily precipitations for Meeuwen station during year 2005.

No major event with IF DD Index larger than 9 cm occurred during year 2006, but we see that a consequent tropospheric activity was present the 14th August 2006 with rain gauges precipitations up to 50 mm/day (see figure 163).

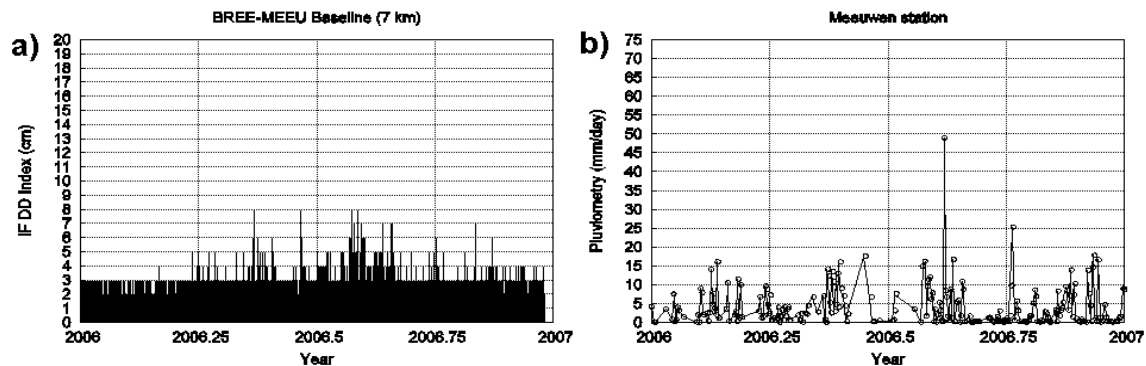


Figure 163: a) Time-series of IF DD Index for BREE-MEEU baseline during year 2006, b) Daily precipitations for *Meeuwen* station during year 2006.

Despite the fact that IF DD Indexes are not larger than 5 cm the 14th August 2006, a tropospheric activity is observed by IF DD Indexes at 18H30 UTC (see figure 164).

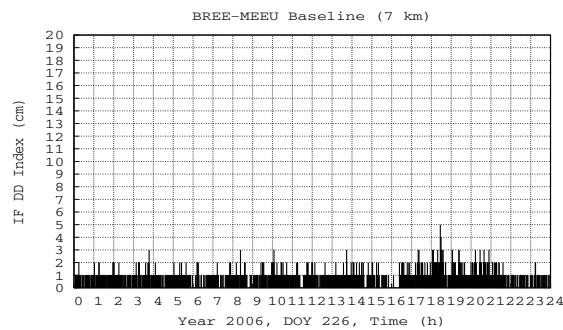


Figure 164: daily IF DD Index of tropospheric activity of BREE-MEEU baseline (the 14th August 2006).

No major event with IF DD Index larger than 9 cm occurred from January to May 2007 (see figure 165).

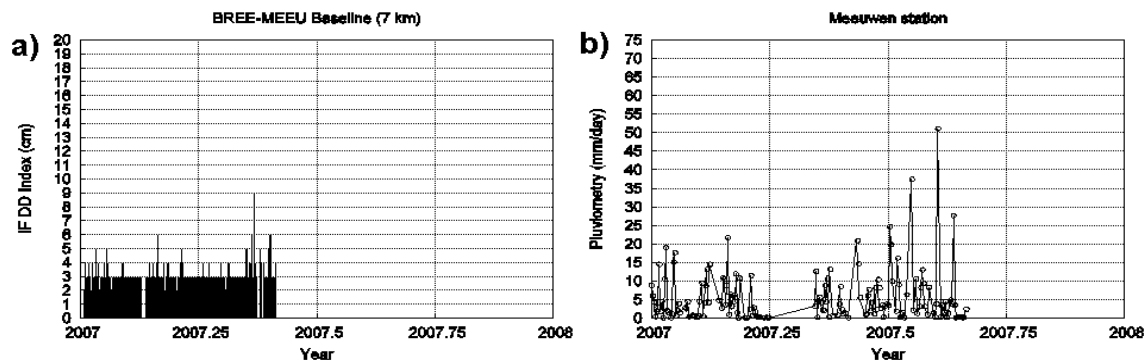


Figure 165: a) Time-series of IF DD Index for BREE-MEEU baseline during year 2007, b) Daily precipitations for *Meeuwen* station during year 2007.

As a conclusion, for the period July 1997 to May 2007, rain gauges measurements of *Meeuwen* station validate every event with IF DD Index larger than 9 cm. Rain gauges measurements of events detected by IF DD Index range from 0.5 mm/day to 35 mm/day.

REFERENCES

Bevis, M., S. Businger, T. A. Herring, C. Rocken, R. A. Anthes, and R. H. Ware: GPS Meteorology: Remote Sensing of Atmospheric Water Vapour Using the Global Positioning System, *J. Geophys. Res.*, 97 (D14), 15,787-15,801, 1992.

Blewitt, G.: Carrier Phase Ambiguity Resolution for the Global Positioning System Applied to Geodetic Baselines up to 2000 km, *J. Geophys. Res.*, 94, 10,187-10,203, 1989.

Brenot, H.: Potentiel de la mesure GPS-Sol pour l'étude des pluies intenses Méditerranéennes, Ph.D Thesis, University of Grenoble, France, 2006.

Brenot, H., V. Ducrocq, A. Walpersdorf, C. Champollion and O. Caumont: GPS Zenith Delay Sensitivity evaluated from High-Resolution NWP Simulations of the 8-9th September 2002 Flash-Flood over Southeastern France, *J. Geophys. Res.*, vol. 111, D15105, 2006.

Chen, G. and T. A. Herring, Effects of atmospheric azimuthal asymmetry on the analysis of space geodetic data, *J. Geophys. Res.*, 102(B9), 20489–20502, 1997.

Davis, J. L., G. Elgered, A. E. Niell, and C. E. Kuehn, Groundbased Measurements of Gradients in the Wet Radio Refractivity of air, *Radio Science*, 28, 1003-1018, 1993.

Delobbe, L. and I. Holleman: Uncertainties in radar echo top heights used for hail detection *Meteorol. Appl.*, vol. 13, 361–374, 2006.

Delrieu, G., V. Ducrocq, E. Gaume, J. Nicol, O. Payrastre, E. Yates, P.-E. Kirstetter, H. Andrieu, P.A. Ayral, C. bouvier, J.D. Creutin, M. livet, S. Anquetin, M. lang, L. Neppel, C. Obled, J. Parent du Chatelet, G.M. Saulnier, A. Walpersdorf and W. Wobrock: The catastrophic flash-flood event of 8-9 September 2002 in the Gard region : a first case study for the Cévennes-Vivarais Mediterranean Hydrometeorology Observatory, *J. Hydrometeorology*, 34-51, 2005.

Dong, D.-N. and Y. Bock: Global Positioning System Network Analysis With Phase Ambiguity Resolution Applied to Crustal Deformation Studies in California, *J. Geophys. Res.*, 94, 3949-3966, 1989.

Ifadis, I. I., The Atmospheric Delay of Radio Wave: Modelling the Elevation the Elevation Dependence on a Global Scale, *Technical Report #38L*, Chalmers University of Technology, Göteborg, Sweden, 1986.

Gradinarsky, L. P., Sensing Atmospheric Water Vapour Using Radio Waves, Ph.D. thesis, School of Electrical Engineering, Chalmers University Of Technology, Göteborg, Sweden, 2002.

Hajj, G., E. Kursinski, L. Romans, W. Bertiger, and S. Leroy: A Technical Description of Atmospheric Sounding by GPS Occultation, *Journal of Atmos. and Solar-Terres. Physics*, 64, 451-469, 2002.

Herring, T. A., Modeling Atmospheric Delays in the Analysis of Space Geodetic Data, Proceedings of the Symposium on Refraction of Transatmospheric Signals in Geodesy, Netherlands Geodetic Commission, *Publications on Geodesy*, Delft, the Netherlands, 1992.

Hopfield, H. S., Two-Quartic Tropospheric Refractivity Profil for Correcting Satellite Data, *J. Geophys. Res.*, 74, 4487-4499, 1969.

King, R. W., E. G. Masters, C. Rizos, A. Stolz, and J. Collins: Surveying with GPS, *Monograph 9*, School of Surveying, University of New South Wales, Kensington, Australia, 1985.

King, R., and Y. Bock: Documentation for the GAMIT GPS Analysis Software, version 10.10, *Tech. rep.*, Mass. Inst. Tech., Cambridge, 2002.

Leick, A.: GPS Satellite Surveying, *Wiley-Interscience*, 1989.

Leick, A.: GPS Satellite Surveying 3rd Edition. *John Wiley & Sons*, New York, 435p., 2004.

Marini, J. W., and C. W. Murray: Correction for Laser Range Tracking Data for Atmospheric Refraction at Elevation above 10 Degrees, *Report X-591-73-351*, NASA GSFC, Greenbelt, MD, 1973.

Niell, A.E.: Global mapping functions for the atmosphere delay at radio wavelengths, *J. Geophys. Res.*, vol. 101, n°B2, 3227-3246, 1996.

Resch, G. M.: Geodetic Refraction, chap. Water Vapour Radiometry in Geodetic Applications, pp. 53-84, *Springer-Verlag*, New York, 1984.

Saastamoinen, J.: Atmospheric Correction for the Troposphere and Stratosphere in Radio ranging of satellites, *Geophys. Monogr. Ser.*, 15, 247-251, edited by S. W. Henriksen, et al., 1972.

Seeber, G.: Satellite Geodesy Second Edition. *de Gruyter*, New-York, 589 p., 2003.

Solheim, F., J. Vivekanandan, R. Ware, and C. Rocken: Propagation Delays Induced in GPS Signals by Dry Air, Water Vapour, Hydrometeors, and Other Particulates, *J. Geophys. Res.*, 104 (D4), 9663-9670, 1999.

Teunissen, P. , A. Kleusberg, Y. Bock, G. Beutler, R. Weber, R. B. Langley, H. van der Marel, G. Blewitt, C. C. Gload and O. L. Colombo: GPS for Geodesy, *Springer*, 2nd Edition, 1998.